Innovative Strategies for Water-in-Diesel Emulsion Separation

Daniel Carwyn Jones

Submitted in accordance with the requirements for the degree of
Doctor of Philosophy

The University of Leeds
School of Mechanical Engineering
Institute of Functional Surfaces

August 2023

The candidate confirms that the work submitted is his/her own and that appropriate credit has been given where reference has been made to the work of others.

Acknowledgements

I would like to thank supervisory team, Prof Nik Kapur, Prof Ardian Morina and Dr Franaz Salehi for their continuous support.

I would also like to acknowledge the support of Prof Anne Neville who was an integral part of my supervisory team prior to her passing.

Additionally, I would like to thank Dr Thibaut Charpentier who prior to leaving the University was my primary supervisor.

Finally, I would like to thank Parker Hannifin, particularly Umer Farooq, for supplying materials and insight throughout the project.

I would also like to thank my friends Rob Jacklin, Harry Bullock, and Raeesa Bhamji and all the other dungeoners for their moral support.

Abstract

The separation of water and particles from diesel is becoming an increasingly pressing issue for the diesel engine. This is as a result of the increase in environmental constraints forcing engine manufacturers to reduce the emissions of their engines (exhaust gasses and particulate matter). In order to do this high-pressure common rail systems were introduced, the increased pressure meant that the tolerances within the engine were made to be tighter. The tighter tolerances mean that the removal of particles and water to avoid the effect of abrasion and corrosion is even more imperative.

This thesis will first examine filters that have been fouled in real engines. The filters have been fouled in three different fuel markets (Sweden petroleum, Brazil petroleum and Brazil biodiesel). The chemical physical changes to the filter as a result of the fouling have been examined. Any differences between the different fuel markets have been noted. It was shown conclusively that there are two main factors that affect the water separation efficiency, the surface free energy and the trans filter pressure (shear force at the pore walls) The findings of this informed the development of a new coating intended to not only increase the immediate water separation efficiency of the filter, but the end-of-life performance as well.

The coating was formed using a modified Stöber process, in which a hydrophobic functionalising agent is used to create hydrophobic microspheres that were applied to the surface of the filter. Three different functionalising agents were examined, two silane-based agents and one acid based. It is shown that it is possible to create superhydrophobic silica spheres using a facile one-pot method for all the functionalising agents examined. It was found that the fluorine containing silane was the most hydrophobic followed by the hydrocarbon-based silane and finally the acid based functionalising agent.

Using a flow rig the immediate effect of the coatings was examined, this will be the most effective method for imitating the real running conditions for the filter. It is shown that all the coatings examined resulted in an increased instantaneous water separation efficiency when compared to an uncoated sample. A novel accelerated fouling technique was developed, this was vital in order to determine the end-of-life performance in a lab environment. It is shown that this technique is representative of what is seen in the samples returned from the field when applied to an uncoated sample. Once the filters were fouled, they were again tested in the flow rig to determine their end-of-

life performance. The coated filters performed significantly better than the filter that was uncoated. The coatings formed with the fluorine containing functionalising agent had the greatest improvement when compared with the uncoated filter.

Table of Contents

List of Tables

List of Figures

Chapter 1
Introduction

1.1 Research Proposal

Water in fuel emulsions are common within diesel engines and can cause issues due to increased corrosion, development of microbial contaminants, and abrasion due to the high pressure (1). Water can enter the fuel in a number of ways, through atmospheric precipitation, changes in humidity and/or temperature or during transport and storage (1). The current technology that is used in diesel engines for the separation of water in fuel emulsions is filtration, the main challenge that is associated with this type of separation is the degradation of the filter due to fouling throughout its operational life. Additionally, it is difficult to ascertain whether a filter is separating water effectively while the filter is installed in the engine. The pressure drop across the filter is measured, but this will not indicate the water separation performance of the filter. The water level within the filter can be measured (2). However, without knowing the initial concentration of water in the fuel, the separation efficiency cannot be known.

Currently, there are two different types of filters that are used in industry to separate water-in-diesel emulsions. One is the depth coalescence filter that uses a convoluted pathway to promote the coalescence of the water droplets within the diesel continuous phase and the effectiveness of this filter is dependent on a number of factors including, pore size distribution, fibre diameter and wettability of the fibres (3). These factors are all affected negatively by fouling. As the filter becomes fouled it loses its effectiveness significantly. The second is a barrier type filter that allows the passage of diesel but stops water from passing through. It is well known that the wettability of the fibres that make up the filter significantly affect the efficiency of the filter (3). It is also relatively well published that applying coatings or modifying surface functional groups changes the wettability of the material (4-6). Again, fouling is the main limitation of this type of filter. The foulant layer effects the wettability reducing the filters effectiveness also the barrier filter is particularly sensitive to blockages because it is a dead end filter (7).

1.1.1 Aims and Objectives

The overall aim of the project is to develop a barrier filter to remove water from water in diesel emulsions. The project will take a barrier filter currently manufactured by Parker Hannifin and improve it in two ways, the instantaneous water separation efficiency should be improved as well as the end of life water separation once the filter has been fouled.

The first aim of the project is to assess the fouling that occurs in the field. It is necessary to determine whether the fuel market has an effect on the type of fouling that is seen. This will help ascertain whether different solutions are required for different fuel markets. Fuel markets can differ in terms of diesel quality, biodiesel blend and running climate.

This will be achieved by:

1. Examining the physical changes that occur during the fouling process. Using filters fouled in different fuel markets assess whether the fuel market has an impact upon the physical change to the filter.
2. Examining the chemical changes to the filter, with particular emphasis to the changes at the surface. Again, the impact of the different fuel markets should be determined.
3. Identify the key factors effecting the water separation efficiency, especially the end-of-life water separation efficiency.
4. Develop a model or index to determine the level of fouling that has occurred and how this is likely to have related to the water separation efficiency.

The second aim of the project will be to develop a superhydrophobic coating that will be applied to the currently used melt blown non-woven polymer filters. The coating will be required to increase the roughness of the fibres and decrease the surface energy.

This will be achieved by:

1. Developing three different one stage processes for forming silica microspheres functionalised with low surface energy compounds.
2. Forming a range of particles with different properties.
    a. Diameter.
    b. Morphology.
    c. Thickness of the functionalised shell.
3. Assessing the hydrophobicity of the of the as prepared microspheres.

4. Applying the microspheres to the surface of the filter material and determining whether the coating process has significantly changed the physical properties of the filter.
5. Selecting an appropriate number of coatings to be examined further based on the key factors that affect the water separation identified in the first aim.

The third and final aim of the project will be to show that the coating has improved both the immediate water separation efficiency and increased end of life performance.

This will be achieved by:

1. Assessing the instantaneous water separation efficiency of the filter. Determine whether the theory that increasing the hydrophobicity results in an improvement in water separation efficiency for water in diesel emulsions.
2. Developing a method for determining the end-of-life water separation efficiency of the coated filters.
    a. Through examining the response of water separation efficiency to an increase in face velocity, mimicking the pore scale increase in face velocity that occurs with pore blinding.
    b. Applying a foreign material to the surface that mimics the physical and chemical changes that were identified in the first aim.

1.2 Motivation

The motivation for this research has come as a result of a number of different changes to both diesel engines themselves and to the fuel being used. In order to comply with tightening environmental regulations, significant developments have been made in the efficiency of diesel engines, one of these developments is the introduction of the high pressure common rail (HPCR) (8). The introduction of HPCR diesel engines allowed for more control over the burn temperature and the completeness of the burn, these are the two driving factors of nitrous oxides (NO_x) and particulate matter production. The high pressure allows for increased atomisation of the fuel, additionally multiple small injection volumes, in the order of micro litres, are used to help control the emissions. This move to small volumes and high pressure result in very small tolerances meaning that the removal of contaminants is even

more pertinent (1). One of the main contaminants that is required to be removed is water, this is because water can contribute to corrosion and microbial growth, also at high pressures the water droplets within the fuel may act like hard particles if sufficient surfactant is present (9).

Another change that has been required is the reduction in sulphur within the fuel, this was done in stages dependant on the geographical location and the regulator of that area. Overall the current limit is around 15ppm for most developed countries (1, 10). The reason that the reduction in sulphur is of concern is that the process of removing the sulphur appears to dramatically reduce the lubricity of the fuel, this resulted in a drastic increase in the number of engine failures that were observed. The decrease in lubricity was found to be caused by the removal of the polar compounds during hydrodesulphurisation. In order to counter the reduced lubricity surfactants are added, the downside of adding the surfactants is that the water droplets within the fuel become more stable and smaller making them more difficult to remove (1).

The addition of biodiesel has become more commonplace in recent years, this also brings with it some issues. It is known that biodiesel is more hygroscopic than petroleum diesel, meaning that it can hold more dissolved water (11). This property means that in humid climates with large fluctuations in temperature will have a higher free water concentration. Not only is this an issue because it means having to remove more water from the system, there is also a possibility that the water may have an adverse reaction with the esters in the biodiesel creating carboxylic acids and alcohols (11).

There would be a significant benefit in developing a coating that can improve the end-of-life performance of a currently used filter. If this were successful it would be possible to continue manufacturing filters using the same methodology with only a slight change in which the filters are coated with the superhydrophobic coating at some point in the process. This would be preferable to developing a novel material because the process of development would be significantly more challenging and the outcome would be significantly more expensive to implement.

Currently there is no commonly used method for determining the water separation efficiency of diesel fuel filters installed on trucks in situ. One motivation is to provide a lab scale method for accelerated fouling that is representative of what is seen in the field. This will allow filter manufacturers to estimate the water separation efficiency based on the pressure drop across the filter, something that is much easier to monitor in situ. This is something

that can be tailored for the specific fuel market in which the filters are being used.

In summary the motivation for this research has come from a change in both the types of engines that are being used and from changes to the fuel market, resulting in reduced performance and premature failure of fuel filters. It is possible that this will be a continuing and even worsening issue as more stringent environmental regulations force more changes to the fuel and to engine running parameters.

1.3 Overview of the issue

Water can enter the fuel system through a number of different routes. The main route is condensation and precipitation or from the humidity in the air, this can happen during transit of the fuel, during the storage of the fuel and to a more minor degree during the refining process (12). Once there is water within the fuel it can exist in two way's dissolved and free water, the water that is dissolved within the fuel cannot be removed through filtration, therefore this project will be focussing on the effects of free water (13). It should be noted that while the dissolved water is not directly being studied the solubility of water is temperature dependant meaning that if the temperature drops some of the dissolved water will become free water provided that the fuel is saturated with water (13).

As can be seen from Figure 1-1 below for pure diesel a drop of 20°C would result in an increase in the free water content of 40mg/kg which is not considerably high. However, the addition of biodiesel has a significant impact of this effect. Biodiesel is more hygroscopic and therefore has a higher dissolved water content when saturated, this means that a drop in temperature would result in an increased amount of free water being released into the system. An example of a saturation curve for pure biodiesel can be seen in Figure 1-2. A saturation curve shows the maximum amount of water that can be dissolved within a specific insoluble liquid for a given temperature. If the liquid at a high temperature is at saturation and the temperature drops, the water in the solution will condense and become free water. It is this water that needs to be removed by the water separation filter being examined in this project.

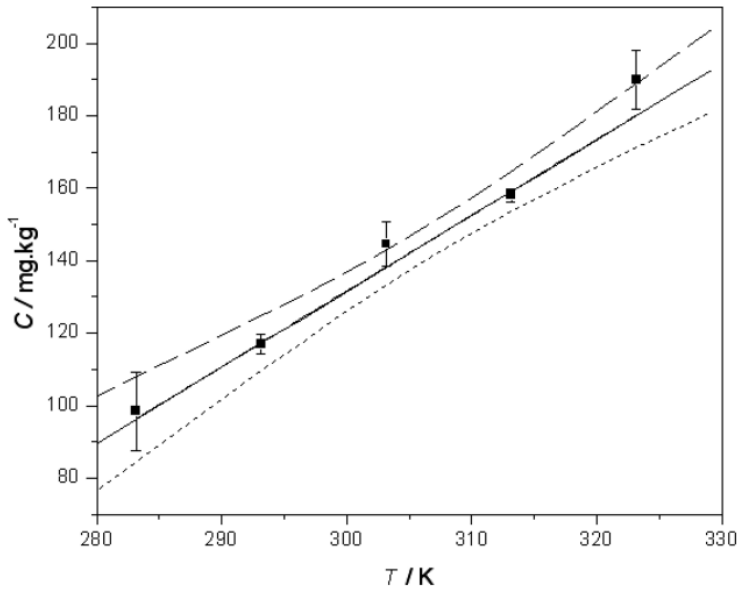

Figure 1-1: Solubility curve for pure diesel [7].

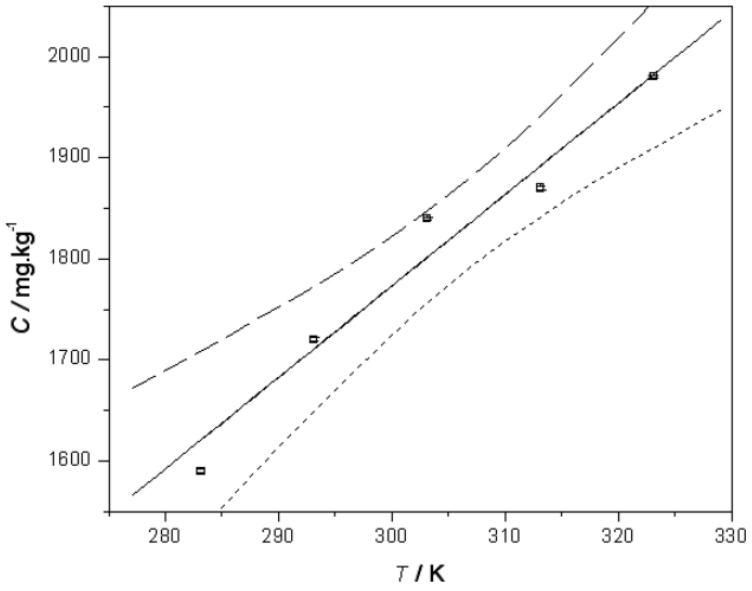

Figure 1-2: Solubility curve for pure biodiesel [7].

The addition of additives results in another issue, due to the fact that some additives are inherently surfactants they result in the reduction of the interfacial tension between the diesel fuel and the water droplets. Interfacial tension is defined as the energy required to create a unit area at the interface between two immiscible fluids (14). This essentially means that smaller droplets (i.e. larger surface area per volume of liquid) will be more stable at lower interfacial tensions due to the fact that the thermodynamic driving force for coalescence is reduced (14). The more stable the smaller droplets are the more difficult it will be to separate the water in diesel emulsion.

Fuel regulation has a significant effect upon the composition of the fuel, this type of regulation strives to provide consistent fuel that will not cause any unexpected harm to the vehicle. Another type of legislation that can have an effect upon the fuel is legislation that concerns the environmental impact of diesel-powered vehicles. This can have an effect because while in some cases it is possible to feasibly modify the engine in order to improve the emissions, it is sometimes necessary to change the composition of the fuel in order to bring the emissions levels within the required constraints (15). The most commonly used example for this is the move to lower sulphur fuels that has been necessary. It should be noted that due to the fact that the composition is primarily controlled through legislation, it is likely that the legislation and therefore the fuel composition are not consistent throughout the world (15).

1.3.1 Sulphur content

The majority of developed countries have particularly strict fuel quality regulations when it comes to the restriction of sulphur. The maximum limits for sulphur content in these developed counties is 50ppm or in some cases 10ppm (10). The EU regulation currently is for a maximum sulphur content of 10ppm, this has come down significantly over the past 20-30 years. The table below summarises the change in maximum sulphur level regulations over time by the EU.

Table 1.1: Change in the maximum sulphur regulations for the EU over time. (16-18)

Year	Sulphur Level (ppm)
1994	2000
1996	500
2000	350
2005	50
2009	10

Similarly in the USA there have also been reductions in the maximum allowed sulphur content. The reduction in the sulphur levels was not done as incrementally as was done in the EU. It reduced to a maximum level of 500ppm in 1993, then down to a maximum level of 15ppm in 2006 and finally to a maximum content of 10ppm in 2017 (19).

Another country with a large market share of the fuel consumption market is China. China overall has not historically had as stringent limits in place to

reduce sulphur associated gases. Up until 2009 the maximum allowable sulphur content in diesel fuel was 500ppm, this was reduced to 350ppm in 2011 (20). There was some variance with mega cities like Beijing requiring more stringent limits (50ppm) to maintain suitable air quality (21). Euro V standards are a regulation put in place by the European Union to regulate the emissions of motor vehicles, it states the maximum allowable nitrous oxides (NO_x) and particulate matter (pm) that can be emitted by vehicles per kilometre (120mg/km – NO_x and 5mg/km – pm) it also sets the maximum allowable sulphur content of liquid fuels (22). It was expected that China would bring its fuel sulphur regulations in line with Euro V standards (10ppm) in 2013, however this was not possible because of the inability to supply sufficient quantities of high quality fuel (23). However, it was possible to supply 50ppm diesel nationwide in 2013 and the 10ppm diesel was made available nationwide in 2017 bringing China in line with the Euro V standards (21).

The other country of interest is India, again due to the fact that India is a developing country the phase in of lower sulphur fuels was slower that was seen for the USA and Europe. There was limited supply of the lower sulphur diesel, therefore in certain cities, mainly Delhi, the lower sulphur limits were implemented earlier (24). In 2001 500ppm diesel was implemented in selected cities, this limit was then brought into effect nationwide in 2005. Also in 2005, the limit of sulphur in fuels was reduced to 350ppm in selected cities, this limit was rolled out nationwide in 2010. Selected cities had the sulphur limits lowered to 50ppm in 2010, with the nationwide rollout coming in 2017. It is planned that the sulphur limit will again be lowered in 2020 to 10ppm to bring the regulations in line with the current Euro V regulations (24).

The majority of countries are widely using ultra-low sulphur fuels, and those that are not have plans to in the near future. This means that if the lowering of the sulphur in fuels is causing an issue with the fouling of filters it is a global issue. It has been well documented that removing the sulphur containing contaminants from the fuel results in a decrease in lubricity (25). It is important that diesel fuel has certain lubricity because it is used to lubricate sliding and rolling parts within the pumps and injectors. It was found that upon the introduction of ultra-low sulphur diesel there was a dramatic increase in the number of engine failures observed, it was concluded that this was caused by the reduction in lubricity (25).

Initially it was thought that the sulphur components were providing the lubricity of the fuel and for that reason removing them was reducing the

lubricity. It was found that by adding sulphur compounds back to the fuel after the hydrodesulphurisation process the lubricity was not returned to the original value, this shows that there is no clear link between the sulphur compounds and the lubricity (25). Some sulphur compounds slightly reduced wear, others had no effect, and some increased the wear. Therefore, it was concluded that some other compound must be removed during the process that provides the lubricity (26). Nitrogen compounds are also removed during the hydrodesulphurisation process, it was shown that there was some correlation between the concentration of nitrogen compounds within the fuel and the lubricity. However, the concentrations that were required to make a significant difference were extremely high (26). It was concluded that the lubricity comes from the combination of all of the polar components within the fuel, not one specific type.

It has been found that the majority of the lubricity in diesel fuels is provided by polar compounds (27). The reason that polar compounds are effective at providing lubricity is that the polar head interacts with the metal oxide and the carbon chain then aids in the formation of an organic film (28). While initially it seems that this would not be a problem for the blocking of filters, in order to counteract the effect of removing the polar components additives were used in order to restore the lubricity of the fuel (29). Generally, the additives that are used for increasing the lubricity are high molecular weight polymers, it should be noted that if a fuel is over treated with additives, then filter blockages can occur. It is also of a concern that the lubricity additives may have adverse reactions with other additives further exacerbating the issue (29). Additionally in some cases biodiesels are used as lubricity enhancers, this is possible because they are predominantly made up of polar fatty acid methyl esters (30). The effect of the biodiesel addition will be discussed further in the next section.

1.3.2 Biodiesel content

There is currently a drive to increase the amount of biodiesel blended with petroleum diesel worldwide. The reason the governments are attempting to increase the concentration of biodiesel is that it is seen as a carbon neutral source of energy, thus reducing the overall carbon footprint associated with transport. Currently the worldwide policy driver for the use of biodiesel is the USA. This has been achieved by enforcing a minimum use of biodiesel per year in the country, this was set at 500 million gallons/ year in 2009 increasing to 1 billion gallons/ year in 2012 this is approximately 2.5% of the total diesel usage (31).

It may be difficult to ascertain whether biodiesel has been added to fuels in the EU because there is no need to label the fuel as such until the concentration is in excess of 5% (32). In low concentrations the biodiesel is used as a lubricity improver as stated in the previous section, however in many countries are attempting to increase the amount of biodiesel in fuels in order to comply with EU directive 2003/30/EU (32). This directive ensures that all member states promote the use of biofuels, it does not give a minimum concentration in regular diesel fuel but rather gives a minimum target for the proportion of the energy for transport that must be provided by biofuels at 2% increasing every year by 0.75% until 2008 when it will be 5.75% (32).

Various countries have used biodiesel indifferent concentrations, Germany has some vehicles that run on 100% biodiesel although this is not widespread. A seemingly more viable and more common method for incorporating biodiesel is by blending it with petroleum diesel, as has been mentioned already this is done in different quantities (32). In the US there are some demonstration fleets that have been successfully run on a blend of 20% biodiesel and 80% petroleum diesel (B20). There are financial benefits of running with biodiesel in the US due to a government backed initiative called the 'Biodiesel Fuel Use Credit Ruling'. However, many fleets do not go with a very high percentage of biodiesel due to concerns that issues may arise with the longevity of engine components. B5 (5% biodiesel blends) are commonly used and this concentration is widely approved by engine manufacturers and often is the standard factory fill fuel (32).

Many different feedstock can be used to create fatty acid methyl esters (FAME) and it has been shown that the feedstock used to create the biodiesel can have an effect upon the tendency of the fuel to block filters (33). An example of a FAME molecule can be seen in Figure 1-3. In a study by Fersner and Galante-Fox (33) various biodiesels from different feedstock were tested for the filter blocking characteristics, additionally differing amounts of sterol glucosides, saturated mono-glycerides and sodium carboxylates were added to assess their effect of filter blocking. The four different feedstock that were tested were rapeseed (RME), used cooking oil (UCOME), coconut (CME) and soy (SME). It was found that when testing B10 (10% biodiesel, 90% petroleum diesel) blends that the following trend with respect to filter blocking was observed UCOME>RME>CME>SME with UCOME performing the best and SME performing the worst. Interestingly when adding saturated mono-glycerides the following trend was seen RME>UCOME>CME>SME (33).

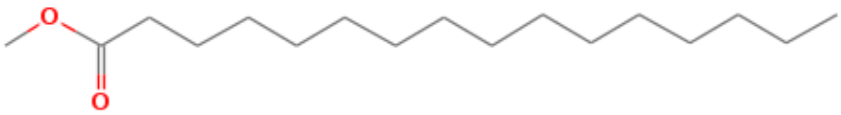

Figure 1-3: Example of a fatty acid methyl ester.

Various countries use different sources of biodiesel, this means that different countries are more likely to have issues with filter blocking related to biodiesel than others. In the US and Brazil the most commonly used feedstock for biodiesel is soy, in the EU the most common feedstock is rapeseed and in Asia palm oil is the most common (34). It is known that biodiesel from a soy feedstock is more susceptible to blocking filters, additionally it is known that the blocking effect is increased significantly with the presence of contaminants like mono-glycerides, sterol glucosides and carboxylate salts. This would suggest that the addition of biodiesel with a soy feedstock is more likely to cause issues, especially if contaminants are present within the fuel (33).

Another important factor to consider is the oxidation stability of the various types of biodiesel. The reason that this is of interest is that the species that are formed as a result of the oxidation are often insoluble, these insoluble species may then contribute to filter blockages (35). Lopes and Geng (36) conducted a study looking at the elemental composition of biodiesels from various feedstock, as a part of this the oxidation stability was assessed using the EN14112 test method (36). In the study biodiesel from the following feedstock were investigated: soy (SME), rapeseed (RME), corn (CME), animal fat (AME) and waste vegetable oil (WVOME). It was found that biodiesel from the soy feedstock has the worst oxidation stability at 3 hours and biodiesel from the animal fat feedstock had the best at 8.5 hours. The complete order was as follows AME>RME>WVOME>CME>SME (36). It is though that the oxidation stability is effect by the degree of unsaturation of the esters in the fuel, with oxidation stability being worse with increasing unsaturation. It was found in a study by Wadumesthrige et al. (35) that SME had significantly larger content of unsaturated species, this helps confirm the link between unsaturation and oxidation stability.

Schwab et al. (37) conducted a study looking at the effect of different additives on internal injector deposits, specifically looking at the problem in the US. It was noted that the issue was not found in engines located in California, there was no theory provided on why this might be. However, in an article in Render magazine it was stated that the major feedstock that is used in

California is corn, followed by animal tallow. As discussed before, in the US the primary feedstock is soy bean (38). This further solidifies the theory that the biodiesel feedstock may have an impact upon the fuel propensity to block filters because the soybean feedstock was found to be the worst in terms of its sensitivity to contaminants and was also had the worst oxidation stability.

1.3.3 Additive interactions

It has been suggested that in some cases the interaction between additives within the fuel can lead to the formation of insoluble compounds. In some cases the additives that are present in the fuel alone may interact with each other, although it is possible that if the fuel becomes contaminated with oil then the additives that are present within the oil could interact unfavourably (39, 40). The interaction between dimer acids that are often used as lubricity enhancers in the fuel and over based detergents that are in the oil can result in aggregations of particles that may contribute to the blockage of filters (40).

Another common problem that is found is the interaction between sodium contaminants and additives within the fuel, this is a problem for both injector deposits and for filter blocking. The primary issue is when acidic additives react with sodium compounds that have found their way into the fuel forming carboxylate salts, these carboxylate salts are insoluble in the fuel and thus precipitate and form deposits on either the injectors of the fuel filters (39). It was shown by Barker and Cook that sodium in the form of sodium hydroxide was the most likely to cause issues with carboxylate formation and subsequent filter blockages (39). It is well known that sodium hydroxide is used in both the hydrodesulphurisation and transesterification processes, although it should be completely removed if good housekeeping practices are observed (39).

Another additive that is known to cause an issue is dodecenyl succinic (DDS) acid that is commonly used to inhibit corrosion. It was found by Schwab et al. (37) that this additive has a high likelihood of reacting with any sodium in the fuel to form insoluble carboxylates. It was found that only very small concentrations of sodium were required for this reaction to occur. In the experiments that were conducted in this study concentrations of 3ppm were used, it was conceded that this is higher than the 1ppm limit that is in place for diesel fuel in the US (the area of interest in the study). However it was concluded that there are many ways that more sodium could be introduced, namely through poor housekeeping in the diesel production system, poor housekeeping in the biodiesel production system or through the introduction of salt during transport (37).

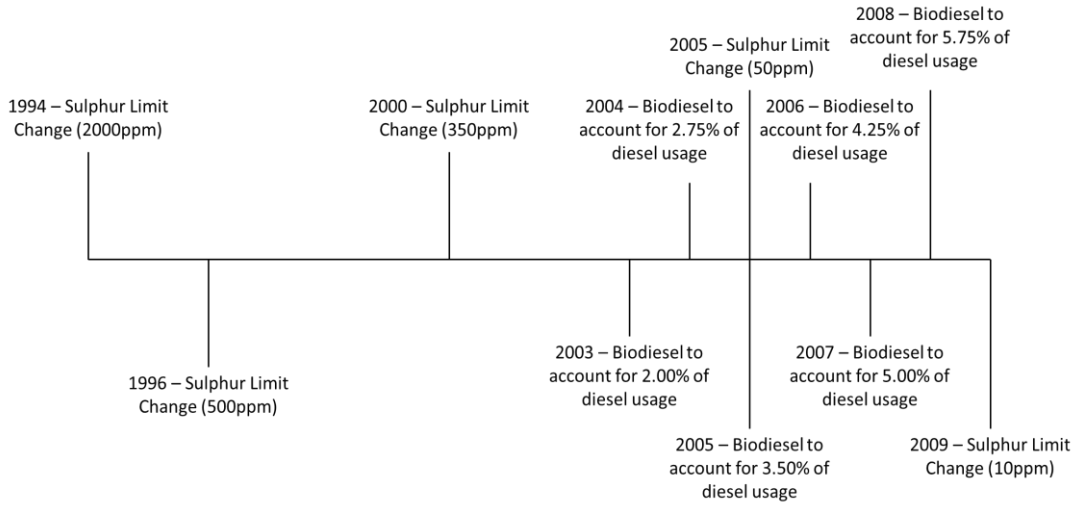

Figure 1-4: Timeline of the known changes to fuel regulation in the EU (16-18, 32)

1.3.4 Conclusion

One of the major drivers for the change in the fuel composition in recent times was increased environmental regulations. This meant that the sulphur content of the fuel needed to be reduced, incidentally the lubricity of the fuel was decreased and an increase in lubricity additives were required. Additionally, there was an increase in the amount of biodiesel that was being blended with conventional diesel, this was also in order to reduce the environmental impact of diesel vehicles. A brief timeline of these events is seen in Figure 1-4 using the EU as the frame of reference. Similar trends are seen for most developed countries, developing countries are slightly behind but in recent times have broadly adopted similar legislation.

It is clear that in reducing the sulphur content of the diesel fuel the lubricity is also reduced, this was a result of the process removing both the sulphur containing components and the polar components. It is important to reintroduce lubricity back to the diesel fuel in order to ensure that the longevity of components (specifically the high-pressure supply pump). There are various additives used to provide this lubricity, one of which is biodiesel. It has been shown that the feedstock of the biodiesel can have a significant role upon the likelihood of the fuel to block a filter.

Another area of concern is the interaction of various additives with either contaminants, biodiesel or other additives. It has been shown that there is a possibility for an unfavourable reaction with additives in the fuel and additives in the lubricating oil if cross contamination occurs. The major area of interest is with the interaction of sodium contaminants and fuel additives,

this can cause the formation of highly insoluble carboxylates that would significantly increase filter blockages.

Overall, there are two major contributors to the increase in fouling seen on diesel filters. The interaction of additives required due to the decrease in lubricity caused by the removal of sulphur and the increase in biodiesel content. The project aims to quantify the impact of the fouling specifically to the water separation efficiency. Using this information a coating will be developed and applied to the surface of manufactured diesel filters in an attempt to improve the end-of-life performance of the filter. This process will not solve the issue and make the filters last longer, it will only ensure that once the filter becomes physically blocked, it is still functioning as a water separator.

Chapter 2
Literature Review

2.1 Techniques for separation

There are a number of possible methods for the separation of emulsions and whilst in this work filtration is the focus, it is important to understand the physics behind other methods and the reasons that they have not been selected for an engine application. This section of the literature review gives background on the reason that filtration is the most appropriate separation technique to be used for the separation of water in diesel emulsions in diesel engines.

2.1.1 Gravity settling

This is a phenomenon that occurs due to the fact that the densities of the two immiscible liquids in question are different. However, this process is very slow especially when attempting to separate emulsions with very finely dispersed droplets. The process is made even more difficult when considering emulsions stabilised by surfactants. (41) The process of purely using gravity to separate a water-in-diesel emulsion would only be feasible in a batch process or continuously with a very large separation vessel compared to the throughput. This is therefore not feasible for an in-line filtration unit within an engine system. There has been some research attempting to improve the effectiveness of this method, discussed in the next section. (41)

2.1.2 Centrifugation

Centrifuges can be used to speed up the process of separation. The effect that is applied using a centrifuge is similar to that that is found in gravity settling, only it is exaggerated, through increasing the effective gravitational constant. The presence of emulsifiers has a drastic effect on the effectiveness of the centrifuge method for separation. It was observed by Hahn and Mittal (42) that having different emulsifiers made a significant difference to the effectiveness of the centrifuge to separate the emulsion. One emulsion was separated to an efficiency of 89%, whereas a second emulsion could only be separated to an efficiency of 7%. The discrepancy is caused by the variation stability of the emulsions formed. In addition to the low separation efficiencies that may be achieved the process takes a significant amount of time, in the region of 2 – 4 hours likely due to the similarity in the density between the two phases.

Equation 2-3 can be used to determine the time it would take to settle a particle (or droplet) of a specified density, it is an adaptation of Stokes' law This is achieved by replacing gravitational acceleration with centrifugal acceleration in the traditional format of Stokes law (Equation 2-1), assuming that the acceleration due to gravity is much smaller than the acceleration due to centrifugation. The equation shown in 2-2 is obtained, then integrating within the limits $r = r$ at $t = 0$ and $r = r_f$ at $t = t$ gives equation 2-3 (43).

$$v = \frac{\Delta\rho D^2 g}{18\mu} \qquad \textbf{2-1}$$

$$\frac{\mathrm{dr}}{\mathrm{dt}} = v = \frac{\Delta\rho D^2 \omega^2 r}{18\mu} \qquad \textbf{2-2}$$

$$\mathrm{t} = \frac{\ln\left(\frac{\mathrm{r}}{\mathrm{r_f}}\right) 18\mu}{\Delta\rho \mathrm{D}^2 \omega^2} \qquad \textbf{2-3}$$

v is the settling velocity, r is the initial position of the particle, $\mathrm{r_f}$ is the final position of the particle, Δρ is the difference in density between the two phases, g is the acceleration due to gravity, μ is the viscosity of the continuous phase, D is the diameter of the droplet, ω is the angular velocity of the centrifuge, t is the time it will take to get from point r to point $\mathrm{r_f}$ and μ is the viscosity of the continuous phase. This equation is only relevant for laminar flow (43). As can be seen increasing the difference in density, the diameter of the droplet or the angular velocity will decrease the settling time. Also, if the viscosity of the continuous phase is decreased the settling time will decrease. These techniques are often used in order to improve the speed of separation processes.

2.1.3 Electrostatically enhanced gravity settling.

The electrostatic enhancement method can only be used in an emulsion in which the water is the dispersed phase, and the oil is the continuous phase. This method of improving the gravity settling method utilises electrodes in order to promote the coalescing of the water droplets within the emulsion. This increases the effect of gravity on these, now larger, droplets, resulting in a reduced time to separate. (44)

An electrostatic coalescing vessel consists of a tank for containing the emulsion, within the tank there would be a set of electrodes with one being earthed, and the other being suspended by an insulator (44). An electrical potential then applied, the electrical potential acts upon the water droplets within the emulsion and polarises them meaning that there is a negative and positive side to the droplet, thus the droplets become attracted to each other

due to the attraction of opposite charges. This attraction promotes coalescence, the larger the droplet becomes due to coalescence the greater the effect of gravity upon it and the quicker the emulsion will separate into two distinct phases. (45) Again, while this method has improved the gravity settling process it is still not fast enough for application within a commercial diesel engine. In addition to this the efficiencies seen are not sufficiently high, Kwon et al. (46) were managing to achieve maximum removal efficiencies of 77%. The time taken to achieve this was in excess of 10hrs.

2.1.4 Microwave enhanced gravity settling

Heating a water-in-oil emulsion is known to increase the settling velocity of the water droplets within the emulsion. It does this by increasing the temperature thus reducing the viscosity of the oil and breaking the outer film of the water droplets, thus increasing the settling velocity of the water droplets. The electrical charge of the droplets is also re-arranged in such a way that promotes the coalescence of the water droplets. (47)

The benefit of using microwaves to heat the emulsion over using conventional heating methods is that it is possible to selectively heat the water within the emulsion. This will dramatically decrease the costs associated with heating the emulsion. Another benefit is that microwave heating is volumetric, this means that the water within the emulsion is heated simultaneously removing the limitations of convective and conductive heat transfer. (48) It was found by Binner et al. (48) that using the microwave heating method resulted in an order of magnitude improvement for separation time. (48) In addition to affecting the interfacial tension between the water and oil it has been suggested that the microwave radiation induces molecular rotation thus neutralising the zeta potential of the droplets in the emulsion. The processes of heating and neutralising zeta potential are usually achieved by conventional heating and chemical addition. (49)

2.1.5 Chemical demulsification

Chemical demulsification occurs in three steps, firstly the surfactant film that is at the surface of the water droplet is displaced, secondly the water droplets flocculate and finally the water droplets coalesce and separate through gravity or other means (50). It is thought that the most important step in this process is the destabilisation of the surfactant film that is surrounding the droplet (51). Chemical demulsifiers are surface active molecules, this means that they have a hydrophilic side and an oleophilic side. This is similar to the

surfactants that are used to stabilise emulsions, however these surfactants promote flocculation and coalescence (52).

The effectiveness of demulsifiers depends heavily on the specific characteristics of the emulsion being separated. In the oil industry chemical demulsifiers are a popular method of aiding the breaking of emulsions. It is common practise in this industry to use trial and error in order to establish the best demulsifier for a specific task (52). It was found by Temple-Head et al. (53) that the solubility of the molecules influenced their effectiveness for breaking emulsions in heavy oil. It was also shown that molecules with long chains tended to promote coalescence better, it was postulated that this was due to the fact that the molecules were poorly packed at the interface resulting in a film that was more elastic (53). The main disadvantage of using chemical demulsifiers is the disposing/ removal of the molecules from either the waste or the product, due to the expense of the molecules it is advantageous to be able to reuse them (44).

2.1.6 Summary of alternative techniques

It has been determined that the alternative techniques are not appropriate for the separation of water in diesel emulsions. Table 2.1 below summarises the shortfalls. The primary shortfall is the fact that the processes are batch processes rather than being continuous. For the centrifuge the radius was assumed to be 50mm, approximately the same radius as a commercial large engine diesel filter. The densities of water and diesel were taken to be 1000kg/m^3 and 785kg/m^3 respectively (54). The viscosity of the continuous phase was taken to be 1.352mPa.s (54).

Table 2.1: Summary of alternative techniques

Process	Settling velocity [mm/s]	Batch/Continuous
Gravity	0.02	Batch
Centrifuge at 5000rpm	3.38	Batch
Centrifuge at 10000rpm	13.5	Batch
Electrostatic	N/A (10hrs to achieve 77% removal of oil from water)	Semi-Batch
Microwave	0.20 (order of magnitude greater than gravity (48))	Batch
Chemical Demulsification	N/A	Batch

The settling velocities for gravity settling were calculated using the Stokes equation (equation 2-1), and the settling velocity for centrifuge settling was calculated using the modified Stokes equation outlined above in equation 2-2. Overall the main problem with these techniques is the fact that they are batch processes. This is without considering the additional equipment that would be required to make the system work would add weight, complexity and maintenance cost to a vehicle that would be unacceptable.

2.2 Filtration overview

As discussed, there are a number of alternatives to the use of filters to demulsify water-in-oil emulsions. However, many of the methods above have serious drawbacks. The main drawback is usually the energy expense of the process, for example centrifuging, electro-coalescence and microwave heating are all energy intensive processes, and this will increase the cost significantly. (42, 44, 48) Any chemical additive is used in order to aid in the de-emulsification usually incurs significant financial cost of materials and potentially will need to be removed after separation is complete. Membrane filtration offers a potential solution to this due to the fact that the membranes themselves are inexpensive to manufacture and provide a very high separation efficiency (55).

Porous filtration membranes work in a relatively simple way, the most basic of which would be to stop particles of a certain size passing through. Typically, filters have micron sized pores if not smaller. For this project

surface active membranes will be required in order to remove the water from a water-in-diesel emulsion. Two approaches will be discussed; firstly, a barrier type filter, this will allow the passage of oil and stop the flow of water thus resulting in separation (56). A general schematic of a barrier filter can be seen in Figure 2-1, the surface wettability combined with the size of the pores allows diesel to pass through freely, whereas the water droplets are stopped at the surface. The second type will be a depth coalescing method, this method relies on the dispersed phase being caught in the fibrous filter and then coalesce with other droplets, and these coalesced droplets should then migrate through the filter medium continuing to coalesce until they are sufficiently large to fall out of the flow due to gravity (57). A schematic diagram of the depth coalescence filter is shown in Figure 2-2, as the droplets flow through the filter they become entrained on the surface of the fibres and coalesce, the average diameter of the droplets increases through the depth of the filter. The aim is to increase the droplets to the size at which they would settle out of the flow within a reasonable time.

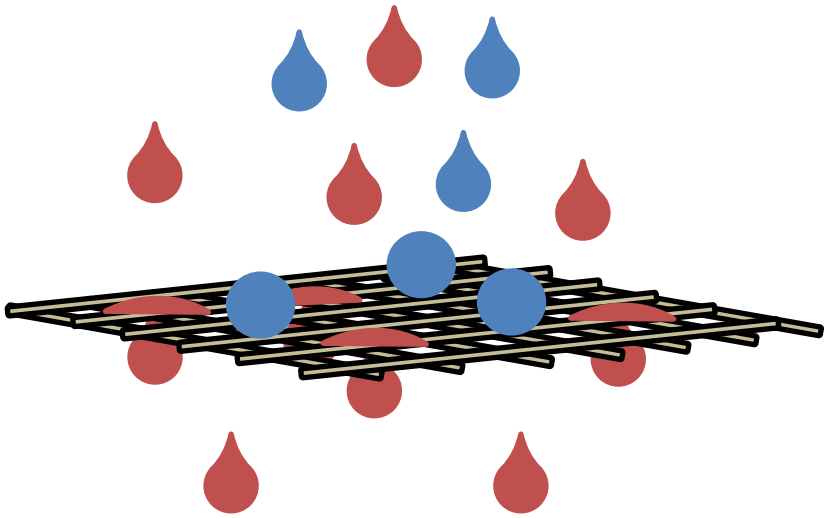

Figure 2-1: Schematic of a barrier filter (red - oil, blue - water)

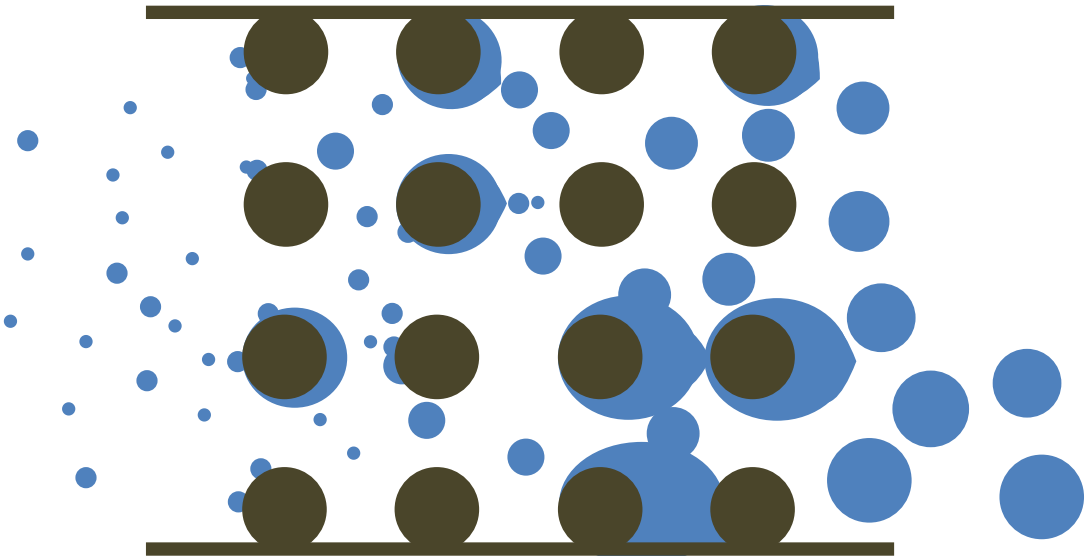

Figure 2-2: Schematic diagram of a depth coalescence filter.

2.2.1 Methods used to assess the efficacy.

In a number of the papers that have been reviewed the efficiency of the filter is not directly evaluated, the reason for this is that the objective of the studies was to create a film/ coating with certain wettability characteristics. In these cases, it was determined that the contact angle was sufficient in order to evaluate the success of the coating, this was more often applied when creating super hydrophobic films (58-61). The contact angle is a quantification of the wettability of a surface. It is the angle that forms between a droplet, usually water but sometimes other liquids, and the surface being examined. An image is taken and the angle is calculated when the droplet is in equilibrium.

When the contact angle is not sufficient to determine the success of a study there are three main factors that tend to be considered: the purity of the filtrate (i.e. the absence of the phase being removed), the separation efficiency defined in equation 2-4 and the comparison of droplet diameters in the feed and the product. These three factors are more applicable to the barrier type filter but are used in some cases for characterising the depth coalescence type filter (however separation efficiency, is usually described as coalescence efficiency). The factors that are more commonly seen when studying depth coalescence filtration are the coalescence efficiency and the quality factor, these are discussed in more detail below (62-64).

The purity of the filtrate can be a relatively crude method of determining the separation efficiency of a filter, the reason this is perhaps not the most appropriate measure is that the final purity is dependent upon the initial concentration of the contaminant. Thus, if there is a disparity between the

initial concentration used between studies it makes any comparison more difficult. Lee and Baik (65) used this method as a proof of concept, however, specific volumes of diesel and water were not used and additionally an emulsion was not formed. Cao et al. (66) also used the purity of the filtrate as an indication of the effectiveness of the filter, however this experiment was more controlled. Surfactant stabilised emulsions were made using four different oil bases and span 80 as the surfactant. In order to prove the stability of the emulsion containers of each were left for 90 days and images of before and after were compared, this showed that the emulsion was highly stable. It was shown that the filter in this case could achieve a final oil purity between 99.96% and 99.98% depending on the oil base used.

Another method that is sometimes used is the droplet diameter distribution, this can be a useful indicator of the ability of a filter to remove certain droplet diameters. Lee et al. (67) used this method in order to show that the filter created in their study was very effective at removing droplets with diameters in excess of 50 micron, however below this diameter the filter was not effective. It was concluded in this study that this was due to the size of the pores in the filter being approximately 50 microns. Cao et al. (66) also used droplet size to supplement the use of the final oil purity, in this study an optical microscope was used in order to image the solution before and after filtration. It was shown that the number of droplets especially large ones had reduced significantly. This is a more rudimentary method than the one that was applied by Lee et al. (67) providing only qualitative data.

By far the most commonly used and therefore the most useful for comparative applications is the separation efficiency. This is usually defined as is shown below in equation 2-4.

$$E = \frac{C_i - C_o}{C_i} \qquad \textbf{2-4}$$

Where C is the mass concentration (kg/m^3) and the subscripts i and o represent inlet and outlet respectively. Due to the fact that the concentration of the droplets is not easily measured the following relationship is often used to relate the number of particles of a specific size to the concentration (12).

$$C = \sum \rho \frac{\pi}{6} D_j^3 n_j \qquad \textbf{2-5}$$

Where C is the concentration (kg/m^3), ρ is the density (kg/m^3) of the droplet, D_j is the diameter (m) of the droplet and n_j is the number of droplets of diameter D_j per unit volume (m^{-3}). A sample is taken from the inlet and outlet and these samples are then run through a particle size analyser to determine

the particle size distribution allowing for the calculation of the separation efficiency. (12, 68, 69)

In some cases, there are more unique methods being used in order to ascertain the water content of filtrates. Zhang et al. (70) added anhydrous cupric sulphate to the solution, anhydrous cupric sulphate is white/grey in colour but reacts with water to form blue copper sulphate pentahydrate. This was used as a visual aid to determine if any water was present in the filtrate. This method is only qualitative, and no experiments were conducted to determine the minimum amount of water required to have a visual effect.

When describing the efficiency of depth coalescence filtration often slightly different methods are implemented, this is due to the difference in the way the filters operate. A depth coalescence filter does not stop the passage of water therefore the concentration at the inlet and outlet will be the same, in order to solve this issue a settling vessel is used prior to taking a sample. (71, 72) The addition of the settling vessel may give results that are higher than the true value due to gravity settling, however if the dispersion is stabilised it is unlikely that the settling vessel will have any effect upon the un-coalesced droplets.

Visual methods are sometimes used in order to determine the effectiveness of a filter Sareen et al. (73) used the clarity of the filtrate in order to give an indication as to the effectiveness of a filter. This was done in two different ways, firstly it was done visually by determining the extent of the turbidity of the filtrate categorising the turbidity into three categories: complete, partial or incomplete coalescence. The categorisation is subjective and does not describe the coalescence well due to the low number of categories available. The second method used the same categories but in order to determine the extent of coalescence, a beam of light was directed at the filtrate. It was found that the more droplets that were present then the more light was reflected. This is relatively rudimentary, but it does remove the subjectivity.

Clayfield et al. (62) also used a visual method for determining the extent of coalescence, however spectrophotometry was used to determine turbidity rather than operator observation. This removes the subjectivity of the operator, it also allowed for a broader range of results because the data were not grouped into categories. In order to relate the turbidity of the filtrate to that of the feed a ratio between the filtrate and the feed was used as the indicator of the effectiveness of the filter, with a value of zero meaning complete coalescence and one meaning no coalescence.

2.2.2 Equipment

In order to measure the values that are described above there are a number of different experimental equipment set ups used. The end goal of the study dictates the type of equipment that is used. For example in some studies the mechanisms of coalescence are what is being observed, for this Basu (74) used a single disk coalescer. The disk could be swapped out for materials with varying wettability and a camera captured the effects of these changes on the capture of droplets on the disk. This equipment would not allow for the collection of data that would lead to one of the efficiency parameters that are described in section 2.2.1. A similar apparatus was used by Moses and Ng (75) to study the breakdown of emulsions in coalescers, the primary difference was that there were multiple disks used. This allowed for the observation of how captured droplets interacted and coalesced with droplets on adjacent disks.

Looking specifically at the barrier filters it is not uncommon for beaker scale apparatus to be used. Zhang et al. (70) placed a filter paper within a funnel and poured the mixture through it, providing that the filter is a success the two phases should be separated with one passing through the filter and the other being held above within the funnel. All of these experiments generally work under the same principle, the mixture is poured over the filter and gravity provides the driving force for the separation of the two phases. Filter holders of various shapes and sizes are used to hold the filters but the same general principle is used (66, 76). Lee et al. (65) used a similar methodology, however the filter was placed above the mixture and a plunger was forced downwards at varying pressures in order to separate the two phases. This has the advantage of having a more controllable pressure in the system allowing for a more accurate representation of reality. Additionally, it was possible to calculate the breakthrough pressure of the repelling phase, this is an important parameter for a barrier filter.

The most common equipment that is used for the depth coalescence filtration analysis is a pumped circuit, an example schematic of this can be seen in Figure 2-3. In many cases there is also a pressure differential measurement device across the filter housing, additionally there are sample points immediately before and after the filter housing in some cases. (62, 64, 71-73, 77, 78) This type of equipment is also used in barrier filtration but it significantly less common.(12, 68, 79) This equipment most accurately represents reality with regards to fuel filtration due to the fact that this is essentially what fuel filtration system may look like within an engine. It also

allows for the control of the pressure that is seen at the filter and the fluid velocity by changing the pumping rate. It allows for the monitoring of the pressure drop across the filter, which is a key parameter when considering fouling. (72)

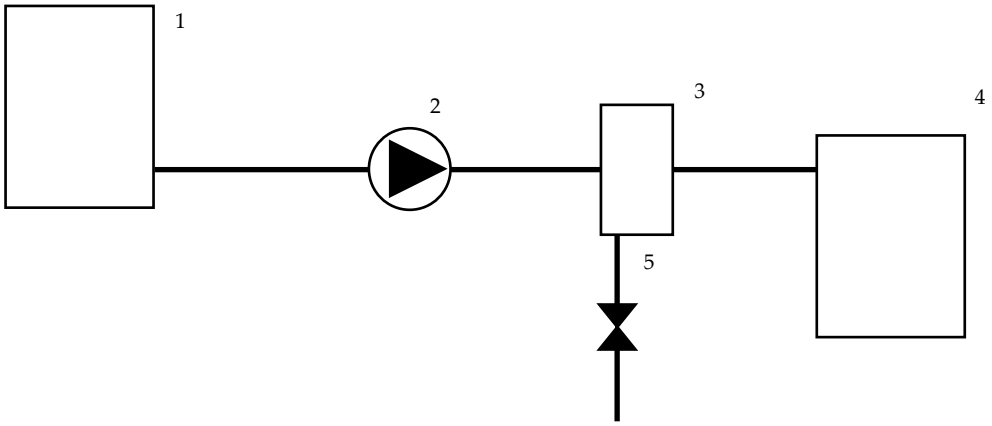

Figure 2-3: Example of a simple pumped circuit. 1. Tank containing the mixture. 2. Pump. 3. Filter housing. 4. Filtrate Tank. 5. Drain Valve

2.2.3 Depth Coalescing Filter

Coalescing has been a cost-effective method of separating emulsions for a long time, the first patent for this kind of separator was submitted in 1908 (80). Othman et al. (81) states that there are three stages in this process, firstly the capture of the droplets by the fibrous bed, secondly the coalescence of the droplets and their migration through the bed, finally the release and removal of the coalesced droplets. This process differs from a regular filter in that the process is a steady state, i.e., the concentration of both phases will be the same on either side of the filter. It is possible for a coalescence filter to coalesce droplets $1/10^{th}$ the size of the pore size of the fibrous bed, this allows the pore sizes to be larger resulting in reduced pressure drop (80).

There are a number of different theories about the mechanisms that control the coalescence of the dispersed phase within the fibrous bed. Austin and Jeffreys (82) suggested that there are three ways that a droplet could coalesce with another. The first is a spontaneous collision of one droplet with another within the dispersed flow. However, Sareen et al. (73) investigated this mechanism and found that it was negligible when compared with the other two mechanisms. The second is collision with the fibrous media, and the third is collision with droplets already attached to the fibrous media. Collision with the fibres (60) the filter medium becomes saturated with the dispersed phase.

The degree to which the filter becomes saturated is dependent on a number of factors, namely, the surface chemistry of the fibres, the surface area of the fibres and the hydrodynamic properties of the flow (82).

There are a number of different factors affect the efficiency of a coalescence filter. There are some that are more important or influential than others. The factors that are most commonly discussed in literature are: Bed depth; fibre surface wettability; flow rate; fibre diameter; and droplet size. (62, 73, 83, 84). It is important to understand the influence that each of these factors has on the efficiency of the filter in order to optimally design a filter for high efficiency operation.

It was shown by Sareen et al. (73) that for the filter thickness there was an optimal value. It was seen that when increasing the filter thickness the coalescence increased, however once a critical depth was reached no further increase in efficiency was seen. It was also noted in this study that increasing the filter thickness also increased the pressure drop, this means that it is important to find out what the critical depth for maximum separation efficiency is in order to maximise efficiency while also limiting the pressure drop. A study conducted by Hazlett (85) yielded results that suggested above a certain minimal value of filter thickness no further improvement in separation efficiency would be seen. Magiera and Blass (86) had again very similar results, however they postulated that above a critical bed depth the droplets that have coalesced begin to break up reducing the performance.

Sokolovic et al. (63) addressed some of the variation in the literature, stating that the reason is usually due to varying operating conditions used, different flow orientations (horizontal or vertical) and differing permeability (63, 77). The general theme seems to be that there is an optimal filter depth, and that this value will not be universal, it will vary from filter to filter depending on the characteristics of the filter, the operating conditions and the dispersion being separated.

Again, there is some disagreement in the literature as to what effect the surface wettability has on the separation efficiency of a coalescence filter. Basu (74) showed that the wettability does have an effect on the separation efficiency of a coalescence filter. In this study an actual coalescence filter was not used, rather disks of two different materials, glass and PTFE, were used in order to demonstrate the effect that wettability has on both water and oil coalescence. It was seen that water would coalesce on the glass surface but not on the PTFE surface whereas, oil would coalesce on the PTFE surface but not the glass surface. This shows that wettability of a surface clearly has an effect

on the coalescence efficiency, however this study cannot be quantitatively applied to a coalescing filter because of its vastly different hydrodynamic properties between the experimental apparatus used and a typical coalescence filter (74).

Sareen et al. (73) found that the wetting characteristic did not play a part in the separation efficiency of the filter. In this study a number of different materials were evaluated to determine what factors had the greatest effect on the separation efficiency, these materials included cotton, Dynel, glass, polyethylene, polypropylene and Teflon. In addition to this a number of different mixtures were evaluated, some oil in water dispersions and some water in oil dispersions. It was found in this study that the cotton performed best for all of the different dispersions used, it was concluded from this that preferential wetting does not have a significant effect on the filter separation efficiency. The postulated reason that this was observed was that the cotton fibres showed significantly greater roughness than the synthetic fibres, this may allow for better adhesion of water or oil droplets resulting in increased coalescence and therefore increased separation efficiency.

Clayfield et al. (62) conducted a study looking at the effect that surface energy has on the separation efficiency of a filter. In order to modify the surface energy of the glass fibres, they were coated with various silanes with different functional groups. In this study glass was used as a substrate, two different fibre diameters were used, 1.5μm and 7.5μm. It was observed that the smaller diameter fibre outperformed the larger diameter fibre in terms of separation efficiency, this was expected due to the increases surface area. The differences in separation efficiency for the different surface coatings were more apparent for the larger diameter fibres, therefore the larger diameter fibres were used in order to make comparisons.

It was found in this study that the surface energy of the coatings did not have any effect on the separation efficiency. It was discovered that a filter with the coating 3-(Heptafluoroisopro - poxy) propyltrichloro – silane with a critical surface tension of 16.7 mN/m had a separation efficiency of only 55.9%, whereas a filter with the coating Perfluoroalkyltriethoxy – silane (branched chain) with a critical surface tension of 17.1 mN/m had a separation efficiency greater than 97%. This shows that wetting is not the only parameter influencing the water separation efficiency, and in certain cases the effect of the other parameters can outweigh that of wettability. The critical surface tension is described as the surface tension required by a liquid to completely wet the surface, this is calculated by plotting the contact angles of various

liquids with known surface tension on to a Zisman plot. It should be noted that this is not the actual surface free energy of the surface, but can be used as an analogue (62).

In order to calculate the critical surface tension in this study, Clayfield et al. (62) applied the surface coatings to a glass microscope slide and not to the glass fibres in order to make the contact angle measurements to add to the Zisman plot. This was done due to the fact that it would not be possible to make accurate contact angle measurements from the glass fibres because of the porosity. During this study a number of other coatings were attempted, however the methods used to adhere the coatings to the glass surface were unsuccessful. The application of the coatings to the fibres was not confirmed with any surface characterisation. It is possible that when using the same method of adherence for the silanes to the glass fibres and glass slides the results were not the same. This would mean that the critical surface tension would not be the same for both a glass slide and glass fibre coated with the same silane, this could explain the fact that there was no correlation seen between critical surface tension and separation efficiency.

Kulkarni et al. (83) looked at the effect that wettability has on separation efficiency in a slightly different way, in this study rather than changing the wettability of the whole filter media hydrophilic and hydrophobic media were layered in different ratios. The hydrophilic media used in this study were glass fibres, two different hydrophobic materials were used polypropylene or polyethylene terephthalate (PET). The concentrations of polymers within the filters varied from 20 – 80% in 20% increments. In order to characterise the wettability of the filter mixtures, the modified Washburn method was used, it was not possible to use the conventional droplet contact angle method because the roughness and porosity of the media stopped accurate reproducible results. The metric that was used in order to compare the relative wettability of the filters was the lipophilic/hydrophilic balance, this is defined in equation 2-6 (83).

$$\frac{L}{H} = \frac{\cos(\theta_O)}{\cos(\theta_w)} \qquad \textbf{2-6}$$

Where θ_O is the contact angle of oil on the surface of the fibres in air, and θ_W is the contact angle of water on the fibres in air. The lipophilic/hydrophilic balance is a ratio between the contact angles formed between oil and water and the surface being examined. The reason this can be a good metric for the wettability of a surface specifically as it pertains to the separation of water in oil (or diesel) emulsions because the driving force (particularly for barrier

filters) is the difference in water and oil wettability. This technique was not used in this project due to the difficulty of measuring the contact angle of diesel on the surface. The value obtained was effectively 0°, resulting in an L/H value of 0, thus giving very little information.

This value was calculated using the modified Washburn equation, it was found using this equation that as the L/H balance increased the pressure drop decreased but so did the separation efficiency. This meant that there must be an intermediate L/H balance that provided the best separation efficiency while minimising the pressure drop. In order to quantify what this was the quality factor was used, this is defined in equation 2-7 (83).

$$Q_F = \frac{-\ln(1 - E)}{\Delta P} \qquad \textbf{2-7}$$

When using this factor, it was found that the optimum L/H balance for polypropylene was between 3 and 10, whereas for PET was approximately 26. Additionally, by making this comparison it was clear that the filters made up of polypropylene were more effective, it was determined that this was due to the lower pressure drop that was seen when using this media. A likely reason for the difference in the pressure drop seen is the difference in permeability of the filters made up of the two polymers, with polypropylene filters having a permeability between 4 and 6 times greater depending on the L/H balance (83).

Another factor that is somewhat related to the fibre wettability is the fibre surface roughness, this is often split into micro and nano roughness. It is well known that the roughness of a surface can affect the both the wettability and the mobility of droplets upon the surface. It was found by Agarwal et al. (87) that in order to effectively separate oil in water emulsions it was necessary to have an oleophilic-hydrophobic fibre with sufficient surface roughness to have good adhesion from the water droplet. Often this surface roughness was required to be in the nanoscale to have the best effect. While this is looking at the separation of oil from water, similar principles will apply for the separation of water from oil emulsions.

Han and Kang (71) conducted a series of experiments looking at the effect that operating conditions have on the separation efficiency. In this study the specific parameter that was varied was the superficial velocity. This is defined as the velocity that would be expected through the filter for a given flow rate if the area reduction due to the presence of the filter media was neglected. It was observed that increasing the superficial velocity of the flow had very little effect on the concentration of water in the effluent flow until a critical value

of superficial velocity was reached, after this point a very drastic increase in water concentration was observed.

The reason for the reduction in separation efficiency was concluded to be due to the increase in hydrodynamic forces that would be experienced by the water droplets (71). It was found that the increase in hydrodynamic shear forces resulted in water droplets having difficulty adhering to the fibres in the filter, this meant that coalescence could not occur as readily. It was also suggested that the three-dimensional net structure of the filter would be loosened, this would allow droplets to pass through the filter without adhering to the fibres more readily resulting in a decrease in the separation efficiency (71). At the higher velocities studied, the difference between the separation efficiencies seen in filters of different thicknesses and porosities was reduced. It was concluded that this was due to the fact that the internal structure of the filter was compromised by the high hydrodynamic forces, this meant that the thickness and porosity became a secondary impact on the separation efficiency (71).

This same effect was seen in another study conducted by Zhou et al. (88), this study differs in that it is looking at oil in water separation rather than at water in oil separation. Having said this the effect, the operating conditions have on the coalescence should be very similar for both types of emulsion. It was noted in this study that increasing the superficial velocity resulted in a decrease in separation efficiency at all levels, however at a certain critical point an extremely large decrease in separation efficiency was observed. Additionally, it was shown that for all of the flow velocities used the separation efficiency was relatively stable, Zhou et al. (88) took this as an indication that there was no breakthrough even under high flow velocities.

It was shown by Sokolovic et al. (72) that having a coalescence system operating in a state above the critical superficial velocity changes how the effluent dispersed phase concentration is affected by other parameters. Again, this study is looking at the coalescence of oil and not the coalescence of water, but the results should be analogous. It was observed that below the critical superficial velocity the inlet oil concentration didn't have a significant effect upon the effluent oil concentration, however for superficial velocities above the critical values there was an obvious correlation between increasing inlet concentration and increasing effluent concentration (72). Additionally, the dependence of the filter depth upon the effluent oil concentration was very different above the critical value for superficial velocity. It was seen that the effluent concentration increased with increasing filter depth to a point, then

began to decrease again. It was postulated that the increase was due to the fact that the coalesced droplets began to break up within the filter due to the increased hydrodynamic shear forces, the subsequent decrease occurred because the droplets began to re-coalesce within the filter (72).

A study by Shin et al. (89) looked at the effect that adding polymer nanofibers to glass fibre coalescing filters has on the separation efficiency. The glass fibres have diameters ranging from 2 to 7 microns, where the nanofibers have diameters in the range 200 to 300 nanometres. In order to apply the nanofibers to the glass fibre substrate the electrospinning process was utilised. Using SEM imaging it was shown that the nanofibers cross over the void between the larger glass fibres, this will result in a more tortuous path for the droplets.

It was observed in this study (89) that the addition of nanofibers to the glass fibre substrate had a positive impact on the separation efficiency. However, it was also shown that after a certain point, the addition of further masses of nanofibers had no discernible effect upon the separation efficiency. As the mass of nanofibers added increased so too did the pressure drop observed across the filter, this means that there would be an optimum mass of nanofibers that yields the highest separation efficiency for the lowest pressure drop (89). It was found that the addition of nanofibers helped in coalescing the small droplets, this was due to the fact that the nanofibers could bridge the pores in the glass fibre substrate. This resulted in reducing the pore size, due to the very small diameter of the fibres the addition of nanofibers has the ability to reduce the pore size without significantly effecting porosity (89).

A study conducted by Magiera and Blass (86) showed very similar results. This paper differed in a number of ways, the primary difference was the fact that the fibres in this study were all one diameter and material (glass). It was observed that as the diameter of the glass fibres reduced it was possible to coalesce smaller droplets, this is the same result as was seen by Shin et al. (89) when adding nanofibers. Similarly it was postulated by Magiera and Blass (86) that the reason for this is the fact that the for a filters with constant porosity but smaller fibre diameters the fibre surface area available for droplets adhering and coalescing increases, this results in greater separation efficiency.

Droplet diameter can have a significant effect on the separation efficiency. The reason for this is related to the reason that fibre diameter effects separation efficiency, in that the decreased separation efficiency due to reduced droplet diameter is because the smaller droplets have more chance of passing through the filter without adhering to the fibres and coalescing. This was observed by

Clayfield et al. (62), when using fibres with average diameters of 7.5μm there was no coalescence of droplets less than 3μm when using plain glass. When using smaller fibre diameters it was found that it was possible to coalesce much smaller droplets (62). This is to be expected considering what was seen with changing fibre diameters.

There are a number of different factors that affect the efficiency of a coalescence filter, some studied in more depth than others in the literature. It is well established that increasing the filter thickness increases both the pressure drop and the separation efficiency, meaning that there is an ideal filter thickness that provides a sufficiently high separation efficiency with the lowest possible pressure drop. This will likely be different for different filter set ups. Similarly, the smaller the fibre diameter the larger both the separation efficiency and the pressure drop will be, an ideal fibre thickness should be found for each application. The factor that appears to have gained the most attention in recent publications is the wettability of the fibres. The likely reason for this is that the effect of the other parameters is relatively well known, and the alteration of these factors is relatively straight forward. There is some dispute as to the effect of the wettability in the literature, however the general theme seems to be that an intermediate wettability is favourable. This is because the droplet would sufficiently wet the fibre in order to adhere and coalesce but would not wet the fibre so much that the accumulation of the water droplets would lead to a significant increase in pressure drop.

Depth filtration summary

While depth coalescence filtration is not directly being examined in this project it is vital that the fundamentals of both separation mechanisms are understood. The reason for this is that physically the only thing that differs between the two types of filtration is the pore size and the wettability of the fibres. This means that depending on the changes to the wettability of the fibres as a result of fouling it is possible that the mechanism of separation might switch from being predominantly a barrier filter to more of a coalescence filter. Understanding the literature on this type of filtration will allow and understanding and an explanation as to why the barrier filter if performing as a coalescence filter would have very poor performance.

2.2.4 Barrier filter

The primary difference between this type of filter and the coalescence filter is that the concentration of water on the inlet and outlet will be different, this means that the filter is not a steady state filter, it is better described as a dead

end filter (80). In order to achieve separation a porous membrane with an extremely low affinity to water must be used, in other words a superhydrophobic material (58). This can be achieved in a number of different ways. Some authors describe methods of creating superhydrophobic coatings or films that are usually formed of some sort of polymer or in some cases carbon nanotubes to apply to a porous substrate (65, 76, 90). Others create a membrane directly from materials that possess the required properties, there are various methods of creating these membranes the most popular in recent research is electrospinning (12, 68). Another method is by phase inversion (56).

One of the major issues that are encountered with this type of filter is the rapid onset of fouling (69). This occurs partially due to the fact that this is a dead-end filter, this means that water molecules that are blocked from passing through the filter may begin to coalesce and cause restriction prior to settling via gravity. This was postulated by Scott et al. (91), the study considered the difference in flux decline between a corrugated and an un-corrugated membrane using a crossflow set up. The rapid decline in flux was deemed to be due to a combination of pore blockage due to water droplets and formation of a cake layer. It was established in this study that the cake layer reduced the flux by adding resistance to flow and changing the pore size distribution. While this is a negative with regards to the lifetime of the filter, it was found that the cake layer improved the separation efficiency of the filter. After the first few minutes of operation with a pristine filter the separation efficiency was improved, likely due to cake layer formation (91).

Another thing that is thought to be an issue is the adsorption of molecules on to the surface of the filter, this is likely to either be hydrocarbon molecules from within the dispersed phase or it is possible that added surfactants will deposit upon the surface. This would be doubly disadvantageous due to the fact that it will add to the reduction in pore volume and thus the flux, additionally it may have an effect on the surface chemistry of the membrane. This is an effect that is well known and has been exploited in the oil industry for a number of years in order to change the wettability of rocks and increase the oil recovery (92). It has been found that the surface wettability can be greatly affected by the introduction of surfactants, it was shown by Somasundaran and Zhang (92) that the wettability can be effectively reversed as can be seen in Figure 2-4(a). Also looking at Figure 2-4(a) it can be seen that with the continued adsorption of surfactant will lead to a further change in

wettability, a possible mechanism for this was proposed and is shown in Figure 2-4(b).

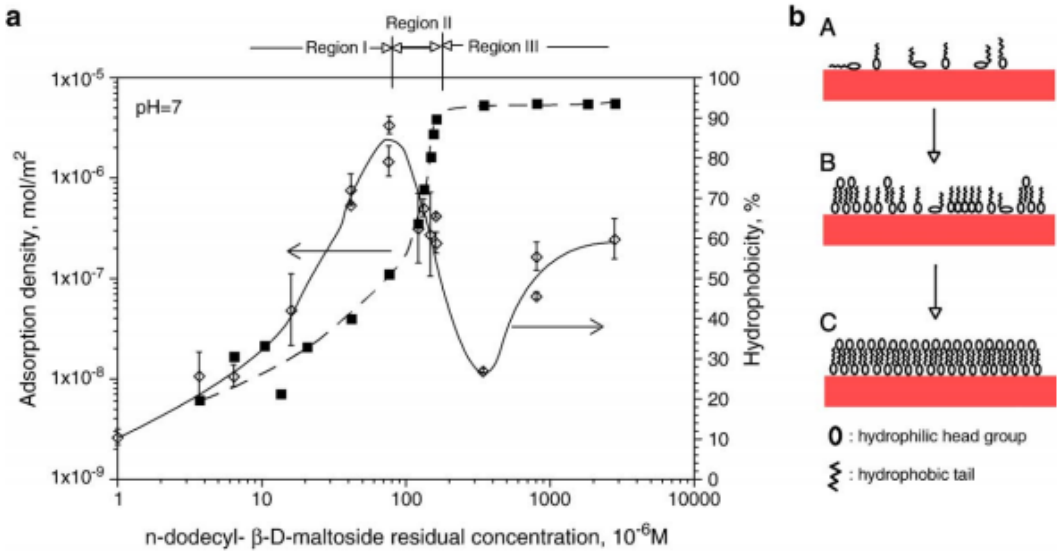

Figure 2-4: (a) change in wettability with increasing surfactant concentration (b) proposed mechanism for the change in wettability observed [102]

If the filter fails in this way it could be very harmful, the reason being that the common method for detecting the degradation of a filter is through differential pressure, however if the filter were to fail due to the fact that it is no longer superhydrophobic the change in differential pressure may not be sufficiently large to detect.

The primary factor that affects the efficiency of a barrier type emulsion filter is its wettability. The hydrophobicity of the filter stops the water droplets from deforming sufficiently to fit through the pores. This effectively causes the water droplets to act like particles becoming trapped on the surface of the filter, they then coalesce as more droplets are deposited and settle via gravity (1). Similar to the depth coalescence filter droplet diameter or pore diameter have a significant effect upon the effectiveness of the filter, however in this case the droplet must not be smaller than the pore size or separation will not occur (5).

The separation mechanics of a barrier filter are relatively similar compared to the mechanics of a depth coalescence filter. Initially it would appear that if the surface is sufficiently hydrophobic, and the pore size is smaller than the droplet being separated then the droplet would be rejected at the surface. While this is true, if the force on the droplet is sufficiently large it is possible to deform it forcing it through the pore. Nazzal and Wiesner (93) developed

a simple model based on Young-Laplace equation to describe the critical pressure that would be required for this deformation.

The critical pressure is defined in equation 2-8 (94).

$$P_c = \frac{2\gamma(\cos\theta)}{r_p} \qquad \textbf{2-8}$$

Where P_c is the critical pressure, γ is the interfacial tension, r_p is the radius of the pore θ is the contact angle as defines in Figure 2-5. This model does not take into account the diameter of the droplets. Nazzal and Wiesner (95) integrated the diameter of the droplet (r_d), the equation developed is shown in equation 2-9.

$$P_c = \frac{2\gamma(\cos\theta)}{r_p}\left[1 - \left(\frac{2 + 3\cos\theta - \cos^3\theta}{4\left(\frac{r_d}{r_p}\right)^3 \cos^3\theta - (2 - 3\sin\theta + \sin^3\theta)}\right)^{\frac{1}{3}}\right] \qquad \textbf{2-9}$$

It was shown in this paper that the model somewhat follows what is observed experimentally. However, it was not a great predictor, highlighting the complexity of emulsion separation problems.

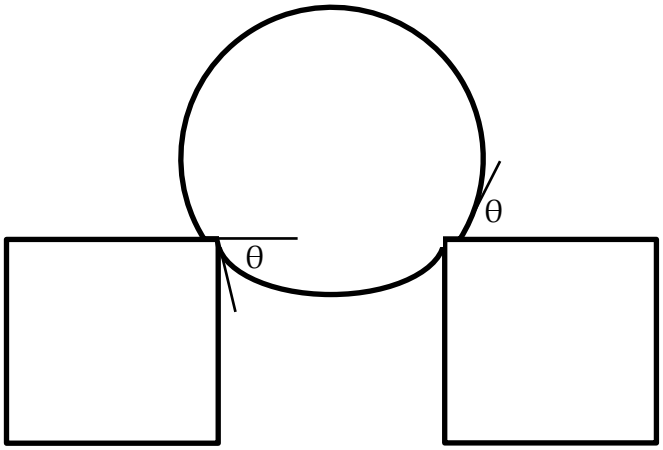

Figure 2-5: Definition of contact angle used in the simple model for critical pressure.

There are a number of reasons that this model does not perfectly represent reality. The model assumes the pore to have no depth, once the droplet is deformed it will require no additional pressure to force the droplet through the filter. In reality the pore will likely be a tortuous path, especially in a fibrous bed. Another of the limitations with these equations is that they describe the interaction between a single droplet and a single pore. If this is applied practically there will be a distribution of both pore and droplet size, and there would be no simple method for determining which droplets will

interact with which pore. In addition to this, droplets will also coalesce in the flow and at the surface making the droplet size distribution dynamic.

The complexity of the mechanism behind the separation of water in diesel emulsions means that developing a purely theoretical model for determining the water separation efficiency is extremely difficult. In addition to this the variables that would need to be input into the model would be impossible to determine for a system in a diesel engine. Therefore, this project will examine the mechanism empirically in order to develop a model to estimate the water separation efficiency based on readily measured variables.

Similar to the problem in coalescence filtration in which there is a trade-off between pressure drop and separation efficiency, there will also be one with a barrier filter. The pore size must be sufficiently small as to stop droplets at the operating pressure, taking into consideration the deformation that will take place. This must also be considered when determining at what point the filter is no longer working optimally. The fouling process will increase the pressure drop for a constant flow rate, it will also have an impact on both the pore size and the contact angle. These changes will affect the critical pressure at which droplets will pass through the filter. All of the parameters are dynamic during the fouling process highlighting the difficulty of using pressure drop alone as the indicator for end of life.

Barrier filtration summary

A number of things have been identified in this section that are important to achieving the aims of the project. The most likely factors that affect the water separation efficiency, namely pressure drop and contact angle, have been identified. This will help achieve the all the aims of the project, particularly it will steer the investigation of the returned filters. The mechanism by which water is separated from a continuous phase is also better understood, this will help inform the strategy for creating a coating for increasing the instantaneous water separation efficiency of the filter.

2.3 Coatings overview

This section will review the literature surrounding the formation of coatings for superhydrophobic applications. This understanding will aid in the achievement of the second aim. It is important to understand the various techniques that are used and their benefits and drawbacks in order to justify the use of the selected coating method.

2.3.1 Plasma

It is well established that increasing the roughness and decreasing the surface free energy of a surface is necessary to create a superhydrophobic surface. Authors have attempted to do this in many ways. One common methodology is to introduce roughness followed by coating the roughened surface with a low surface energy layer. Vasiljevic et al. (96) did this using a plasma etching technique, in this study cellulose fibres were roughened using a H_2O plasma followed by a sol-gel coating of a fluorinated alkyl silane. It was found that plasma treatment increased the contact angle from 150° to 154° and decreased the sliding angle from 15° to 7°. It was thought that while the increase in contact angle was quite small, the decrease in the sliding angle was important with respect to the self-cleaning applications of fabrics.

Fernández-Blázquez et al. (97) adopted a similar approach, however the plasma treatment used in their study was an oxygen plasma. Additionally, the fibres used were not cellulose but a polymer. Similarly, the resultant roughened surface was coated with a low surface energy substance, in this case 1H,1H,2H,2H-perfluorodecyltrichlorosilane. Interestingly, once the fibres were treated with the plasma and prior to coating with the low surface energy substance it was found that the contact angle decreased. This was attributed to the fact that the plasma treatment increased the polar oxygen containing compounds at the surface of the fibres, a change in the composition due to the plasma treatment process was also found by Vasiljevic et al. (96).

Fernández-Blázquez et al. (97) examined the effect that time under plasma treatment had on the hydrophobicity of the surface. It was found that initially there was a sharp increase in the contact angle as the treatment time increased, however after 20 minutes there was very little difference. The sliding angle continued to decrease up to 60mins of treatment (no longer treatment time was evaluated). This continued decrease was attributed to the increasing length of the nanofibrils, after 2-5mins the nanofibrils had a height of 70nm, whereas after 60mins this had increased to 150nm.

Balu et al. (98) used plasma etching in order to introduce roughness. Oxygen plasma was implemented using a similar methodology to Fernández-Blázquez et al. (97). However, in this case cellulose was used as the substrate. The more interesting aspect of this study was the use of plasma to provide the low surface energy coating, in order to do this CF_4 gas plasma was used. The process consisted of first creating a roughened surface by etching the fibres with the oxygen plasma at a high power, followed by a shorter process of coating the fibres at a lower power with the CF_4 plasma. The effect of the

oxygen etching was examined by preparing two samples, one that had been etched and then coated with the CF_4 plasma and one that was only coated with the CF_4 plasma. It was found that both methods produced a fibrous structure with a very high contact angle, however the etched sample had a significantly lower contact angle hysteresis, which is analogous to sliding angle (3.4°). It was found that without etching droplets of water could not be removed from the surface under the force of gravity alone. This proved that the roughening process was key in making a self-cleaning surface.

Yang et al. (99) studied the effect of applying a CF_4 plasma coating to a PVDF membrane filter used for filtering salt water to create fresh water. It was found that by applying the coating that the contact angle was increased to 165° from 130°. The process of applying the coating also etched the surface somewhat leading to an increase in the pore size, after a period of time (20mins) the pores began to close again. This was attributed to the coating starting to encroach into the pores once a full layer had been produced. This study is interesting in that it showed the practical application of plasma etching and coating, the efficiency of the process of removing salt could be increased by 30% in using this method.

2.3.2 Chemical Etching

Another method commonly used in increasing the roughness of surface is chemical etching, this is usually followed again by coating with a low surface energy compound. This is done for a number of different substrates, Yin et al. (100) used nitric acid to etch a magnesium alloy surface. It was shown that it was possible to etch this surface, then coat the roughened surface with a silane to create a superhydrophobic surface. Using this technique, a maximum contact angle of 157° was achieved and the sliding angle was found to be less than 10°. The etching process produced pillar like structures similar to those seen on the surface of a lotus leaf, these pillars were spaced approximately 5micron apart. One important thing that was noted was that the pillars showed a dual roughness with the pillars themselves being roughened. This dual roughness was theorised to increase the contact angle and reduce the sliding angle. It was shown that this method of coating the substrate increased the corrosion resistance.

Another way that is often used to chemically etch surfaces is using an alkaline etching chemical, by far the most commonly used alkaline compound is aqueous NaOH. Xue et al. (101) used aqueous NaOH to introduce a roughness to a polymer substrate before coating with PDMS. It was possible to create a fibrous surface with a contact angle greater than 160° and a sliding angle of

8°. One important thing to note is that the etching process reduced the average fibre diameter from 11.45micron to 9.68micron, this is something that should be considered for systems in which the strength or the porosity of the structure is important (101). Again, in this study it was found that the etching was not as important for increasing the contact angle as it was for decreasing the sliding angle. It is postulated in this paper that the reason for this is that the increase in roughness results in a transition from the Wenzel state to the Cassie-Baxter state (101).

The Wenzel and Cassie-Baxter models are two different models used to describe the interaction between three phases. Typically, a rough solid, air and a liquid droplet. The Wenzel model supposes that the droplet is completely in contact with the surface, this means that with increasing roughness the wettability will either increase or decrease depending on whether a smooth surface is hydrophobic or hydrophilic (102). The Cassie-Baxter model supposes that air can become trapped within pockets provided by the roughness, this means that an increase in roughness will always result in a decrease in wettability (103).

Jin et al. (104) also used NaOH in order to etch the substrate they were using. In this study cellulose was being examined. First NaOH was used to increase the roughness of the surface, followed by also using 2M CH_3COOH to help continue the etching process. Next a titanium layer was applied using a sol-gel process followed by a fluorinated alkyl silane. The resultant fabric had a contact angle of 158°, in this study the sliding angle was not examined. Again, it was found that the etching process removed material, in this case 9.2% of the material was removed (104). This could be concerning for work in filtration. Another interesting discovery was that the cellulose's crystalline structure was altered by the alkaline treatment, this is something that should be considered if using this methodology (104).

Another technique that can be used when etching cellulose is to use an enzyme. Cheng et al. (105) used the enzyme papain in order to etch cellulose, followed by coating with methyltrichlorosilane to induce superhydrophobicity. It was possible to create a surface with a contact angle of 156.7° and a sliding angle of 8.5°. The etching process increased the rms roughness from 1-5nm to 30-35nm, interestingly the process of applying the methyltrichlorosilane coating resulted in a further increase to 86-91nm. The coating was applied through a simple chemical vapour deposition method, the increase in roughness was interesting due to the fact that usually the process of coating reduced the roughness. This process of etching was found

not to change the chemical composition at the surface, confirmed by XPS (105). One thing that seemed to be true for all the studies that tested for it was that abrasion did not affect the contact angle significantly, but the sliding angle was increased significantly.

2.3.3 Alternative Application Using Microspheres/ Nanospheres

One of the more common methods of applying a superhydrophobic coating is using microspheres. This is sometimes done by creating a superhydrophobic microsphere and adhering it to the surface, alternatively by adhering a microsphere and subsequently applying a superhydrophobic coating. Arfaoui et al. (4) applied ZnO nanospheres to a cellulose fibre structure and then used a fatty acid to create a superhydrophobic layer. It was found that it was possible to grow ZnO nanorods on the surface of the fibres. It was shown that the rods were hexagonal in shape with a diameter of 70nm and a length of 2.5micron. Stearic acid was used in order to create a superhydrophobic surface, in order to confirm that the nanorods grown were vital a pure cellulose sample was also coated with stearic acid. It was shown that without the roughness caused by the nanorods the contact angle was only 120° whereas with the nanorod induced roughness the contact angle was increased to 148°. This is an interesting result because it has been possible to create a highly superhydrophobic surface without the use of fluorine containing compounds, which is often seen as undesirable due to the potential toxicity of these compounds (106).

Wu et al. (107) used a similar approach however a glass slide was used as the substrate instead of cellulose. In this study a ZnO microsphere roughness was created by growing the ZnO structures from a seed layer on the surface. A solution of zinc acetate was sprayed on the surface in an oven at a temperature of 180°C for 30mins, then the glass slide was placed in a solution of zinc acetate at 180°C for 4hrs to create a roughened surface. It was shown that after this coating was completed the contact angle had decreased from 70° to approximately 0° (107). The Wenzel state is dominant at this stage, indicated by this drop in contact angle. The surface was then spin coated with Teflon, this resulted in an increase of the contact angle to 168°. Using SEM, it was possible to show that the pillars had a dual scale roughness, the tips of the nanorods formed had a rose petal like structure. Using a surface that had a ZnO nanowire coating that didn't display the dual scale roughness it was found that the addition of the dual scale roughness resulted in an increase in contact angle from 159° to 168° (107). It is likely that the reason for this is an

increased Cassie-Baxter effect, the dual scale roughness allows a higher portion of air to be trapped beneath the examined droplet.

Zhu et al. (108) also grew ZnO nanoparticles on the surface of a substrate. First the substrate was coated with a PDMS layer, achieved by dissolving PDMS and a cross linking agent in THF and submerging the fibres in the solution followed by drying. A carboxylic salt of zinc was subsequently dissolved in sodium hydroxide and the fibres were then submerged in this solution for 6hrs to allow the ZnO nanoparticles to grow (108). The resultant structure was then coated again with PDMS in the same was as before. The resultant fibres had a contact angle greater than 165° and a sliding angle less than 10°. The introduction of the ZnO nanoparticles increased the RMS roughness from 8.7nm to 64.9nm. One thing that was found is that similar to the etched samples abrasion did not have a significant effect upon the contact angle but did increase the sliding angle significantly (108).

Another nanoparticle that is sometimes used to increase the roughness of a surface is TiO_2. Ogawa et al. (109) used a multi-layer approach creating layers of TiO_2 with poly acrylic acid in between. The final layer used was a fluorinated alkyl silane as a low surface energy component. It was possible to create a nanofibrous surface with a contact angle of 162° and a sliding angle of 2°. The number of layers was analysed in this study there was an optimum number of layers to produce the largest contact angle and the lowest sliding angle. This was found to be 10 layers, the reason that this was the optimum was related to the roughness imparted to the fibres. Without the final low surface energy layer, the surface was not made to be superhydrophobic, so it was concluded that this was a vital step in the process (109).

Zhang et al. (110) formed a dual scale roughness structure from a composite of poly(vinylidene fluoride-hexafluoropropylene) (PVDF-HFP) and graphene via gelation. PVDF-HFP was dissolved in DMF and adding a percentage of graphene, as this ages by absorbing water vapour a hybrid gel is formed. These gels were then subjected to solvent replacement by submerging in water followed by freeze drying. The most interesting finding in this study is that the dual scale micro/ nano-roughness resulted in a superhydrophobic surface. There was no attempt in this work to assess any water separation efficiency, additionally this process would likely not be applicable as a coating because the formation process does not create individual particles (110).

Gao et al. (111) used nonsolvent assisted electrospraying to create polymer (PMMA) microspheres with a hierarchical porosity. This is similar to the electrospinning process in which fibres are formed, however the viscosity of

the solution is controlled in such a way as to form particles instead of fibres. In this specific process, hexanol is used as the nonsolvent, as the particles are deposited on the receiver the solvent (dichloromethane) is evaporated first and the hexanol migrates to the surface. This is what causes the hierarchical porous particles. It was again shown that the roughness played a significant part in the increase of superhydrophobicity. A thin film of PMMA had a lower contact angle than a solid PMMA microsphere coating which had a lower contact angle than the porous PMMA microsphere coating.

2.3.4 SiO_2 for superhydrophobic applications

Alone SiO_2 microspheres would not impart hydrophobicity, unmodified SiO_2 is inherently hydrophilic. The increased roughness caused by the microspheres will increase the hydrophilicity (112). In order to achieve hydrophobicity, the microspheres must be modified with a hydrophobic material. Commonly fluorine containing materials are used to impart the hydrophobicity.

Brassard et al. (113) formed nanoparticles using the Stöber process, followed by a functionalisation with a fluoroalkylsilane. The Stöber process is a hydrolysation-condensation reaction in which a silicate in an alcoholic solution is reacted with water to form SiO_2 spheres. Brassard et al. (113) examined the effect of applying numerous layers of the coating, 7 layers of the as prepared particles are required in order to impart superhydrophobicity. The coating is effective when applied to various different substrates, it was applied using a spin coating method to aluminium and two different types of glass. It is theorised that the roughness plays an important part in the superhydrophobic properties. The randomly oriented spherical particles are grouped and separated by cracks leading to a dual micro-nanoscale roughness. This roughness leads to the trapping of air resulting in superhydrophobicity as described by Cassie-Baxter (103). It was found by Wu et al. (107) that a dual scale roughness increases the water contact angle, likely because the ratio of the droplet that is in contact with the air compared to the surface is increased as a result.

Gao et al. (6) created a coating of SiO_2 nanospheres subsequently coated with polyvinylidene fluoride (PVDF) giving a contact angle of 162° and a sliding angle of 1°. This was done by dissolving PVDF in DMF followed by adding pre-prepared SiO_2 nanospheres, this solution was then electro sprayed onto the desired substrate. This resulted in a surface covered in superhydrophobic nanospheres made of agglomerates of PVDF and SiO_2 nanospheres. It was found that with increasing concentration of SiO_2 the eventual particle sizes on

the surface of the substrate also increased (6). The contact angle was also shown to be related to the particle sizes and thus the concentration of SiO_2, it was found that there was an optimum concentration of SiO_2 at 4wt%. The coating showed excellent self-cleaning properties, carbon black could easily be removed from the surface by simple spraying with water. The adherence to the surface was also good, this was tested by performing multiple cycles of oil water separation tests. There was very little reduction in separation efficiency or flux (6).

Zhang et al. (114) used a very similar method to create a superhydrophobic surface. Again, pre-prepared SiO_2 nanoparticles were used. In this case first the SiO_2 particles were hydrolysed using a piranha solution. trichloro(1H,1H,2H,2H-perfluorooctyl) silane was added to the hydrolysed solution in order to fluorinate the surface. Then a coating PDMS was dissolved in ethyl acetate and a set amount of the fluorinated nanoparticles were added. The desired effect of the PDMS was to increase the adhesion of the particles to the substrate. This was done twice to create a dual layer coating. A high contact angle of 157° was achieved, the sliding angle was not examined in this case (114). One of the main benefits of this type of coating is the abrasion resistance, after 200 cycles with a pressure of 250kPa there was only a decrease of 10°. It would have been interesting to see what effect there was on the sliding angle, this would show whether the microsphere method is better at maintaining abrasion resistance compared to the etching methodologies (114).

Vasiljevic et al. (115) created Stöber particles by hydrolysing tetraethyl orthosilicate, this was done in a number of different ways in order to produce different size Stöber particles. Various temperatures, pH ranges and solvents were examined to determine the best combination. Having said this it appears that either all combinations were not examined, or they were found to be ineffective and not included in the paper. Again, and similar to findings by others a fluorinated alkyl silane was used as a final coating to reduce the surface energy and induce superhydrophobicity (115). It was found that the smallest particles were created when using ethanol as the solvent and hydrolysing at 40°C, while the largest particles were created by using propanol as the solvent and hydrolysing at 50°C. Table 2.2 below describes all of the methodologies that were used in this study to create the Stöber particles (115).

Table 2.2: Table showing the tests done by Vasiljevic et al. (115).

Code	Type	Diameter	Solvent	Temp (°C)	T (min)	H_2O/NH_3 (mol/l)
SP1	Pre-prepared	50	Ethanol	40	60	4/0.3
SP2	Pre-prepared	230	Ethanol	RT	60	6/0.2
SP3	Pre-prepared	780	Propanol	50	60	4/0.5
IS	In situ	-	Propanol	50	15	4/0.5

The Stöber particles were then coated onto the surface of the cellulose fibres. Various combinations of the Stöber particles were used in conjunction with each other. The combination that gave the greatest contact angle (>160°) and the smallest sliding angle (<5°) was IS combined with SP2. The sliding angle was greatly affected by washing samples, this is similar to what has been seen in other work. It was concluded that the low abrasion resistance of the fluorinated layers was the reason for this (115).

In some cases, there are a combination of SiO_2 microspheres and polymer microspheres. Yu et al. (116) used a combination of polystyrene microspheres and fluorinated silica nanospheres to create a durable superhydrophobic coating. This was achieved by creating a colloidal mixture of the two compounds followed by spraying onto the substrate. The coated substrate was then hot pressed forming the durable coating. The hot press technique brings the temperature close to the melting temperature of the polystyrene leading to mobility of the polymer and the formation of a continuous network. A temperature higher than the melting point resulted in the roughness being removed and a drop in the contact angle observed (116).

While fluorine-based compounds are often used in order to reduce the surface free energy of the SiO_2 molecules, there have been a number of attempts to use other functionalising agents. Zhao et al. (117) used hexadecyltrimethoxysilane (HDTMS) as a functionalising agent, the process of forming a HDTMS layer on the surface is similar to the Stöber process. However, in this study an acid catalysed process was used. A colloidal solution of pre prepared SiO_2 was made and TEOS and HDTMS were added along with a hydrochloric acid (HCL) catalyst. The pre prepared SiO_2 molecules act as a nucleation point for the hydrolysis condensation reaction.

Some basic separation testing was performed and a water separation efficiency greater than 99% was achieved. It should be noted that the separation testing was very basic, the fluids were not emulsified, and the driving force was gravity (117).

A similar study was performed by Xu et al. (118) again this process was performed by adding pre prepares SiO_2 nano-spheres and HDTMS to anhydrous ethanol. The difference in this experiment is that no catalyst was used for the hydrolysis condensation reaction. Superhydrophobic particles were formed with contact angles in excess of 170°. However, to achieve this a significant excess of HDTMS was required. This was likely required because of the lack of catalyst and the low reaction time of approximately 1hr.

Another functionalising agent of interest is oleic acid. Li et al. (119) showed that it was possible to create surface modified SiO_2 particles by stirring oleic acid in a colloidal solution of SiO_2 and hexane at a temperature of 60°C for 4hrs. It is postulated that the oleic acid reacts with the SiO_2 by way of esterification. This will form a similar particle to what is formed with the other functionalising agents. Baniasadi et al. (120) also created surface modified SiO_2 particles using oleic acid, this was performed at a higher temperature (80°) for a shorter period of time (1hr).

The majority of the surface modification is a minimum of two steps, the formation of SiO_2 particles followed by the surface modification. However, there are some studies in which the process is combined into one step. This makes the formation significantly easier increasing the potential commercial viability. Wang et al. (121) performed a co-hydrolysis of TEOS and a number of different functionalising agent including HDTMS and a fluoroalkyl silane. It was shown that it was possible to achieve a superhydrophobic surface by a one pot method.

2.3.5 Polydopamine coating

Polydopamine has been used as a functionalising agent for a number of years, the first reported use was by Lee et al. (122) It was shown that polydopamine can be applied to a number of different surfaces by self-polymerisation, this paper suggest that it can be used as an adhesive layer for further functionalisation. The inspiration of the use of polydopamine comes from studying the way in which mussel's utilise adhesive proteins (123). One of the most challenging aspects of finding a coating to use in the accelerated fouling process was finding a substance that would adhere to the low surface energy surfaces. One of the primary benefits of using polydopamine is that it will

adhere to surfaces with very low surface energies. For example Cao et al. (124) coated electrospun poly(vinyldene fluoride) membranes.

In addition to the superb adhesion properties of the polydopamine coating it is well documented that the coating thickness is relatively well controlled through reaction time. It is shown by Orishchin et al. (125) that the thickness of the coating is linearly proportional to the reaction time. In addition to this it is also shown that the thickness of the coating can be controlled to the order of 10's of nanometres. This is vital for this thesis because the polydopamine coating will not add any significant additional resistance to flow but will impact on the surface free energy.

The primary use of the polydopamine in this thesis is to alter the surface chemistry during the accelerated fouling process. The desired effect is to change the surface from hydrophobic to hydrophilic. It is shown by Cao et al. (124) that applying the coating to the surface of poly(vinylidene fluoride) resulted in the surface becoming hydrophilic. It was also shown by Kang et al. (126) that a superhydrophobic surface could be made hydrophilic having been coated with polydopamine.

2.3.6 Summary of the coatings overview

The review of the literature relating to the coating was mostly to support the understanding required to achieve the second aim of the project, to develop a coating that improves both the instantaneous and end-of-life water separation efficiency. The literature shows that two things are critical to the success of a superhydrophobic coating, the surface free energy and the roughness. The reasoning behind using a modified Stöber process to form the microspheres was that it is consistently shown that the size of the particles can be controlled by varying the composition of the solution allowing variation in the roughness produced by the microspheres. Additionally, it has been shown by a number of authors that the microspheres can be functionalised to produce hydrophobicity. This means that this method is able to achieve the two primary requirements of the coating in a facile one-step process.

2.4 Fouling

This section will provide the understanding for two of the three aims. Clearly it will help inform the techniques required to analyse the filters returned from the field. In addition to this an understanding of the fouling is required in order to develop an accelerated fouling technique that can be used to assess the end-of-life performance of filters with respect to the water separation efficiency.

2.4.1 Foulant types

The types of foulant can be split into three categories: inorganic, organic and bio-foulant (127). It has also been postulated by some authors that inorganic matter can be further split into two categories namely suspended particles and scale (128). It is also possible to further characterise the type of fouling by other measures namely fouling position within the membrane, fouling reversibility or fouling mechanism. Firstly, the main categories will be discussed followed by the other sub-categories.

2.4.1.1 Inorganic Foulant

As has been mentioned this type of fouling can come in the form of either suspended particles or scale. Suspended particles generally refers to particles of inorganic origin that are found within the flow. For example in bioreactors suspended particles of sludge are carried to the membrane surface in the flow, the type of particle may vary in different processes (129, 130). Most of these suspended particles are rejected at the surface of the membrane, this results in the formation of a cake layer (128). It is well known that the formation of this cake layer is disadvantageous because it increases the resistance to flow, this will therefore decrease the overall flux of the membrane (131). Specifically in the case of emulsion separation depending on the type of particles that are forming the cake layer the effects could be doubly troublesome, on one hand the flux will be decreased, but also it is possible that the cake layer will have disadvantageous wetting characteristics that may significantly decreases the effectiveness of the filter.

Scale can form at the membrane surface as the precipitates of dissolved ions and salts are deposited (128). Zhang et al. (127) state that the main two compounds that are the most common cause of scale in membrane filtration are calcium sulphate and calcium carbonate. The main fouling mechanism is crystallization on the membrane surface, this occurs at nucleation sites and then grows to form a scaling layer. The disadvantages of this are very similar to the cake layer that would be formed from the suspended particles

mentioned above. This type of fouling is more likely in systems where water is the continuous phase, so it is unlikely that this would be the dominant fouling mechanism for this project (127).

2.4.1.2 Organic Foulant

Chang et al. (128) state that oil and grease can also form a cake on the surface of the membrane leading to blockages. It is likely that this would be more prevalent in systems where water is the continuous phase because the oil would create a layer of immiscible contaminants. Zhang et al. (127) also state that the organic matter would form a gel or cake layer on the surface of the membrane, but could also be in the form of pore blockage. This could happen in a diesel system as partially soluble compounds precipitate out of solution as a result of temperature changes, or adverse reactions forming new insoluble compounds.

2.4.1.3 Bio-foulant

Bio-foulant is deposited onto the membrane surface and subsequently grows to be larger, thus increasing the negative effects on the efficiency of the filter. The most common type of bio-foulant is are extracellular polymeric substances that are secreted by microbes like algae, this will only happen in systems where microbes are present (128). Membranes easily adsorb microorganisms that will then grow into a gel like biofilm, this provides the ideal environment for microorganism growth. The microorganisms that are grown result in irreversible fouling that will lead to not only a decline in flux but also will change the surface chemistry of the membrane. For a diesel system it is unlikely that microbes would be present unless there was significant amounts of water (127).

2.4.2 Bio-Diesel Specific Issues

Since the introduction of biodiesel there has been an increase in the amount of filter plugging that is seen in diesel systems, this is not an issue that plagues systems that exclusively use biodiesel but also systems in which a mixture is used. A possible reason for this is that there are contaminants that are present within the biodiesel that have undesirable interactions with additives within the diesel. The majority of investigations look at the effect that this has upon the fouling at the injectors. However, this will also be an issue in the filtration process as well (39).

A particular contaminant that is known to cause issues is sodium ions, this is not a contaminant that can be solely attributed to bio-diesel because a sodium containing compound is also used in the refining of ultra-low sulphur diesel.

Providing that good housekeeping is implemented the sodium entering through the petroleum diesel stream should be extremely minimal. It enters the bio-diesel fuel stream because it is commonly used as a catalyst for the esterification process for producing fatty acid methyl esters (FAME), the main component of bio-diesel there is a limit of 1mg/kg of sodium in biodiesel however in isolated incidents this may be breached (39). The reason that sodium content can be seen as an issue is that when it reacts with an acid it may form soap deposits that will block filter pores. Acidic additives are sometimes used as lubricity enhancers, also carboxylic acids are known to form as a decomposition product of bio-diesel and an oxidation product of petroleum diesel (39).

In a study by Barker et al. (39) various different additives were used and are detailed in Table 2.3 below.

Table 2.3: Table detailing the acids used by Barker et al. (39)

ID	Acid
A1	Di-acid corrosion inhibitor
A2	Dimer acid corrosion inhibitor
A3	Mono acid lubricity additive
A4	Ester based lubricity additive

These additives were combined in different ways together with various sources of sodium including NaCl and NaOH. It was found that when running the system with the A3 additive and the NaOH that the filter blocked, after performing both FTIR and EDX analysis it was concluded that this was due to the presence of carboxylate salts, however it was also found that there was a significant amount of calcium present, which was unexplained. A similar experiment was run with A1 and A4 additives and NaOH, in this experiment no filter blocking was seen and when examining the injector nozzles under EDX after performing engine testing there was very little sodium. However, again there was evidence of calcium deposits that could not be explained. The A3 additive was examined again but using NaCl as the sodium source, in this experiment the filter did not block and there was no evidence of carboxylate salt in the filter. It was found that when using a fuel soluble sodium salt with the additive A3, that there was no filter blocking but there was some carboxylate salt deposits found at the injector (39).

2.4.3 Fouling Characterisation

In some cases when using membranes, it is possible to remove the foulant that is deposited on the surface. When the foulant can be removed through physical methods it is called reversible fouling (132). There are a number of methods that can be used to remove the foulant including backwashing/ back pulsing, which is usually considered the most facile method for removing foulant layers and is achieved by running the stream in the opposite direction to normal removing some of the deposited particles (132). Other methods include pneumatic cleaning that uses air to remove non adhered particles, mechanical cleaning using some of external object to scour the surface or ultrasound irradiation using sound waves to break the filter cake (132).

In many cases in addition to reversible fouling there is also an element of irreversible fouling, this is usually defined as fouling that cannot be removed by conventional processes. Often this is foulant that is deposited inside the structure of the porous membrane and not at the surface (128). Juang et al. (133) have found that in some cases that the irreversible fouling can account for up to 80% of the total membrane resistance. In this case biofilms formed within the internal structure of a fibre membrane.

There are a number of methods that are used for characterising the type of fouling that has occurred. These can broadly be split into two categories, destructive and non-destructive. A destructive technique would require the removal of the membrane and cannot be completed in-situ, some of the most common methods that are employed are scanning electron microscopy, energy dispersive x-ray spectroscopy and Fourier transform infrared spectroscopy (134). Using FTIR Wang et al. (135) were able to characterise the type of organic foulant that was found in the gel layer of a membrane filter within a bioreactor system, it was possible to identify inorganic elements using EDX, whilst confirming that the gel layer completely covered the surface using SEM. In situ fouling characterisation is slightly more challenging, and likely will not be used in this project. However, it is possible to do this using techniques such as direct observation using optical probes, magnetic resonance imaging, x-ray micro-imaging and electrical impedance spectroscopy (134).

Another method that has been used to quantify the level of fouling/ the type of fouling that is observed is using an atomic force microscope. Using this piece of equipment, it is possible to measure surface roughness to a relatively high accuracy. It has been found that higher roughness in membranes tends to increase the level of fouling that is seen, this is due to the fact that the

increased roughness provides a larger surface area for the foulant to adhere to. If roughness measurements are taken from a fouled membrane it is possible to relate the level of roughness to the level of fouling that is seen, it may also be possible to determine the type of foulant when combined with other methods because the change in roughness is highly related to the type of foulant that is adhering (136). It is also possible to calculate the pore size using atomic force microscopy, it should be noted that using this method will likely yield different results to what would be achieved using a technique like porosimetry. This is because porosimetry calculates the smallest aperture of a pore whereas AFM calculates the size of the pore opening (136).

2.4.4 Fouling control

There are a number of methods that are used in order to help control the amount of fouling that accumulates. These methods include backwashing, chemical scrubbing, chemical pre-treatment of the feed solution and modification of the membrane surface (128). The most viable option to be explored for the system being studied in this project is the modification of the membrane to reduce the fouling. It has also been reported that the type of fouling control must be based upon the size of the pores, for example for a microfiltration membrane used to filter biological sediments can effectively be controlled by a process of back flushing and air aeration. However, this process would not be as suitable for a reverse osmosis membrane (128).

There have been significantly fewer studies completed on the fouling mechanisms, and therefore the fouling mitigation, which can be implemented for nano-filtration and reverse osmosis membranes. Both RO and NF membranes have extremely small pores, this means that back flushing is not a viable fouling control mechanism which generally is one of the more popular methods in MF. This means that the methods that must be used are limited to pre-treatment of the feed, chemical cleaning or modification of the surface of the membrane (137).

It is suggested by Mohammad et al. (138) that the most effective method of fouling mitigation is pre-treatment of the feed. In this study the focus is specifically focussed on the filtration of wastewater, having said this there should be parallels with diesel filtration, if not in the exact treatments at least in the methodology. Although it is possible to remove a significant proportion of the foulant by pre-treating, it is noted that there will still be some foulant that could not be removed meaning that additional fouling controls should also be in place.

The hydrodynamic conditions also have a significant effect upon the fouling rate, and also the type of fouling that occurs within a membrane. It was found by Kaya et al. (139) that in a cross flow wastewater system higher pressures result in reversible cake formation being the dominant mechanism, whereas at lower pressures irreversible pore blocking was dominant. It is also shown that in some cases having a lower initial flux and higher cross flow velocity may lead to a slower decline in flux in cross flow applications, the reason for this is that in this case calcium ions were facilitating the deposition of humic acid (a common foulant in wastewater systems). The increase in the crossflow velocity resulted in the increase in the shear stresses, which ultimately resulted in the reduction of the calcium ions acting as a facilitator for the deposition of humic acid (138).

Another possible method for controlling the deposition of foulant is chemical cleaning, as has been discussed above. When determining the type of cleaning agent that should be used it should be considered that the cleaning agent could have a negative impact on the membrane itself, a suitable cleaning agent that has no effect upon the membrane should be chosen. It was found by Simon et al. (140) that using a caustic cleaning agent containing sodium hydroxide caused an increase in the pore size and thus a noticeable decrease in the efficiency of the filter. Commonly either acidic or basic cleaners are used, the cleaning efficiency of the candidate cleaners should be determined. In some cases, it is advantageous to use a mixture of acidic and basic processes in order to remove the maximum amount of foulant possible. Cleaning efficiency is the parameter that is used to determine this and is defined as the membrane flux recovery ratio (138).

2.4.5 Low-fouling membranes

There have been numerous attempts to create anti-fouling or low-fouling membranes, Gzara et al. (141) created an anti-fouling membrane for use in the water industry. Gzara et al. (141) found that the most commonly used material, Polyethersulfone (PES), had poor antifouling properties because it is hydrophobic. Additionally, it was noted that the main type of fouling that was seen was biofouling, therefore it was important to stop colony formation on the surface. In order to create an anti-fouling membrane cobalt nanoparticles were used because of their anti-bacterial properties, it was found that having cobalt nanoparticles present significantly decreased the degree of fouling that was observed (141).

Another use of cobalt was found by Liu et al. (142), the focus of this study was to find a membrane that could separate oil and water surfactant stabilised

emulsions whilst also showing good anti-fouling properties. This was achieved by using a copper mesh substrate with pore sizes of 50μm coated with an agglomeration of zinc oxide and cobalt (ii, iii) oxide. The benefit of combining the two oxides was the deposition properties. It was found that the zinc oxide would deposit into the pores of the copper mesh but was washed away easily when used to separate emulsions, however when combined with the cobalt oxide that was deposited on top of the copper mesh and the zinc oxide within the pores the resultant membrane was much more robust. It was found that the membrane has barely any reduction in flux after 50 separation experiments, therefore it was determined that this membrane had good antifouling properties. Having said this each experiment only used a small amount of emulsion, and after every experiment the membrane was washed with acetone, this may have halted any growth of cake layer (142).

Zhang et al. (56) created a polyvinylidene fluoride (PVDF) membrane by a modified phase inversion technique. In this technique ammonia is added to the solution prior to the phase inversion process, this promotes the coagulation of the PVDF chains. The coagulation results in a micro/ nanostructure, this will result in an increase in the observed contact angle due to the fact that the roughness would be increased significantly (56). It was thought that the excellent chemical inertness of the PVDF material would help reduce the amount of fouling that is seen, it was shown that there was a steady reduction in flux over 20 cycles of an experiment of fixed emulsion volume with no sharp decline. It was concluded from this that the membrane showed relatively good anti-fouling properties. However, the experiment in this case was not continuous and between each cycle the membrane was washed with ethanol. This may have had an impact upon the growth of foulant layers that could happen in a continuous filtration environment.

Shi et al. (143) created an ultrathin single walled carbon nanotube (SWCNT) film on ceramic membrane. It was thought that due to the extremely thin nature of the SWCNT film that the flux would be very high, additionally the thinness of the film allows the pore size to be very small without overly compromising the flux. It should be noted that the film was not fixed to the ceramic membrane, the membrane was there merely for structural support. Again, a similar experiment was conducted in order to show the anti-fouling properties of the film, in which a small volume of emulsion (10ml) was passed through and then the membrane was washed with ethanol (15ml). Clearly, while it was possible to show that here was very little flux decline over 20 cycles of this experiment it is not indicative of what would be seen in a real

system. The amount of substance used to wash the membrane exceeded the amount of emulsion that was being separated by a factor of 1.5 (143).

Significant amounts of research have also gone into attempting to find an antifouling membrane technology for the separation of oil from water, this would have applications in oil spill clean-up, wastewater treatment and other sectors. Huang et al. (144) developed a membrane to separate oil and water, the antifouling property was based upon the assumption that the majority of the foulant would be in the oil phase. This membrane is underwater superoleophobic, this means that the contact of the oil phase with the membrane would be decreased significantly. The membrane was formed of free-standing graphene oxide and was supported by Polyamide porous membrane. It was shown that the thickness of the graphene oxide film had a direct effect upon the recoverability of the flux in the cyclic experiments. These experiments were different to the majority of the experiments that have been described previously, in that the time that the membranes were separating emulsions was much longer (120min) prior to stopping and cleaning the membrane. It was shown that there was a sharp decrease in flux initially, but eventually the rate of decline decreased (but not to zero). While it was shown that the graphene oxide membrane performed better than the polyamide membrane alone, there was still a significant decrease in the flux during continuous use. Having said this it was shown that for certain film thicknesses that the flux was almost completely recoverable by washing with pure water (144).

2.4.6 Fouling mechanisms

Solid particles would initially be deposited in pore openings blocking the pores, or in some cases on the pore walls. This can be broken down into three categories (described in Figure 2-6): 1. Standard pore blocking in which particles are deposited around the pore entry resulting in a restriction of flow. 2. Complete pore blocking in which large enough particles completely cover the pore blocking flow completely. 3. Intermediate pore blocking that is a combination of the two previous categories in which particles are deposited at the edge of pores and begin to block over the whole pore (7). This type of fouling is sometimes considered the most severe, especially if the particles are deposited within the membrane structure, the blockages that occur internally are much more difficult to remove and are often described as irreversible fouling (7).

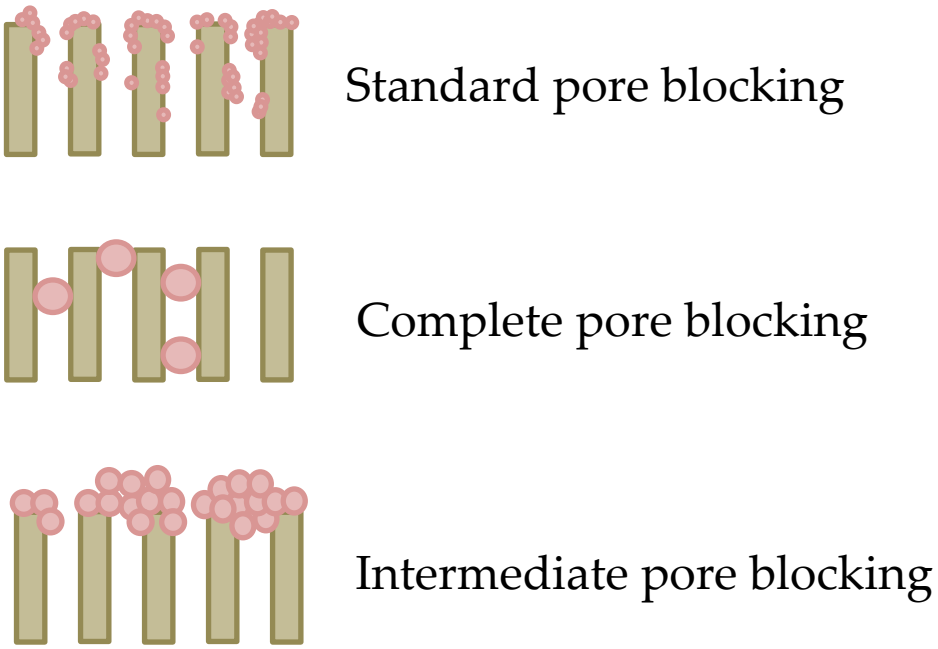

Figure 2-6: Visual representation of the types of pore blockage

Once sufficient particles have been deposited to cover the surface of the filter completely it is known as the cake layer. Once a cake layer has been formed it will degrade the flux significantly, to the point that the cake layer dominates the flow resistance of the membrane system (128). Once the cake layer has been formed it effectively takes over the role of the membrane, in some cases cake layers are built up deliberately in order to aid in the removal of certain impurities, these are known as dynamic membranes (145). The rate of flux decay is not only impacted by the types and concentration of foulant but operating conditions as well, Pearce (146) showed that increasing the transmembrane pressure increased the rate of decline of the flux. The reason for this was thought to be the compression of the cake layer resulting in a reduction in permeability. If there is some system in place for cleaning of the membrane for example back flushing or chemical cleaning then a cake layer can be removed relatively easily (7).

2.4.7 Diesel system studies

There have been a limited number of studies examining the fouling in diesel fuel filters. Barker et al. (39) examined the interactions between sodium contaminants and fuel additives. This has been discussed in section 2.4.2 above. In another study by Barker et al. (147) the deposition of foulant material on the high pressure equipment in new (at the time) diesel engines was examined for two fuels, one with a high propensity for deposit formation the other with a low propensity. While this was not looking specifically at fuel filters, some of the results found were of interest. It was found that both

sodium and zinc were present in both fuels examined, however there was no correlation with the amount of deposits formed leading to the conclusion that a measurable amount of metal ions aren't a necessary prerequisite for deposit formation (147). Similar results were found for the mass spectrometry analysis, the compounds thought to be the cause of deposit formation were present in both fuels. Overall, the complexity of the problem was highlighted.

Csontos et al. (148) examined the foulant from real samples. Three different filters were examined, all the filters were fouled on Euro V, 450 horsepower engines. The trucks were run for 10,000km using B10 fuel. It was shown using gas chromatography – mass spectroscopy that there was glycerol and sterols present in the foulant material. It was also possible to show that there were multiple different long chain carboxylic acids present in the foulant material, it was postulated that these were likely in the form of carboxylic soaps (148). Using x-ray florescence and energy dispersive x-ray spectroscopy it was determined that calcium is the most prominent metal and likely the metal ion present in the soaps. Overall, the general structure was identified as being a mixture of glycerol, sterols and carboxylic soaps. There was very little variation between samples.

2.4.8 Summary of fouling

During the literature review of the fouling, the fundamentals of fouling were assessed. This is a key area that will be important in achieving the first aim of the project. One thing that is clear is the number of diesel specific fouling studies is very limited, this is one of the key things that is novel about the first aim of the project. Additionally, there were no studies examining the fouling effect on prepared water separators or any that developed a lab scale accelerated fouling technique. This is a key gap found in the literature.

2.5 Summary

There have been a limited number of studies examining the foulant material that is removed from samples fouled in real engines. The studies were concentrated on determining the composition of the fouling material, the consensus is that the fouling material is made up of a combination of carboxylate salts, sterols and glycol derivatives. There has been very little work looking at the effect of different fuel markets on the fouling process. However, indirectly the fouling tendency of fuels has been related to the feedstock of biodiesel that is blended. It is known that different countries are more likely to use certain feedstocks due to availability, from this some

information can be determined with regards to the blocking tendency of fuels in different markets.

The method by which a surface filter is able to separate an emulsion is well known, it is necessary to have sufficiently small pores combined with favourable wetting characteristics. In the case of water separation from oil or diesel a superhydrophobic filter is required. There are a number of ways that this could be achieved, it is possible to form fibres from low surface energy materials like PTFE, fibres can be chemically etched, or plasma coated to create superhydrophobicity or the most facile with regards to equipment required is the formation and application of a coating. It is known that surface roughness is an important factor in superhydrophobicity, therefore a coating formed of low surface energy microspheres imparts both an increased roughness and reduced surface energy is ideal.

2.5.1 Gap in the literature

While there have been a limited number of studies looking at the composition of foulant material from real samples, and within the context of filtration, there remain a number of areas that still require to be investigated. The limited studies that do look at the fouling material are focused on the composition with the aim of determining the cause of the fouling. The first aim of the project is to assess the effect that fouling has specifically on the factors effecting the water separation efficiency. This will be done from two standpoints. A comparison will be made between the fuel market and the chemical composition of the fouling material and the effect that this has on the wettability characteristics of the filter. The effect of the physical characteristics of the filters that are returned, and the effect that this has on the performance with respect to water separation efficiency.

While there has been extensive research into the formation and application of superhydrophobic microspheres, the majority of the studies only focus on the contact angle and sliding angle achieved once the particles have been applied. In some cases, the contact angle decline after being subjected to harsh conditions (e.g., abrasion, high pH, low pH etc.). There are a smaller number of papers that examine the water separation efficiency of coated materials. However, the majority of these test the water separation efficiency with gravity as the driving force and for mixtures that are not emulsified. The second aim of this thesis is to show that using the modified Stöber process superhydrophobic microspheres can be formed and applied successfully to the surface of polymeric fibres. The impact that the morphology of the coating

has on the factors that will eventually affect the water separation efficiency will also be assessed.

Finally, there has been some research looking at the fouling resistance of superhydrophobic filters. However, the major for bio-fouling resistance, this is not a major contributor to diesel fuel filter blockages. Additionally, the majority of papers looking at the fouling resistance are from the standpoint of reducing flux decline. The third aim of this thesis will determine whether the superhydrophobicity imparted by coatings will improve the fouling resistance with respect to water separation efficiency. This will help fill the gap in the literature related to fouling resistance specifically as it relates to water separation filters. Using the findings found in the first section it will be possible to determine whether the application of superhydrophobic microspheres will improve the end-of-life performance of water separating diesel fuel filters. Additionally, developing an accelerated fouling technique will be a key addition to the literature, allowing the end-of-life water separation to be more readily studied because currently there is no papers on this topic.

Chapter 3
Methodology

3.1 Theory

3.1.1 General Theory

In this subsection the general theory for the procedure of separating water from diesel emulsions. Primarily, the aspects that are covered are wettability, and the general mechanisms of filtration.

Factors affecting wettability.

In order to achieve the separation in either barrier or depth coalescence filters, specific surface chemistries are desirable (149). The particular property that is of interest is the wettability of the fibres making up the membrane. This property is commonly defined by the contact angle that the liquid has with the surface. An example of contact angle can be seen in Figure 3-1.

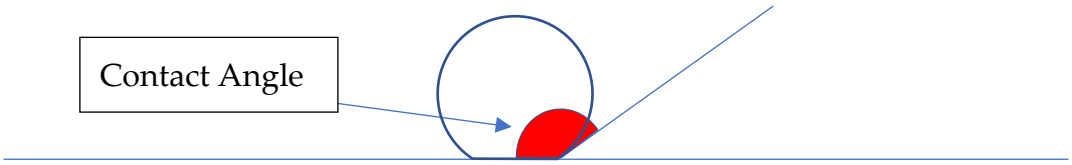

Figure 3-1: Example of contact angle

As can be seen from the figure the larger the affinity of the surface and droplet the lower the contact angle will be, meaning that for water a super-hydrophilic surface would have a contact angle tending towards 0°. Conversely Feng et al. (58) defined a super-hydrophobic surface as having a contact angle of greater than 150° (58). An additional criterion for a surface to be defined as superhydrophobic is having a sliding angle that is lower than 5°. The sliding angle is the angle at which the surface needs to be tilted to for a droplet to roll off the surface due to gravity (150). This is not a very well-defined parameter due to the fact that the size of the droplet is very rarely quoted, and the size of the droplet could have a significant effect upon the sliding angle observed.

There are three main models that should be considered when attempting to define or modify the wettability of a surface: Young's model (151), Wenzel's model (102) and the Cassie-Baxter model (103). All of the equations use contact angle as a determination of wettability. Young's equation determines

the contact angle based upon the surface free energies of the components in the system and both the Wenzel and Cassie-Baxter equations describe the effect of surface roughness on the wettability (152).

Young recognised that there was a connection between contact angle and surface tension in 1805, he found that when a droplet was in equilibrium on a surface that there must be a balance of the cohesive and adhesive forces. A visual representation of this can be seen in Figure 3-2. It shows that three interfacial tensions are in equilibrium with each other, this is true of any stationary three phase contact line. In knowing this it is then possible to manipulate a surface tension in order to change the contact angle to the desired point (151).

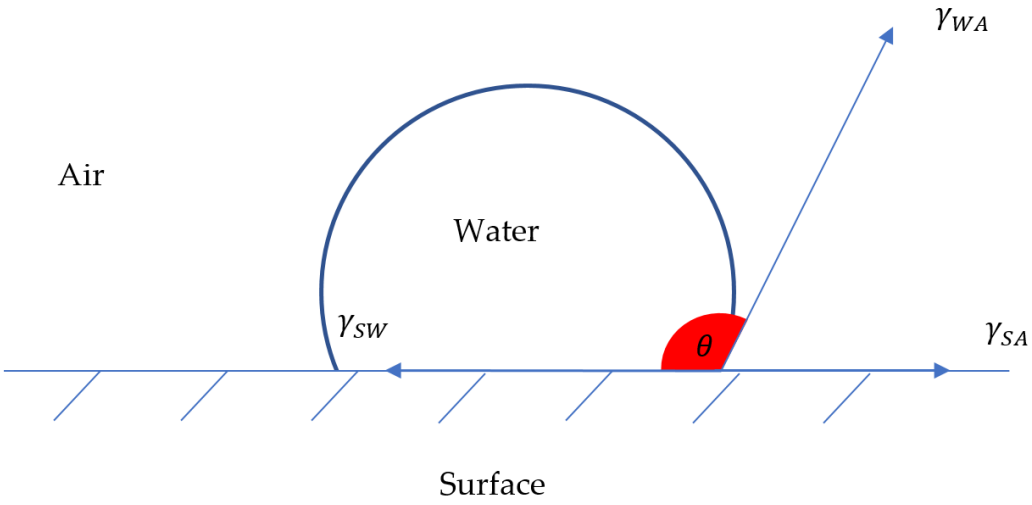

Figure 3-2: Visual representation of Young's equation

From this Young's equation can be represented as follows (151):

$$\gamma_{sw} = \gamma_{SA} - \gamma_{WA}\cos(\theta)$$
$$\theta = \cos^{-1}\left(\frac{\gamma_{SA} - \gamma_{SW}}{\gamma_{WA}}\right) \quad \textbf{3-1}$$

In which γ is the interfacial tension and the subscripts SW, SA and WA represent solid-water interface, solid-air interface and water-air interface respectively. From this equation it can be deduced that in order to produce a larger contact angle the term within the arc-cos function must be reduced to as close to negative one as possible, conversely in order to produce a low contact angle the term must tend towards positive one. In order to do this the interfacial tensions must be changed, this can be done in a number of ways e.g., using chemical surfactants or changing the surface free energy of the solid. For this project the only option that is available is changing the composition of the surface because the properties of the liquids are fixed.

A common element that is used in order to increase hydrophobicity is fluorine, a material with one of the lowest surface free energies is polytetrafluoroethylene (18.5mN/m (153)). The reason that fluorine is an effective element for lowering the surface free energy is that it has a small atomic radius and the largest electronegativity, this large electronegativity combined with carbons small electronegativity results in a large electron density being located away from the centres of mass of the two atoms. This is desired for low surface energy because it reduces the polarity of the molecule as a whole, with the low electronegativity of the carbon atoms cancelling the high electronegativity of the fluorine atoms (154).

Another method for changing the apparent wettability of a surface is increasing the roughness. In order to describe the effect that changing surface roughness has on the contact angle there are two primary models, the Cassie-Baxter and the Wenzel models. The Wenzel model states that the droplet is always in contact with the surface as can be seen in Figure 3-3. The model is described using equation 3-2 (155).

$$\cos(\theta_W) = r\cos(\theta_Y) \qquad \textbf{3-2}$$

Where θ_W is the actual contact angle according to the Wenzel model, r is the roughness defined as the ratio between the actual surface area and the apparent surface area and θ_Y is the contact angle on a completely smooth surface (Young's contact angle). Thus, according to Wenzel's model increasing the roughness will result in increasing the hydrophobicity or hydrophilicity of the surface depending on the Young's contact angle. I.e., if the smooth surface has a contact angle of 110° increasing the roughness will increase the contact angle, whereas if the smooth surface had a contact angle of 70° increasing the roughness would decrease the contact angle.

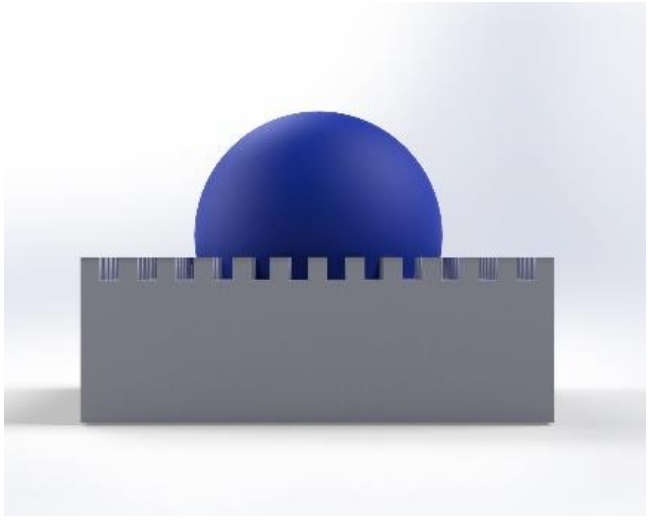

Figure 3-3: Visual representation of Wenzel's model

The Cassie-Baxter model differs from this in such that the wetting can be described as being heterogeneous rather than homogenous as is seen in the Wenzel model. This essentially means that there will be pockets of air trapped within the roughness of the surface. The equation that is associated with the Cassie-Baxter model is shown in equation 3-3 (155).

$$\cos(\theta_{CB}) = r_f f \cos(\theta_Y) + f - 1 \qquad \textbf{3-3}$$

Where θ_{CB} denotes the contact angle according to the Cassie-Baxter model, f is the fraction of the projected area of the surface that is wetted, r_f is the roughness ratio of the wet area. A visual representation of the Cassie-Baxter model can be seen in Figure 3-4.

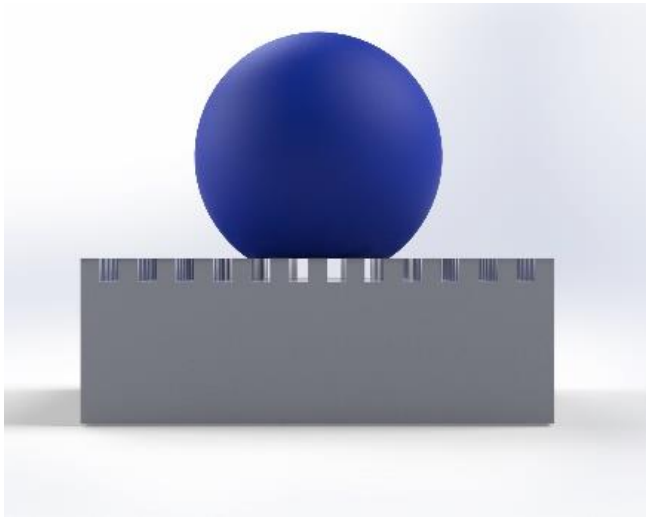

Figure 3-4: Visual representation of the Cassie-Baxter model

As can be seen from equation 3-3 if the fraction of the projected area of the surface that is wetted is 1, the equation becomes the same as the Wenzel

equation. If the Cassie-Baxter model accurately describes the situation then an increase in roughness will always result in increasing the contact angle, and therefore the hydrophobicity. Figure 3-5 shows graphically the difference between the two models.

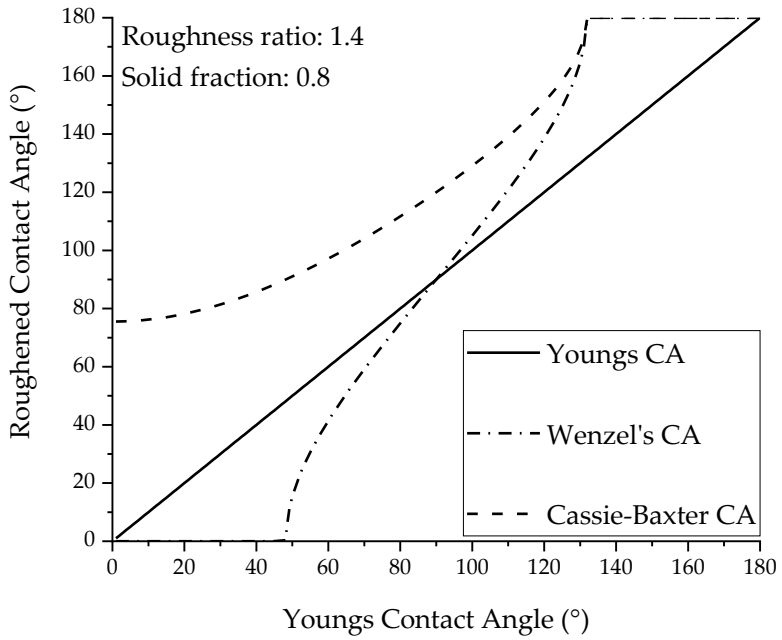

Figure 3-5: Graphical representation of the Cassie-Baxter and Wenzel models

An interesting study by Liang et al. (61) shows the effect that roughness can have on a surface, in this study aluminium was roughened by using a high speed wire electrical discharge machining. This method managed to impart a highly ordered microscale roughness. This microscale roughness manages to increase the contact angle from 61° to 154 +/- 1° with no additional chemical treatment. This shows that the introduction of roughness to a surface can have a drastic effect on the contact angle that is observed, it was found by Liang et al. that changing the distance between the protrusions decreases the contact angle, while increasing the diameter of the protrusions increases the contact angle, it was also shown that increasing the height decreased the contact angle (61).

It should be noted that only three varying measurements were made for each of the roughness parameters, it is possible that different results would be seen if further variation was investigated. It was also shown in this study that the Cassie-Baxter model predicts the contact angle relatively well. It was expected that the Cassie-Baxter model would describe the behaviour more accurately

than the Wenzel model due to the fact that the surface transitions from hydrophilic to hydrophobic, showing a tendency towards heterogeneous wetting. (61)

Methods for determining wettability.

There are a number of different methods that can be utilised in order to determine the wettability of a surface. Additionally, authors have different metrics by which they measure wettability. The most common and probably the simplest is purely by using the equilibrium contact angle. However, other parameters of interest are the advancing and receding contact angles, the surface free energy and the surface roughness.

1. Contact angle.

The most common method for measuring the equilibrium contact angle is by using an optical contact angle measurement device (65, 67, 70, 156). This method takes an image of the droplet and then applies a model in order to determine the angle that is made with the substrate. There are two other measurements that are of interest when looking at the contact angle, namely the advancing and receding contact angles. These are sometimes defined as the maximum and minimum contact angles, the difference between these two values is the contact angle hysteresis. Hysteresis often used as an indication of the ability that a droplet will have to roll off the surface, a surface with a lower contact angle hysteresis will allow the droplet to roll off more easily (157).

In some cases, rather than calculating the contact angle hysteresis the rolling angle is experimentally determined instead. The rolling angle is defined as the angle at which when tilted a droplet will roll off a surface under the influence of gravity, an example of this is seen in Figure 3-6. The smaller this value is the smaller the contact angle hysteresis will be. It can therefore be used as a qualitative measure of contact angle hysteresis (158). In order to calculate the advancing and receding contact angles directly the sessile drop method can be used. In order to implement this method a contact angle goniometer should be used, volume is then added to the droplet using a needle without changing the area that is in contact with the surface, and the angle measured this is the advancing contact angle. For the receding angle the volume of the droplet is reduced as much as possible without reducing the area in contact with the surface and the angle is measured (159).

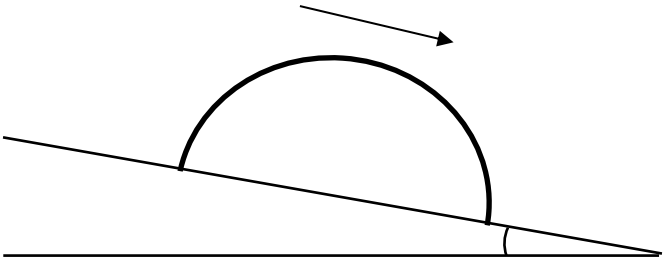

Figure 3-6: Visual representation of the rolling/ sliding angle.

Once the image of the droplet has been captured it is then possible to apply a fitting model to the image in order to determine the contact angle accurately. Some issues may arise when completing this step, due to the fact that the droplets deform under gravity it may become difficult to get an accurate reading. Zhang et al. (157) found that when using various different fitting models, a broad range of results were achieved, for the same droplet image a range between 152° and 179.8° was calculated using different fitting models. Zhang et al. (157) postulated that the reason for this is that the deformation due to gravity skewed the results for most of the models. It was also stated by Zhang et al. (157) that due to the effect of gravity on the droplets, for the most common droplet size (4-5μl) the maximum contact angle that was possible would be approximately 156°. In order to achieve a more accurate contact angle measurement a smaller droplet should be used; however, it is very difficult to obtain a droplet with a volume less than 4μl. In another paper Zhang et al. (160) found a possible way of obtaining a smaller water droplet. In this paper the stability of a superhydrophobic surface was being studied, a contact angle measurement was taken on a droplet and then 40 minutes later another measurement was taken on the same droplet. It was found that the contact angle had increased from 156° to 173°, it is unlikely that this would have happened for any other reason than the reduction in volume due to evaporation (from 4μl to 0.3μl) resulting in a more accurate reading of the contact angle because of the reduced gravitational effect.

2. Roughness

Surface roughness is often characterised using the root mean square of the deviations from the centre line average (161), it can be split into two different grades of roughness: micro and nano-roughness. The surface roughness is characterised by local maxima and minima (hills and valleys). The most common parameter used to describe roughness is the variations in the height

of a surface relative to a reference plane. The reference plane is often the arithmetic average but can sometimes be the root mean square. Providing that the measurement doesn't need to be on the atomic scale, mechanical or optical methods are sufficient. Measurement can be split into two broad categories, contact and non-contact. It is possible that contact type measurement may damage the sample due to the contact of a measurement instrument, this would particularly be the case for soft and/or delicate roughness (162).

Mechanical Measurement

The most common method for mechanically determining the surface roughness is the mechanical stylus method, a stylus is run across the surface and then the vertical motions are amplified and recorded. It is possible to either move the stylus across a stationary surface at constant speed or move the surface underneath the stationary stylus at constant speed. A grid pattern can be sampled across the surface in order to achieve a 3D topographic representation of the surface using this method. There are some significant errors that can occur with this method, the most common introduction of error comes from the ability of the stylus tip to accurately trace the topography. It is possible that the tip is too large to fit into all the crevices meaning that some resolution will be lost, an example of this can be seen in Figure 3-7.

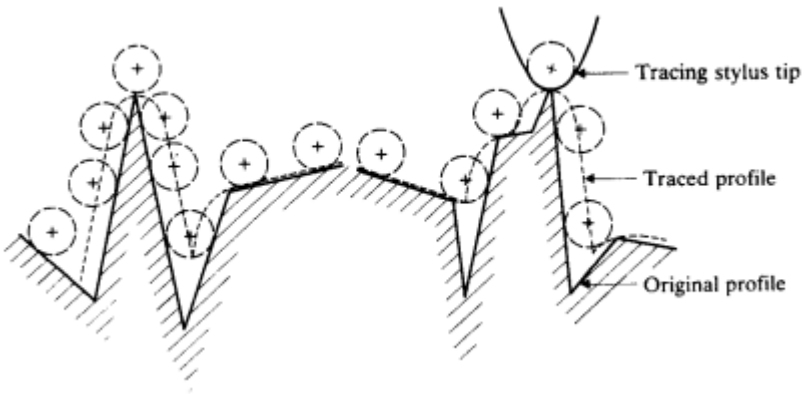

Figure 3-7: Error introduction in mechanical roughness evaluation (162)

Another source of error may be due to the fact that the stylus is moving too quickly with too little load in order to stay in contact with the surface for the whole of the time, this would cause distortion in the topographical profile. Conversely is the stylus load is too high then it is possible that the sharp stylus may cause elastic deformation of the surface resulting in phantom roughness (162).

Optical methods

Another set of methods that are used are optical methods. This is based on the theory that when electromagnetic radiation is incident on a surface it is reflected according to Snell's law. In order to use this to calculate roughness a second transparent reference surface is used this is placed parallel and above the sample surface. Some of the incident beam is reflected by the transparent reference surface and the rest is reflected by the sample surface. There two reflected beams interfere with each other creating fringes, the spacing of these fringes is a function of the distance between the two surfaces. This means that it will be possible to determine the precise height of the hills and valleys that make up the roughness. In reality a slightly different set up is used, utilising mirrors and a beam splitter but the same principle applies (162).

While surface roughness is an important factor when determining the wettability, the scalar value that is often used to describe the surface roughness may not be an appropriate system to relate it to wettability. The reason for this is that the height of the hills and valleys is not the only thing that effects the wettability due to roughness. The reason that the roughness changes the wettability is generally that air pockets manage to reside underneath a droplet, this means that the shape of the roughness will have some effect upon the amount of air that can reside there (61). For example looking at Figure 3-8 it can be seen that very different surface topographies can have the same value for roughness.

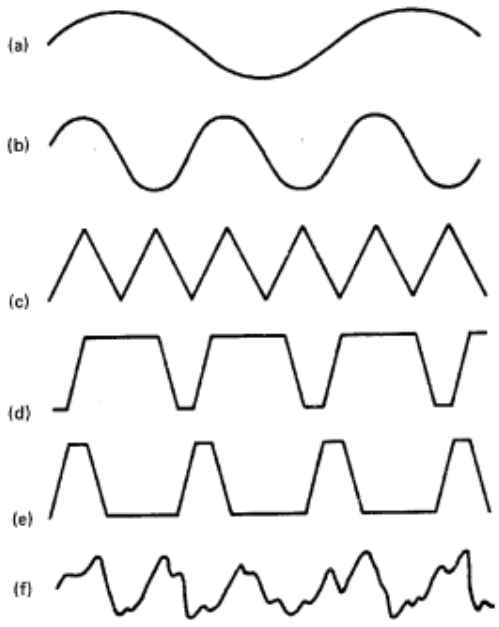

Figure 3-8: Different surface topographies with the same roughness value (162)

3. Surface Free Energy

In cases where the contact angle is easily obtained there are a number of different methods that can be applied in order to calculate the surface free energy of a solid. In order to do this a number of authors have attempted to modify Young's equation defined in equation 3-1 in order to make it solvable for γ_{SA} with experimentally determinable parameters. The most widely used method utilised to do this is the partition of surface free energy into its components. This was pioneered by Fowkes (163), he postulated that the solid free energy could be split up as described in equation 3-4 (163).

$$\gamma_s = \gamma_s^d + \gamma_s^p + \gamma_s^h + \gamma_s^i + \gamma_s^{ab} + \gamma_s^o \quad \textbf{3-4}$$

Where, γ_s^d, γ_s^p, γ_s^h, γ_s^i, γ_s^{ab} are the dispersion, polar, hydrogen, induction and acid-base components respectively. γ_s^o represents any remaining forces. From this it was postulated by Fowkes (163) that the following equation was true for the solid liquid interface free energy for a completely dispersive system (164).

$$\gamma_{sl} = \gamma_s + \gamma_l - 2\left(\gamma_s^d \gamma_l^d\right)^{0.5} \quad \textbf{3-5}$$

This was adapted by Owens and Wendt (164), who grouped all interactions that were not due to dispersion into the polar group, this can be seen in equation 3-6. It should be noted that the p superscripts for this equation differ from the ones used in Fowkes equation (164).

$$\gamma_s = \gamma_s^d + \gamma_s^p \quad \textbf{3-6}$$

The grouping of these terms allowed for the following equation to be obtained.

$$\gamma_{sl} = \gamma_s + \gamma_l - 2\left(\gamma_s^d \gamma_l^d\right)^{0.5} - 2\left(\gamma_s^p \gamma_l^p\right)^{0.5} \quad \textbf{3-7}$$

From these equations both Fowkes (163) and Owens and Wendt (164) have two mathematically similar but procedurally different methods for obtaining the surface free energy of a solid. Fowkes (163) first requires the use of a liquid that only has a dispersive component with a known quantity in order to calculate the dispersive component of the solid surface being used. This is done by combining equation 3-5 with Young's equation (equation 3-1) and simplifying, this yields:

$$\gamma_s = \gamma_s^d = 0.25\gamma_l(1 + \cos(\theta))^2 \quad \textbf{3-8}$$

Using this liquid, the dispersive component of the solid free energy is calculated. The next step is to get another contact angle measurement, this time using a liquid that is not completely dispersive and the components of the liquids surface free energy are known. Fowkes (163) accepts Owens and Wendt's (164) suggestion that the solid free energy can be split into two components, namely dispersive and polar. Using this premise the following equation is then used in order to calculate the polar component of the surface free energy (163).

$$\gamma_s^p = \frac{0.25\gamma_l^2(1-\cos(\theta)) - \gamma_s^d\gamma_l^d}{\gamma_l^p} \qquad \textbf{3-9}$$

The Owens and Wendt (164) method is relatively similar mathematically, it uses a rearranged version of equation 3-9 shown in equation 3-10. The method differs slightly in that while again two liquids are used it is not necessary for one to be completely dispersive.

$$\left(\gamma_s^d\gamma_l^d\right)^{0.5} + \left(\gamma_s^p\gamma_l^p\right)^{0.5} = 0.5\gamma_l(1+\cos(\theta)) \qquad \textbf{3-10}$$

By using two liquids to get data, two linear equations are formed. The benefit of this method over using the Fowkes' (163) method is that the independence of polar and dispersion interactions doesn't need to be assumed. The Owens Wendt (164) method is the most popular method for calculating the surface free energy. (165)

Another method that is often used in order to calculate the surface free energy is the Zisman method. Saying that this method calculates the surface free energy is not exactly correct, in actual fact what this method calculates is the critical surface free energy. This is defined as the maximum surface tension of a liquid that completely wets the surface i.e., the contact angle is zero. Therefore, this method only gives an approximation of the surface free energy. In order to calculate the critical surface free energy, the contact angles of liquids with various surface tensions are measured. The cosines of the contact angles are then plotted against the corresponding surface tensions creating a Zisman plot an example of which can be seen in Figure 3-9. The trend line is then extrapolated to the point $\cos(\theta) = 1$, this then gives the critical surface free energy. (166) This method is not often used for two reasons, one it is experimentally time-consuming and two it doesn't give the actual surface free energy. (165)

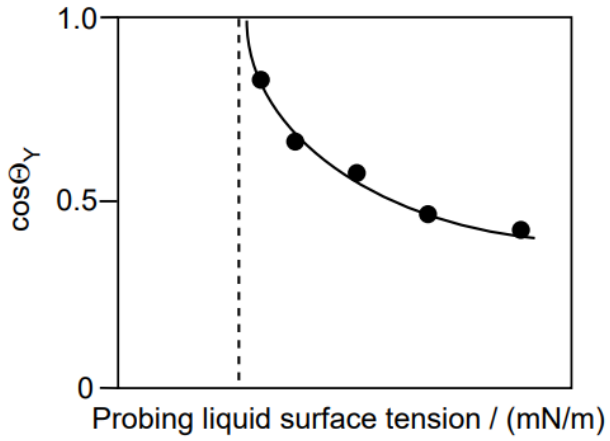

Figure 3-9: Typical Zisman plot (167).

All of the methods that have been outlined above require the measurement of the contact angle of a liquid on the surface in question. In cases where the surface is porous, as is the case for this study, this may not be possible. Some authors have circumvented this by using a non-porous piece of the same material, or have applied the surface coating to a non-porous glass slide to get the contact angle measurement but this is not always possible. (62, 89) Another method of circumventing the need for direct contact angle measurement is using the modified Washburn equation, this method relates the rate at which a liquid is drawn into a porous medium by capillary forces. A sample is lowered to a test liquid until it touches the surface. The mass that is gained by the sample is measured over time, using the modified Washburn equation, defined in equation 3-11. The mass gained over time is related to the contact angle. Once this contact angle has been obtained it is then possible to use one of the methods that are outlined above (83).

$$w^2 = \frac{c\rho^2\gamma_l \cos(\theta)t}{\eta} \qquad \textbf{3-11}$$

The modified Washburn equation is shown above where ρ is the density of the liquid, γ_l is the surface tension of the liquid, θ is the contact angle, t is time, w is the weight gained, η is the viscosity of the liquid and c is a clustered constant that is defined in equation 3-12 (83).

$$c = \frac{r_{eff}\varepsilon^2 A^2}{2} \qquad \textbf{3-12}$$

Where, r_{eff} is the effective radius of the pores, ε is the porosity, A is the cross-sectional area of the sample. This constant is difficult to quantify due to the fact that the effective radius is difficult to measure, having said this it is possible to determine it experimentally. In order to determine this experimentally a liquid that completely wets the surface must be used

(contact angle = 0°) to perform the experiment. This will mean that the $\cos(\theta)$ term will be equal to one and the constant can be calculated. It should be noted that the Washburn equation assumes that the sample is made up of vertically aligned capillaries, due to the fact that this would not be the case there will be some error in the calculated value. (83)

<u>SiO_2 formation – the Stöber process</u>

One of the aims of this thesis is to improve the water separation efficiency of a prefabricated filtration material. As has been shown in the previous theory sections, increasing both the roughness and decreasing the surface free energy will result in an increase in hydrophobicity. A facile method of increasing the roughness is the addition of nanoparticles, the method selected for producing the nanoparticles is the Stöber process. Additionally, it is possible to modify the produced silica nanoparticles in order to increase the hydrophobicity.

A facile method for forming SiO_2 nanoparticles is the Stöber process, prior to the inception of this method there was no method for forming monodisperse silica nanoparticles (168). It was possible to form highly disperse silica by the combustion of silicon tetrachloride in a hydrogen torch. It was noted by Stöber that a researcher named Kolbe had reported the formation of monodisperse silica particles, however upon attempting to recreate these findings Stöber was unsuccessful (168).

The Stöber process is the hydrolysis condensation reaction of alkyl silicates in an alcoholic solution under basic conditions. Stöber et al. (168) look at the effect of different alcohols, namely methanol, ethanol, n-propanol and n-butanol. It was found that the reaction rates were fastest with methanol and increased with increasing chain length, it was also shown that the particle sizes were smaller and the distributions were more narrow with a methanol solvent, compared to a molecularly larger alcohol (168).

The chemical equations are shown in equations 3-13 and 3-14, where equation 3-13 displays the hydrolysis of the alkoxysilane and equation 3-14 shows the condensation of the monomers (169).

$$Si(OC_2H_5)_4 + 2H_2O \xrightarrow[\text{alcohol}]{NH_3} Si(OH)_4 + 4C_2H_5OH \qquad \textbf{3-13}$$

$$Si(OH)_4 \xrightarrow[\text{alcohol}]{NH_3} SiO_2 + 2H_2O \qquad \textbf{3-14}$$

The formation of particles in this case occurs in two stages, nucleation followed by growth. The nucleation stage is relatively well understood, but there has been some debate as to how the growth phase occurs. There are two

main schools of thought, the first is that the particles grow according to an aggregation model in which nucleated particles aggregate to form larger particles. The other is that they grow according to an addition model, in which monomers are added to the surface of the formed particle by condensation (169).

The aggregation model is based on the premise that the particles formed are colloidally unstable, this causes them to aggregate to form more stable particles that have a collective reduction in surface area (170). If the aggregation rate is slower to two large particles aggregating than it is for either a small and large or two small particles aggregating, then the narrow size distribution that is seen in the Stöber process can be achieved. Lee et al. (171) proposed an aggregation model for the Stöber process, it was shown to have relatively good agreement with experimental data.

The experimental data showed that is the concentration of ammonia is high and/or the water concentration is optimal for maximum particle size, the aggregation was fast compared to nucleation. This results in intermediate size particles being made extinct and the main aggregation is between newly formed nuclei and larger aggregates (171). If the concentration of ammonia is low and/or the water concentration is not optimal, the nucleation rate is high compared to the aggregation rate. This results in a significant portion or intermediate particles while the nucleation rate remains high, once the silicate reagent begins to run out the nucleation rate drops and the number of intermediate size particles drops quickly due to the aggregation rate being faster than the nucleation rate (171).

A study by Masalov et al. (172) examined the idea of aggregation further looking at the effect of adding additional alkoxysilane once the initial reagent had been depleted. This is in a way is forced aggregation. It is postulated by Masalov et al. (172) that once the depleted reagent was replenished nucleation restarted and is the dominant reaction. Once the concentration of the reagent decreased the newly formed particles begin to aggregate on the larger pre-formed particles. This was shown quite conclusively using scanning electron microscope images, in the first minutes after the increase in reagent concentration the large smooth particle looks unchanged, but after a short period of time a clear roughness appears on the surface. After approximately 60mins the particle is returned to being smooth as the aggregation phase completes (172).

It has been shown by Matsoukas and Gulari (173) that the growth stage of the process is controlled by the hydrolysis portion of the reaction. It is shown

experimentally that the nucleation is limited to the early stages because the number of particles was conserved through the main growth period. The fact that no more nucleation occurs but the particle size increases implies that monomer addition must occur. This was achieved using dynamic light scattering and Raman spectroscopy. In another study by Matsoukas and Gulari (174) a model based on monomer addition is presented, it is suggested that once the total number of particles reached a steady state growth then occurs by monomer addition. It was noted that providing the concentration of monomers remains low growth by monomer addition was favoured, however if the concentration rose nucleation and subsequently aggregation would occur.

The understanding of this theory is important in being able to produce a variation of differently sized particles. Additionally, being that the aim of this work is to modify the Stöber process to crease hydrophobic silica particles an understanding of the process is required in order to explain the variation in results.

Filtration

Filtration is a separation process for removing contaminants from a mixture of contaminants and useful fluids. In an ideal world the separation would be 100% efficient, however in reality this is rarely possible. Contaminants will be able to pass through the filter if they have a diameter less than the pore size of the filter. Filters are usually rated to remove a specific percentage of contaminants of a certain diameter, this allows the designer to determine an allowable level of filtration. This will likely be a trade-off between filtration performance and pressure drop (175).

The type of filtration being examined is dead end filtration, sometimes called surface filtration. The filtration occurs at the upstream surface of the filter. A schematic of this is shown in Figure 3-10. In a pure surface filtration system in which the surface is infinitely thin, the particle being separated from the flow will have one chance at an interaction with a pore. The particle will either be trapped at the surface of the filter or will pass through. this type of filtration will inevitably lead to blockages and potentially cake layers if there is sufficient particles within the flow (175).

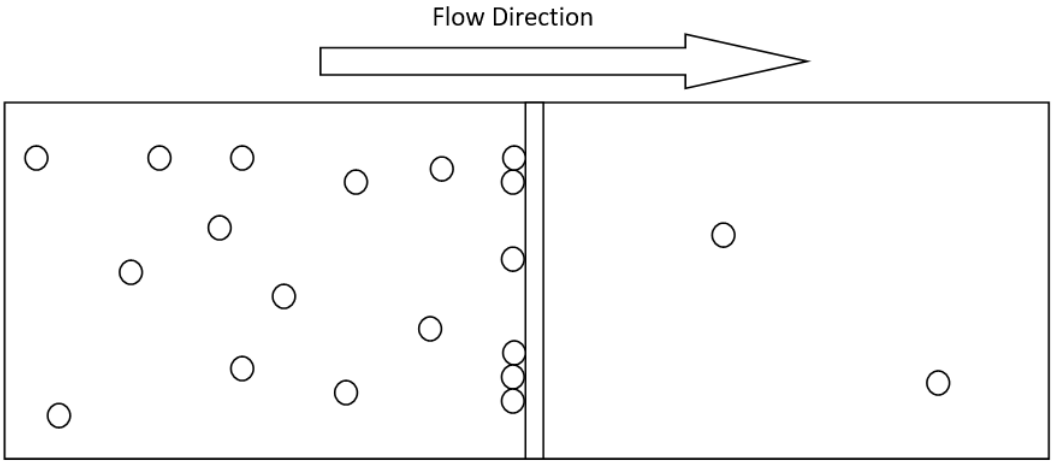

Figure 3-10: Schematic of dead-end filtration

In a situation where the pores are smaller than the particles being captured, the mechanism for capture is simple, this process is sometimes called surface straining (175). It is also possible to capture particles that are smaller than the size of the pores. The capture mechanism in this case is a matter of probability. There is some amount of probability that the particle will pass through the filter untouched, however if the particle interacts with the surface there is a chance that it will become suck through adhesion or electro deposition (175). In real systems the surface will not be infinitely thin, this will give rise to an element of depth filtration. The particle will come into contact with significantly more fibres, increasing the probability that it will be captured. This will still inevitably lead to pore restriction and potentially blockage (175).

While most of this has been describing solid particles within a liquid system, many of the same principles can be applied to immiscible liquid-liquid systems, where one phase is captured by the fibres. The one major difference is that the droplets within this system are less discrete than particles, having the ability to deform and pass through pores. It is possible to estimate the pressure that is required for a droplet to be deformed and forced through a pore. Nazzal et al. developed an equation to determine this based on the young-Laplace equation (93). The variables that effect the breakthrough pressure are, the contact angle, the diameter of the pore, the diameter of the droplet and the interfacial tension between the two phases.

3.1.2 Techniques Theory

The theory behind some of the more advanced techniques are covered in this section. It is important to have a good understanding of the theory behind these techniques for two reasons. Firstly, it is important to understand the

theory so that the method is applied correctly. Secondly, if any results are difficult to analyse, a good understanding of the theory is vital.

Scanning electron microscopy

Scanning electron microscopy is the process of creating a beam of electrons that make contact with a surface that is to be examined. This is used in all elements of this project in order to visualise the changes to the surface of the filter as a result of either coating or fouling, or both. The beam is created by a thermal field emission gun. The beam of electrons interact with atoms of the relatively high-density surface of the solid being examined and lose energy and alter their well-defined path. The interactions produce three things of interest, back scattered electrons (BSE), secondary electrons (SE) and x-rays. These can all tell the user something about the surface, both the BSE and the SE can be used to image the surface with high resolution, while the x-rays give information regarding the composition of the surface. It is important that the sample chamber is in a high vacuum state because any interaction with molecules in the air in between the electron gun and the sample or the sample and the detector would result in distortion of the data (167).

There are two main types of scattering processes, inelastic and elastic scattering. Inelastic scattering describes the process of reducing the energy of a beam of electrons and transferring the energy to the surface atoms by interactions with the inner shell atomic electrons and the valence shell electrons. SE are formed as a result of this type of interaction, the electron beam interacts with the atoms and results in the ejection of the weakly bound valence electrons, these SE will have the same energy as the binding energy of the valence electron. The x-rays are also formed from this type of reaction, although in this case the electrons from the inner shell are ejected. This ejection also causes the emission of x-rays with a specific energy that corresponds to the binding energy of the electrons, this allows the composition of the surface to be calculated. BSE are created through elastic scattering; this occurs when an electron in the electron beam is deflected by the electrical field of an atom. The BSE will have a relatively high energy of nearly the same energy as the beam that is created by the field emission gun (167).

Charging is a common issue in SEM. The beam of electrons that are being applied to the surface of the specimen can be considered to be a flow of current. The backscattered and secondary electrons should be considered to also be flows of current, however combined these two phenomena only make up around 40% of the total current that is sent to the specimen via the electron

beam. This means that the remaining current must flow to ground to avoid charge accumulation. If the specimen is not a good conductor, then there is more of a chance that charge will accumulate, this accumulation of negative charge will decelerate incoming electrons from the beam distorting the image (167). This is the reason the BSE were used in this project, the materials being examined are not good conductors and therefore are susceptible to charging, the BSE have a much higher energy than the SE and therefore experience less of an affect from charging.

Capillary flow porometry

This technique is used to determine the drop in permeability as a result of the fouling experienced by the filters in the field. It is also used to determine the effect of the coating on the permeability of the filters.

The sample is placed in a sealed compartment. The porometer allows compressed air to be passed through the sample and pressure sensors on either side calculate the pressure drop. Two pressures against flow curves are collected, one dry curve in which only air is passed through the sample, and one in which the sample is covered with a wetting liquid (Galpore – surface tension 16.9mN/m) and air is used to force the liquid through the sample. The difference between these two curves is then used to calculate the pore size distribution. An example of the two curves is shown in Figure 3-11.

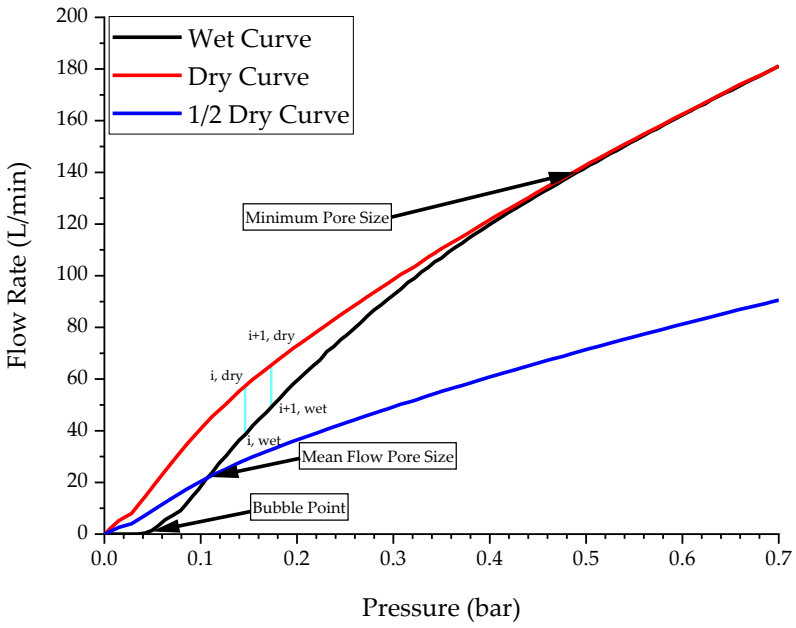

Figure 3-11: Example of the curves produced by the porometry process.

The point at which the wet curve crosses the ½ dry curve is related to the mean flow pore size, the point at which the wet curve converges with the dry curve is related to the minimum pore size and the point at which the wet curve increases from zero is related to the maximum pore size or bubble point. Equation 3-15 is the equation that relates the pressure to the pore diameter. It should be noted that the diameter that is calculated is the minimum pore throat for the respective pore, a visual explanation of this is shown in Figure 3-12.

$$d = \frac{4\gamma \cos(\theta)}{P} \qquad \textbf{3-15}$$

Where γ is the surface tension of the wetting fluid (N/m), θ is the contact angle of the wetting fluid on the media being analysed, P is the pressure (Pa) and d is the diameter of the pore (m). The normal methodology for this is that the wet curve is obtained first, followed by the dry curve in order to ensure that all of the wetting liquid has been removed using the pressure that was selected. In this case however, it was necessary to complete the dry curve first followed by the wet curve because the process of completing the wet curve may remove some of the foulant material.

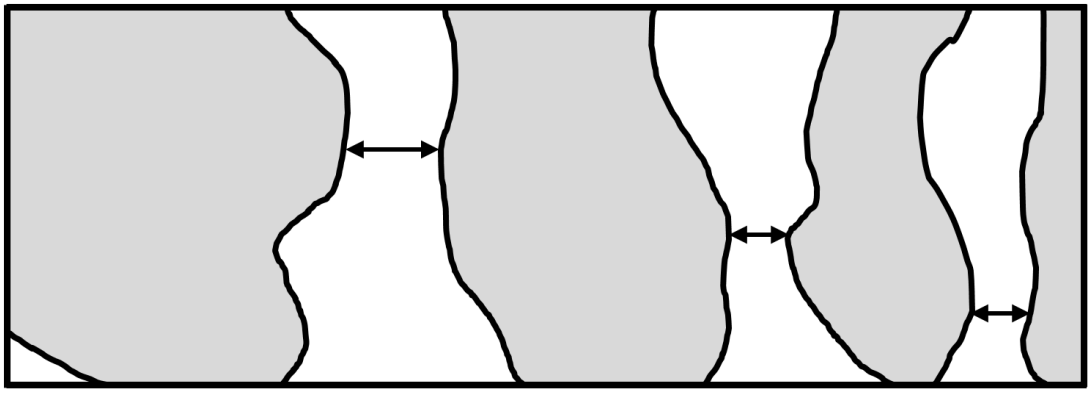

Figure 3-12: Visual representation of minimum pore throat.

While the maximum, minimum and mean pore sizes can be determined easily from the wet and dry curves, calculating the pore size distribution is slightly more involved. Equation 3-15 is again used to calculate the pore size at each pressure step. Using equation 3-16 and the flow data at each pressure step the differential curve can be calculated, which shows the percentage of pores present at that pressure.

$$[DIF]_i = \left(\frac{\left(\frac{flow\ i+1, wet}{flow\ i+\ 1, dry} - \frac{flow\ i, wet}{flow\ i, dry} \right)}{\sum_{j=0}^{n} \left(\frac{flow\ j+1, wet}{flow\ j+\ 1, dry} - \frac{flow\ j, wet}{flow\ j, dry} \right)} \right) \times 100 \qquad \textbf{3-16}$$

In this system it is the pressure steps that are controlled, this results in a variation in the pore size step as the pressure is increased. While the pressure is quite low, the pore size steps will be quite large, but will decrease as the pressure increases. In order to counter this effect, the differential curve must be corrected. Each fraction is divided by the difference in pore size as shown in equation 3-17, this is then commonly taken as the pore size distribution.

$$[CDIF]_i = \left(\frac{\frac{[DIF]_i}{pore\ size(i) - pore\ size(i+1)}}{\sum_{j=0}^{n} \left(\frac{[DIF]_j}{pore\ size(j) - pore\ size(j+1)} \right)} \right) \times 100 \qquad \textbf{3-17}$$

Water content determination

This process was necessary for all separation testing, therefore was vital in order to gain the results in the first and third results chapters. The equipment used in this project is a coulometric Karl Fischer titration device (Mettler Toledo C20 coulometric KF titrator). This means that there are two solutions being used, separated by a semi permeable membrane. The main reaction that inspired the Karl Fischer titration method was the Bunsen reaction (3-18) used for determining the quantity of sulphur dioxide in aqueous solutions (176).

$$SO_2 + I_2 + 2H_2O \rightarrow H_2SO_4 + 2HI \qquad \textbf{3-18}$$

This process can also be used to determine the amount of water in a solution if SO_2 is present in the reagent. During the testing of solvents for this reaction it was found that it only occurs quickly and stoichiometrically between a pH of 5 and 7 (177).

Dynamic light scattering

Dynamic light scattering is a method that can be used to determine the size of particles in suspension, this is used in order to assess the size of the particles formed in the Stöber process used for coating. The process requires a colloidal solution to be hit with a monochromatic light source, a detector is located at 173°. As the light source hits the colloids within the solution the light is scattered. In dynamic light scattering the fluctuations of the intensity at the detector are examined. These fluctuations are caused by the Brownian motion of the particles within the solution, the Brownian motion is related to the size of the particles within the solution (178).

The movement of the particles are related to the diameter using the Stokes-Einstein equation 3-19. Where,D_t is the translational diffusion coefficient, k_B is the Boltzmann coefficient, T is the temperature, η is the viscosity of the solution and R_h is the hydrodynamic radius (178).

$$D_t = \frac{k_B T}{6\pi\eta R_h} \qquad \textbf{3-19}$$

The reason for this is that as the diameter of the particle increases, the frictional forces also increase. This results in slower movement due to Brownian motion.

Dip coating

There are three stages in the dip coating process, as shown in Figure 3-13. The first stage in which the sample is immersed in the coating solution must be long enough for the sample to be completely wet. In the second stage the sample is withdrawn leaving a thin layer of the solution (In this case colloidal solution of solvent and microspheres) is deposited on the surface. During the third stage the solvent is evaporated and the microspheres remain on the surface (179). This process was used to coat the filters due to its facile nature and the fact that no specialist equipment is necessary.

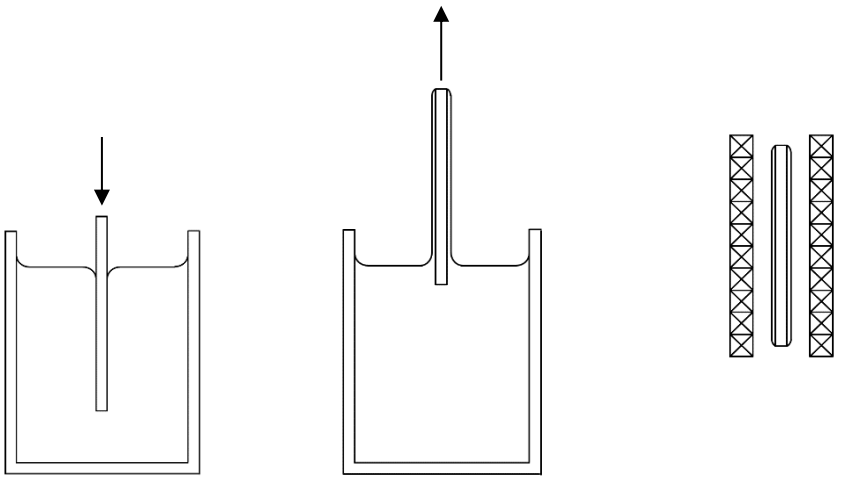

Figure 3-13: Schematic of the dip coating process

There are a number easily of controllable parameters that will have an impact on the final thickness of the film formed. Most notably is the velocity at which the sample is withdrawn from the solution. Generally, the faster the sample is withdrawn from the solution the thinner the film will be. In addition to this the concentration of colloids, the density, the viscosity and the evaporation rate of the solution will also have an impact on the final film thickness. For this work the thickness of the film was not being examined. However, knowledge of this technique was required in order to ensure that the coatings were applied consistently.

3.2 Practical Methodology

3.2.1 Returned pleat stack preparation.

Before the returned filter elements could be tested for water separation efficiency they needed to be removed from the casing, an example of the filters received is in Figure 3-14. Once the metal outer casing was removed, the pleat stack was cut out in its entirety, as shown in Figure 3-14. From this the samples for analysis were cut. All samples were cut from the centre of the pleat stack to reduce the effect of any hysteresis present in the filters. For the separation testing a circular sample was cut, with a diameter of 110mm. For porometry, a circular sample of approximately 25mm was cut from the pleat stack. For the contact angle experiments, scanning electron microscope (SEM) imaging and Fourier transform infrared spectroscopy (FTIR), small squares (roughly 1cm x 1cm) were cut out. All of these samples, aside from the FTIR samples (processing described in section 3.2.3), were placed in an oven at 120°C for 1hr to remove any diesel whilst removing as little foulant material as possible.

Figure 3-14: Example of the filters received (left) and the removed pleat stack (right)

3.2.2 Contact angle.

The contact angle was measured using a goniometer (KSV instruments). All tests were done in air using de-ionised water, the droplet sizes were 10µL. The samples were used as prepared by the method described in section 3.2.1. There is some difficulty in obtaining the contact angle from fibrous samples because the fibres can interfere with the fitting algorithm, an example of this is shown in Figure 3-15.

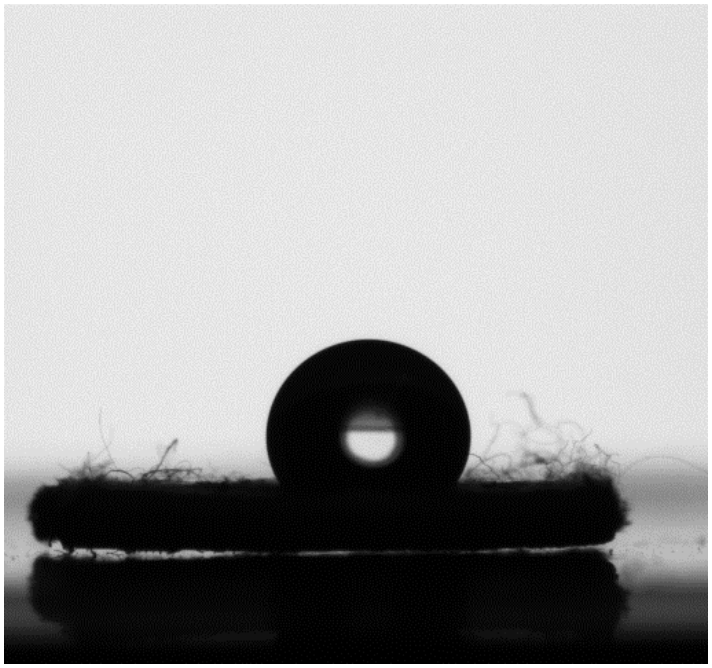

Figure 3-15: Example of fibres interfering with the fitting algorithm

If it was found to be an issue, then the samples were cut as small as possible (so that there was only enough room for the droplet on the surface) to reduce the amount of foreground and background fibres that were in view. In almost all cases this reduced the fore and background fibres to the point that the fitting algorithm can pick the edges.

3.2.3 Fourier transform infrared spectroscopy.

The specific type of Fourier transform infrared spectroscopy that was used was attenuated total reflection spectroscopy. This utilises an internal reflection element (IRE), a high refractive index crystal that the sample is placed upon. Figure 3-16 shows a simple path of a ray through the internal reflection element, the ray will penetrate the sample to a small degree and specific wavelengths are absorbed allowing for the characterisations of materials (180).

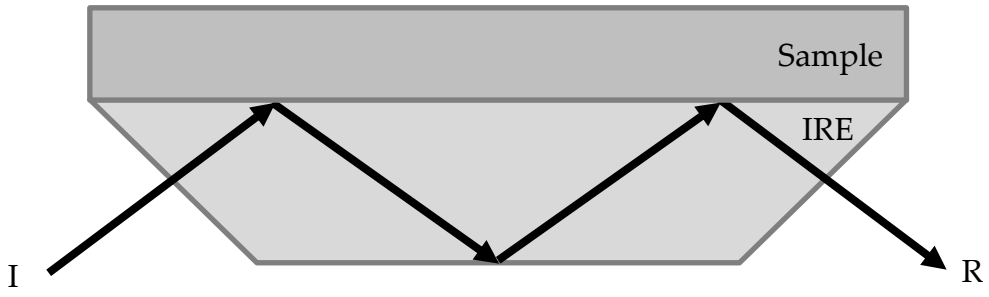

Figure 3-16: Schematic diagram of the ray path for ATR-FTIR (I = incident beam, R = reflected beam)

The main focus of this analysis was looking at the foulant therefore It was necessary to isolate the foulant material from the filter. In order to remove the foulant from the surface a section of filter was cut and placed in 50ml of solvent. (The solvent chosen was heptane because it is nonpolar, similar to diesel and therefore should dissolve as little of the foulant as possible.) The filter sample and 50ml of solvent was placed in an ultrasonic bath at room temperature for 30mins to mechanically remove the foulant material. The filter sample was then removed and discarded. The resultant solution of heptane and foulant colloids were placed in a centrifuge at 12000rpm for 30mins, the separated heptane was discarded and replaced with 50ml of fresh heptane and the centrifugation process was repeated. This ensured that any fuel is removed and only insoluble foulant material remains. The resultant foulant material was then dried in an oven at 120°C to remove the excess solvent.

Once the foulant was isolated and the excess solvent was removed it was applied to the crystal of the attenuated reflection Fourier transform infrared spectrometer. The sample was then run with a resolution of $4cm^{-1}$ between the wavenumbers $3300cm^{-1}$ and $650cm^{-1}$, this will capture all the peaks of interest. An average of 10 scans were taken and the crystal was cleaned thoroughly with iso-propanol between each sample run.

3.2.4 Scanning electron microscope

The pristine filters are dry, so very little pre-processing was required in order to ensure that they were suitable for a vacuum environment. However, the material that makes up the filter is not conductive causing potential for the image that is produced by the scanning electron microscope (SEM) to be distorted. In practice it was found that this was not too much of an issue.

In order to combat this distortion when it occurred, the sample was sputter coated with a thin layer (5 – 20nm) of conductive iridium. The following settings were used for the collection of the SEM data using the Hitachi TM3030Plus tabletop scanning electron microscope.

- 15kV acceleration voltage.
- ~50000nA emission current.
- 1500mA filament current.
- Backscattered electron detector using the charge up reduction function.

The settings when using the Carl Zeiss EVO MA15 SEM were as follows.

- 20kV acceleration voltage.
- Backscattered electron detector using the charge up reduction function.

When using SEM to analyse the returned engine samples some pre-processing was required in order to make them suitable for use in near vacuum conditions. When the filters were returned, they were saturated in fuel, if this was subjected to the near vacuum environments present in the SEM, a significant amount of off-gassing would occur potentially causing damage to the detectors. To avoid this issue the filters were first dried in an oven at 100°C for a minimum of 2 hours, this caused any volatile components to evaporate. Washing with a solvent was considered although it was thought that this may remove some of the foulant that was being analysed. Again, where necessary the dried samples were sputter coated with iridium to stop image distortion. Also, the same image analysis was performed.

3.2.5 Capillary flow porometry

Capillary flow porometry allows for the calculation of the pore size distribution. The method involved cutting a small circle (25mm diameter) of the sample being analysed. For the returned samples an attempt was made to take the sample area in between the pleats in order to reduce any effect that they may have. This sample was then placed into the sample holder of the porometer (Porolux 100NW), an O-ring was then placed on top, and the lid was screwed on tightly.

The wet and dry curves were collected. Traditionally it is recommended that the wet curve is collected first. However, it was found that the liquid used in collecting the wet curve had a tendency to remove some of the foulant material. To combat this the dry curve was taken first.

3.2.6 Air permeability

Using the Porolux 100NW, it was possible to determine the air permeability of the filter samples. This was beneficial to get an insight into the severity of the blockage from a quantitative standpoint that was not provided by simply looking at microscopic images. The process was relatively simple, the filter was placed in the same sample holder and a flow of air was applied.

The differential pressure measurement was made and using Darcy's equation (equation 3-20) the air permeability was calculated. In order for this to be accurate the thickness of the samples was required; this was done using a high precision electronic thickness gauge. All experiments were conducted at a pressure of 0.8 bar.

$$k = \frac{q\mu L}{A\Delta P} \qquad \textbf{3-20}$$

In which k is the permeability, q is the flowrate, μ is the viscosity, L is the characteristic depth of the sample, A is the area of the sample and ΔP is the pressure drop.

3.2.7 Water separation efficiency

Equipment

The water separation experiments were performed using a rig designed in the University of Leeds, a diagram of which is shown in Figure 3-17. In all experiments reference grade diesel fuel supplied by Parker Hannifin was used. The water injected into the system was de ionised water from the laboratory supply. The filter samples were contained within a filter housing designed in a previous project shown in Figure 3-18 (181).

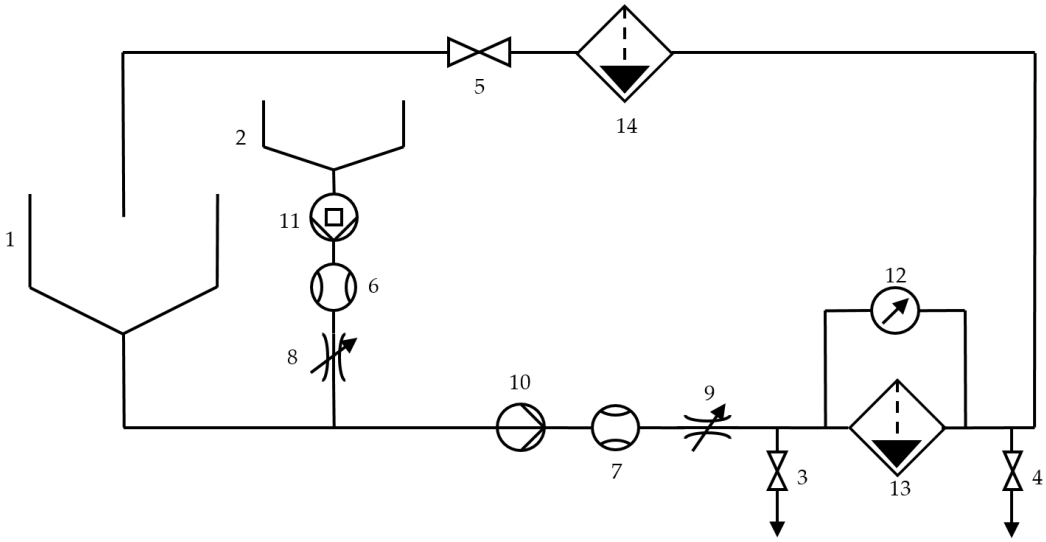

Figure 3-17: Flow diagram of the separation rig
1. Fuel Tank. 2. Water Tank. 3, 4, 5. Ball Valves. 6, 7. Flow Meter. 8, 9. Adjustable Valve. 10. Centrifugal pump. 11. Peristaltic Pump. 12. Differential Pressure Meter. 13. Test Filter Housing. 14. Clean-up Filter.

The main centrifugal pump is a Stuart Turner pump with a maximum working pressure of 6 bar, the peristaltic pump used to inject water into the flow is a Watson Marlow peristaltic pump. The flowmeter measuring the flow in the main loop is a Porter (B-250-8), the flowmeter used to measure the flow of water is a Porter (A-157-1). The differential pressure meter used is a Dwyer 496 series digital manometer. The clean-up filter is full 3 stage filter unit, supplied by Parker Hannifin.

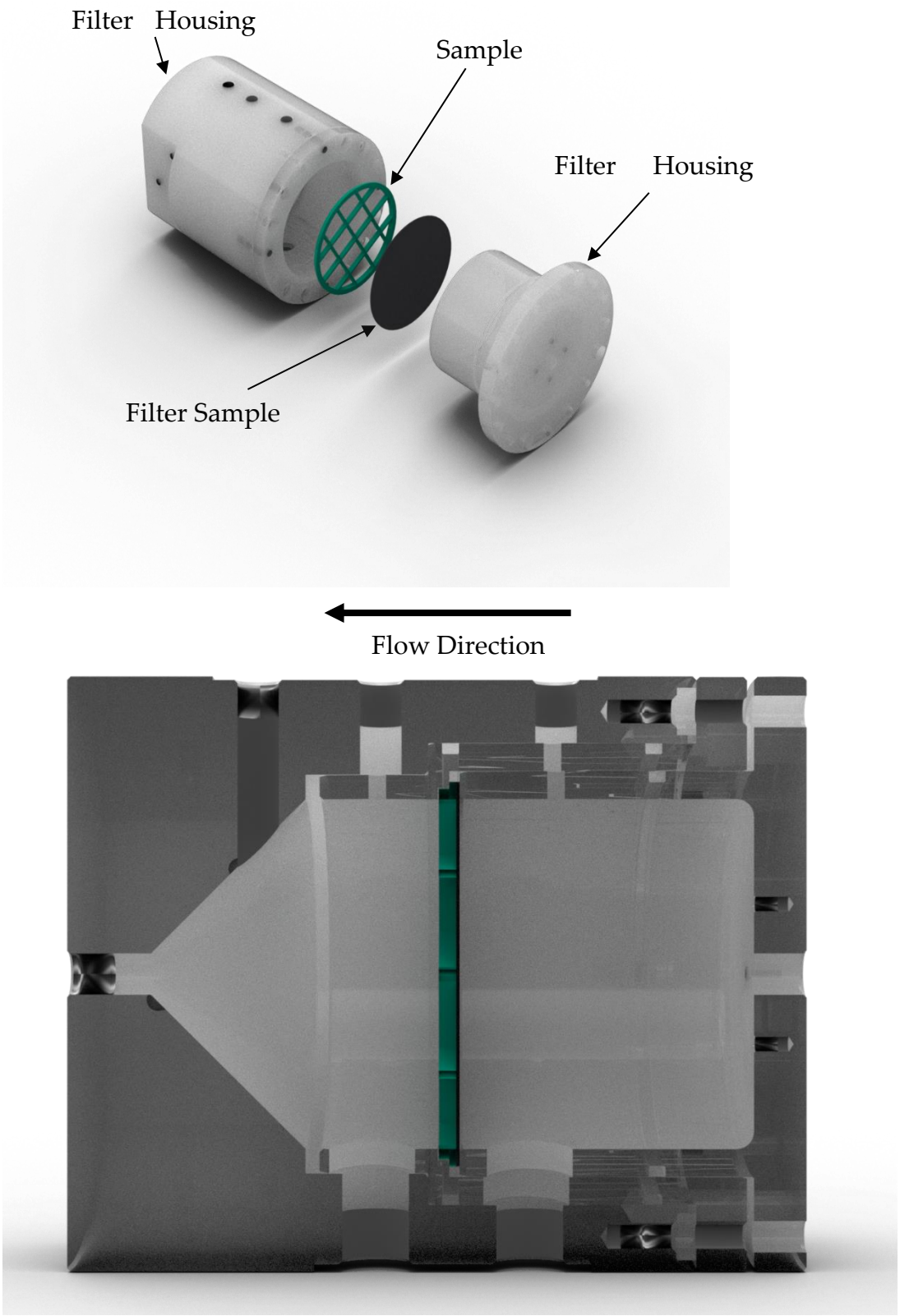

Figure 3-18: Filter housing

For the filtration unit to work effectively. The flow should be fully developed by the time that it reaches the filter face. There is a large expansion that will create potential dead zones. Using equation 3-15, where ρ is density, u is

velocity, D is the diameter and μ is the viscosity, the Reynolds number for the flow in the housing was calculated to be 37.

$$Re = \frac{\rho u D}{\mu} \quad \textbf{3-21}$$

A study conducted by Dagtekin and Unsal (182) estimated the length of pipe required to return to fully developed flow following an abrupt expansion for various Reynolds numbers and levels of expansion. It was shown that for a Reynolds number of 50 (the lowest examined) and an expansion factor of 10 the length required was approximately 30 pipe diameters. This is in excess of the 12 that there are in this set up. However, the Reynolds number is lower that examined by Dagtekin and Unsal (182) and if there flow is not completely fully developed it is unlikely to have a massive impact on the results of this work.

Basic Testing

To perform the experiment first the centrifugal pump was started, the filter housing was filled (all the air was bled out) and the flow was allowed to settle. The total flow rate was set in order to achieve a face velocity at the filter of 0.75mm/s. The peristaltic water pump was started at this point t = 0. The water flow rate was set to achieve a weight percentage of approximately 1% of the total flow. At t = 15 minutes a sample was taken (approx. 50ml) from the inlet sample point (3 on Figure 3-17) and the outlet sample point (4 on Figure 3-17). This was also done at 30, 45 and 60 minutes. At these measurement points, the differential pressure across the filter housing was recorded.

Once the samples had been taken, they were immediately taken to the Karl Fischer titration equipment to determine the amount of water. The reason for testing the samples immediately was to reduce the amount of gravity settling that could occur within the samples. While this wasn't an issue in the inlet sample, some of the droplets that had not been trapped by the filter had coalesced, increasing the droplet size in the outlet sample. This was particularly prevalent in the fouled samples that had a reduced hydrophobicity.

Varying Face Velocity

For the coated samples, as a facile measure of comparing the ability of the coatings varying the face velocity was used. The flow rate was increased in intervals to achieve face velocities of 0.75, 0.9, 1.2 and 1.5 mms^{-1}. The final pressure at the 1.5 mms^{-1} was in the region of the higher flow rates that were

seen in the most blocked of the return samples. The response to the increasing face velocity is then used as an analogue for the response to fouling.

3.2.8 Water content determination

The process being used in this project is coulometric titration, as has been mentioned. This differs from volumetric titration in that the reagent is generated using an electric current rather than being added dropwise using a burette. In the Karl Fischer titration process iodine is formed by electrolysis from an iodide containing reagent. It is important that the process is 100% current efficient, and that no side reactions occur. It was found that the maximum current that was possible to satisfy this is 400mA, otherwise the temperature increased resulting in side reactions.

In order to detect the end point of the reaction a separate electrode from the generator electrode. This is usually a double platinum wire electrode. The end point detection used in this case is bivoltameric, a small current is applied across the electrode (50μA) the voltage is then recorded. The voltage is dependent of the amount of water in solution, typically it is relatively high with excess water (680mV) and lower with excess iodine (100mV) (176). The equipment in this case has a generator electrode with a diaphragm, a schematic of this is seen in Figure 3-19. The reason that this is used is the relatively low conductivity of diesel and the low amounts of water in the solution.

In this set up there are two solutions required, the anolyte and the catholyte. For this project the anolyte selected was Hydranal coulomat AG-H (CAS no: 67-56-1) because it is appropriate to use with the hydrocarbons that will be used in the analysis. The standard Hydranal coulomat CG (CAS no: 14426-21-2) was used for the catholyte. The anolyte is located in the main beaker during running, and the catholyte is located within the generator electrode. Iodine is formed from the catholyte using electrolysis. The cumulative current required to bring the voltage back down to the steady state is then related to the amount of water because the current produces the iodine that subsequently reacts with the water.

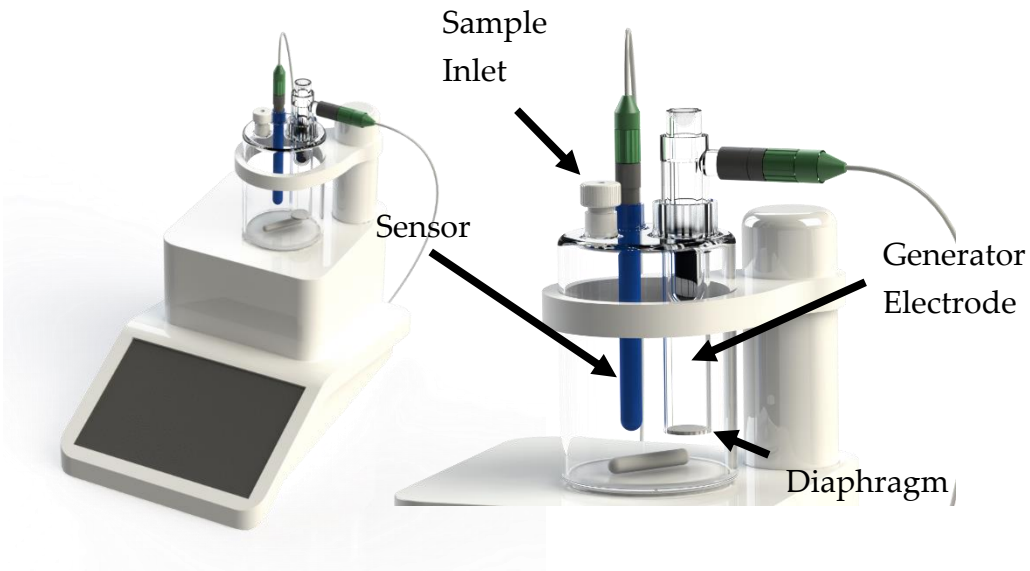

Figure 3-19: Model of the Karl Fischer titration equipment

Samples were collected during all water separation testing. For each timestep a sample was taken from the upstream and downstream of the filter being tested. Approximately 50ml samples were taken, but not all of this was required for the titration.

Once the samples were collected the Karl Fischer titration was completed immediately, this reduces the possibility that the sample separated through gravity settling. Some of the sample was drawn into a syringe and weighed on a digital scale (MyWeigh iM01), approximately 0.5g was then injected into the main beaker and the syringe containing the remaining sample was weighed again. The exact weight of the sample was inputted into the Karl Fischer in order to convert the mass of water detected into a concentration. The values outputted were then logged for analysis.

3.2.9 SiO_2 microsphere formation

SiO_2 microspheres have been selected as the method for increasing both the roughness and hydrophobicity of the filter material, with the aim of increasing the instantaneous and end of life water separation performance. In order to create a nanoparticle sol of fluorine functionalised silane, tetraethyl orthosilicate (TEOS) (CAS no: 78-10-4) and the selected functionalising agent were co-hydrolysed under basic conditions, the three functionalising agents selected are listed in Table 3.1. The process used to form the nanoparticles is the Stöber process, described in section 0.

Table 3.1: List of functionalising agents used in the SiO_2 nanoparticle formation.

Functionalising agent	Abbreviation	CAS number
Perfluorooctyltriethoxysilane	FAS	51851-37-7
Hexadecyltrimethoxysilane	HDTMS	16415-12-6
Oleic Acid	OA	112-80-1

The additional reagents that were used are listed in Table 3.2.

Table 3.2: List of reagents used in the SiO_2 nanoparticle formation.

Reagent	Abbreviation	CAS number
Ammonium hydroxide	NH_4OH	1336-21-6
Ethanol	EtOH	64-17-5
De-ionised water	H_2O	N/A

In order to gain an understanding of the effects of each reagent a testing matrix was developed using latin hypercube sampling. For each functionalising agent the concentrations that were varied were: NH_4OH, H_2O and the functionalising agent itself. Table 3.3 details the testing matrix.

Table 3.3: Testing matrix

Test ID	Concentration ($molL^{-1}$)			
	TEOS	**Functionalising agent**	**NH_4OH**	**H_2O**
1	0.261	0.0181	0.772	2.20
2	0.264	0.0328	0.524	1.95
3	0.250	0.0631	0.601	3.88
4	0.234	0.0150	1.54	5.86
5	0.251	0.0223	0.434	4.93
6	0.243	0.0125	2.36	2.44
7	0.257	0.0141	0.857	2.96
8	0.263	0.0356	0.711	1.69
9	0.230	0.0218	0.499	8.90
10	0.254	0.0469	1.07	2.39

The points within the matrix were selected randomly within the test space using a latin hypercube function available within Matlab in order to minimise overlap between the values.

The mass of TEOS was maintained throughout every experiment, but due to the slight changes in volumes of the other components, the concentration varied slightly. In each iteration of the experiment the TEOS, 30ml of EtOH and the functionalising agent material were measured and mixed together under magnetic stirring in a beaker. In a separate beaker 4ml of EtOH, the H_2O and the NH_4OH were again mixed under magnetic stirring. Once the mixtures had been sufficiently mixed (5 – 10mins) the second mixture was next added dropwise to the first. This solution was then left under magnetic stirring for a minimum of 12hrs. A visualisation of this is shown in Figure 3-20

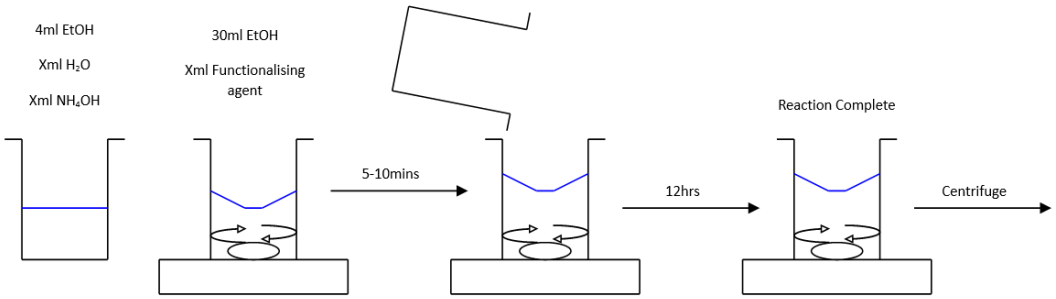

Figure 3-20: Visualisation of the Stöber process used.

Once the reaction was complete the resulting solution was placed in the centrifuge at 12000rpm for 30mins to separate the nano/micro particles from the solvents. Once this was complete as much solvent as possible was removed manually, the centrifuge container was then refilled with ethanol and the centrifugation was repeated. This washing process was repeated once more, and the resultant colloidal suspension was assumed to be ethanol with the hydrophobic particles.

3.2.10 Dynamic light scattering

In order to determine the sizes of the particles that are produced during the Stöber process a dynamic light scattering (DLS) technique was used.

For these experiments a Malvern Zetasizer was used using standard disposable plastic cuvettes. The temperature of the experiment is very important for DLS because Brownian motion is affected by the temperature and the viscosity of the continuous phase. For these experiments the temperature was set to 20°C. Prior to the experiments the particles being examined were placed in methanol and put in an ultrasonic bath for a minimum of 10 minutes to break up any aggregates formed during the drying process.

Once the particle size distribution has been calculated within the software a calculation is performed to determine the polydispersity index. This is a measure of the mono-dispersity of the particles being analysed. The results of the DLS are being compared with the results of particle size analysis using SEM imagery. It is also useful to compare the polydispersity index of the two methods as well. Therefore, in order to determine the polydispersity of the particle size distribution determined through SEM imagery, equation 3-22 is used, where PDI is the polydispersity index, σ is the standard deviation and μ is the mean particle size.

$$\mathrm{PDI} = \left(\frac{\sigma}{\mu}\right)^2 \qquad \textbf{3-22}$$

This means that a lower polydispersity index means that the particles are more monodisperse.

3.2.11 Artificial fouling with carbon black

In order to simulate the fouling that occurs within the engine in a lab setting carbon black was used as the foulant. In the field the fouling will occur over a significant amount of time, the lowest amount of miles that a vehicle travelled before changing the fuel filter was 29,383km. Assuming a fuel efficiency of 9mpg (183), the full pleat stack will filter in excess of 9000 litres of fuel. The total surface area of the filtration material was measured to be approximately $1m^2$, this results in $0.9L/cm^2$ of fuel being filtered. The sample size used in the test rig was a circular section of 11cm, giving a surface area of $95cm^2$. This would therefore require the filtration of 85L of fuel. In addition to this the fuel in an engine undergoes thermal and pressure cycling while being circulated through the fuel system. Using the test rig, it was not possible to simulate this, resulting in the formation of solid contaminants. For this reason, a rapid fouling process was required.

Carbon black was used as a fouling material because it is composed of small particles. The small particles means that the type of fouling observed on the field samples will be replicated. Figure 3-21 gives an example of what the surface of an artificially coated filter looks like. This is representative of what was seen in the returned field samples. A cake layer is formed on the surface, but there are still some pores remaining for fluid flow.

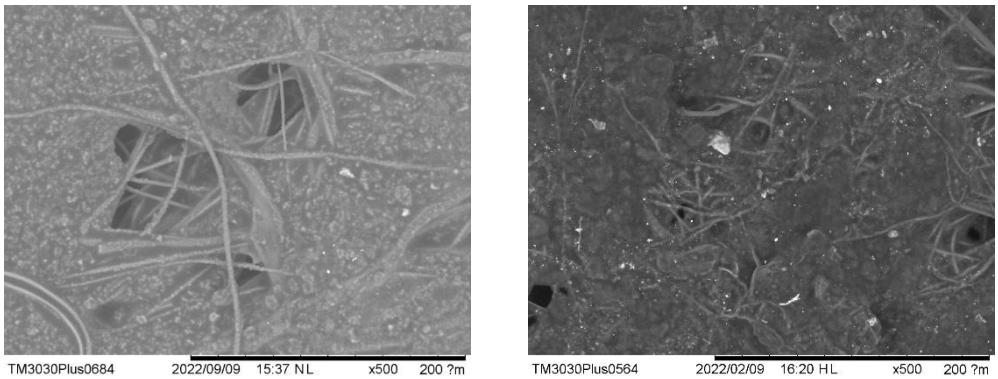

Figure 3-21: Example of carbon black fouled surface (left) compared to an engine fouled filter (right).

In order to achieve this. A solution of reference grade diesel and carbon black was made at a concentration of 2g/L. This was then stirred with a magnetic stirrer for 5 minutes to make a homogenous suspension; the carbon black was immiscible in the diesel which was desired for this process. The sample holder from the water separation rig was used to hold the sample being fouled. The

suspension was poured through the filter (being driven by gravity) and the filtrate was collected. The collected filtrate was then poured through the filter again. This was repeated so that the suspension had passed through the filter three times. The filter was then dried in an oven at 110°C for 15 minutes to remove any excess diesel. Once this was complete the sample was ready for analysis.

3.2.12 Polydopamine decoration

It was found that the carbon black fouling process was successful in replicating the physical fouling process that is seen in the field. However, in addition to physically blocking the filter there were also some chemical changes that occurred. The main result of this from a water separation efficiency was the reduction in contact angle. The carbon black did have an impact on the water contact angle of the filters; however, it was only reduced to approximately 120°C. This was not sufficiently low. Further modification was required in order to achieve a sufficiently accurate representation of the fouling that occurs in the field.

The modification technique that was identified was polydopamine decoration. The reason this was selected was that it creates a very thin film on the surface and is also known to have very good adhesive properties (184). The process of creating polydopamine is an alkali induced oxidation of dopamine. In order to achieve this a buffer solution was created using a tris buffer at a concentration of 0.05M and a pH of 8.5, the pH was achieved using concentrated HCl. Dopamine was then dissolved in 500ml of the buffer solution to create a concentration of 4g/L of dopamine. The details of the reagents used are shown in Table 3.4. The sample being coated was then placed in this solution and stirred using magnetic stirring for 24hrs. The sample was then removed from the solution and washed using de ionised water. The sample was then placed in an oven at 110°C for 15 minutes to dry. Once this was completed the sample was ready for analysis.

Table 3.4: Reagents used in the formation of polydopamine.

Reagent	Abbreviation	CAS number
Tris(hydroxymethyl)aminomethane	Tris	1185-53-1
Hydrochloric Acid	HCl	7647-01-0
Dopamine hydrochloride	DA	62-31-7

3.2.13 Dip coating

In order to determine the efficacy of the coatings performed, as well as determining the properties of interests on smaller sections of filter material. Dip coating is a commonly used method for coating, it is popular due to the ease of the process. It is possible to dip coat products as part of a continuous process, in this case a batch process was more appropriate (185). The sample is immersed in the nanoparticle containing solution, the sample is then withdrawn at a steady rate. The sample was then cured in an oven at 120°C for 30mins.

In order to ensure that the coatings were consistent a solution of methanol with a concentration of $1gL^{-1}$ of the as prepared microspheres was made. The substrates were immersed in the solution for 30 seconds to allow for completer wetting. The substrates were withdrawn as a speed of $10mms^{-1}$, this process was done by hand. Therefore, it is possible that there is some error introduced here but the control of the other parameters should ensure that this error is minimised.

Chapter 4
Analysis of field samples

4.1 Introduction

This chapter will assess returned filter samples, looking at the fouling behaviour and its effect upon the water separation efficiency. The used filters were provided by Parker Hannifin. These filters were used in three different fuel markets namely the Swedish petroleum diesel market, the Brazilian petroleum diesel market and the Brazilian biodiesel market (B100). It is known that even in petroleum diesel markets that there is a percentage of biodiesel blended to increase lubricity and reduce carbon emissions (186). For this analysis, it is assumed that the Brazilian petroleum diesel had a 10% blend of biodiesel (B10), whereas the Swedish petroleum diesel had a 7% blend of biodiesel (B7). These samples were fouled outside of a lab environment; therefore, it was not possible to control or test the fuel that was being used.

This chapter will achieve the first aim of the project, to analyse the filters used in the field and determine whether the fouling seen is specific to the region in which it was used. Additionally, the effect of the foulant on the water separation efficiency will be quantified. The physical changes to the filter will be examined using SEM for visual characterisation of the foulant material, the porometer to determine the change in pore size distribution after the fouling and again the porometer for determining the changes to permeability. The chemical change will be examined using contact angle as an analogue for the changes to the surface free energy and FTIR will be used to determine the composition of the foulant material. The changes will then be linked to the changes in water separation efficiency in order to determine any trends between the location of fouling and the drop in performance.

4.2 Materials and Methods

4.2.1 Samples being examined.

Table 4.1 shows the filters that were examined as part of this study. The ID is specific to an engine, with the number representing a unique service window. E.g., Pompe represents the vehicle, the #4 means this is the fourth filter that has been removed and sent to Parker Hannifin for analysis. Unfortunately, it was not possible to receive all the filters sent for analysis because some destructive testing is performed, not related to this project. The filters were

either removed as part of regular maintenance or if the pressure drop became so high that the engine was being partially starved of fuel. The mileage represents the distance travelled with this particular filter installed, not the mileage of the vehicle. It is immediately apparent that the Brazilian market filters (both B10 and B100) show significantly lower mileage.

Table 4.1: Filters being examined including their origin and mileage (filter ID format: 'vehicle ID' & 'filter number').

Filter ID	Country	Fuel	Mileage (km)
Pompe #4	Brazil	B100	43,836
Pompe #5	Brazil	B100	36,534
Pompe #10	Brazil	B100	29,383
Pompe #11	Brazil	B100	36,757
Adams #4	Brazil	B10	46,018
Renata #3	Brazil	B10	64,788
Renata #6	Brazil	B10	43,920
Renata #7	Brazil	B10	64,756
Hudson #2	Sweden	B7	156,414
Cook #2	Sweden	B7	159,785
Lewis #2	Sweden	B7	165,203

4.2.2 Methods

For this chapter the fouled samples returned from use in the field are examined in various ways to assess the physical and chemical changes occurring. The methods used are described in the block diagram shown in Figure 4-1. The general details of each method are given in the Methodology, if there are any deviations from this general method they will be stated below. All experiments were completed a minimum of three times using separate samples from the returned field filters. All error bars shown in figures are a standard deviation of the three results. For the FTIR results a representative result was shown, the results were extremely consistent for all samples indicating the chemical consistency of the foulant being deposited.

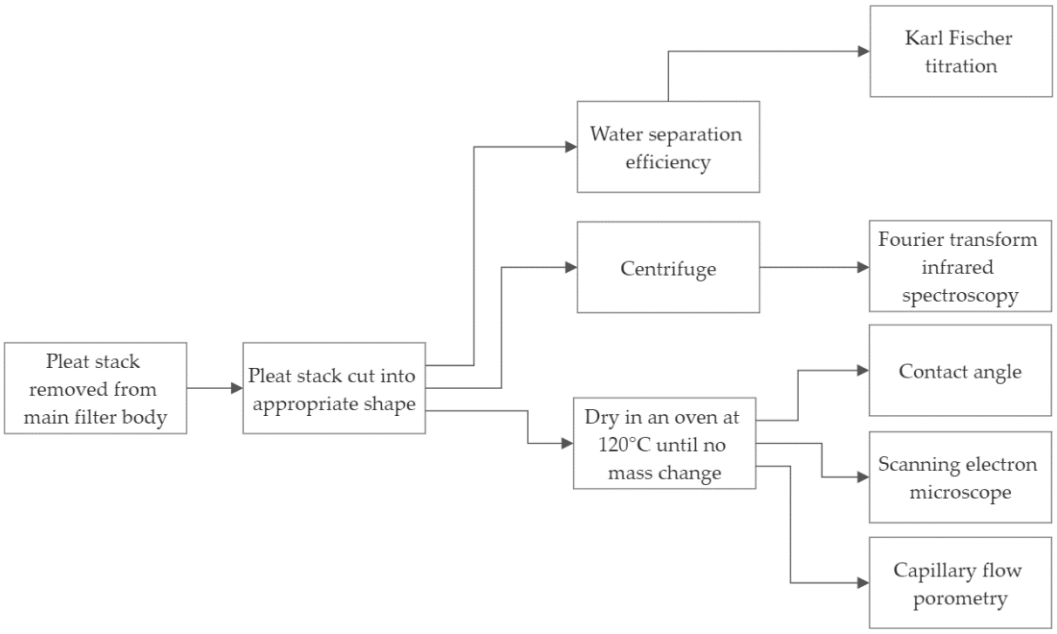

Figure 4-1: Flow diagram of the methodology for testing returned field filters.

4.3 Results

4.3.1 Water separation efficiency

Using the filter flow equipment two critical measurements were taken, the pressure drop and water separation efficiency. Table 4.2 is the data collected from the flow rig, alongside some of the gathered data during the use of the filters. In all cases the base filter material, which has not been fouled, was tested alongside the returned filters from the field. The ID of this is MSR37.

Table 4.2: Data collected from the filtration flow rig.

Filter ID	Country	Fuel	Mileage (km)	Pressure Drop (mbar)	Water separation efficiency (%)
MSR37	N/A	N/A	0	40.3	81.3
Pompe #4	Brazil	B100	43,836	62.7	56.5
Pompe #5	Brazil	B100	36,534	103.3	47.5
Pompe #10	Brazil	B100	29,383	69.7	46.1
Pompe #11	Brazil	B100	36,757	51.0	59.5
Adams #4	Brazil	B10	46,018	130.0	25.3
Renata #3	Brazil	B10	64,788	96.0	33.1
Renata #6	Brazil	B10	43,920	67.3	47.6
Renata #7	Brazil	B10	64,756	97.3	38.3
Hudson #2	Sweden	B7	156,414	71.0	33.0
Cook #2	Sweden	B7	159,785	53.0	75.8
Lewis #2	Sweden	B7	165,203	54.3	71.1

As the filters are used, insoluble particles in the fuel will become trapped within or on the surface of the filter. A simple way that this can be investigated is by examining the pressure drop across the filter at a set flow rate. The pressure drop should be a good analogue for the number of insoluble particles that have been deposited on or within the filter. Figure 4-2 shows that there is not a significant correlation between the mileage and the pressure drop.

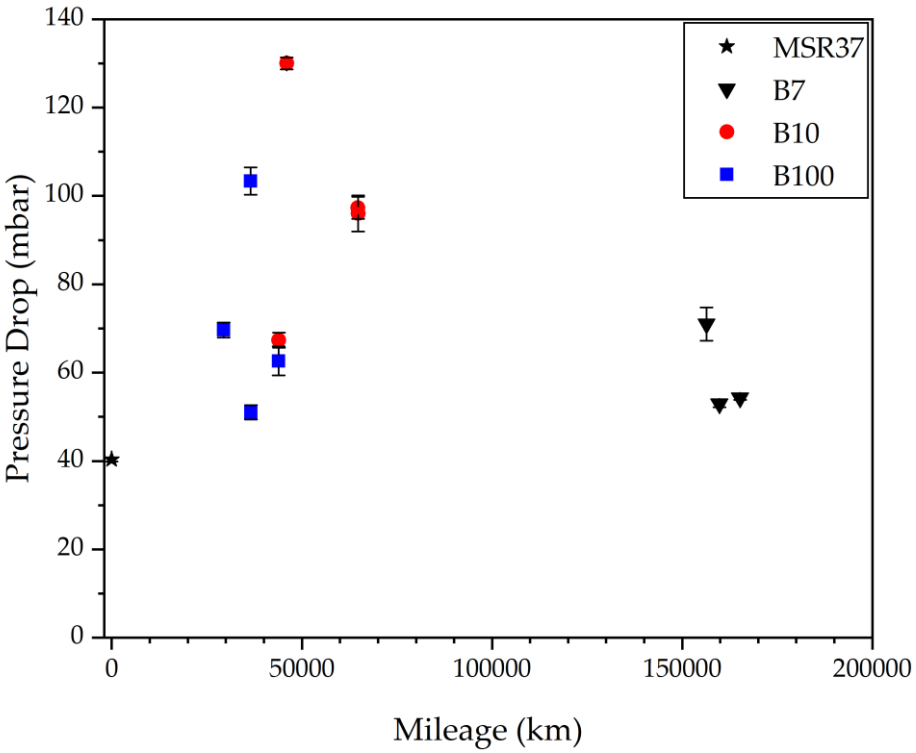

Figure 4-2: Mileage v pressure drop for the returned filter elements.

Figure 4-3 shows a comparison between the mileage and the water separation efficiency for the returned elements, including the unfouled material. Again, there does not appear to be any correlation between the mileage and the water separation efficiency looking at Figure 4-3. Table 4.2 shows the data collected for the filters examined. This suggests that the process is influenced by more than just the amount of fuel being passed through the filter. It is not the case that as the filter is used the performance declines in a predictable manner.

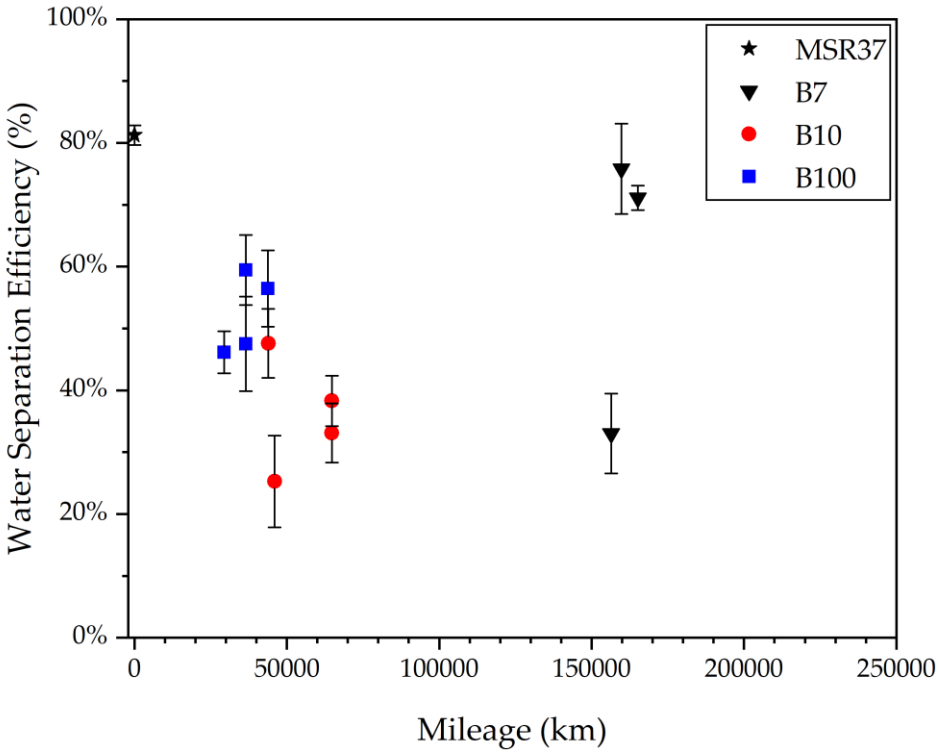

Figure 4-3: Mileage vs water separation efficiency

While it was not possible to show any correlation between the data collected from the filtration flow rig and the mileage of the filters, it was possible to show that there was a correlation between the pressure drop and the water separation efficiency. Figure 4-4 shows that a straight trendline can explain 84% of the variation in the data. While it is possible to fit a non-linear trendline to this data that provided what would appear to be a better fit, the small number of data points are susceptible to over fitting. The Boltzmann curve, shown in Figure 4-5, fit gave the fit that was best able to explain the variation in the data without obviously over fitting to the relatively small sample size.

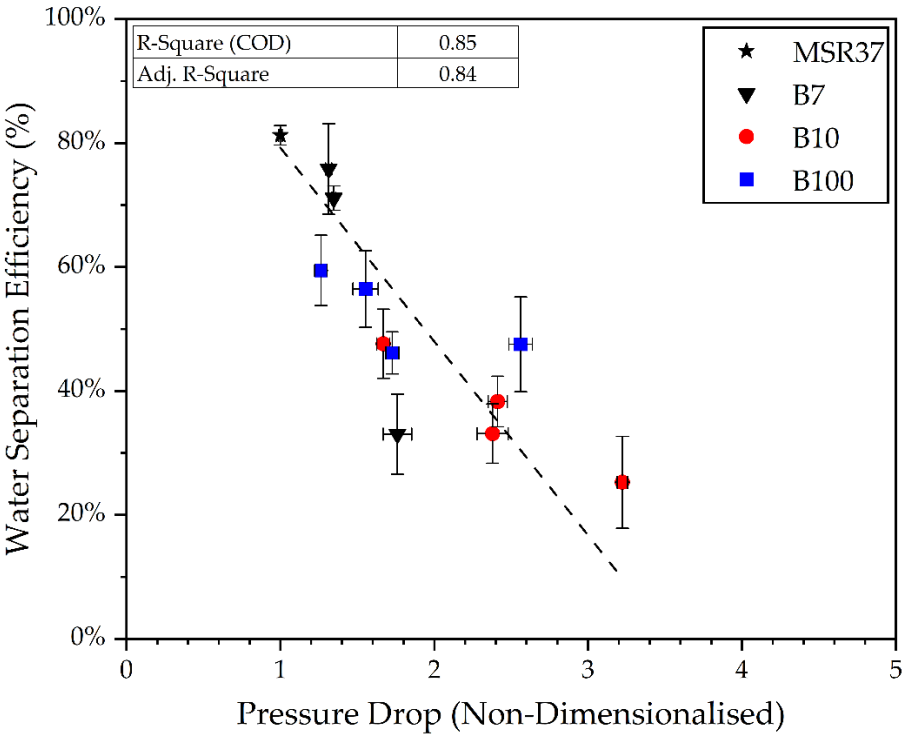

Figure 4-4: Pressure drop vs water separation efficiency: linear fit.

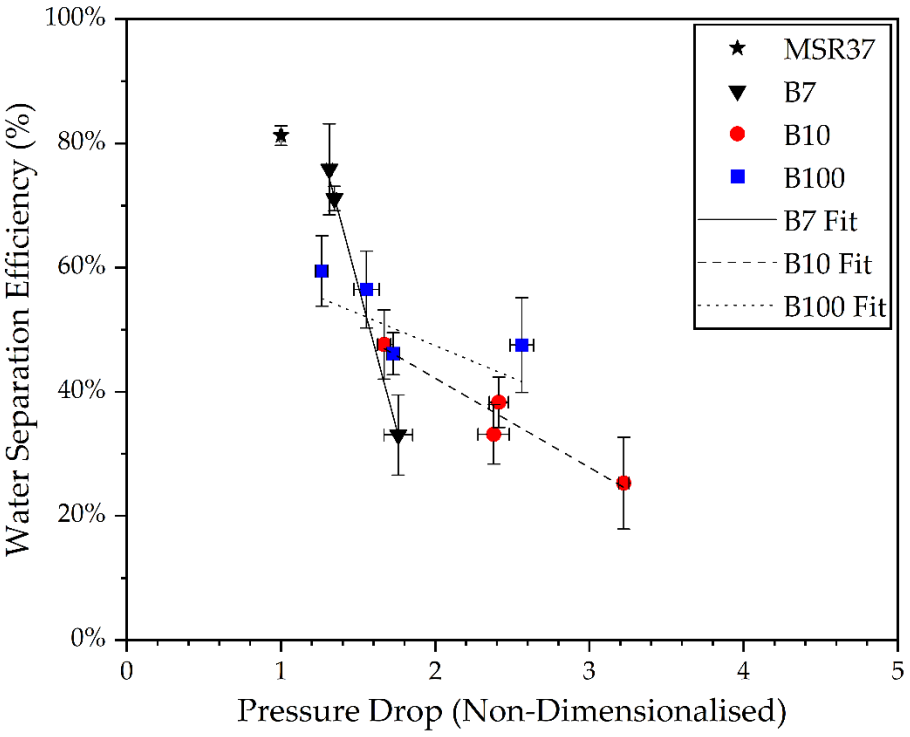

Figure 4-5: Pressure drop vs water separation efficiency: Individual fits.

4.3.2 Contact angle.

The pressure drop is a good analogue for the physical changes that occur within the filter, but there will be chemical changes that also occur. One of the key things that is needed in a surface filter that separates water in diesel

emulsions is a hydrophobic surface. As the fibres at the surface are coated in foulant material, the hydrophobicity is likely to decrease. The reason for this is that diesel is a non-polar solvent, meaning that the compounds that are most likely to be insoluble are polar (187). It is also well known that polar surfaces will result in hydrophilicity (188). Figure 4-6 compares the water contact angle measured with the water separation efficiency determined using the flow rig.

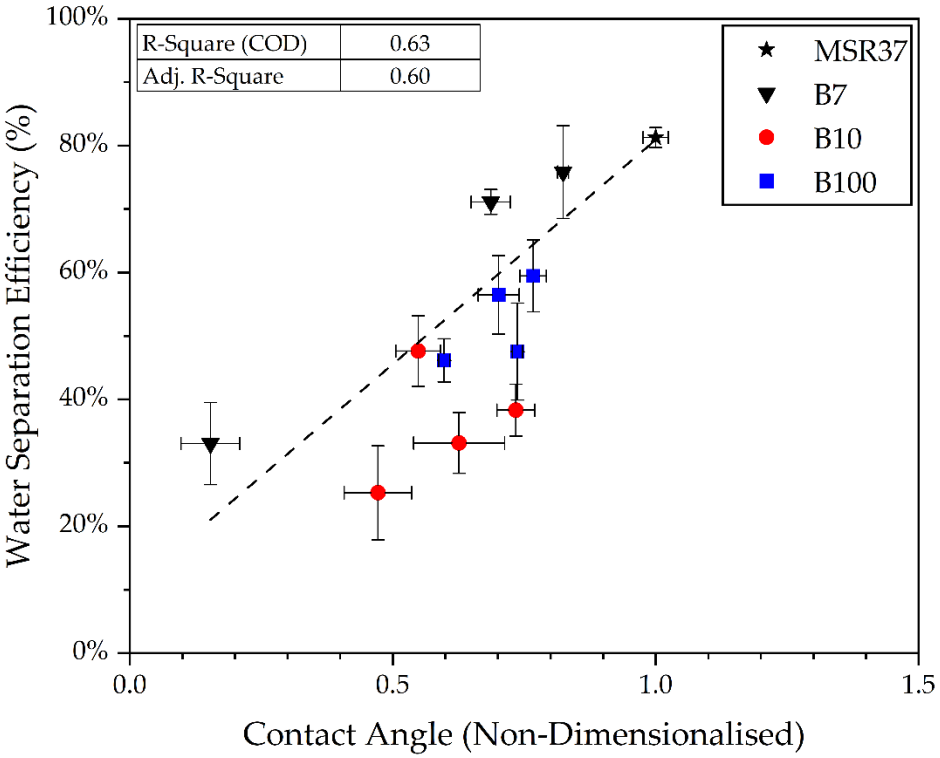

Figure 4-6: Contact angle vs water separation efficiency: linear fit.

Figure 4-6 shows that there is a clear relationship between the water contact angle and the water separation efficiency. It is not possible to analyse the effects of contact angle and pressure drop separately using the returned samples, this is a potential issue because there is an interdependency between them, shown in Figure 4-7. The interdependency is present because the root cause is foulant material being deposited on the surface. Foulant material has two effects, it blocks pores resulting in an increase in pressure drop across the filter. It also is hydrophilic and as it coats the fibres the contact angle is decreased.

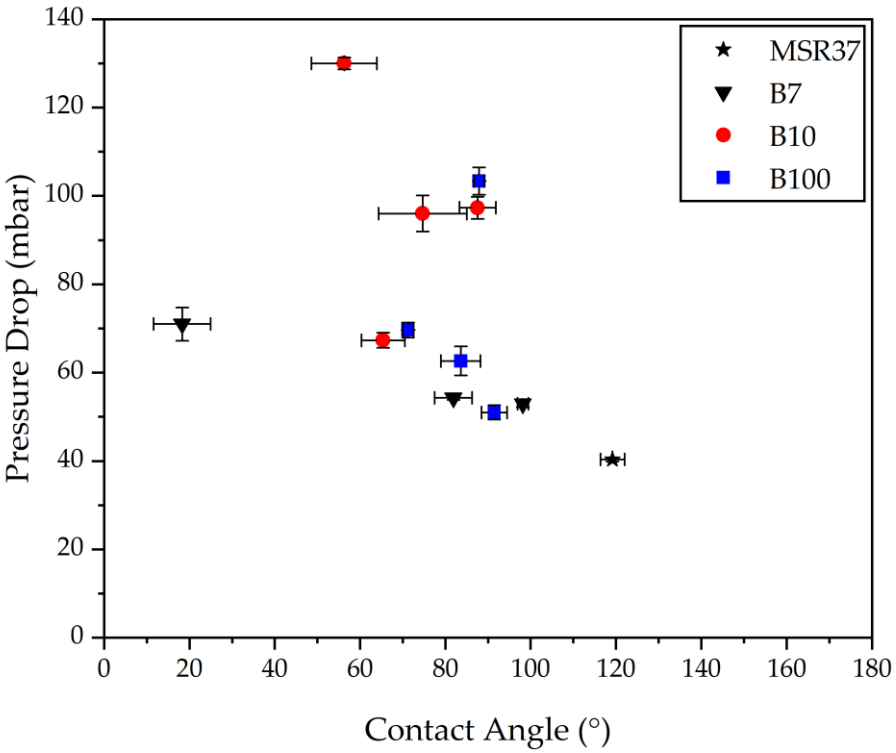

Figure 4-7: Interdependency between contact angle and pressure drop.

4.3.3 Scanning electron microscope

While it has been possible to show that the pressure drop is a relatively good analogue for the level of restriction, the way in which this restriction presents itself is also of interest. Using SEM imaging it has been possible to show the general type of fouling that is seen on the surface of the fibres. Figure 4-8 shows the clean fibres, where Figure 4-9 through Figure 4-19 show the fouled filters. Using these images, the type of fouling behaviour was categorised into either, inter-pore fouling, partial cake layer, full cake layer, or a combination of inter-pore fouling and partial cake layer. Table 4.3 shows the types of fouling behaviour as determined from the SEM images.

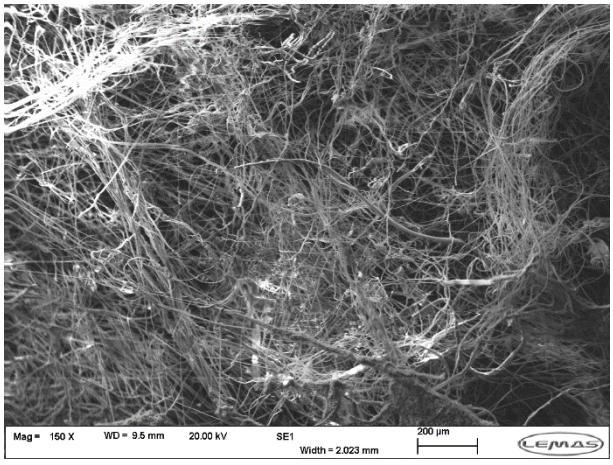

Figure 4-8: SEM image of clean filter material.

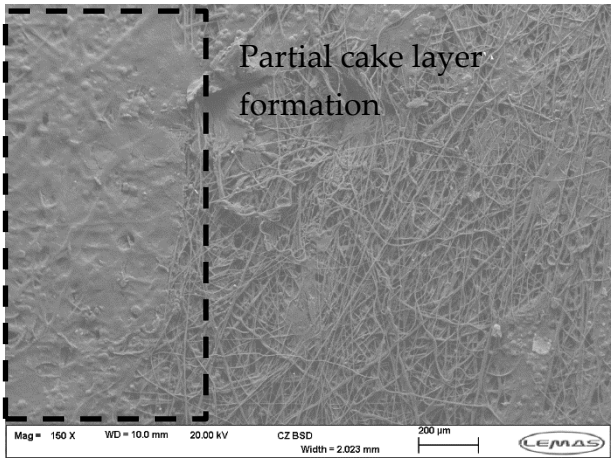

Figure 4-9: SEM image of Hudson #2 (B7)

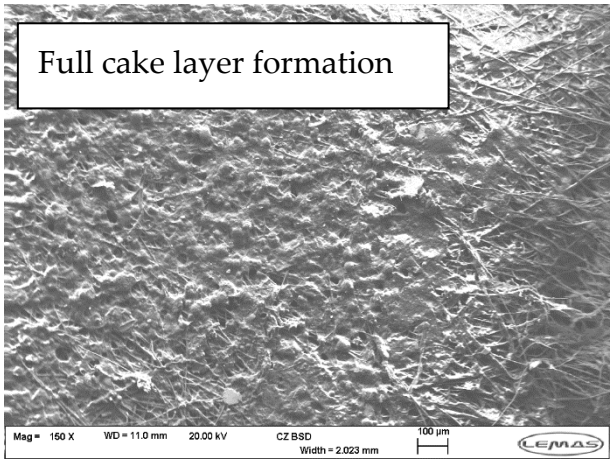

Figure 4-10: SEM image of Cook #2 (B7)

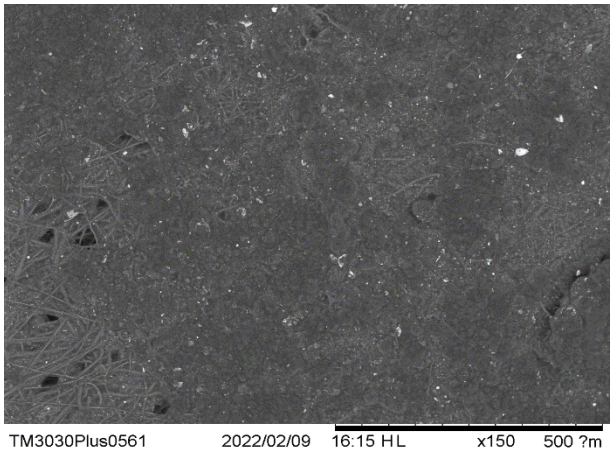

Figure 4-11: SEM image of Lewis #2 (B7)

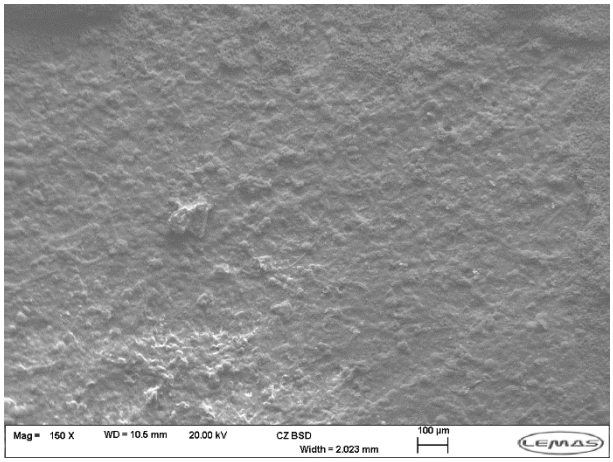

Figure 4-12: SEM image of Adams #4 (B10)

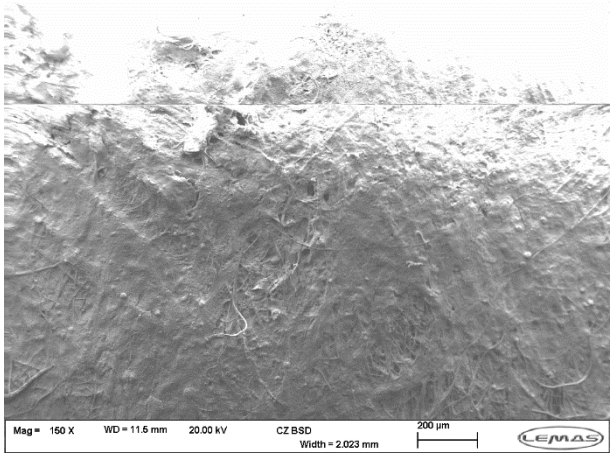

Figure 4-13: SEM image of Renata #3 (B10)

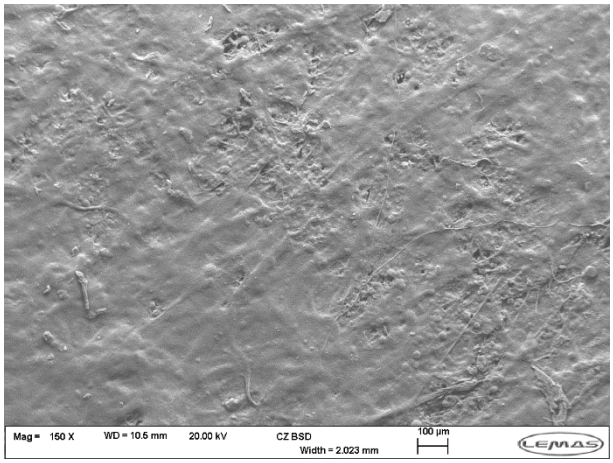

Figure 4-14: SEM image of Renata #6 (B10)

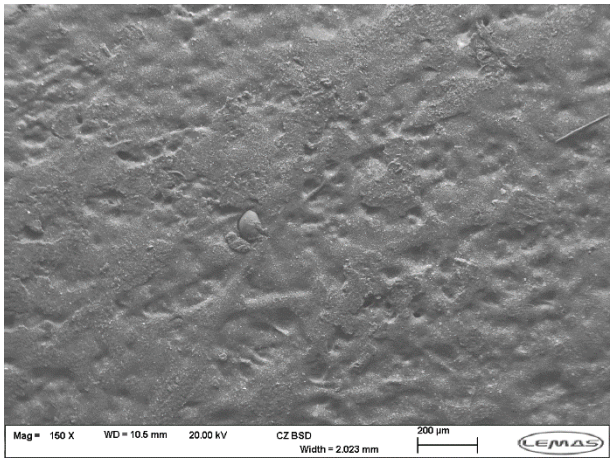

Figure 4-15: SEM image of Renata #7 (B10)

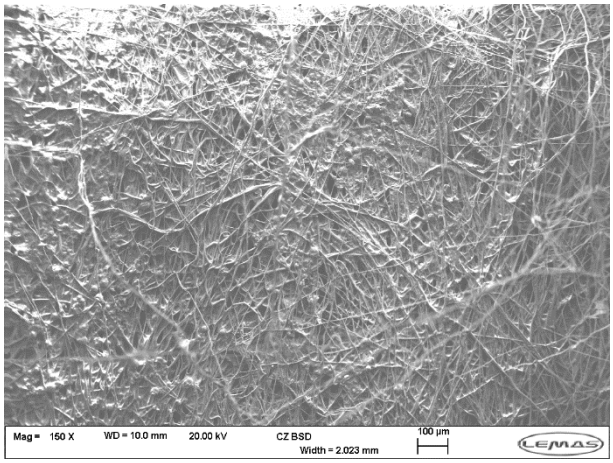

Figure 4-16: SEM image of Pompe #4 (B100)

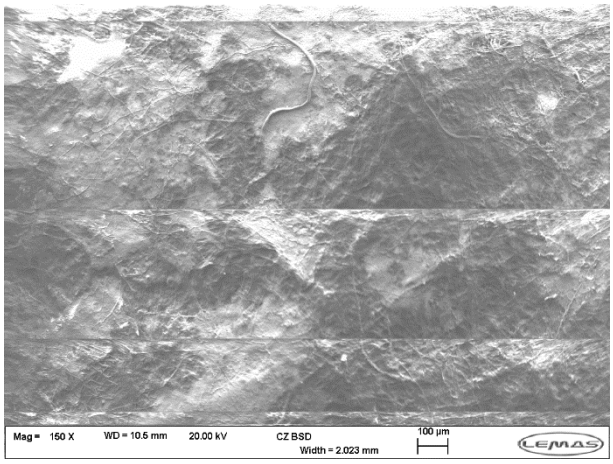

Figure 4-17: SEM image of Pompe #5 (B100)

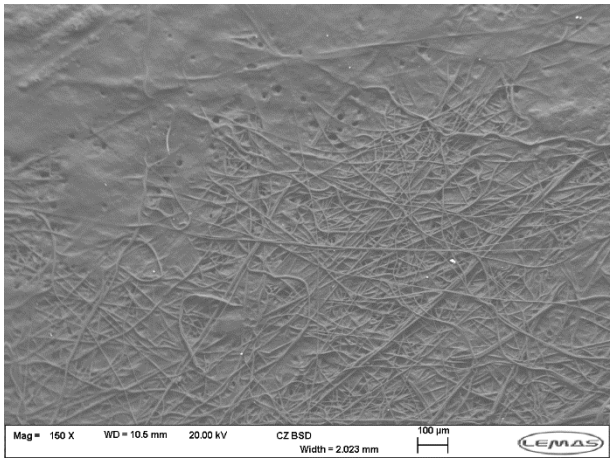

Figure 4-18: SEM image of Pompe #10 (B100)

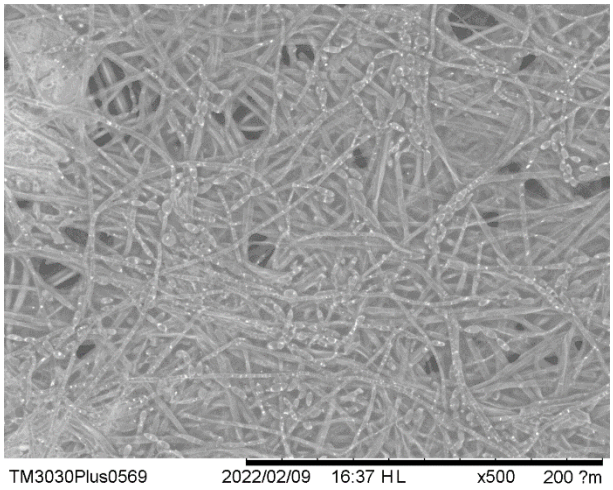

Figure 4-19: SEM image of Pompe #11 (B100)

Table 4.3 shows the type of fouling that was identified using the SEM imagery, in all cases the images are representative of what was seen. The type of fouling was determined from a minimum of 5 different points around the sample or through examining the surface during the scanning process. It should be noted that the samples examined were very small in comparison to the filter pack as a whole. No attempt was made to determine if there was a difference in fouling at different points on the filter, it was assumed to be homogenous.

Looking at the relationship between the type of fouling seen and the cake layer, there doesn't appear to be any significant correlation between the pressure drop and the type of fouling. This could suggest two things, the fouling is not as homogenous as first thought. The other possibility is that the fouling at the surface is not the factor that is determining the increase in restriction seen in these samples. It is likely that the fouling through the depth of the filter is more significant, this is not something that could be determined using SEM imagery.

Table 4.3: Table of the fouling behaviours identified using SEM imaging.

Filter	Fuel Market	Type of fouling	Pressure Drop (mbar)
Hudson #2	B7	Partial cake layer	62.7
Cook #3	B7	Inter pore & partial cake layer	103.3
Lewis #2	B7	Full cake layer	69.7
Adams #4	B10	Full cake layer	51.0
Renata #3	B10	Full cake layer	130
Renata #6	B10	Inter pore & partial cake layer	96
Renata #7	B10	Full cake layer	67.3
Pompe #4	B100	Inter-pore	97.3
Pompe #5	B100	Partial cake layer	71
Pompe #10	B100	Inter pore & partial cake layer	53
Pompe #11	B100	Inter-pore	54.3

4.3.4 Pore size distribution

It is possible to determine the pore size distribution using capillary flow porometry; this can give information on how the fouling behaviour has influenced the pore size distribution, the technique is fully explained in Chapter 3 (Methodology). Figure 4-20 through Figure 4-22 show the pore size distributions of the returned filters grouped into the fuel markets in which they were used.

The general trend seen in the B7 fuel market (Figure 4-20) is that the average pore size decreases. It should be noted that the pore size distribution gives no information on the number of pores, only the percentage of the total pores that are of a certain size. There is an obvious exception to this rule in Hudson #2. A possible way in which fouling could present itself in this data is that after a low level of fouling pores begin to restrict creating smaller pores as shown for The Cook and Lewis filters. As fouling continues more of the smaller pores are blocked completely leaving only the larger pores open. If

this were true it would be expected that the pressure drop for Hudson #2 would be higher, this is the case (71mbar compared to ~53mbar) so this theory is possible. A different deposition mechanism in which the smaller pores are preferentially blocked is another possible theory. The difference in pressure drop does not rule this out. As mentioned, the main contributor to pressure drop is the number of available pores. However, the SEM image (Figure 4-9) does not show this, instead showing a partial cake layer being formed and no preferential deposition. If smaller pores were being preferentially blocked, it would be expected that some form of inter-pore fouling would be dominant.

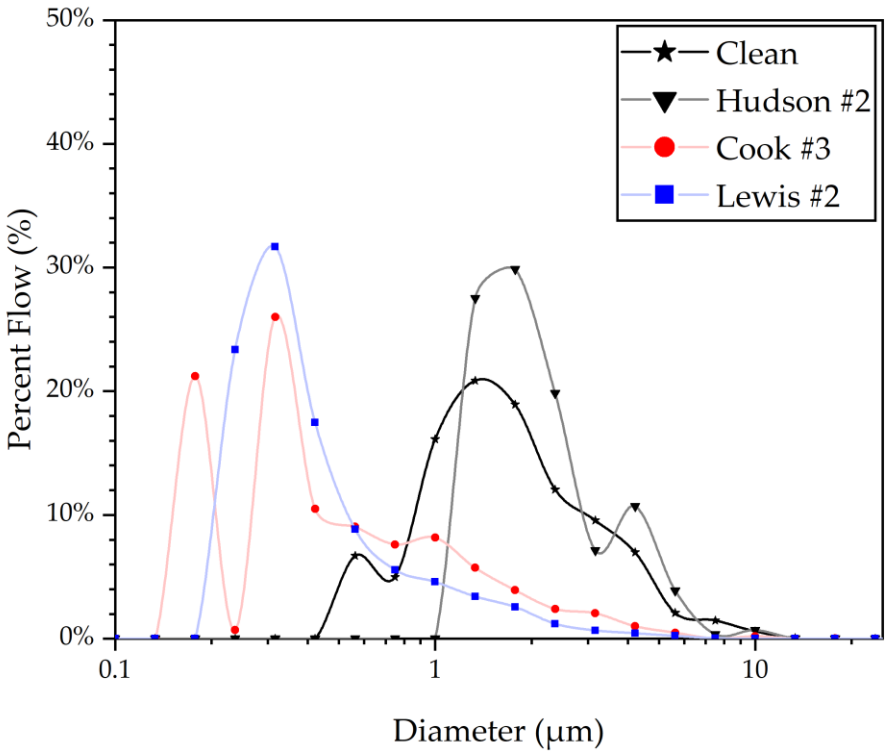

Figure 4-20: Pore size distribution for filters fouled in the B7 market.

The B10 fuel market appears to favour the formation of cake layers resulting in a reduction in the average pore size. The one filter that does not follow this trend is Renata #6. However, it does appear that a partial cake layer has formed on the surface. Again, it is theorised that Renata #6 is in an early stage of the fouling process compared to the other three filters fouled in this market, this is confirmed when looking at the SEM images. A facile method for confirming this is to look at the pressure drop. For the filters with a cake layer, the percentage increase in pressure drop compared to a clean filter is between 138% and 223%. The Renata #6 sample shows only a 67% increase in pressure drop. This gives some confidence to the theory that the Renata #6 sample is in an earlier stage of fouling.

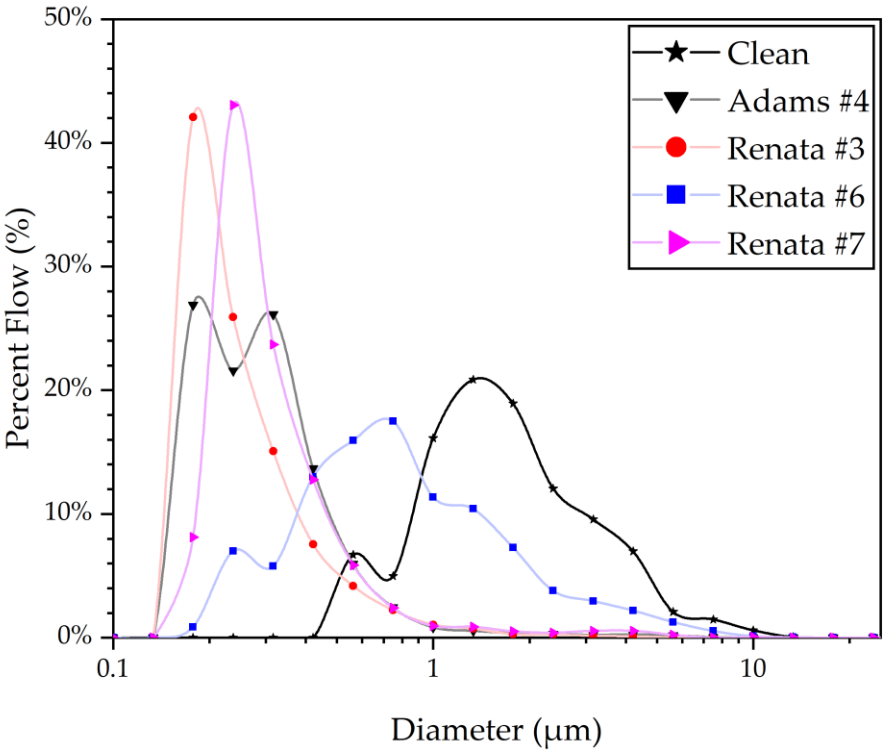

Figure 4-21: Pore size distribution for filters fouled in the B10 market.

The filters fouled in the B100 fuel market appear to exhibit a tendency towards inter-pore fouling and partial cake layer. Two of the filters display a slight reduction in the average pore size (Pompe #4 and Pompe #5, Figure 4-22). One filter saw an increase in average pore size (Pompe #11, Figure 4-22). The final filter saw a decrease in average pore size, similar to what is seen in the cake layer samples (Pompe #10, Figure 4-22). The filter with the greatest increase in pressure drop was Pompe #5, with an increase of 156%. This highlights the danger of characterising with SEM imaging or pore size distributions alone, looking at both of these data it would not be expected that the pressure drop would be highest compared to the other B100 filters. A possible reason for this is that the fouling is occurring within the depth of the filter, which will not be seen by the SEM looking at the surface.

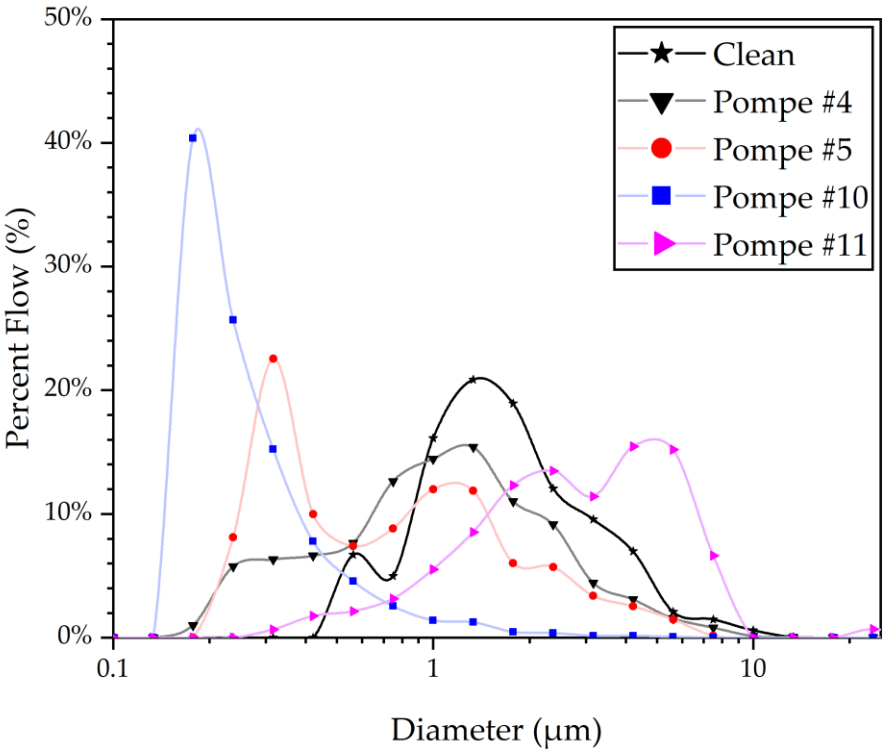

Figure 4-22: Pore size distribution for filters fouled in the B100 market.

Grouping the filters into the fouling behaviours that were identified and tabulated in Table 4.3, makes it possible to better identify the effects that the fouling behaviour has on the pore size distribution. Figure 4-23 shows the pore size distributions of the filters identified as having cake layer formation. All of the average pore sizes have decreased significantly, and now lie in the 0.1 – 0.5µm range. The consistency of pore sizes for this type of fouling behaviour gives confidence to the SEM method for identifying cake layer formation. The same cannot be said for identifying partial cake layer formation (Figure 4-24), the two filters identified as having this type of fouling behaviour exhibit drastically different changes in pore size distribution. One possible reason for this is the inherent heterogeneity of the fouling, and possible fouling below the surface of the filter that cannot be seen by the SEM.

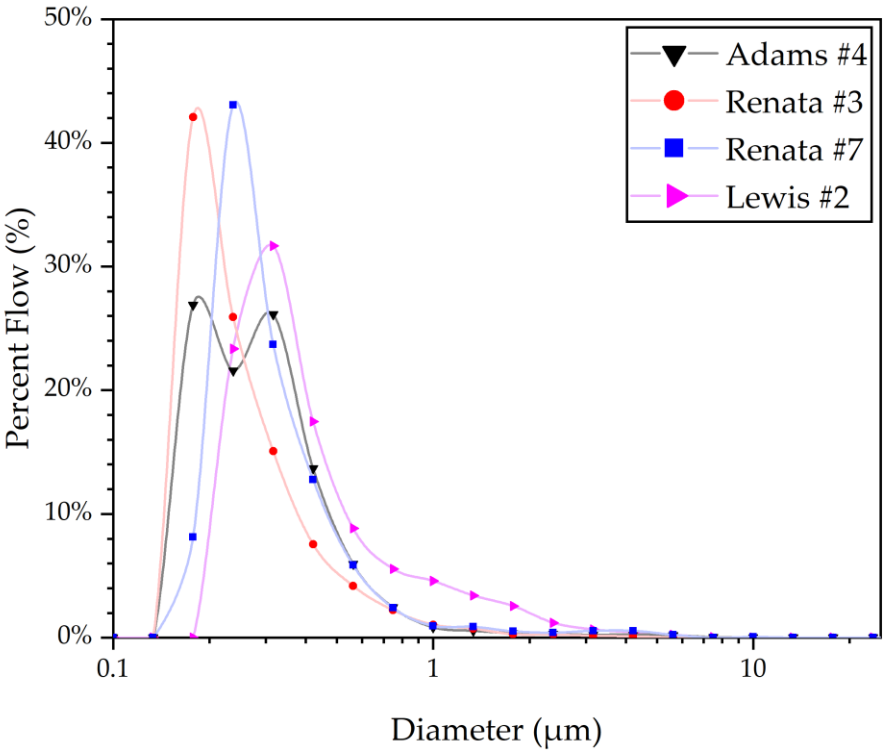

Figure 4-23: Pore size distribution for filters identified as having a full cake layer.

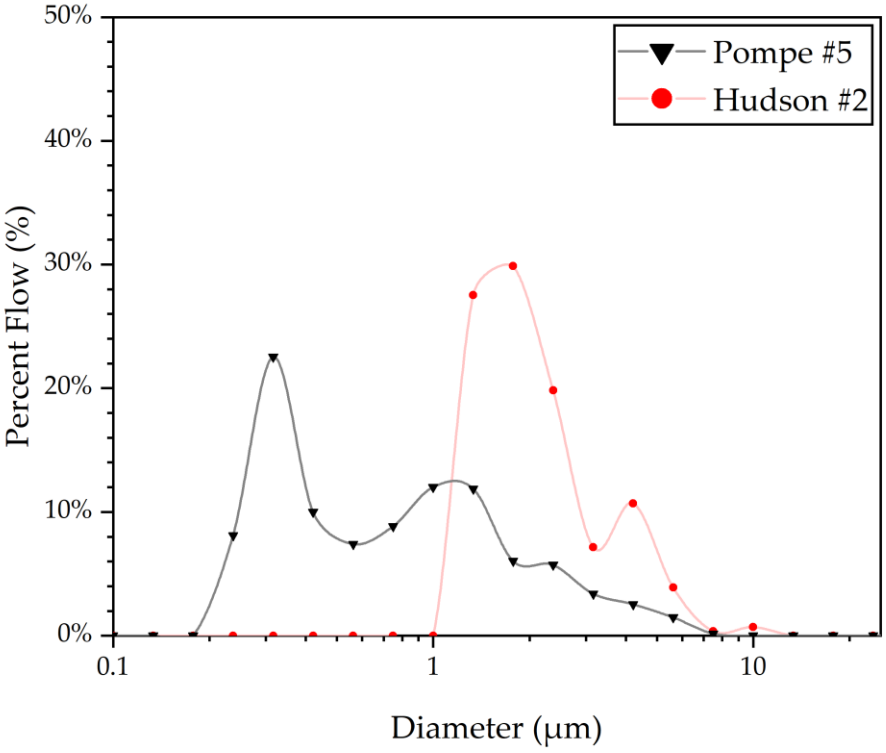

Figure 4-24: Pore size distribution for filters identified as having a partial cake layer.

There are again some stark differences when comparing the pore size distribution of filters identified as having inter pore fouling (Figure 4-25), one

thing in common between the two filters is a broadening of the distributions. Where they differ is the average size shift. A similar observation can be made for the filters identified as having inter pore fouling and a partial cake layer (Figure 4-26). Overall, there is a general trend of the average pore size reducing, however the degree to which this happens is quite varied.

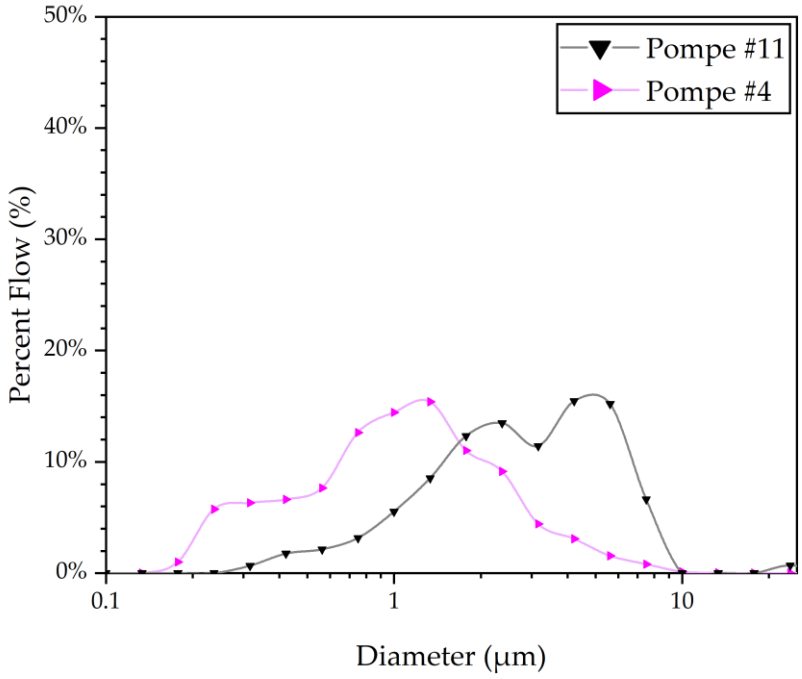

Figure 4-25: Pore size distribution of filters identified as having inter pore fouling.

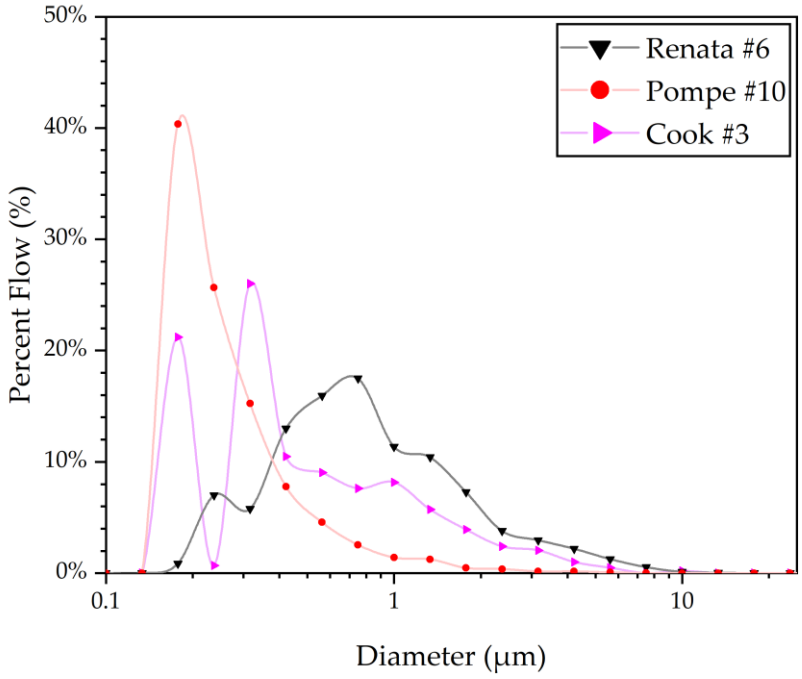

Figure 4-26: Pore size distribution for filters identified as having inter pore fouling and a partial cake layer.

4.3.5 Air permeability

In addition to pressure drop, air permeability was also used as a secondary measure of the level of blockage seen in the filters. It would be expected that the pressure drop, and air permeability would be proportional. However, it was found that this rule did not hold. There is a large jump in air permeability for the clean filter compared to fouled filters; this is not reflected in the pressure drop data. The relationship between the pressure drops and air permeability for the fouled filters is linear as would be expected.

One thing to note is that the pressure drop measurements were made during the water separation testing. This may result in the deposition and coalescence of water droplets on the surface. It is likely that once the foulant has been deposited on the surface the roll off angle will be increased leading to the capture of water on the surface. This will result in increased pressure drop through pore blockage. However, this will not be captured by the air permeability measurement. Figure 4-27 shows the relationship between pressure drop and the air permeability measured. The filters have been separated into the fuel markets in which they were fouled to see if there is any correlation.

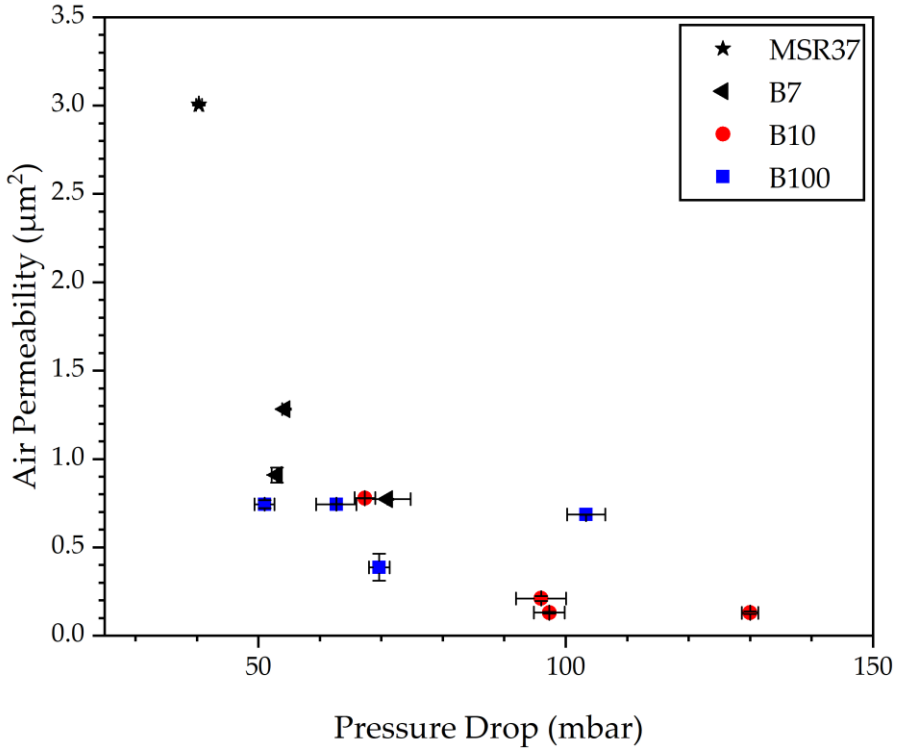

Figure 4-27: Relationship between pressure drop and air permeability.

There is a trend in the air permeability with respect to the fuel market with B10 fuel market followed by B100 and finally the B7 fuel market.

4.3.6 Fourier transform infrared spectroscopy.

For this work only the general structure of the molecules that have fouled the filters is of interest. It is possible to compare the structure of the foulant material deposited in different fuel markets. The most important aspects of the FTIR spectra in this case is the oxygen functionality, an increase in oxygen functionality will likely mean an increase in polarity. As has been mentioned previously an increase in polarity would result in an increase in hydrophilicity eventually leading to filter failure with respect to water separation efficiency.

Figure 4-28 shows the B7 fuel market FTIR spectra, Figure 4-29 shows the B10 fuel market FTIR spectra and Figure 4-30 shows the B100 fuel market FTIR spectra. Two peaks that are common in all of the spectra are at 2920cm^{-1} and 2850cm^{-1} (189); they are associated with symmetric and asymmetric methylene stretching respectively. There are also two partially obscured peaks present one at approximately 2955cm^{-1} and the other appears as a shoulder slightly lower than 2850cm^{-1} (189), these are associated with symmetric and asymmetric methyl stretching respectively. The lack of prominence of the methyl peaks suggests that the carbon chain lengths are relatively long. Additionally, there is a peak at 720cm^{-1} which is often attributed to the methylene $-(CH_3)_n-$ rocking, where $n \geq 3$. This supports the theory that the chain lengths of the hydrocarbons are relatively long (189).

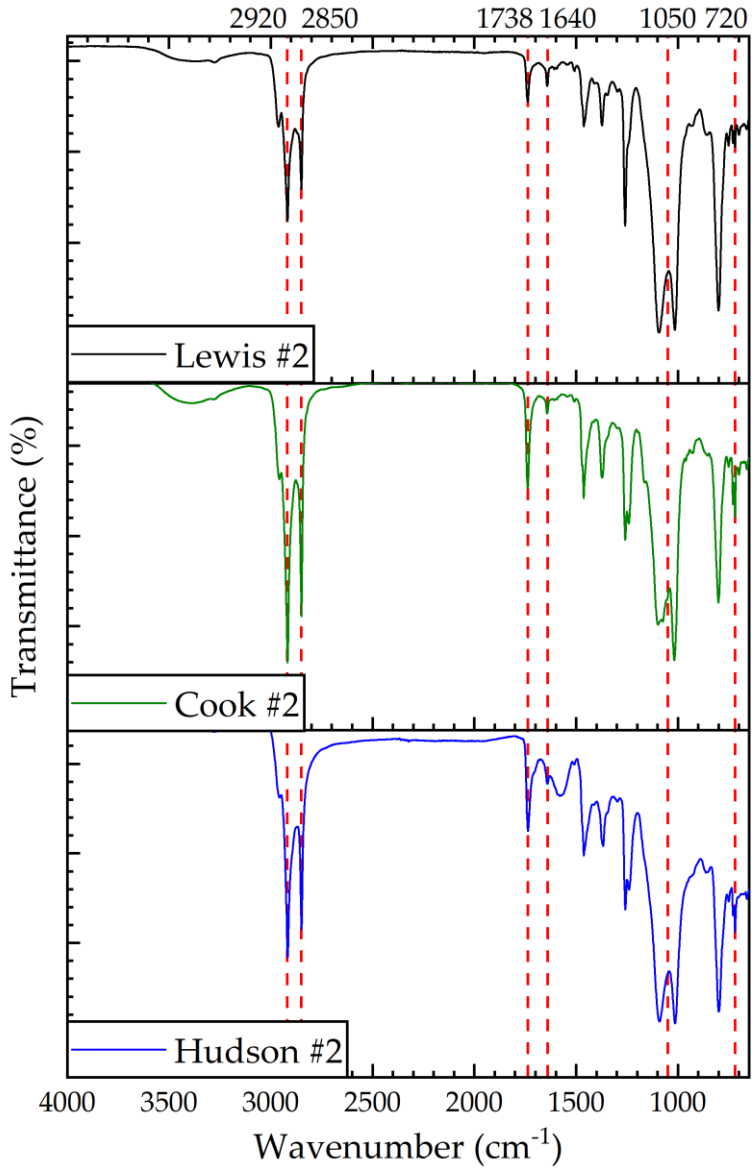

Figure 4-28: FTIR spectra for the foulant found in the B7 fuel market.

The peak at approximately 1640cm^{-1} is not present in all spectra, showing greatest intensity in Renata #3 and Renata #7 (Figure 4-29). The most likely cause of this peak is from the C=C bond in unsaturated hydrocarbons, this is probably present in a complex system similar to an asphaltene. A peak at approximately 1560cm^{-1} indicates the presence of carboxylate salts, a well reported contaminant leading to premature filter blockages (37, 190-192).

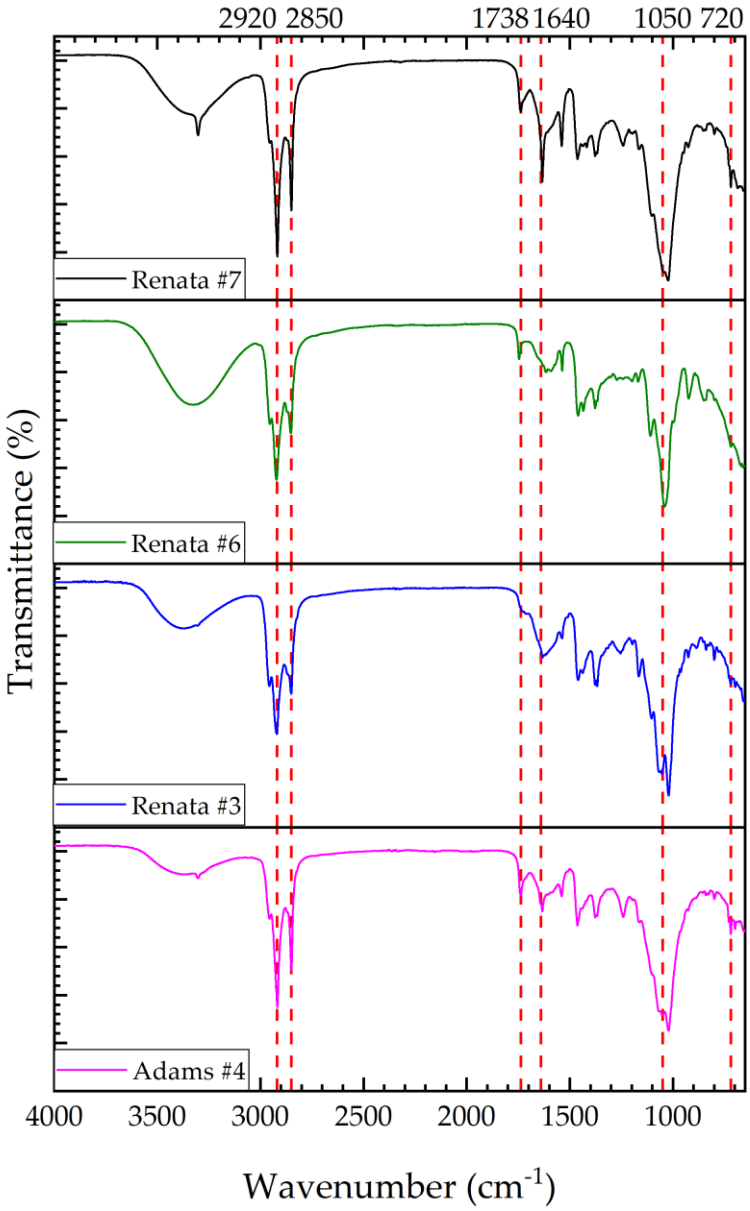

Figure 4-29: FTIR spectra for the foulant found in the B10 fuel market.

Oxygen functionality is represented by a number of different peaks. The broad peak at 3350cm^{-1} is caused by O-H stretching from a hydroxyl group; this is seen most prominently in the B10 filters. The peak at 1738cm^{-1} is associated with the C=O stretching from an ester, this is indicative of the biodiesel content in the fuels being used (189). Renata #3 (Figure 4-29) is the only spectrum that does not exhibit a prominent peak at 1738cm^{-1}, however there is a shoulder on the adjacent 1640cm^{-1} peak. The relatively prominent peak at 1640cm^{-1} is likely merging with the peak at 1738cm^{-1} obscuring it from view (189).

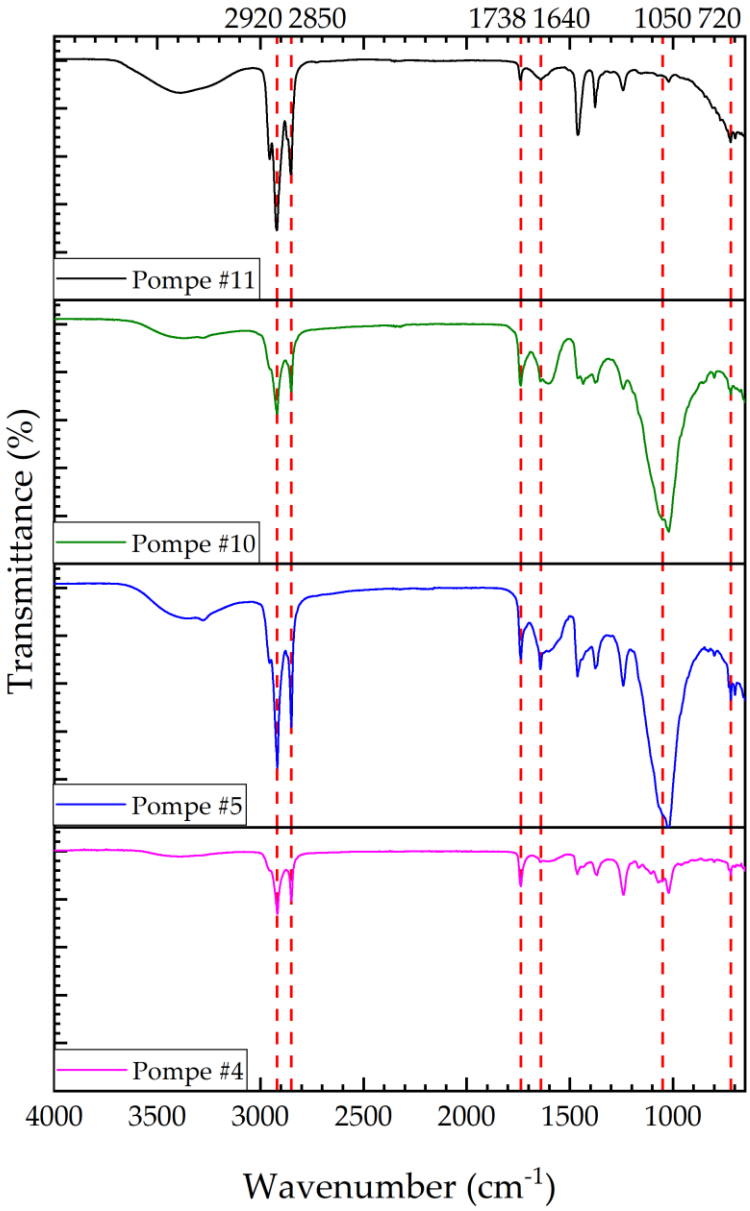

Figure 4-30: FTIR spectra for the foulant found in the B100 fuel market.

Other peaks that are known to represent oxygen functionality are seen between 1200cm^{-1} and 1000cm^{-1}, there are a number of peaks in this area making the identification of individual peaks challenging. Stretching of the O-CH$_3$ bond will exhibit a peak between 1188cm^{-1} and 1200cm^{-1}, this is indicative of biodiesel content. Another peak also caused by esters can be seen between 1050cm^{-1} and 1150cm^{-1} is caused by C-O stretching (193). There are numerous possible alcohol C-O bond stretches between 1050cm^{-1} – 1150cm^{-1} (194). Compounds of interest that can be identified by peaks in this section of the spectrum are glucosides, it is well reported that glucosides can cause significant increases in filter blocking rates (195). Using both FTIR and time of flight secondary-ion-mass-spectrometry, Felder et al. (191) determined that the glucosides exhibited peaks between 1000cm^{-1} and 1200cm^{-1}.

4.4 Discussion

There is a general trend of the B10 filters exhibiting higher pressure drop on average followed by the B100 and finally the B7 filters. It should be noted that these filters have a large range in mileages with the European B7 fuel market filters being able to run for a significantly higher mileage, therefore a lower rate of blockage when compared to Brazilian fuel markets. The main reason for this is likely the fuel quality. It was not possible to determine the fuel quality directly because the filters were fouled in real engines; it was not feasible to get fuel samples from these engines. Even if fuel samples were taken at the time the filters were removed, it could not be guaranteed that this would be representative of the fuel seen by the filter throughout its life.

The quality control of the biodiesel is a vital to avoiding premature blockage of filters. Metal contaminants are known to react with carboxylic acid-based additives forming carboxylic soaps. These compounds are insoluble in diesel causing them to become trapped at the surface of the filter (196). The FTIR spectra (Figure 4-28 through Figure 4-30) show that the carboxylate salts identified by a peak at 1560cm^{-1} are more prominent in the Brazilian fuel markets. Another element related to fuel quality is the feedstock used for the biodiesel, there are many different feedstocks used throughout the world. Examples are rapeseed oil, palm oil, soy bean oil, castor oil or animal tallow (197). The most common feedstock used in Brazil is soy bean oil, whereas in Europe the most common feedstock is rapeseed oil (198).

It has been reported that different feedstocks can lead to varying levels of blocking tendency. Fersner and Galante-Fox (33) conducted a study looking at the blocking tendency of B10 biodiesel blends in which the biodiesel was sourced from various feedstocks. The feedstocks examined were cooking oil, soybean oil, coconut oil and rapeseed oil. It was found that the rapeseed oil had the lowest filter-blocking tendency, while the soybean oil had the worst filter-blocking tendency (33). This concurs with what has been seen in our study, both the Brazilian fuel market filters become blocked at far lower miles than the Swedish filters.

The general structure of the foulant material has been identified using FTIR; it was identified as a relatively long chain hydrocarbon with a fair amount of oxygen functionality. There were some notable differences between the filters fouled in different fuel markets. The B7 fuel market filters have far fewer carboxylates (identified by the 1560cm^{-1}) when compared to the B10 fuel market filters. The presence of carboxylates is usually associated with

increased blocking (196), being that the B10 fuel market filters block at a faster rate compared to the B7 fuel market filters it follows that the carboxylate content is higher. The intensity of a peak cannot be directly compared to the intensity of another peak to determine compositional fractions. Lacey et al. (190) identified carboxylates on injector deposits, it was found that the identifying peak (1560cm^{-1}) was very prominent. This is not the case for the spectra produced in this study, suggesting that the proportion of carboxylates in the foulant material is quite low comparatively.

Another contaminant is often reported as having an impact upon the rate of blocking is glucosides. As has been mentioned the peak that is likely associated with this is located between 1000cm^{-1} and 1100cm^{-1} (191, 199-201). The filters fouled in the B100 fuel market shown in Figure 4-30 show an interesting trend here. Pompe #5 and #10 have prominent peaks between 1000cm^{-1} and 1100cm^{-1} that can be attributed to sterol glucosides, in contrast Pompe #4 and #11 do not show peaks here. The interesting aspect can be seen when looking at the pressure drop; the filters showing the presence of glucosides have significantly higher pressure drops when compared to the ones without.

The contact angle is also somewhat dependant on the fuel market in which the filter was used. This is only true for the B100 and B10 fuel markets, with the B10 overall having lower contact angles than the B100. The B7 fuel market filters have a broad range of contact angles. This does not agree with the results of the FTIR spectroscopy, which suggested that the composition of the foulant material was relatively constant. It may be that a small fraction of the composition is having a more significant effect upon the wettability than was first thought.

One possible reason for this is the physical nature of the foulant. If a cake layer is formed on the surface, a relatively impermeable layer is present for the droplet to sit on. However, if the fibre is coated in foulant material, there are a large number of open pores, and the wettability is lowered to a point below and equivalent 90° contact angle the droplet will likely fall through the porous network leading to a lower contact angle. It should be noted that the size of the droplet in the contact angle experiment is significantly larger than the droplets in the water separation experiments. This means that while the cake layer is relatively impermeable with respect to the size of droplet in the contact angle experiment, it does not mean that it will be impermeable to the smaller droplets within the water separation experiments.

It was shown that the contact angle has an inversely proportional relationship with the water separation efficiency (Figure 4-6); this is what would be expected from theory. According to the Young-Laplace equation the lower the contact angle the lower the force required to force a droplet through a porous surface (95).

SEM imaging was used to display that the B10 fuel market filters had the most prominent cake layer formation. The B7 filters did not show any consistent type of fouling and the B100 filters showed a tendency towards inter-pore fouling (Table 4.3). This is also shown in the capillary flow porometry data, a full cake layer results in a significant decrease in average pore size, along with a narrowing of the distribution (Figure 4-23). A similar trend is seen for the partial cake layer and partial cake layer with inter pore fouling, Figure 4-24, the average pore size decreases. Having said this there is more variability in the pore size distribution for the filters displaying partial cake layer formation. The nature of partial cake layer formation leads to heterogeneity; this explains the larger variation in the pore size distribution. Additionally, the area examined using the SEM is relatively small, this could lead to categorising incorrectly. There are not sufficient filters identified as having inter-pore fouling to make any comments on the change to pore size distribution.

The air permeability does not match up with the pressure drop observed. The air permeability of the clean filter is significantly higher than would be expected, if the relationship between air permeability and pressure drop was linearly inversely proportional. Darcy's equation (3-2) shows that theoretically permeability (k) is inversely proportional to the pressure drop (ΔP). As a result of the fouling process the contact angle is reduced, additionally it is likely that the roll off angle is increased. This will result in droplets of water being trapped at the surface. This will lead to a form of fouling in which the droplets will effectively block the pores.

It has been possible to show that as expected there are two things that affect the water separation efficiency. The flow dynamics of the emulsion through the filter, examined primarily using the pressure drop, and the chemical changes to the surface of the filter, examined primarily using the contact angle. As the filter was fouled the pressure drop increased the water separation efficiency decreased, using pressure drop alone it was possible to explain approximately 84% of the variation in the data. Contact angle could only explain 60% of the variation in the data if used as the lone predictor. It

was also shown that the pressure drop and contact angle were interdependent.

If both parameters are combined, it is possible to improve the prediction. The parameters are combined by dividing the pressure drop (inversely proportional) by the contact angle (proportional). The contact angle was non-dimensionalised by dividing the filters contact angle by the contact angle of a pristine filter. The pressure drop was non-dimensionalised using the Euler number. The equation defining the Euler number is shown below. ΔP is the pressure drop, ρ is the density and u is the fluid velocity.

$$Eu = \frac{\Delta P}{\rho u^2} \qquad \textbf{4-1}$$

Figure 4-31 shows that by combining the analogues used in this work to describe the physical and chemical changes.

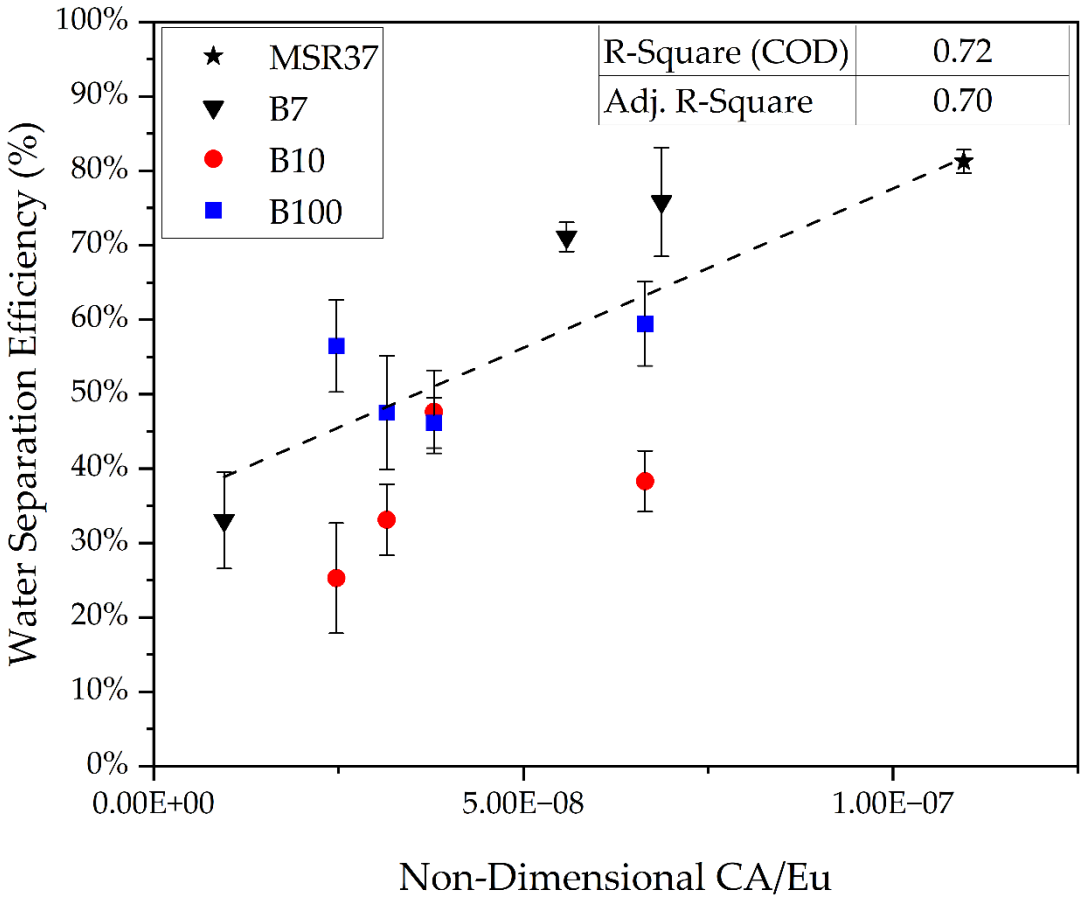

Figure 4-31: Water separation efficiency vs contact angle/ differential pressure

If the data is split into its requisite fuel markets, it is apparent that the fuel market has a bearing upon the water separation efficiency. Firstly, the B10 and B100 fuel market filters are grouped, whereas the B7 fuel market filters span

the full range. The gradients for each of the fuel markets are different; the B10 fuel market filters have a steeper gradient, while the B100 fuel market filters show the flattest gradient. This suggests that there are other effects related to the fuel market that are not captured by examining the contact angle and pressure drop alone. While this is an interesting observation there are only a small number of samples from each fuel market, therefore this is difficult to say for sure.

This technique for predicting the water separation performance of fouled diesel filters has not been implemented previously. With the addition of more returned samples, it would be possible to fully develop a predictive model for the water separation efficiency. The method for developing this model has been established through this work and would be a significant addition to the literature regarding fouled diesel filters. In addition to this there is very little published work on the effect of fouling on diesel filters with respect to the water separation efficiency, while the results of this study confirm what would be expected there would still be merit in publishing the results, especially showing that the fouling is largely consistent between different fuel markets.

4.5 Conclusions

It has been shown that the fuel market in which a filter is used has a significant impact upon the fouling tendencies of fuel filters used in HGVs. It was shown using FTIR that overall, the general structure of the foulant material is relatively consistent for all filters, the material is long chain hydrocarbons with some oxygen functionality. The filters fouled in the B10 fuel market show a tendency to form cake layers rapidly, the filters fouled in the B100 fuel market have a higher likelihood of displaying inter-pore fouling.

The pressure drop and contact angle were used as analogues for the chemical and physical changes caused during the fouling process. Both the contact angle and pressure drop are good analogues for the changes that occur during use. However, there is a variable related to the fuel market that could not be accounted for. Analysis of air permeability indicated that the fouled filters are more susceptible to fouling from water droplets due to a decrease in contact angle hysteresis. It was possible to show the effects of different fouling mechanisms on the pore size distribution within the filters, however it was not possible to link this directly to the water separation efficiency.

This chapter highlights the complexity of the fouling process in field samples, meaning that the current use of pressure drop as an indicator for end of life can lead to the failure of the filter with regards to water separation without any indication. It also shows that when applying a coating, particular attention should be given to any changes that occur to the flow dynamics through the filter. The water separation efficiency is sensitive to this type of change.

The aim of this chapter was to determine whether the fuel market in which the filter was used has an impact on the performance of the filter after being fouled. This has been achieved, it is immediately obvious that the rate of fouling is impacted by the fuel market, the filters fouled in the Brazilian market blinded significantly quicker than the filters fouled in the Swedish market. The most likely reason for this is postulated to be the composition of the biodiesel feedstock. It has been shown in the literature that soybean biodiesel used in Brazil has a higher blocking tendency when compared to rapeseed biodiesel used in Europe.

It was shown however, that the composition of the biodiesel was substantially similar both physically and chemically. It was possible to confirm that the two primary factors affecting the water separation efficiency that are impacted by the fouling are the shear stress at the pore walls (represented by the pressure drop) and the surface free energy of the fibres (represented by the contact angle). Using the data gathered it was possible to create the basis of a model that could be used to estimate the water separation efficiency of a filter based on some relatively easily measured values.

Chapter 5
Formation and characterisation of SiO_2 microspheres for coating

5.1 Introduction

This chapter will outline the process of forming silica microspheres and the subsequent hydrophobic treatment. Three functionalising agents have been selected for creating hydrophobic silica particles, they are detailed in Table 5.1.

Table 5.1: Functionalising agents used for the formation of hydrophobic silica microspheres.

Functionalising agent	Abbreviation	CAS No
Perfluorooctyltriethoxysilane	FAS	51851-37-7
Hexadecyltrimethoxysilane	HDTMS	16415-12-6
Oleic acid	OA	112-80-1

As was described in the methodology section the effect that the concentration of three chemicals have on the effectiveness of the hydrophobic particles produced is investigated. The variables that are being examined are the concentration of deionised water (H_2O), ammonium hydroxide (NH_4OH) and the functionalising agent (Table 5.1). The method being used is a one pot method, in which the functionalising agent is added alongside the tetraethyl orthosilicate (TEOS). It is theorised that a core and shell arrangement will be formed between the silica and the functionalising agent, depicted in Figure 5-1. The 'as-formed' particles will then be applied to the fibrous filter through a simple dip coating method.

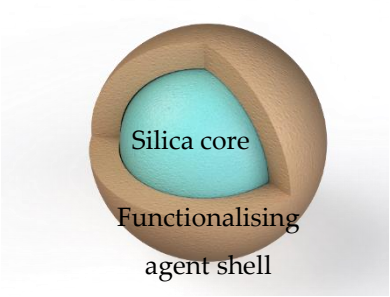

Figure 5-1: Example of the core and shell silica-functionalising agent particle

This chapter will achieve the second aim of the project. A coating is developed to improve the water separation performance of the filters. A number of different particles were formed using the Stöber process, the process was modified slightly to allow for the silica particles formed to have a hydrophobic shell as described above. The hydrophobicity of the particles prepared was analysed using the contact angle technique, this was done having applied them to the fibres. In order to assess the size of the particles formed two methods were used, dynamic light scattering and scanning electron microscopy. It was found that the particles aggregated and using the two methods it was possible to approximate the degree of aggregation.

It was also necessary to determine the impact that the coating has on the physical properties of the filter. This was achieved using capillary pore porometry and air permeability testing. It is important that any coating applied has a minimal impact on the physical change, because as identified in Chapter 4 the blockage of pores decreases the performance of the filter.

5.2 Materials and Methods

5.2.1 Testing matrix

To effectively determine the effect that each parameter has on the final properties of the microspheres a testing matrix was created. This was done using a technique often used in computational modelling called Latin hypercube sampling. This creates a random spread of particles that are well distributed over a sample space. The testing matrix used for each functionalising agent is shown in Table 5.2. In total, 30 tests were carried out.

Table 5.2: Experimental matrix for the SiO_2 formation, each test ID was repeated for each functionalising agent.

Test ID	Concentration ($molL^{-1}$)			
	TEOS	**Functionalising agent**	**NH_4OH**	**H_2O**
1	0.261	0.0181	0.772	2.20
2	0.264	0.0328	0.524	1.95
3	0.250	0.0631	0.601	3.88
4	0.234	0.0150	1.54	5.86
5	0.251	0.0223	0.434	4.93
6	0.243	0.0125	2.36	2.44
7	0.257	0.0141	0.857	2.96
8	0.263	0.0356	0.711	1.69
9	0.230	0.0218	0.499	8.90
10	0.254	0.0469	1.07	2.39

There is some variation in the concentration of TEOS. The mass of TEOS and the other unvaried reactants were kept the same throughout the testing, therefore the small changes in volume of the varied parameters results in some small fluctuation in the concentration of TEOS. The reason the mass was maintained the same was to attempt to keep the eventual mass of particles in the solution used for coating the same.

5.2.2 Methods

The general method for forming the SiO_2 microspheres is described in the methodology section (section 0). This methodology was used any time that microspheres were created.

Following the formation of the microspheres, a number of experiments were conducted in order to determine the efficacy of the particles to impart hydrophobicity. Figure 5-2 describes the testing completed.

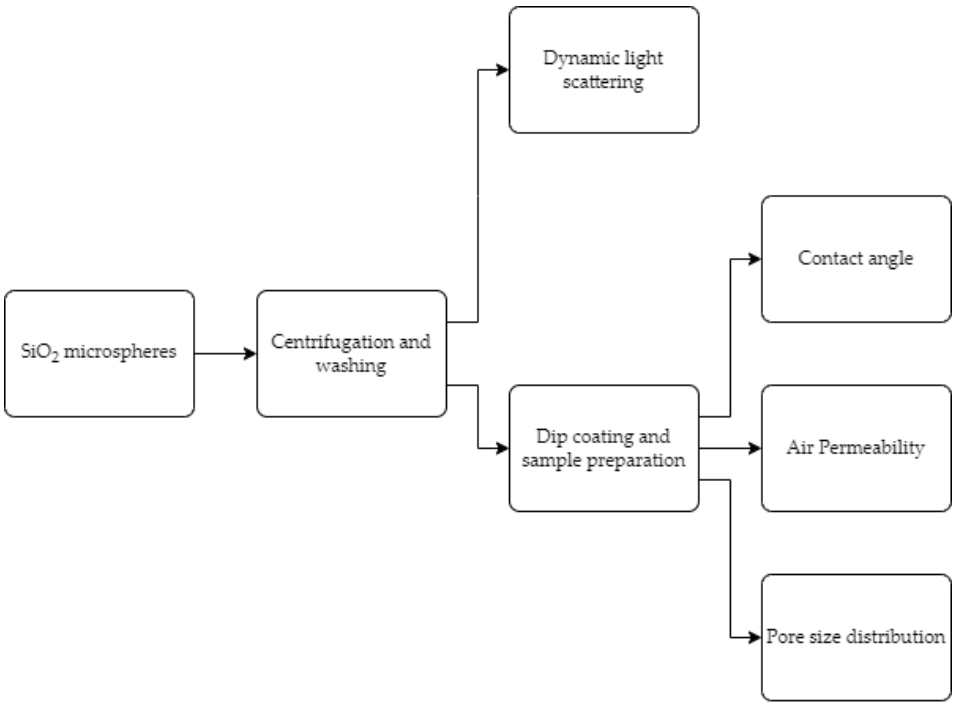

Figure 5-2: Flow diagram of the methodology for testing as formed hydrophobic silica microspheres.

The stages within the block diagram are described within the methodology section. Dynamic light scattering is performed in order to determine the size distribution of the particles formed. The contact angle is measured after applying the particles to the filter through dip coating. The fibrous nature of the filter material made the measurement of the sliding angle impractical, the lack of data for the sliding angle means that the coatings cannot truly be called superhydrophobic. Air permeability and pore size distribution are used to assess the changes to the physical characteristics of the filter. This should be kept to a minimum to ensure that the hydrodynamics of the flow are maintained as best as possible.

5.3 Results

5.3.1 Particle Sizes

Using a Malvern Zetasizer, it has been possible to determine the particle sizes by utilising dynamic light scattering (DLS) produced using the modified Stöber method. This will show how the addition of the functionalising agents affects the production of the microspheres by way of utilising the Stöber process. The diameters of the particles were confirmed using SEM imagery because it was found that there was significant poly-dispersity in the Zetasizer measurements.

5.3.1.1 FAS

Looking first at the results for when using the FAS functionalising agent. The particle sizes for ID 1-10 as defined in Table 5.2 are shown in Figure 5-3 through Figure 5-7.

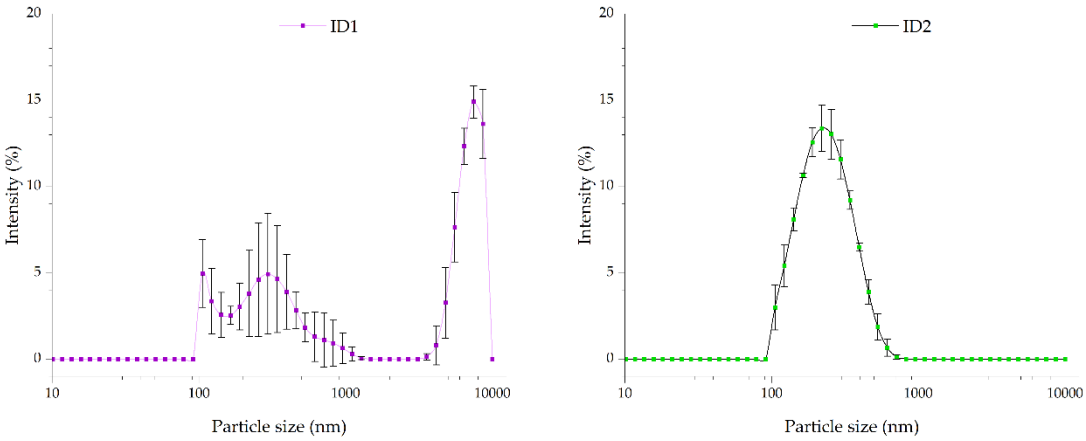

Figure 5-3: Particle sizes for ID 1 & 2 with the FAS functionalising agent.

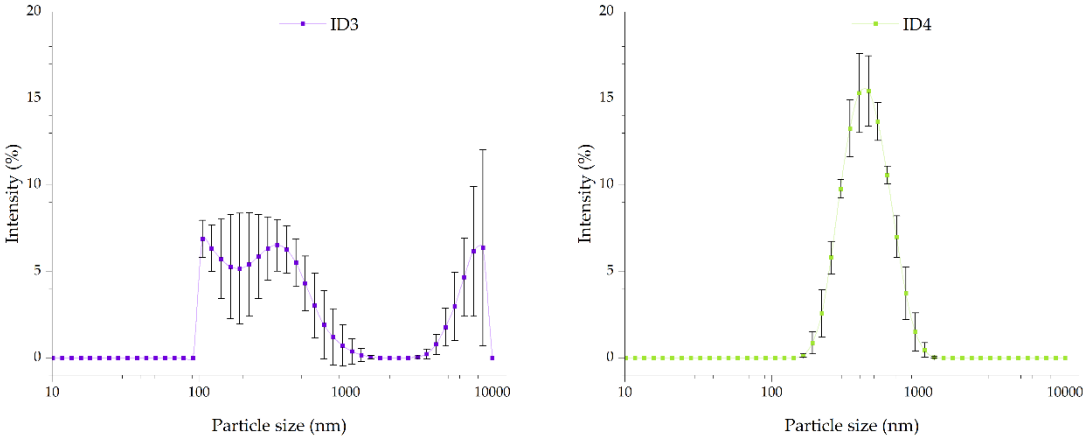

Figure 5-4: Particle sizes for ID 3 & 4 with the FAS functionalising agent.

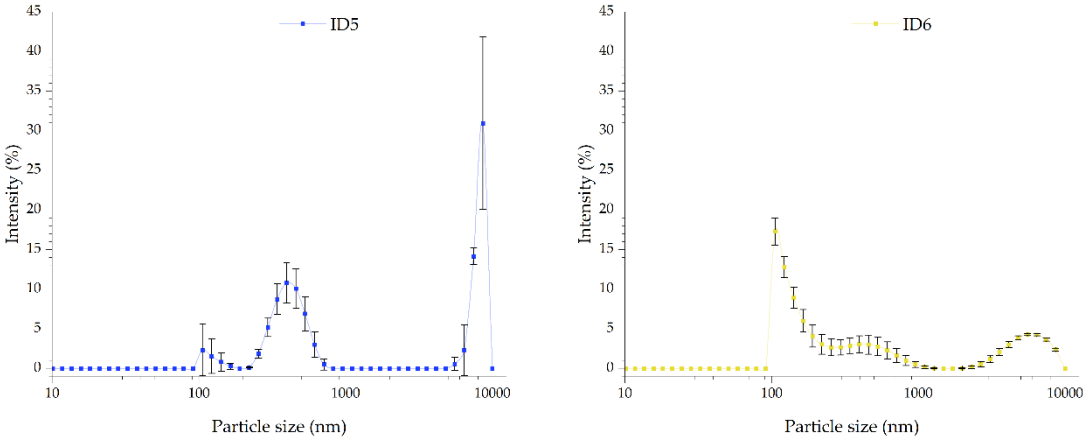

Figure 5-5: Particle sizes for ID 5 & 6 with the FAS functionalising agent.

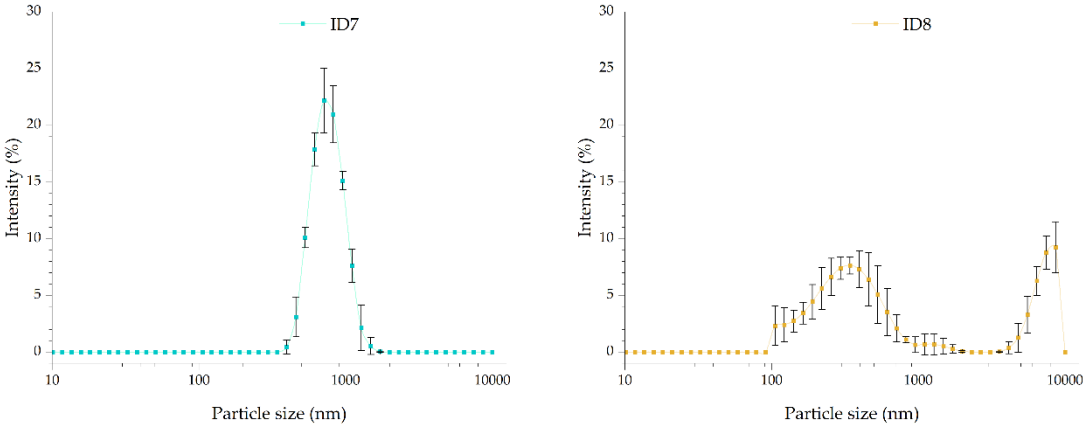

Figure 5-6: Particle sizes for ID 7 & 8 with the FAS functionalising agent.

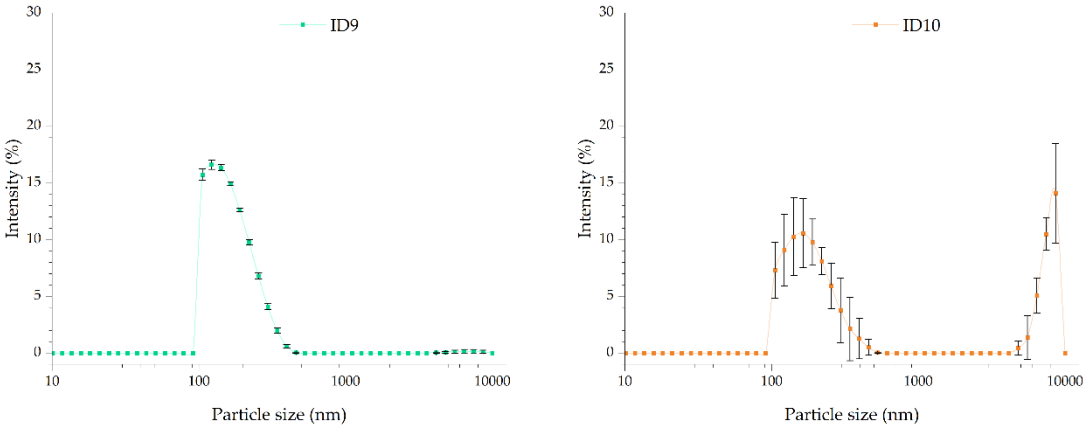

Figure 5-7: Particle sizes for ID 9 & 10 with the FAS functionalising agent.

There are some important things to note from these figures. It is well reported that the Stöber process forms relatively uniform spherical particles (202). However, looking at these data collected from the particles formed in this work, it appears that this is not the case. There is a large amount of polydispersity in many of the samples (ID1, 3, 5, 6, 8 and 10). Wang et al. (203) showed using TEM that when utilising the Stöber method with TEOS and FAS that uniformly sized particles were formed. This suggests that the addition of the functionalising agent doesn't result in polydispersity in all cases. The likely cause of this polydispersity is aggregation of the particles.

Bogush et al. (204) examined the Stöber process and how the concentration of each reactant effects the size of the silica spheres produced. In excess of 100 experiments were conducted for this. Bogush et al. (204) developed an equation based on empirical data to determine the diameter of a Stöber particle from the concentration of the reagents. The equation is shown in equations 5-1, 5-2 and 5-3.

$$d = A[H_2O]^2 \exp\left(-B[H_2O]^{\frac{1}{2}}\right) \qquad \textbf{5-1}$$

Where,

$$A = [TEOS]^{\frac{1}{2}}(82 - 151[NH_3] + 1200[NH_3]^2 - 366[NH_3]^3) \quad \textbf{5-2}$$

And

$$B = 1.05 + 0.523[NH_3] - 0.128[NH_3]^2 \quad \textbf{5-3}$$

These models are based on the formation of Stöber particles in the traditional method, without the presence of a functionalising agent. Figure 5-8 shows how the particle sizes measured in this work compare to this empirical model. Clearly the correlation is poor, this could be caused by several factors including aggregation, the addition of the functionalising agent or experimental controls.

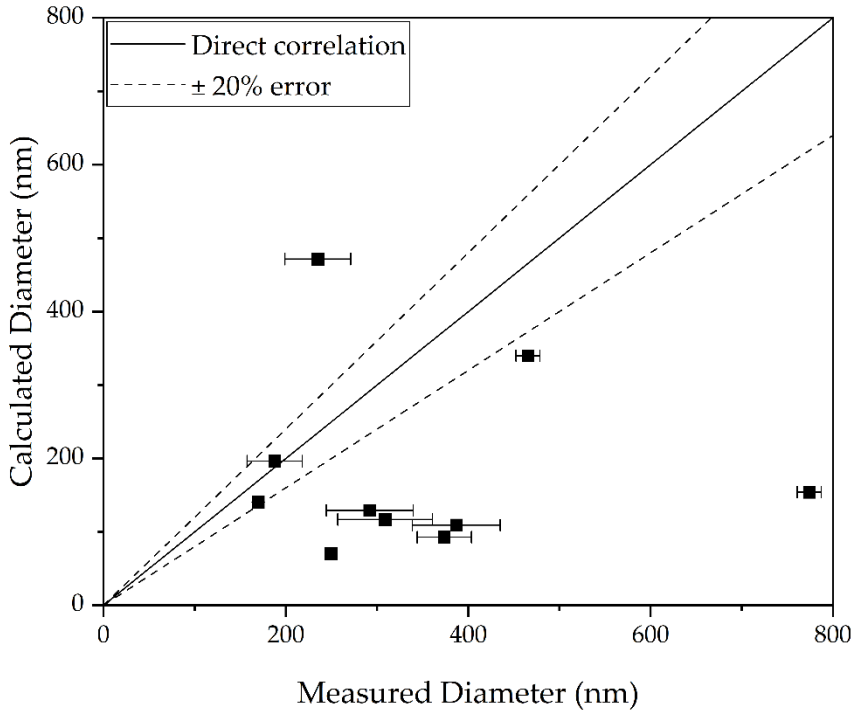

Figure 5-8: Calculated diameter vs measured diameter for the FAS functionalising agent microspheres.

The aggregation that is seen in these samples is problematic for determining the true particle sizes. The most facile method for determining the particle sizes without aggregation being a problem would be through imaging. Using SEM, the particles were directly imaged. The resultant images were then analysed to determine the particle size distribution. Figure 5-9 shows an example of the image collected for the ID7 particles, along with the resultant particle size distribution.

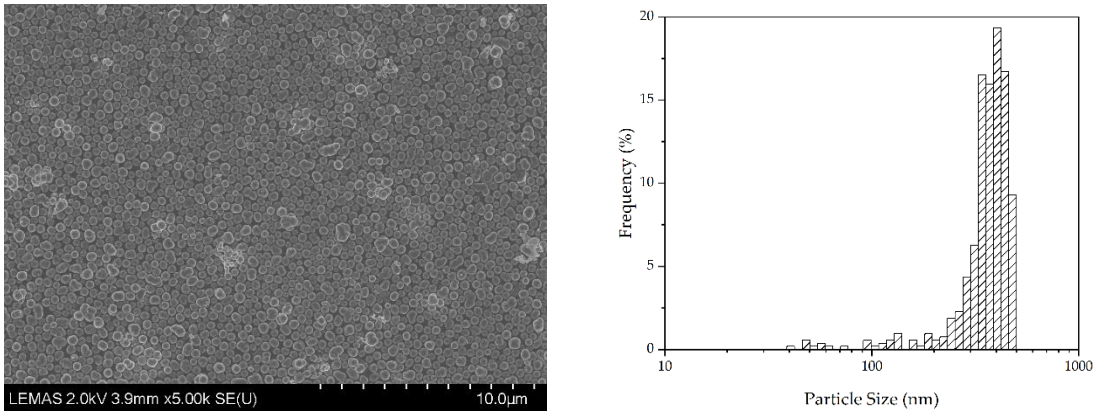

Figure 5-9: Left: image of the microspheres created (ID7). Right: histogram of the particle sizes (ID7).

This analysis resulted in an average particle size of 400.1 ± 66.5nm, compare this to the 774.1 ± 13.2nm measured using DLS it is clear that there is an element of aggregation even in the relatively large particles. Looking at Figure 5-10 it can be seen that the effect of aggregation is even greater in other samples. The particle size measured with DLS (387.0 ± 48.3nm) is over ten times greater than the particle sizes measured with the SEM images.

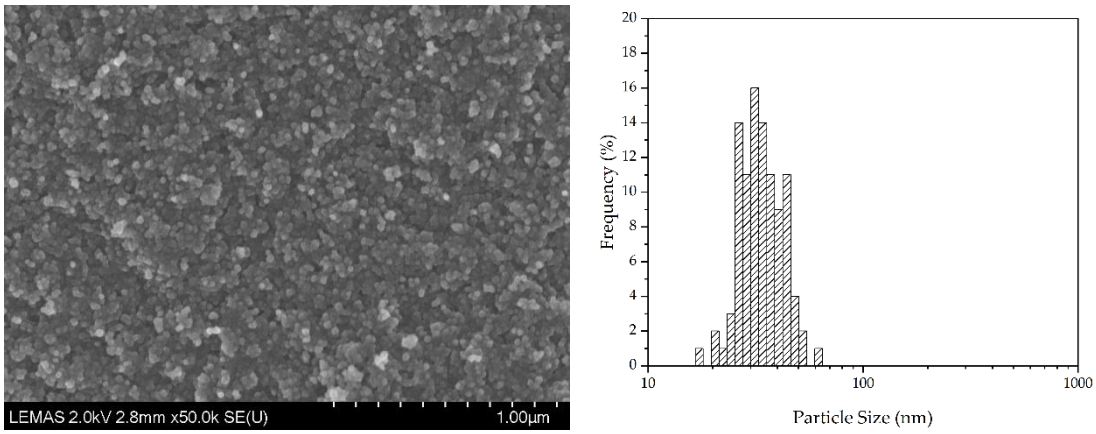

Figure 5-10: Left: image of the microspheres created (ID5). Right: histogram of the particle sizes (ID5) for the FAS functionalised microspheres.

While it has been possible determine the actual apparent size of the particles formed, it is not possible to show using SEM imaging the extent to which the particles aggregate. The theoretically calculated particle sizes still do not correlate with the observed particle sizes measured using SEM, Figure 5-11 shows this relationship.

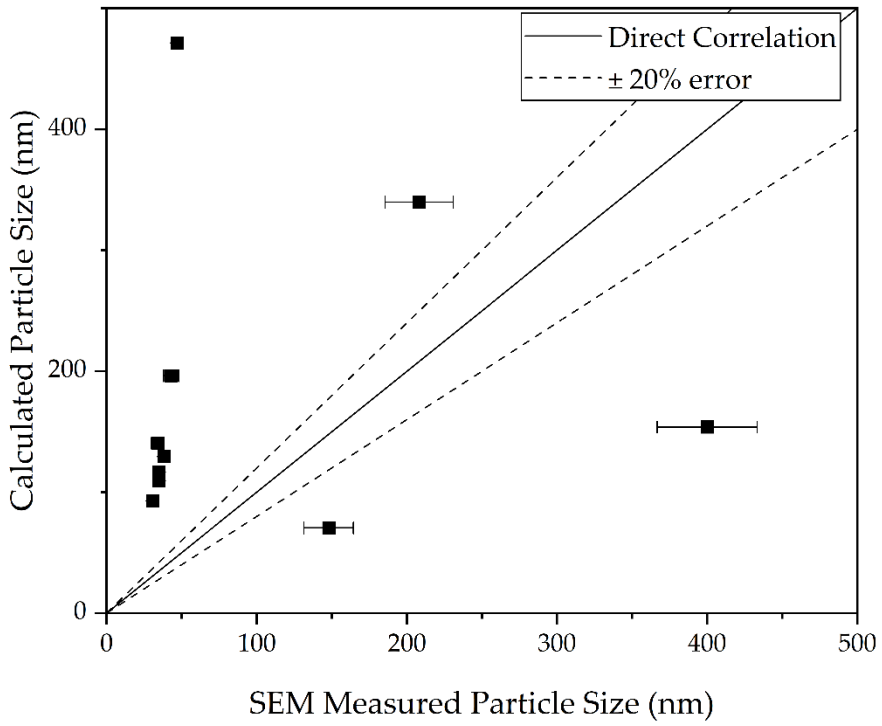

Figure 5-11: Correlation between the measured particle size (using SEM) and the theoretically calculated particle sizes for the FAS functionalised microspheres.

It is likely that the addition of the functionalising agent has altered the way in which the particles are formed changing the particle sizes. This could explain the deviation of the particle sizes from what would be expected from theoretical calculations. It is an interesting result, which should be noted. However, the purpose of examining the Stöber process was to achieve a range of particle sizes. This has been achieved; therefore, an alternative methodology is not required.

5.3.1.2 HDTMS

Using DLS again the diameter of the particles formed with the HDTMS functionalising agent. Figure 5-12 to Figure 5-16 show the particle size distributions. There are several important things to note in the particle size distributions, in Figure 5-13 and Figure 5-16 the particle size distributions for ID3 and ID9 show no distribution. This is caused by the large apparent particle sizes for these ID's, the Malvern Zetasizer being used does not supply distribution data for particles in excess of 10000nm. This is likely caused by aggregation of the particles formed. The aggregation is also exemplified in the distributions showing a secondary peak in the order of thousands of nanometres.

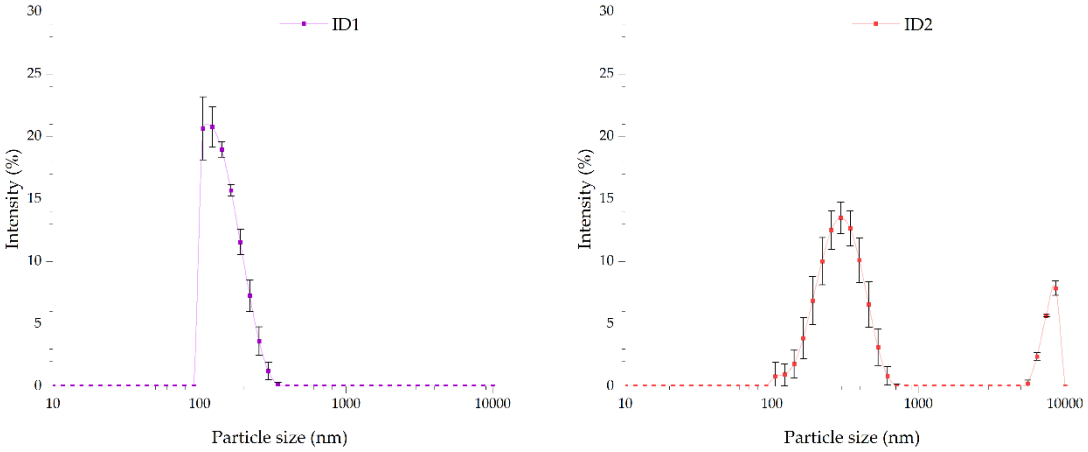

Figure 5-12: Particle sizes for ID 1 & 2 with the HDTMS functionalising agent.

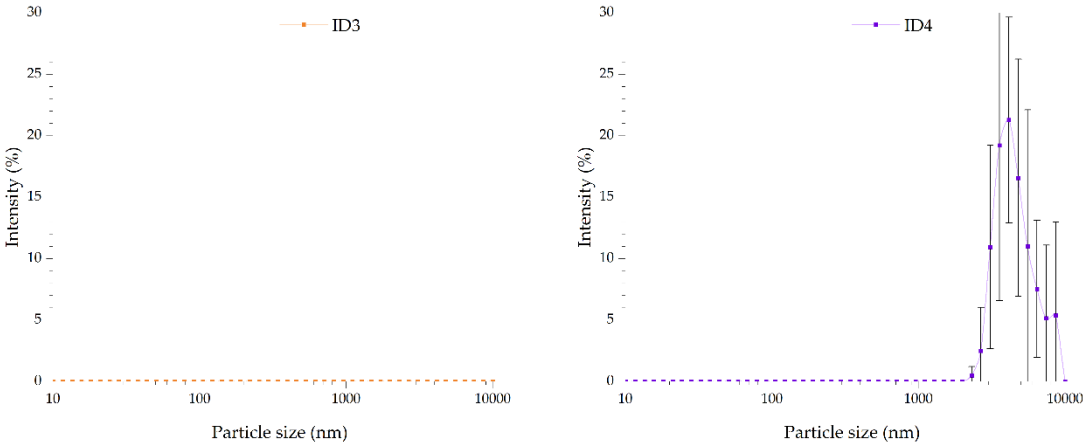

Figure 5-13: Particle sizes for ID 3 & 4 with the HDTMS functionalising agent.

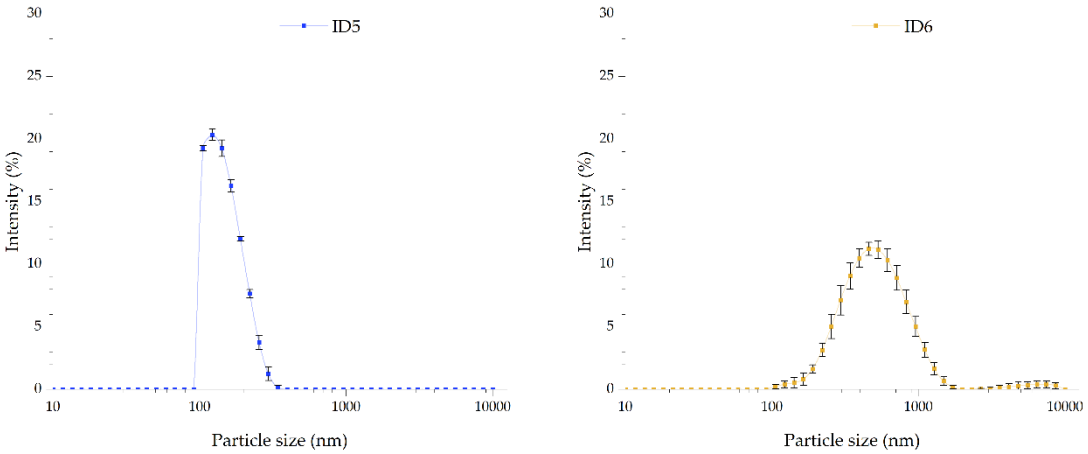

Figure 5-14: Particle sizes for ID 5 & 6 with the HDTMS functionalising agent.

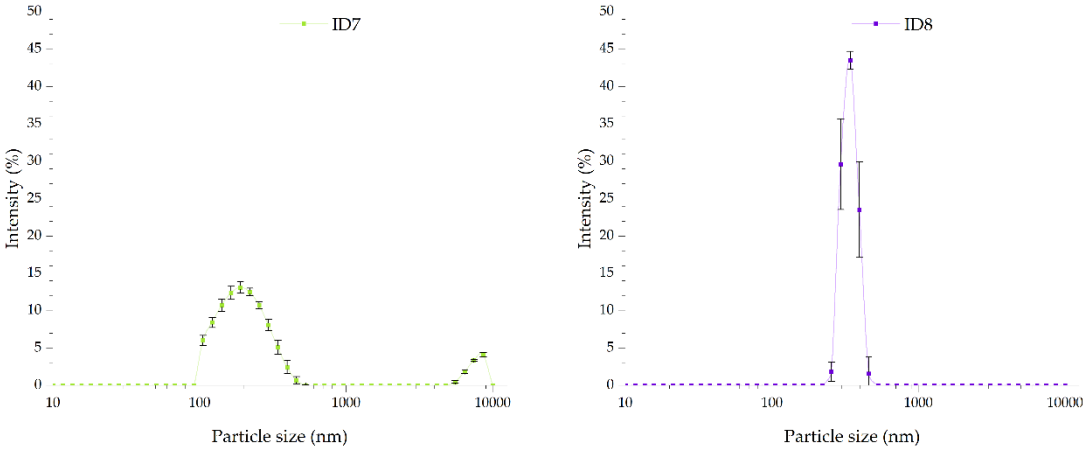

Figure 5-15: Particle sizes for ID 7 & 8 with the HDTMS functionalising agent.

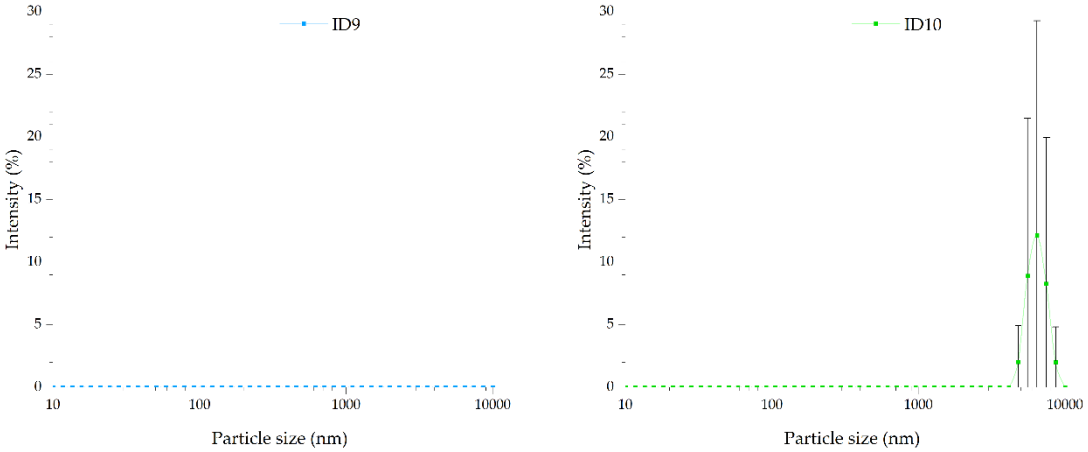

Figure 5-16: Particle sizes for ID 9 & 10 with the HDTMS functionalising agent.

The aggregation is exaggerated in the HDTMS functionalised particles when compared to the particles made with FAS as the functionalising agent. This is exemplified in Figure 5-17. Many of the points on this figure are out of range, because the measured size is much larger than the calculated value. This suggests that the aggregation is a more prominent problem when using the HDTMS functionalising agent. In some cases a surfactant can be used to mitigate the aggregation (205). However, in this case the addition of surfactants would likely lead to changes in the surface chemistry, so this was not an option.

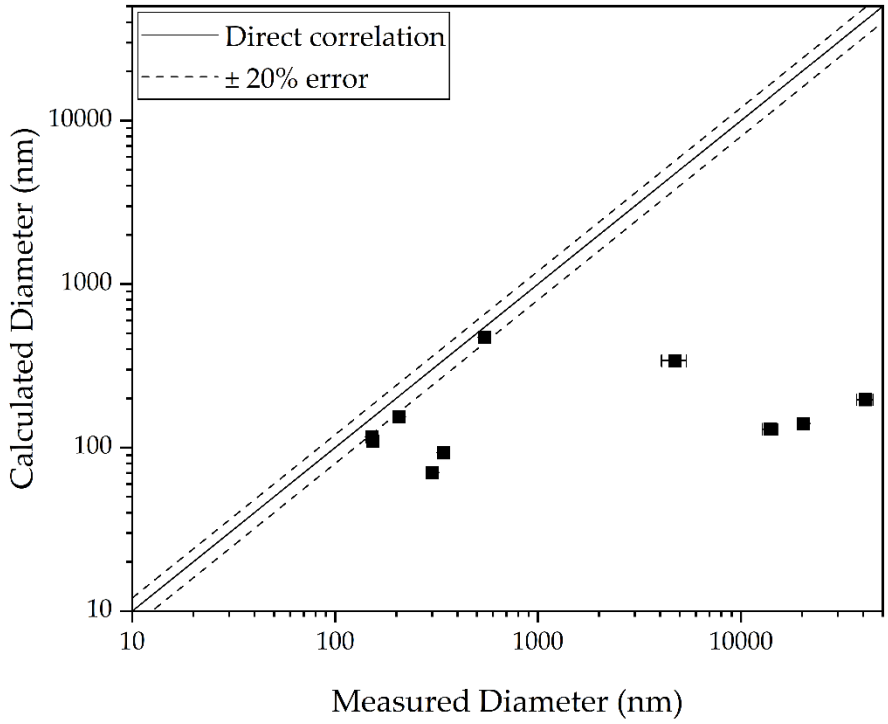

Figure 5-17: Calculated diameter vs measured diameter using DLS for the HDTMS functionalising agent microspheres.

The difference between the particle sizes measured with DLS and the theoretically calculated particles is more apparent than was seen for the microspheres formed with the FAS functionalising agent. This is likely caused by aggregation, again SEM imagery was used to confirm the actual size of the particles formed. It was shown in Figure 5-10 that for the FAS functionalised coatings aggregation was significant in some cases. This was also seen in the HDTMS functionalised particles. Figure 5-18 shows an SEM image of coating ID10 functionalised with HDTMS alongside the particle size histogram using the SEM image. This coating was selected as the coating functionalised with HDTMS that had the most discreet particles, and even here aggregation is widespread.

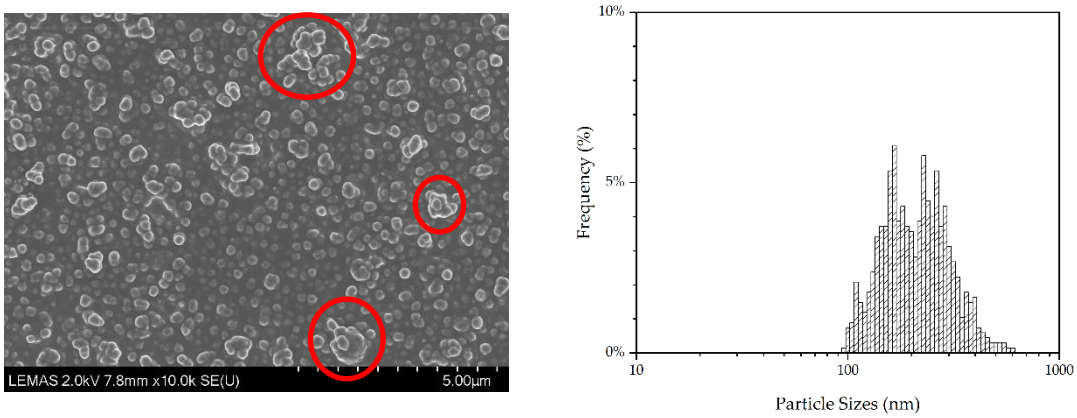

Figure 5-18: Right: SEM image of HDTMS ID10 with the aggregation highlighted. Left: histogram of the particle sizes for the HDTMS ID10 coating.

A more representative coating for what is seen in the HDTMS functionalised coatings is shown in Figure 5-19. There are large aggregates of discreet particles. For all further analysis the sizes of the particles measured using SEM were taken to be the size of the discreet particle, rather than the aggregation. The particle size histogram is also included, for reference.

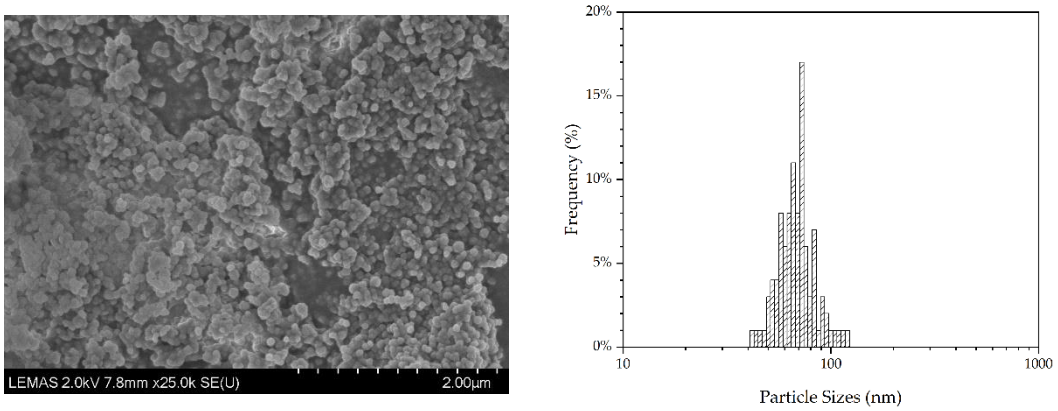

Figure 5-19: Right: SEM image of HDTMS ID5. Left: histogram of the particle sizes for the HDTMS ID5 coating.

Using the same method as was done for the FAS functionalised microspheres, the expected particle sizes were calculated. Figure 5-20 shows the comparison between the calculated and measure particle sizes. Again, there is large disparity between these two values. The particle sizes fall well outside the ± 20% error boundaries for the most part, with only two of the ten samples falling within this range. This again is attributed to the introduction of the functionalising compound.

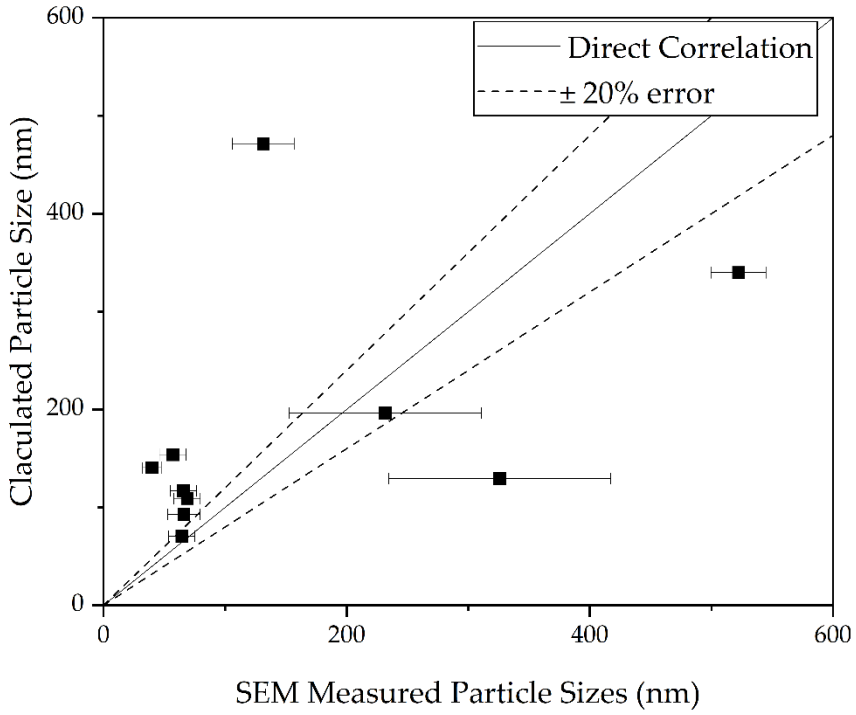

Figure 5-20: Calculated particle sizes vs measured particle sizes using SEM for the HDTMS functionalised microspheres.

5.3.1.3 OA

DLS is able to show the particle sizes for the microspheres created using oleic acid as the hydrophobic functionalising agent. The particle size distributions are shown in Figure 5-21 to Figure 5-25.

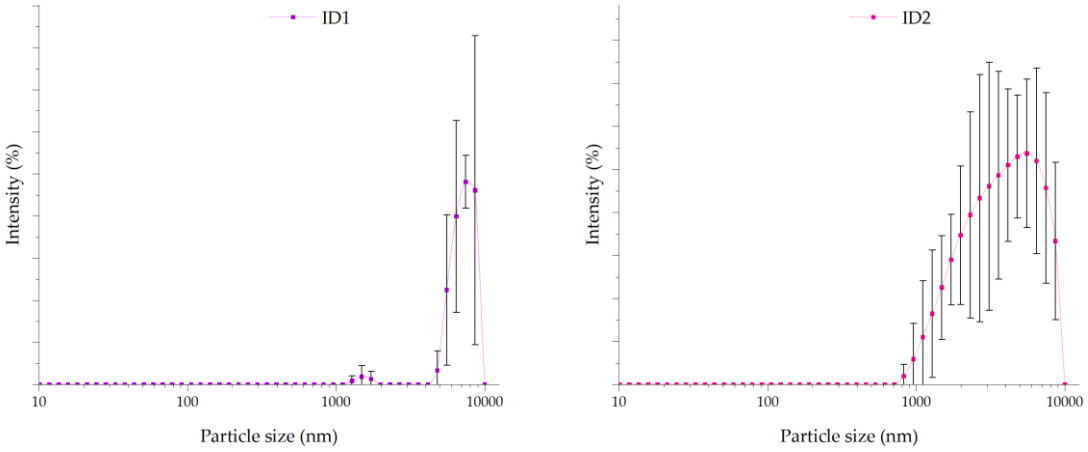

Figure 5-21: Particle sizes for ID 1 & 2 with the oleic acid functionalising agent.

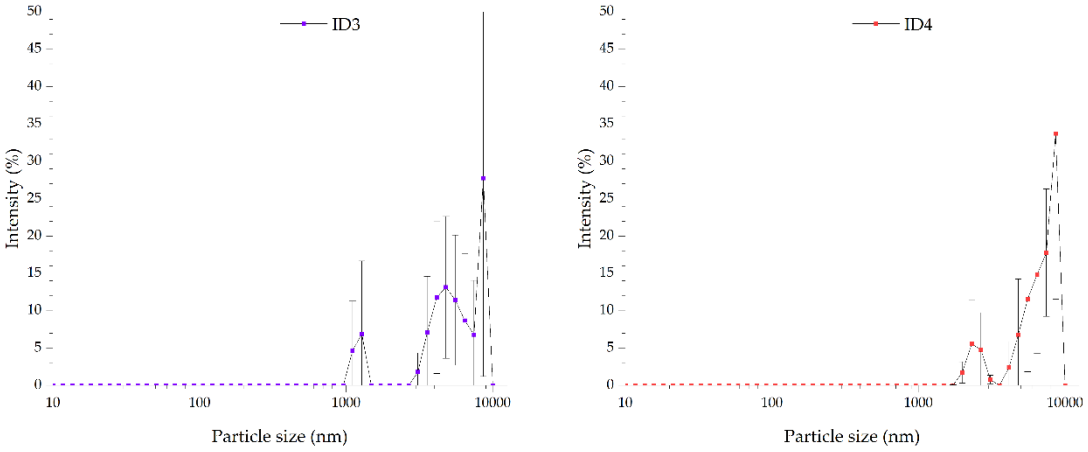

Figure 5-22: Particle sizes for ID 3 & 4 with the oleic acid functionalising agent.

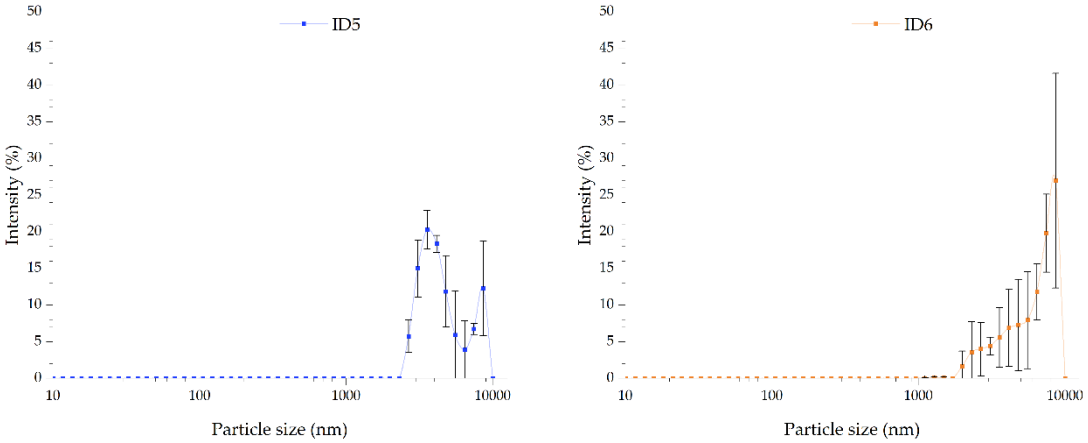

Figure 5-23: Particle sizes for ID 5 & 6 with the oleic acid functionalising agent.

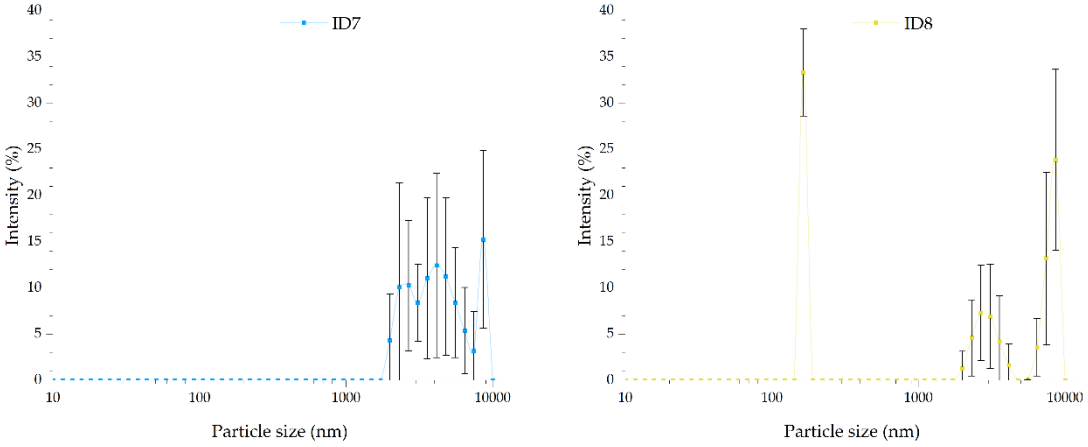

Figure 5-24: Particle sizes for ID 7 & 8 with the oleic acid functionalising agent.

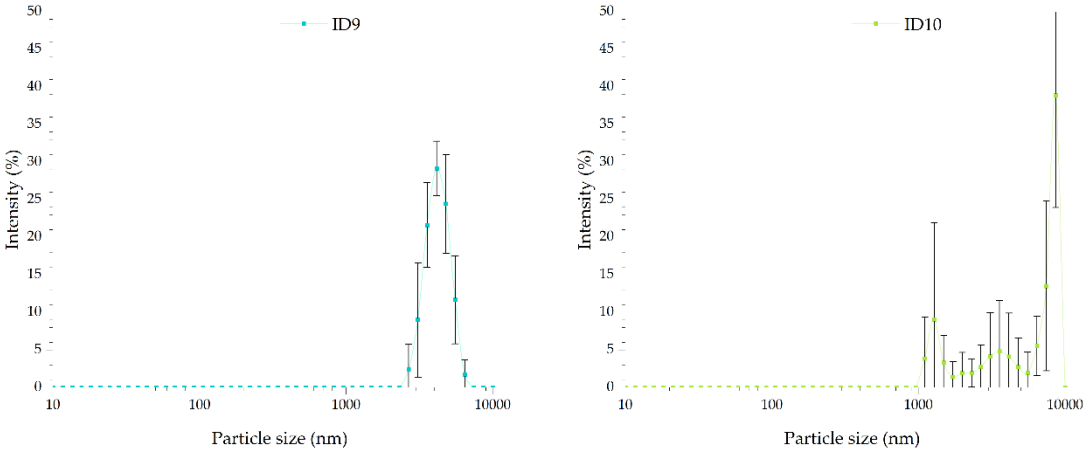

Figure 5-25: Particle sizes for ID 9 & 10 with the oleic acid functionalising agent.

The average particle size for the microspheres formed using oleic acid as the functionalising agent have a significantly higher average particle size compared to both the HDTMS and FAS functionalising agents. It is unclear from the particle size distribution data alone whether this is as a result of aggregation or if the particles are simply much larger. In the HDTMS and FAS samples aggregation was identified by the polydispersity, the oleic acid functionalised particles do not present two peaks (one aggregate and one actual particle), but only one larger aggregate peak. The expected in this instance is what has been shown empirically by Bogush et al. (204), a comparison between measured and expected particle sizes is shown in Figure 5-26. The measured diameter is significantly greater for all the microspheres formed using oleic acid as a functionalising agent. However, there is a correlation between the measured and calculated values, this suggests that the oleic acid is causing the change in diameters from what would be expected.

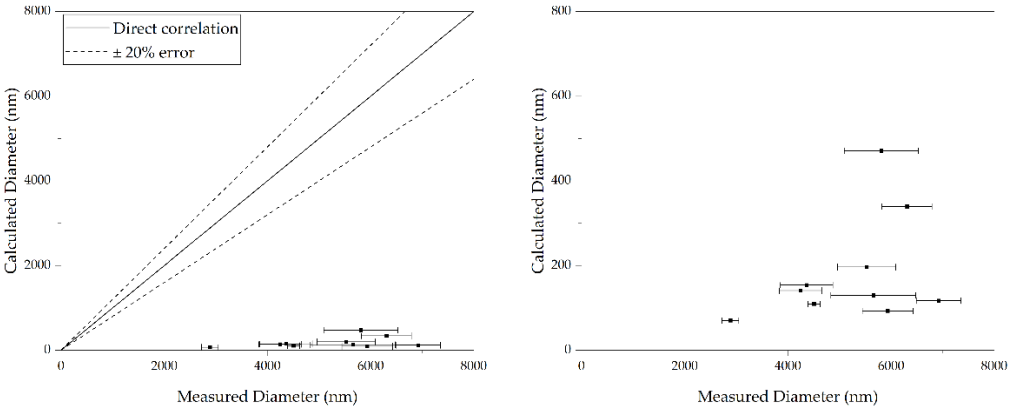

Figure 5-26: Calculated diameter vs measured diameter for the OA functionalising agent microspheres (left: equal scale to show correlation, right: scaled to show trend).

Again, using SEM imagery, it has been possible to determine more accurately the size of the microspheres formed. Figure 5-21 to Figure 5-25 suggest that aggregation is again prevalent in these samples. This is confirmed using SEM. Figure 5-27 shows a typical aggregate that is formed along with the corresponding particle size histogram. As was done for the other aggregates the discreet particle sizes were analysed, not taking into account the size of the aggregates. The reason for this is that the size of the aggregates in the samples imaged is likely a function of the drying, this will not be representative of the final coating added to the fibres (206).

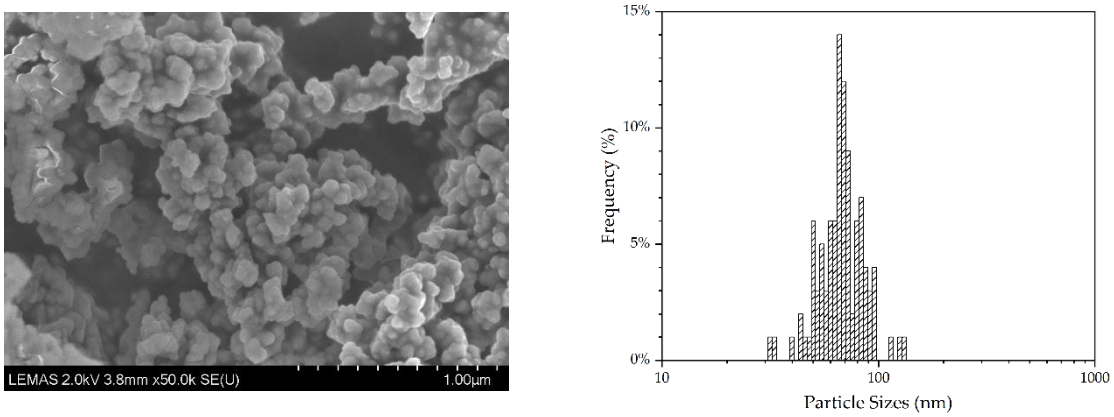

Figure 5-27: Right: SEM image of OA ID1. Left: histogram of the particle sizes for the OA ID1 coating.

Using this method of determining the particle sizes the average particle size for each iteration of the OA functionalised coating, it is possible to determine whether the addition of the functionalising agent has an impact upon the expected particle sizes. The correlation between the calculated particle size and the measured particle size is shown in Figure 5-28, comparing this with the correlations for the FAS and HDTMS functionalised coatings (Figure 5-11 and Figure 5-20) it is clear that the OA functionalising agent has a lesser impact upon the discreet particle size.

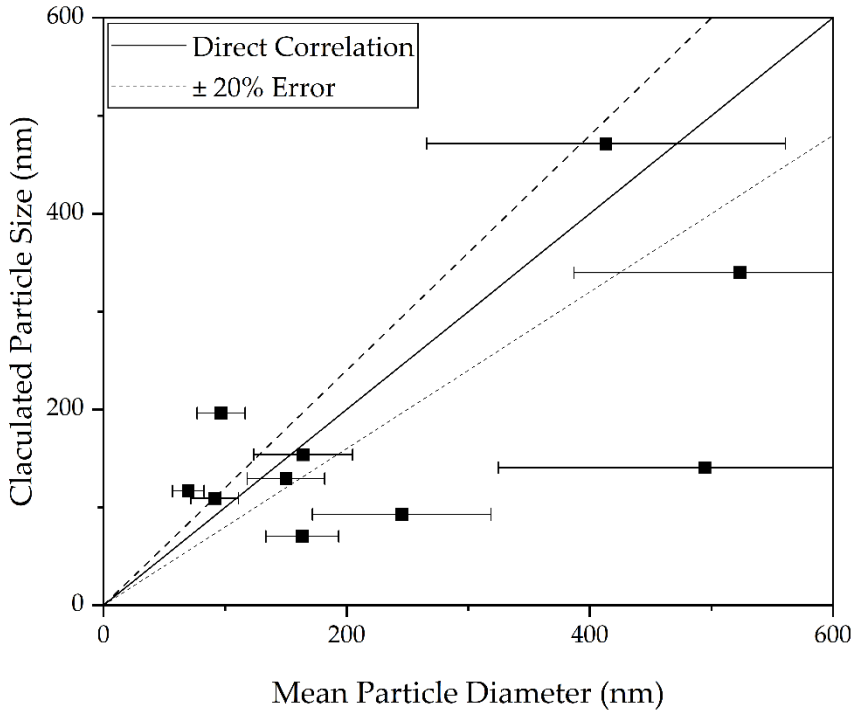

Figure 5-28: Calculated particle sizes vs measured particle sizes using SEM for the OA functionalised microspheres.

While the correlation is not perfect, it is much improved when compared to the correlations for the other functionalising agents. This is likely as a result of the difference in type of functionalisation. This will be discussed more thoroughly in the discussion section of this chapter.

5.3.2 Contact angle.

In order to determine whether the coatings have been successful in increasing the hydrophobicity contact angle has been used. The coatings were each applied to the surface of the filter material being examined as described in section 3.2.13. It was not possible to determine the sliding angle because of the nature of the samples. The filter material is corrugated, causing the sliding angle to be extremely inconsistent. The static contact angle will be sufficient to determine the efficacy of the coating.

5.3.2.1 FAS

It has been shown that the addition of the silica microspheres that have been functionalised with FAS always result in an increase to the contact angle observed as shown in Figure 5-29. This is expected for two reasons, firstly the FAS functionalised microspheres will reduce the surface energy of the fibres. The second is the increase in roughness relative to uncoated fibres.

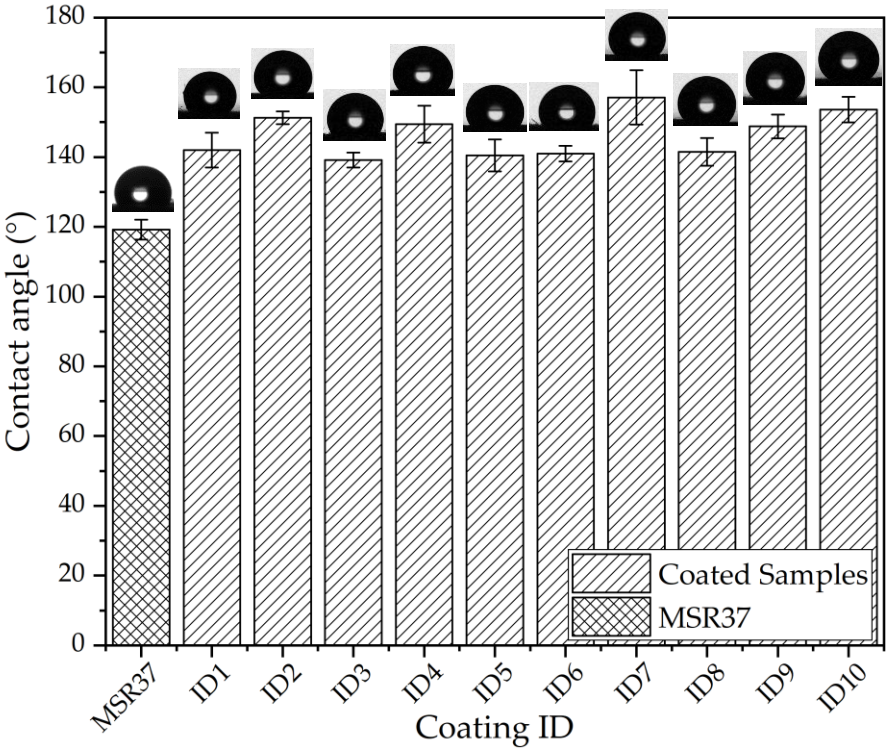

Figure 5-29: Contact angle vs coating ID for FAS functionalised silica

The effect of the particle sizes on the subsequent contact angle is shown in Figure 5-30. It does not appear that there is a significant correlation between the particle size and the contact angle. It may be possible to say that the contact angle is highest for either extremely small or large particles.

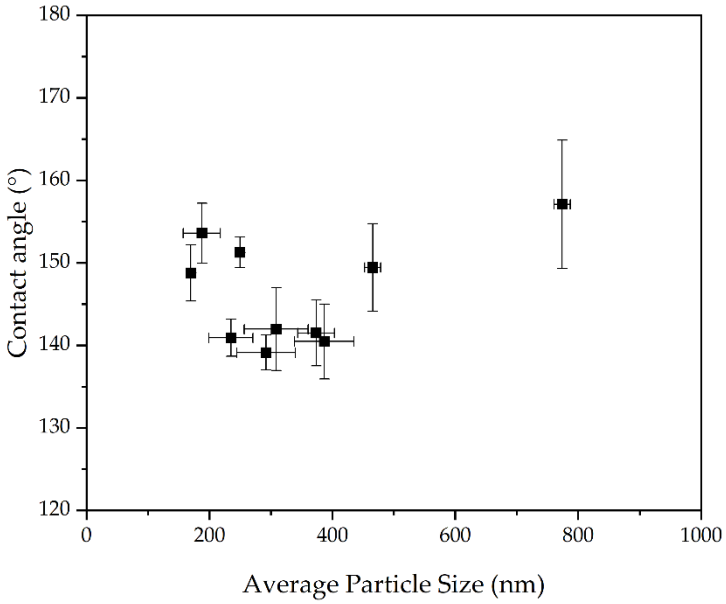

Figure 5-30: Contact angle vs DLS measured particle size for the FAS functionalised nanoparticles.

It is also important to consider the particle sizes measured using the SEM. This will give an indication as to whether the size of the aggregates or the size

of the discreet particles has the greatest impact upon the contact angle observed. Figure 5-31 shows the relationship between the particle sizes measured using the SEM and the contact angle.

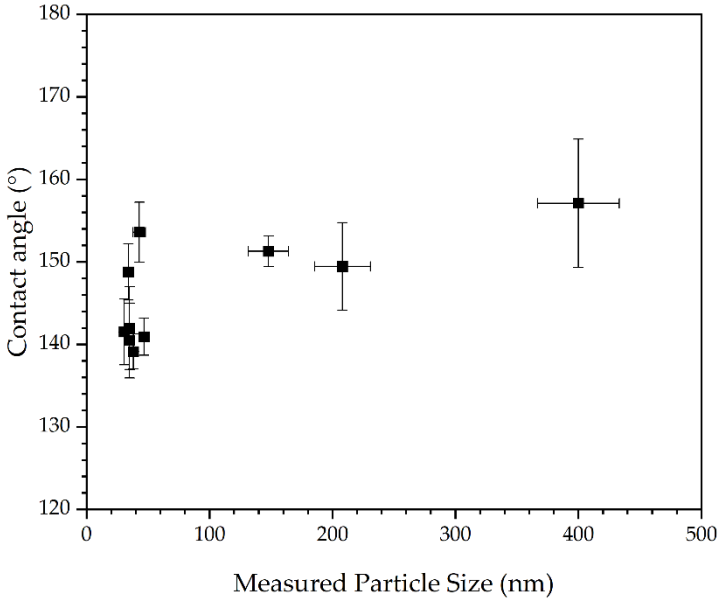

Figure 5-31: Contact angle vs SEM measured particle size for the FAS functionalised nanoparticles

While there didn't appear to be a strong correlation between the particle size measured using DLS and the contact angle ($R^2<0.1$), there does appear to be a correlation between the particle size measured using SEM and the contact angle ($R^2 = 0.4$). With larger particles resulting in increased contact angles. The likely reason for this is the change in roughness caused by the differing particle sizes. This will change the amount of air that is able to be trapped within structure, this will change the contact angle as described by the Cassie-Baxter model (103).

There does appear to be a correlation between the polydispersity index based on the measurements made using DLS and the contact angle. It is shown in Figure 5-32 that the contact angle increased for a lower polydispersity index. In the context of the particle sizes measured with DLS this can be viewed as a measure of the degree of aggregation because as two peaks form (one for the actual size of the particles and the other of the aggregates) the PDI will increase. The greater the aggregation the closer to 1 the polydispersity index will be.

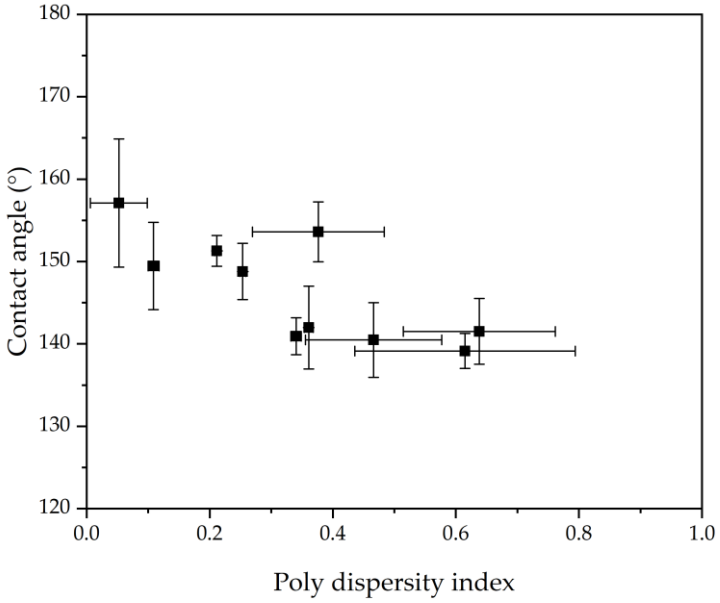

Figure 5-32: Contact angle vs polydispersity index measured using DLS for the FAS functionalised nanoparticles.

Overall, it has been shown that as aggregation increases in the FAS functionalised coatings the contact angle is decreased. It is also interesting to examine the effect of the polydispersity with respect to the particle sizes measured using the SEM method. This will determine whether it is more beneficial to have a more mono disperse microsphere coating with respect to increasing contact angle. The polydispersity index was calculated in the same way as above, using equation 3-22, and the relationship between polydispersity and contact angle is shown in Figure 5-32.

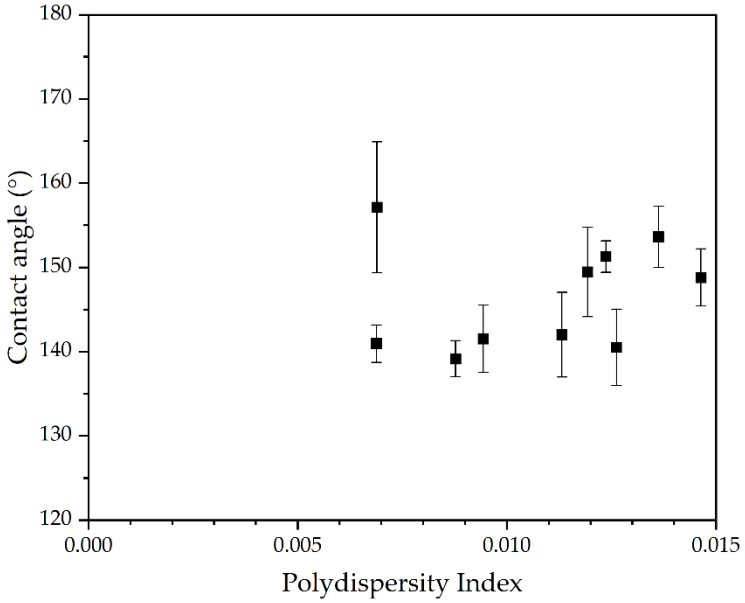

Figure 5-33: Contact angle vs polydispersity index for the particle sizes measured using SEM imagery for the FAS functionalised coatings.

The opposite trend is seen for the polydispersity index of the particles when measured with the SEM images. This suggests that the more variation in size in the discreet particles resulted in increased contact angles. There is one obvious outlier to this, the likely cause of this is the fact that this datapoint displays an extremely low tendency for aggregation (as indicated by the low polydispersity measured with DLS).

Both parameters aren't directly linked but have an impact upon the final contact angle, and when combined display a relatively good predictor for the contact angle as shown in Figure 5-34. This implies that for a maximum contact angle a coating that is quite disordered and has a low tendency for aggregation is beneficial.

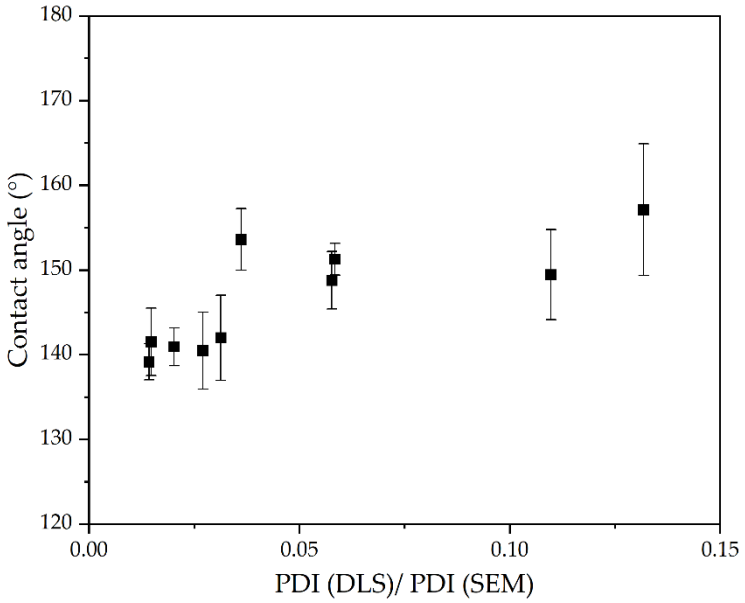

Figure 5-34: Contact angle vs the polydispersity index calculated with DLS over the polydispersity index calculated with SEM for the FAS functionalised coatings

5.3.2.2 HDTMS

Using HDTMS in order to functionalise the silica nanoparticles has also been shown to be effective in increasing the hydrophobicity. Figure 5-35 shows the contact angles achieved using HDTMS as the functionalising agent. All the nanoparticles functionalised with HDTMS increased the contact angle significantly when compared to the untreated fibres. Similar to the FAS functionalised nanoparticles it would be expected that the contact angles would be increased because the roughness would be increased, and the surface energy would be decreased.

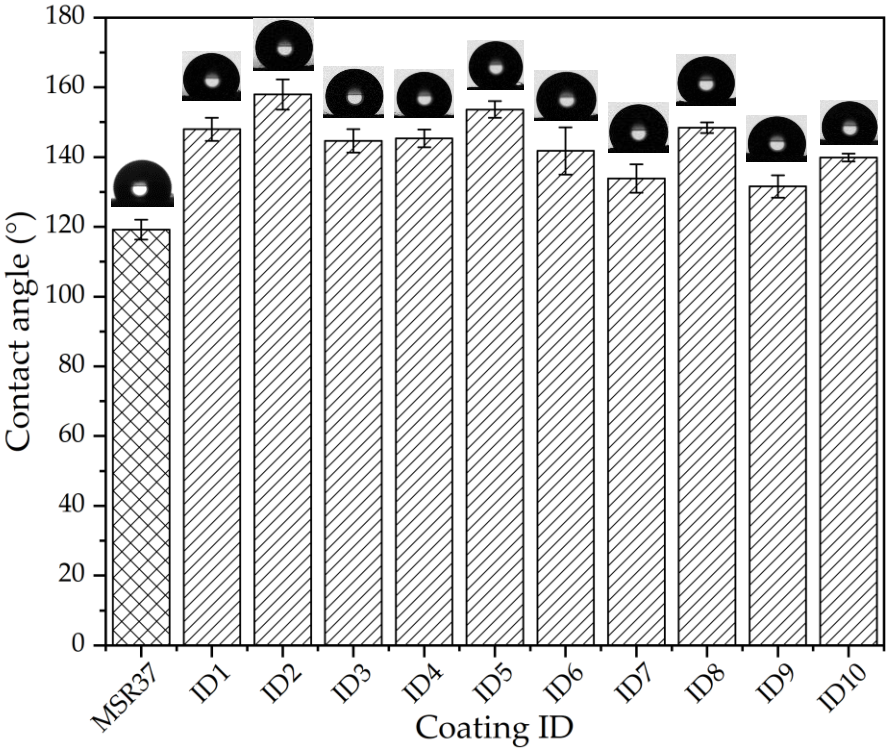

Figure 5-35: Contact angle vs coating ID for HDTMS functionalised silica

Figure 5-36 shows the relationship between the contact angle and the average particle size for the silica nanoparticles functionalised with HDTMS.

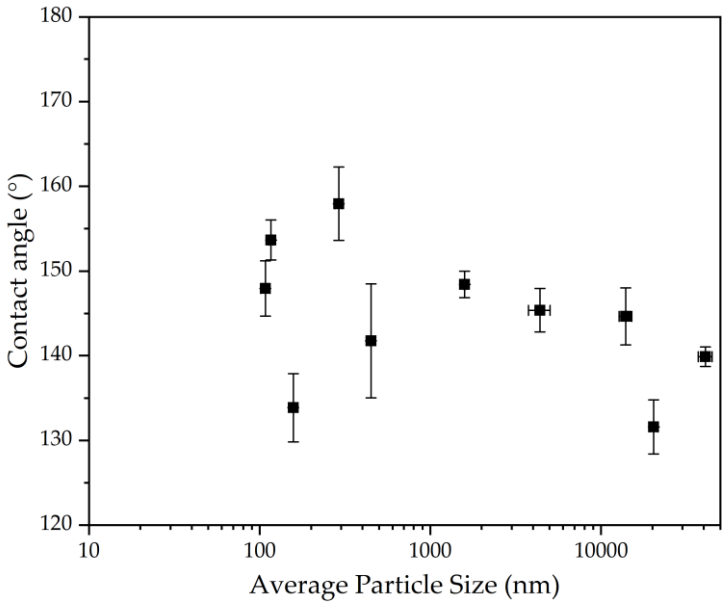

Figure 5-36: Contact angle vs particle size for the HDTMS functionalised nanoparticles

There is a correlation, as the particle size increases the contact angle decreases. It should be noted that the particle sizes are on a logarithmic scale for the HDTMS functionalised particles, where they are on a linear scale for the FAS functionalised particles. Again, using the data gathered from the SEM images

it is possible to determine whether the discreet particle size has an impact upon the contact angle for the HDTMS functionalised microspheres. Figure 5-37 shows the relationship between actual particle size and the contact angle. There isn't a significant correlation between the particle sizes as measured by the SEM and the contact angle, this is likely because the aggregation is so significant that the size of the particles becomes less relevant.

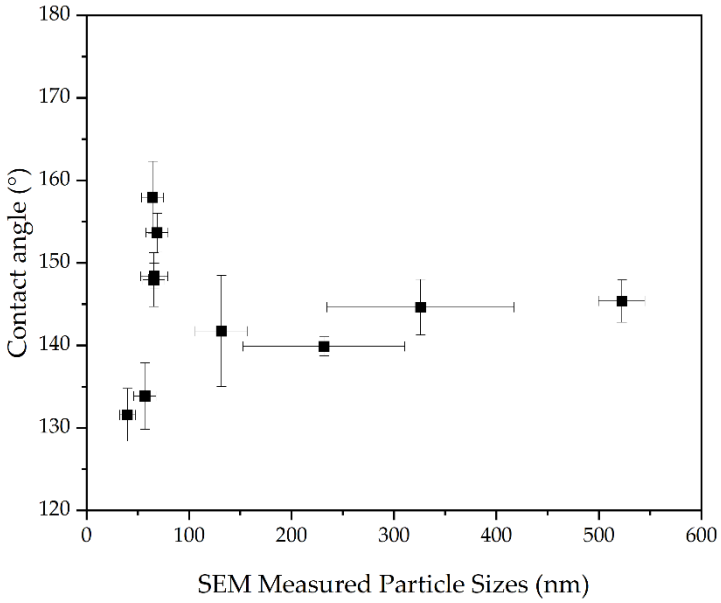

Figure 5-37: Contact angle vs SEM measured particle size for the HDTMS functionalised nanoparticles

There was found to be no correlation between the poly dispersity index, as calculated from the DLS measurement, and the contact angle for the HDTMS functionalised nanoparticles. For the HDTMS functionalised coatings the degree to which the particles agglomerated is significantly worse. Therefore, using the polydispersity index as measured by DLS to indicate the degree of aggregation isn't valid. However, the size of the aggregates is vastly greater than the actual size of the particles. Therefore, the size of the particles measured using DLS is the size of the aggregates in this case meaning that particle size is a better analogue for the degree of aggregation.

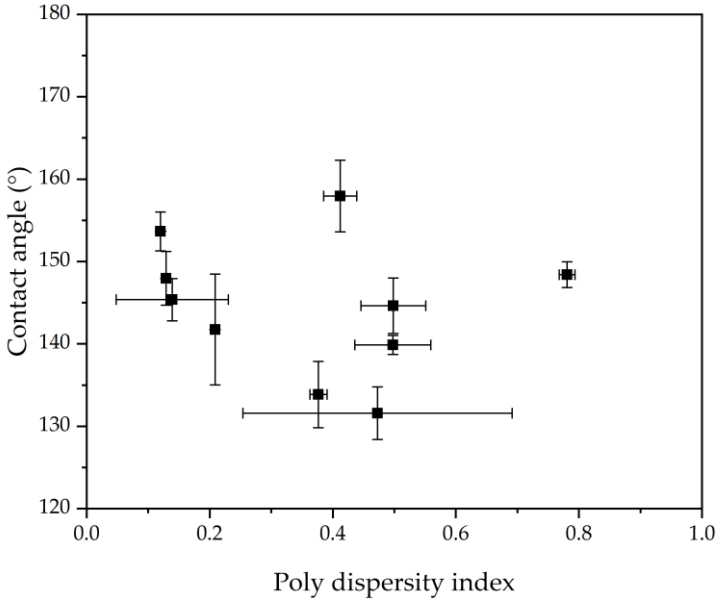

Figure 5-38: Contact angle vs polydispersity index measured with DLS for the HDTMS functionalised nanoparticles.

It was also possible to calculate the polydispersity index for the HDTMS functionalised coatings using the measurements made with the SEM images. There is a very slight correlation between this polydispersity index and the contact angle. However, there is a large variation in the data. This is what was expected, it is likely that the extent of the aggregation is the determining factor in controlling the contact angle (as indicated by Figure 5-36). The correlation between the PDI calculated from the SEM size measurements and the contact angle is shown in Figure 5-39. The same analysis was performed to determine if both the polydispersity.

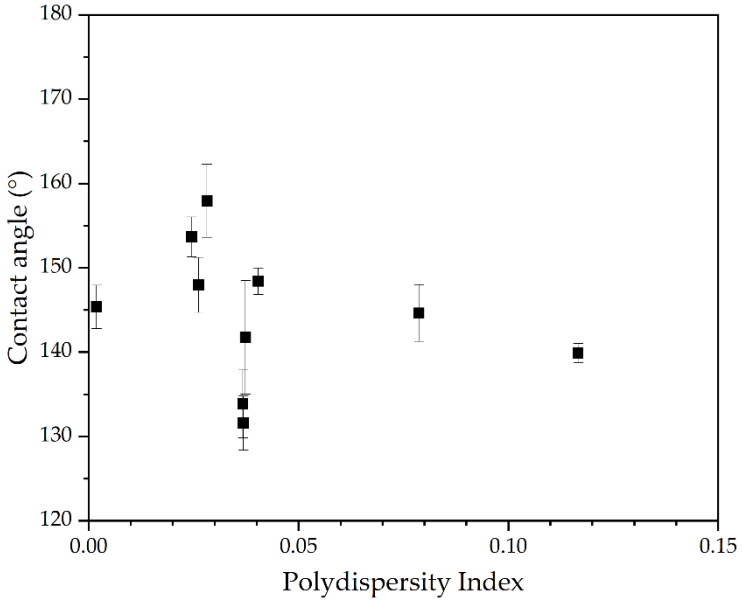

Figure 5-39: Contact angle vs polydispersity index for the particle sizes measured using SEM imagery for the HDTMS functionalised coatings.

5.3.2.3 Oleic acid

It has been shown that using oleic acid to functionalise the surface of silica nanoparticles has been successful in a one-pot method. Figure 5-40 shows that for all the concentrations used in the formation of oleic acid functionalised silica nanoparticles the contact angle was increased compared to the base fibrous material.

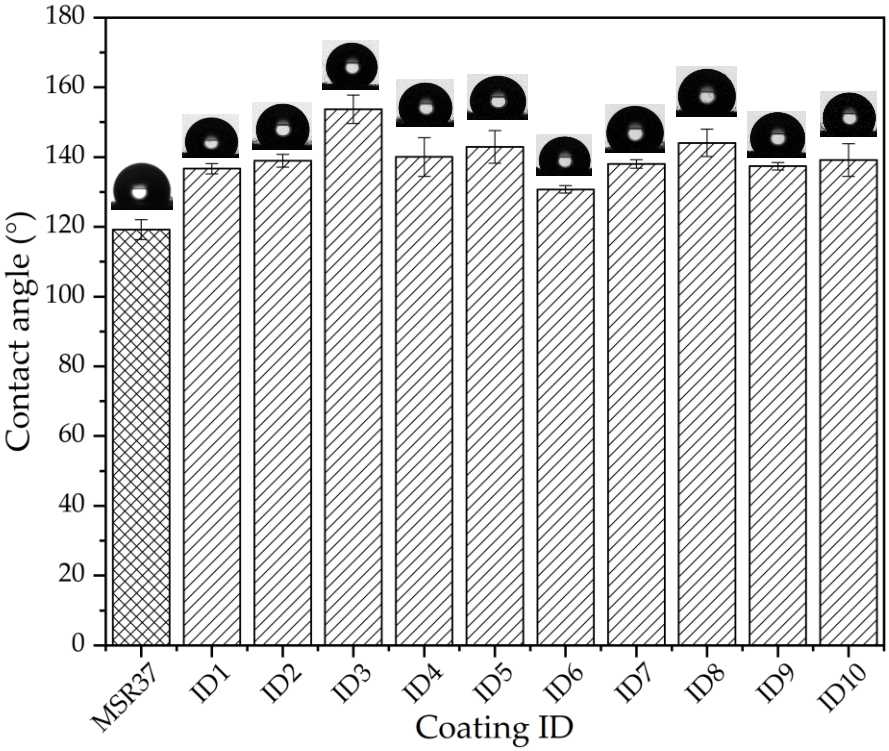

Figure 5-40: Contact angle vs coating ID for HDTMS functionalised silica

Figure 5-41 shows the relationship between the contact angle and particle size measured using DLS, there is very weak correlation between the two parameters, with the contact angle decreasing with increasing particle size.

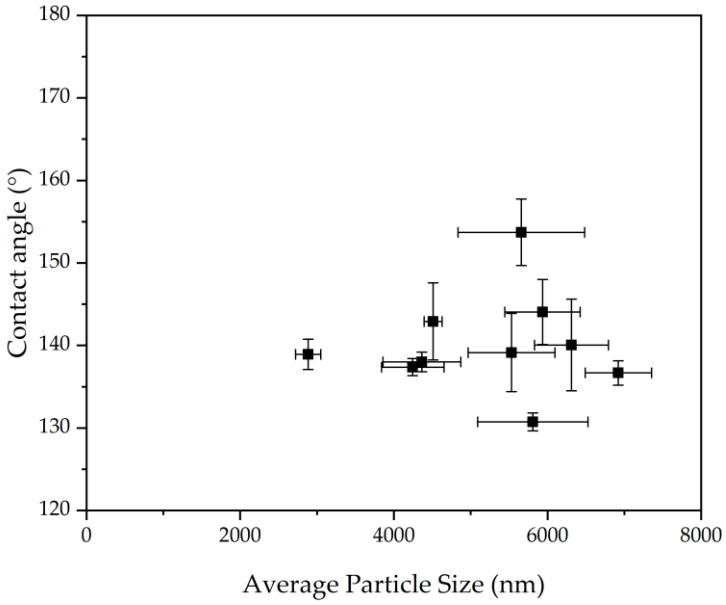

Figure 5-41: Contact angle vs particle size measured using DLS for the oleic acid functionalised nanoparticles.

Looking at the size of the particles measured using SEM imagery and their relationship, it appears that there is a more pronounced relationship between the size of the discreet particles and the contact angle. This relationship is

shown in Figure 5-42. It should be noted that while the relationship is stronger than for the particle sizes measured using DLS, it is still relatively weak, with a linear trendline only having an R^2 value of 0.27.

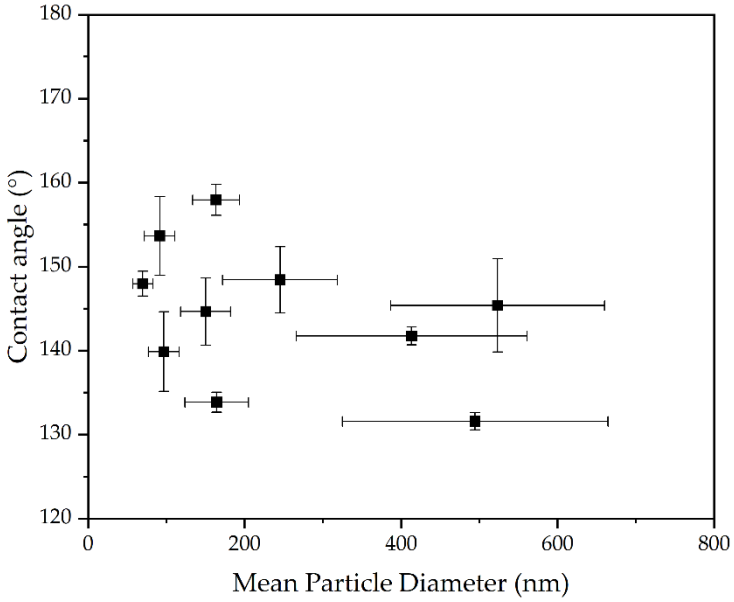

Figure 5-42: Relationship between contact angle and particle size measured using SEM imagery for the OA functionalised coatings.

Figure 5-43 shows the relationship between the PDI calculated using DLS and the contact angle. There is a positive correlation between the two parameters. The correlation is again quite weak and the standard deviation for these measurements were very high. The high standard deviations were a result of the high level of aggregation in some of the samples. However, the observed polydispersity was not as consistent as was seen in the FAS and HDTMS functionalised coatings. This shows that the particles were aggregating during the measurements, possibly suggesting that the aggregates are less stable.

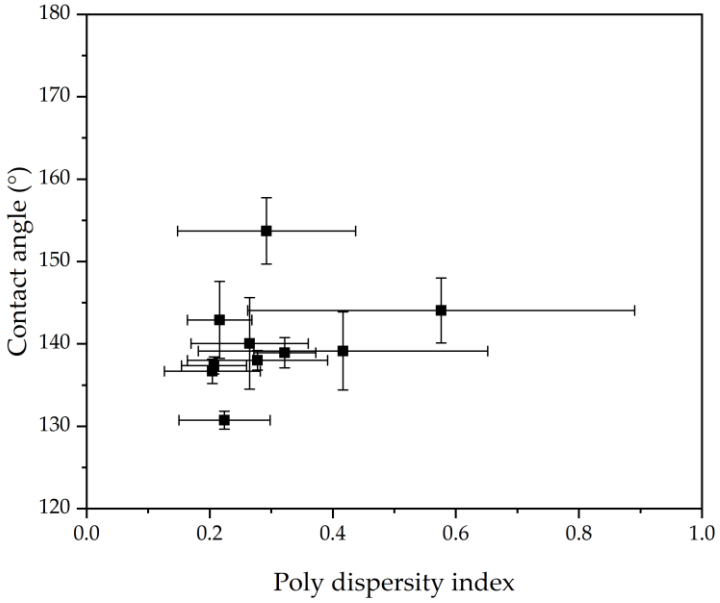

Figure 5-43: Contact angle vs polydispersity index calculated using DLS for the OA functionalised nanoparticles.

As was done for the other functionalising agents, the polydispersity index was calculated from the measurements made using SEM imagery. It appears that there is a negative correlation between the polydispersity index calculated using SEM images and the contact angle. This means that if the particles formed are more uniform in size the contact angle will be increased.

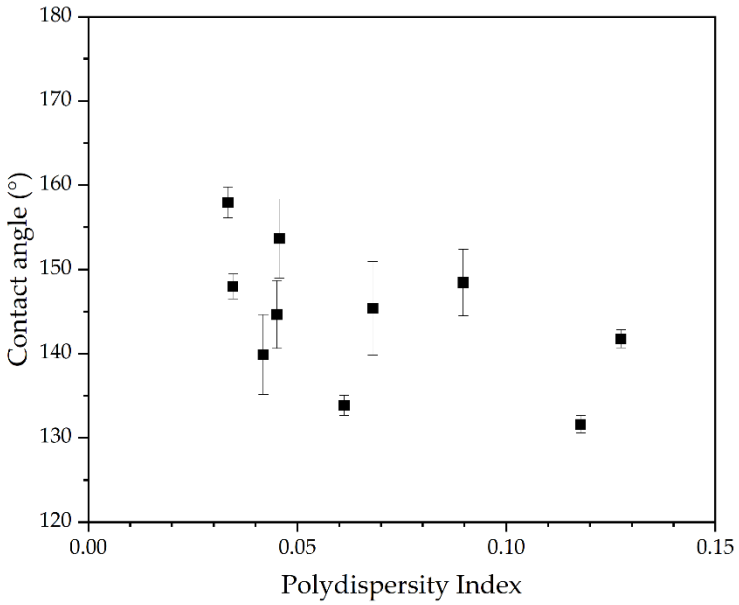

Figure 5-44: Contact angle vs polydispersity index calculated using the SEM images for the OA functionalised coatings.

For the OA functionalised particles, it is more challenging to find an analogue for the degree of aggregation due to the apparent instability of the aggregates. This is shown in Figure 5-43, the large error in the measurements are a result

of a broad range of instable particle sizes due to aggregation and subsequent break up of aggregates during the measurement. It is likely that similar to the HDTMS functionalised coatings, the particle sizes measured with DLS is the best analogue for aggregation. However, there isn't a strong relationship between the DLS measured diameter and the contact angle. This means that for the OA functionalised coatings the size and dispersity of the discreet particles controls the contact angle observed.

5.3.3 Air permeability

As was shown in the previous chapter, the hydrodynamics of the flow through the filter have a significant bearing on how well the filter performs with regards to water separation efficiency. It was shown that increased resistance resulted in diminished water separation efficiency. Therefore, it is important when applying a coating to have as little impact as possible on the resistance to the flow. The method used to measure this is air permeability.

5.3.3.1 FAS

Figure 5-45 shows how the air permeability was affected by the application of the coatings functionalised with FAS. In all cases the air permeability has been decreased, this is to be expected because material is being added to the fibres.

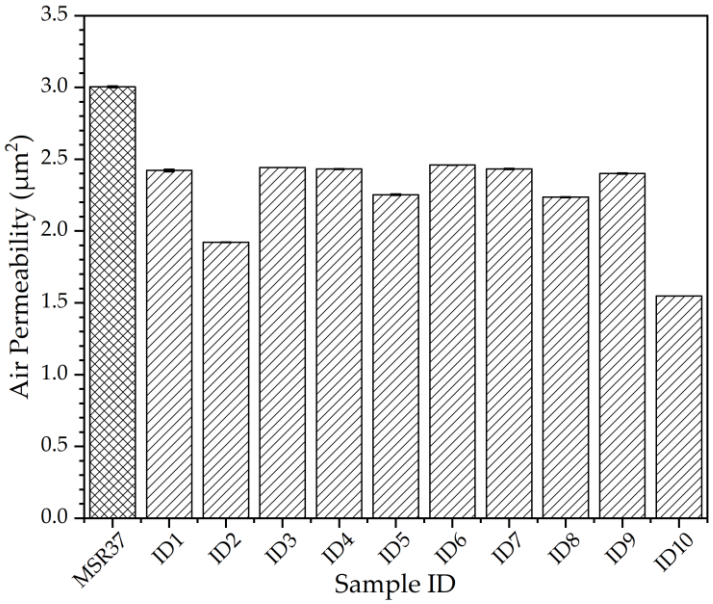

Figure 5-45: Air permeability against sample ID for the nanoparticles functionalised with FAS.

There are several characteristics of the particles that have an impact upon the air permeability. Figure 5-46 shows the relationship between the concentration of the compound used to functionalise the silica nanoparticle and the air permeability. There is an inverse proportionality between the air

permeability and the concentration of the functionalising agent. However, there is a large outlier that disagrees with this theory.

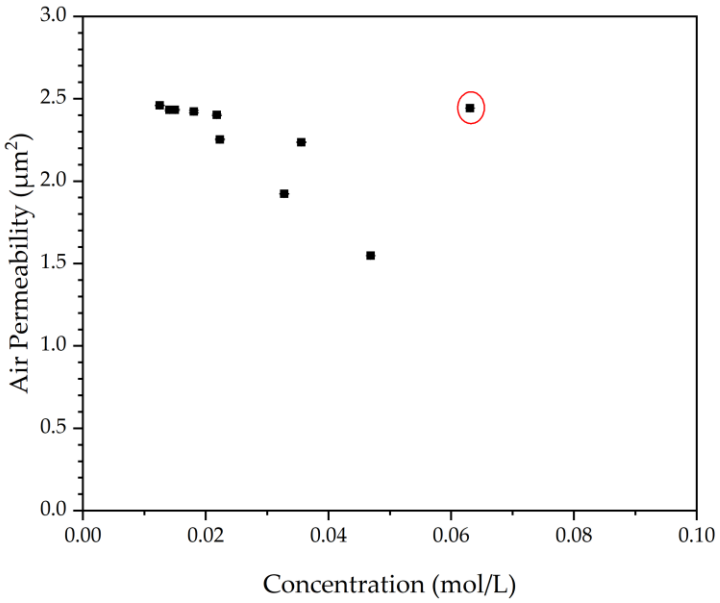

Figure 5-46: Air permeability vs concentration of functionalisation compound (FAS)

There is also a relationship between the air permeability and the average particle size. Figure 5-47 shows this relationship, generally smaller particles lead to increased resistance to flow. However, this trend is not particularly strong.

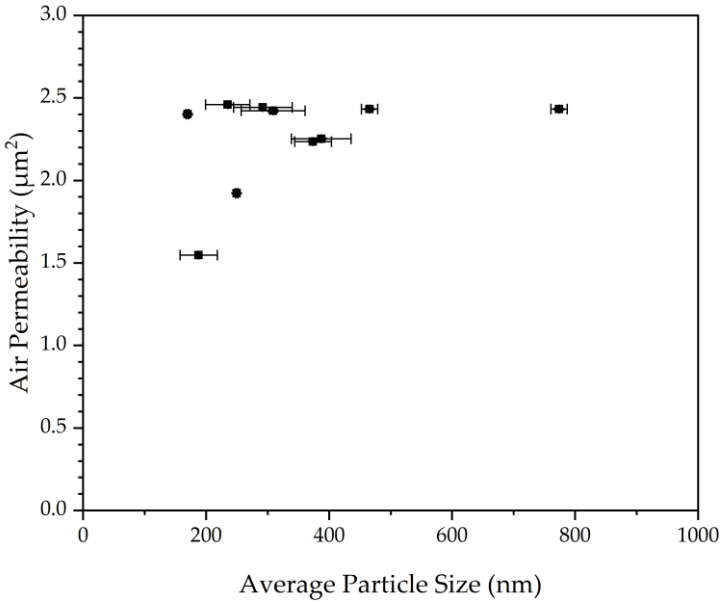

Figure 5-47: Air permeability vs particle size measured using DLS for the FAS functionalised silica nanoparticles.

As was done when analysing the air permeabilities, it is important to consider the sizes of the discreet particles as measured using SEM imagery. Figure 5-48

shows this relationship. There is no appreciable trend between the size of the particles measured using SEM and the air permeability.

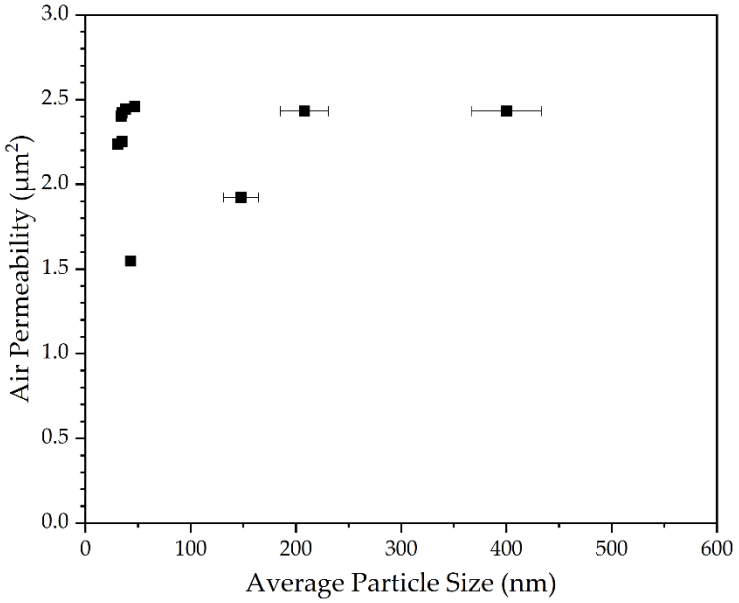

Figure 5-48: Air permeability vs the particle size measured using SEM for the FAS functionalised nanoparticles.

The effect of the polydispersity index on the air permeability was also assessed. It was found that the poly dispersity index for the particle size determined using SEM had a slight bearing on the air permeability of the final filter. It was theorised that the higher polydispersity index would lead to a more densely packed coating that may have been able to bridge smaller pores more effectively, resulting in decreased air permeability (207). There is a slight negative correlation between the PDI measured with SEM, shown in Figure 5-49.

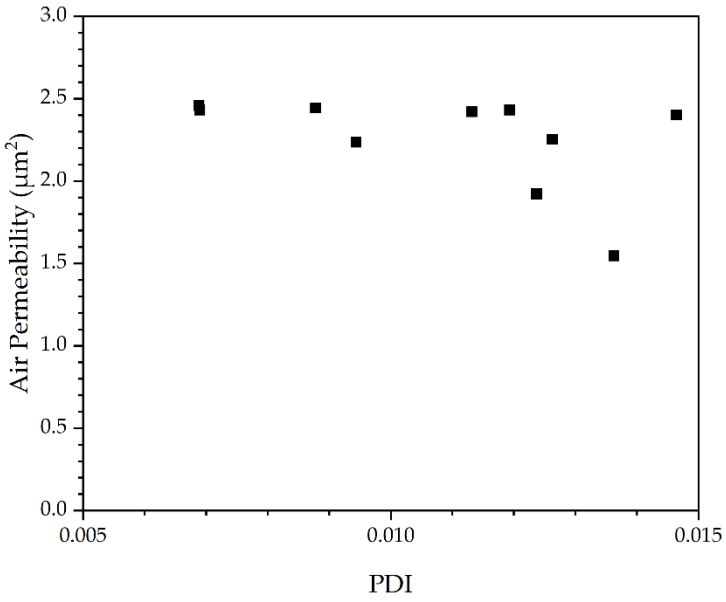

Figure 5-49: Air permeability vs PDI measured with SEM for the FAS functionalised coating.

The concentrations of the other compounds used in creating the microspheres were also assessed. Figure 5-50 shows how the concentrations of these compounds effect the air permeability. There is no relationship between these parameters and the air permeability.

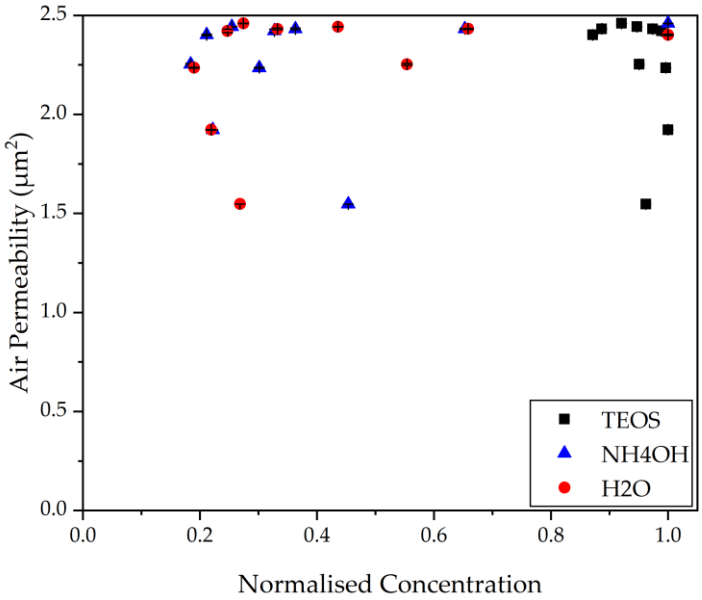

Figure 5-50: Air permeability vs concentration of silica forming reactants (FAS)

5.3.3.2 HDTMS

Figure 5-51 shows that the air permeability is again negatively affected by the application of the coating. The HDTMS functionalised coating has a greater impact upon the air permeability compared to the FAS functionalised coating.

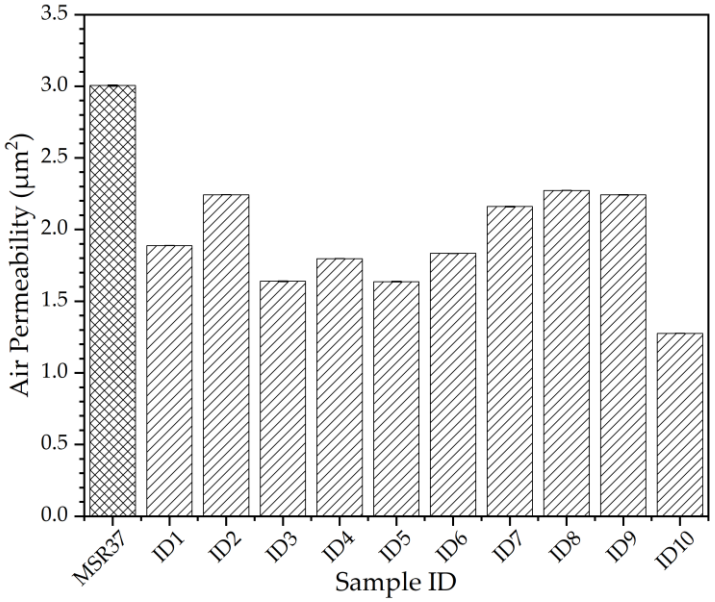

Figure 5-51: Air permeability against sample ID for the nanoparticles functionalised with HDTMS.

Figure 5-52 shows the weak negative correlation between the concentration of the functionalising compound and the air permeability. There is a negative correlation between the concentration and the air permeability, this is the same as what was seen for the FAS functionalised particles.

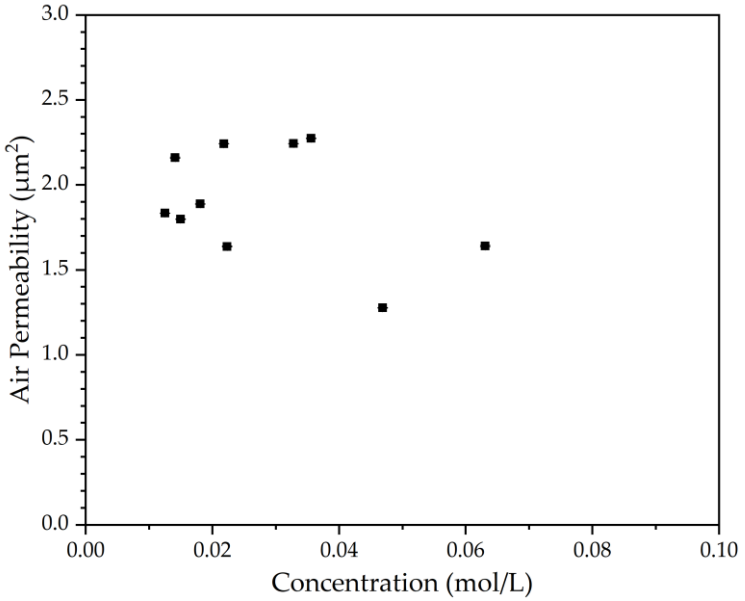

Figure 5-52: Air permeability vs concentration of functionalisation compound (HDTMS)

Figure 5-53 shows the relationship between particle size and air permeability. There is a weak negative correlation between the particle size and air permeability. It should be noted that the x-axis is on a logarithmic scale, this

differs from Figure 5-47 in which the same relationship is shown for the FAS functionalised nanoparticle coatings.

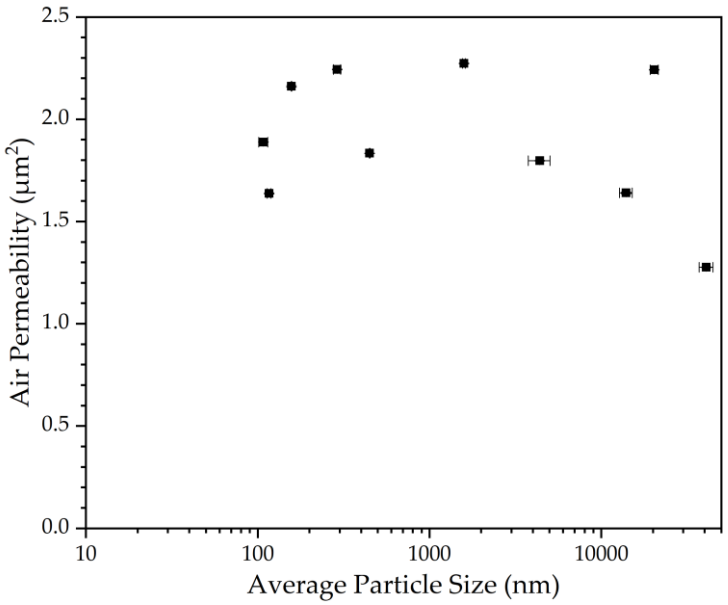

Figure 5-53: Air permeability vs particle size for the HDTMS functionalised silica nanoparticles

Figure 5-54 shows the relationship between the size of the discreet particles measured using SEM and the air permeability. There is a negative correlation between the size of the discreet particles and the air permeability. The larger particles result in reduced air permeability. The larger particles block the pores to a higher degree, resulting in a decreased air permeability.

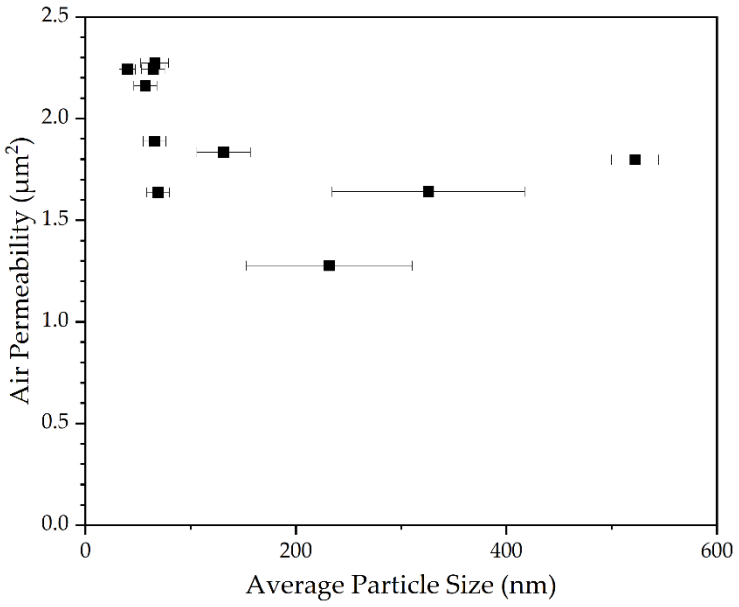

Figure 5-54: Air permeability vs average particle size for the HDTMS functionalised coatings

For the HDTMS functionalised particles, the polydispersity index calculated using SEM showed a correlation with the air permeability. The relationship is shown in Figure 5-55. This aligns with the theory that as the particles become more disordered the coating formed is denser making it more effective at blocking pores.

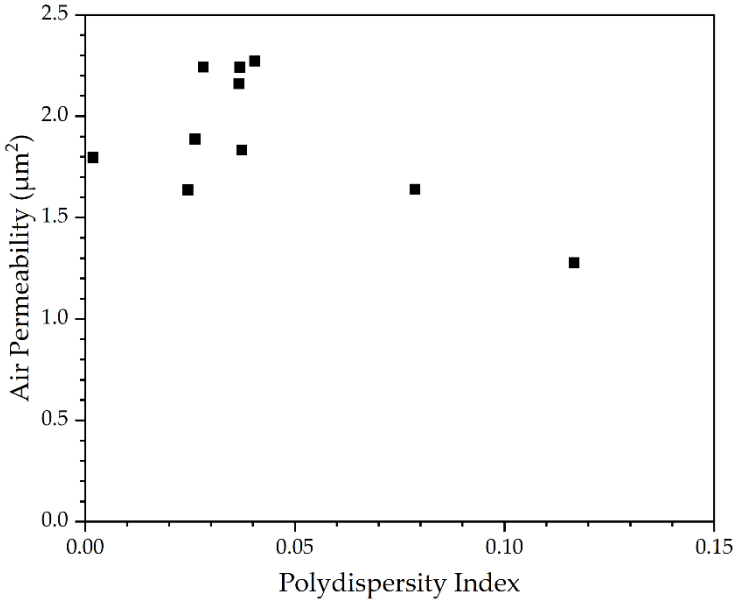

Figure 5-55: Air permeability vs polydispersity index calculated using SEM imagery for the HDTMS functionalised coating.

Figure 5-56 confirms that there is no correlation between the concentration of the reagents used to form the silica microspheres.

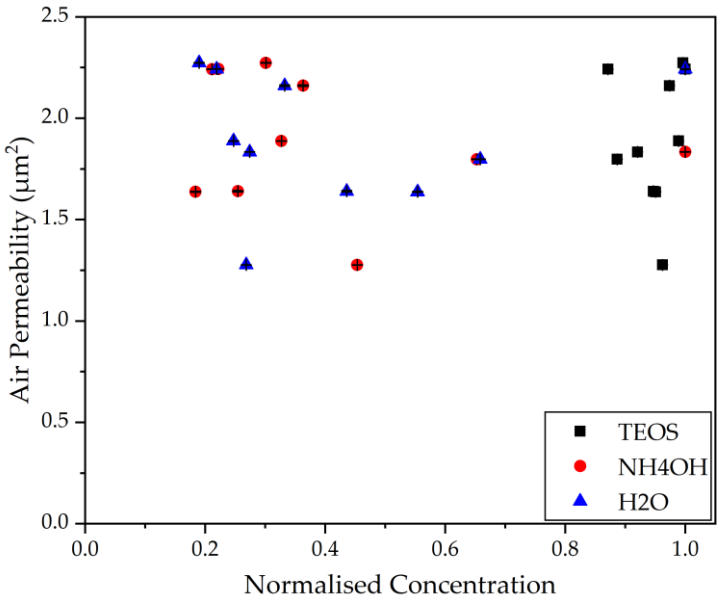

Figure 5-56: Air permeability vs concentration of silica forming reactants (HDTMS)

5.3.3.3 Oleic acid

Again, as expected the air permeability is reduced as a result of applying the coating, shown in Figure 5-57. On average the air permeability is higher that was seen in the HDTMS functionalised coating, but lower than for the FAS coating. There are two coatings (ID2 and ID4) that display quite high air permeability compared to the others.

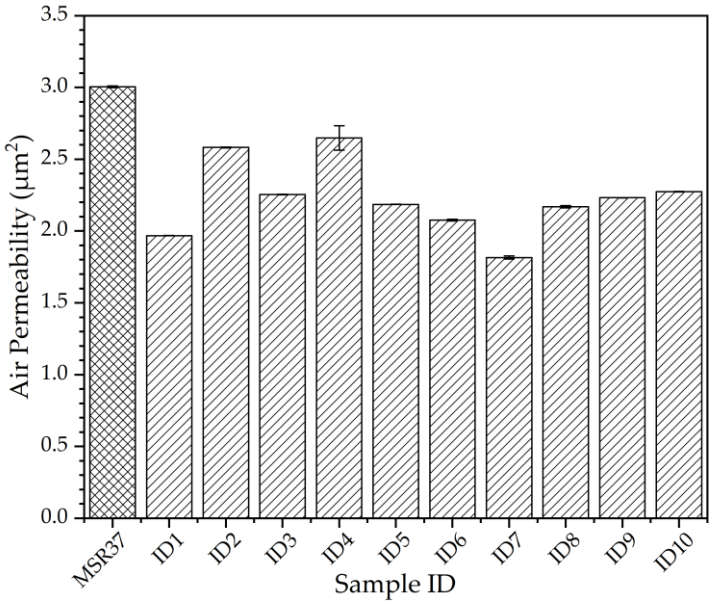

Figure 5-57: Air permeability against sample ID for the nanoparticles functionalised with OA.

There is a weak positive correlation between the air permeability and the concentration of oleic acid used to functionalise the silica microspheres, shown in Figure 5-58. This is the opposite of what is seen for the HDTMS and FAS functionalised coatings.

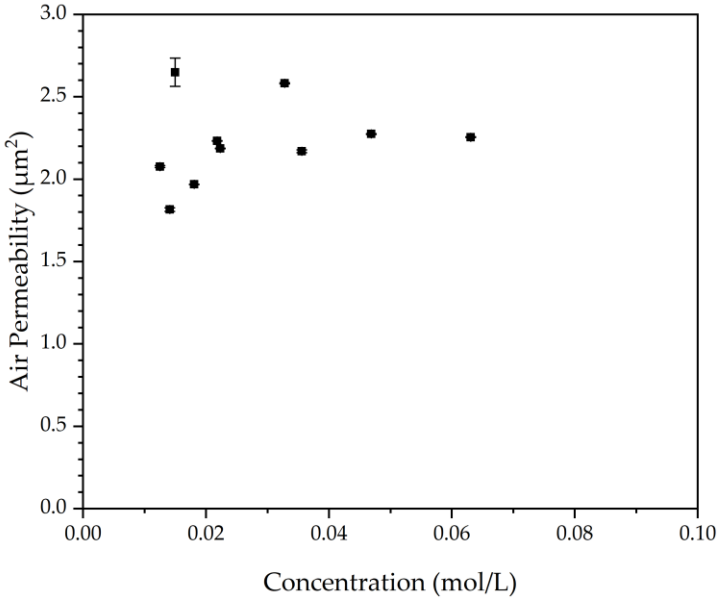

Figure 5-58: Air permeability vs concentration of functionalisation compound (OA)

There is a negative correlation between the air permeability and the average particle size, shown in Figure 5-59. However, this correlation is quite weak.

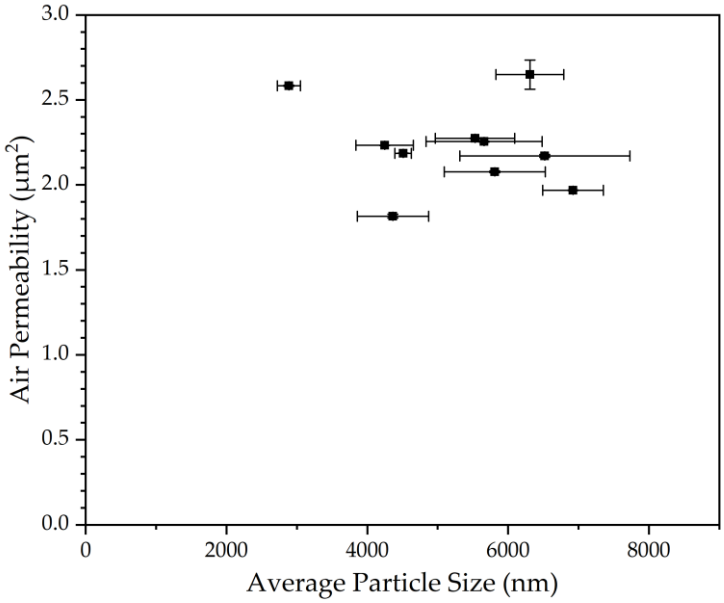

Figure 5-59: Air permeability vs particle size measured using DLS for the coating functionalised with oleic acid.

The relationship between the average particle size measured with the SEM and the air permeability is shown in Figure 5-60. There is a positive correlation between the average particle size of the individual particle and the air permeability. This suggests that larger particle sizes result in increased air permeability. This is likely because smaller particles form a tighter denser coating that is more capable of spanning pores without collapsing.

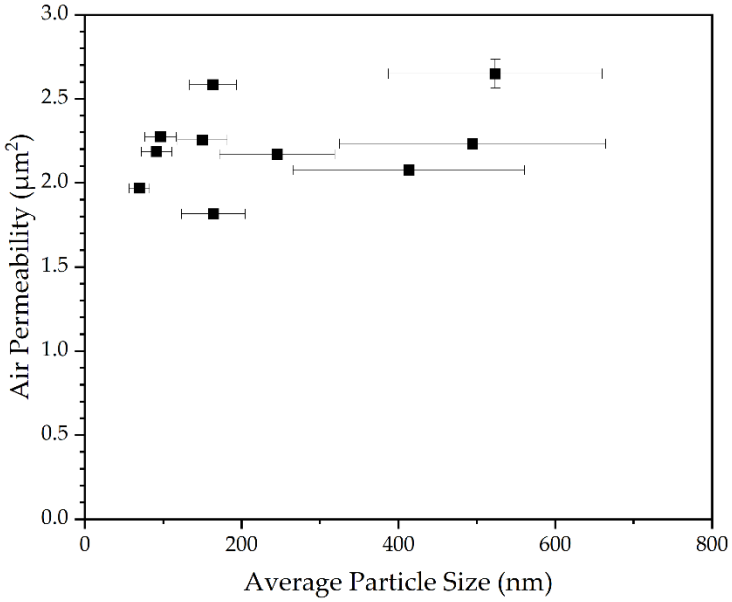

Figure 5-60: Air permeability vs particle size measured using SEM for the OA functionalised coatings.

There was found to be no correlation between the polydispersity index calculated with either DLS or SEM. For this coating the particle sizes had a greater impact upon the air permeability than the order of the particles. Figure 5-61 shows that there is no correlation between the concentration of the reagents used to form the silica microspheres.

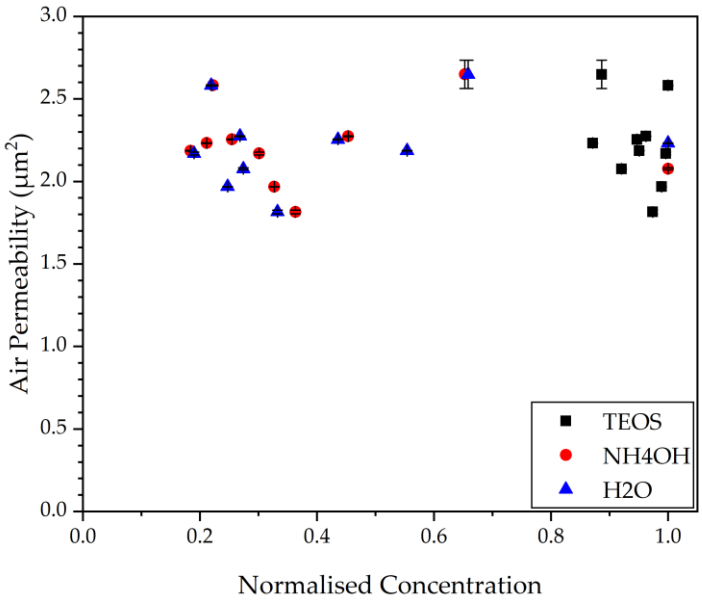

Figure 5-61: Air permeability vs concentration of silica forming reactants (OA)

5.3.4 Pore size distribution

It was shown in Chapter 4 that the fouling process changes the pore size distribution. This in turn had a negative effect upon the water separation

efficiency. With this in mind it is desirable for the pore size distribution to be affected as little as possible.

5.3.4.1 FAS

Overall, the pore size distribution is relatively unchanged when compared to the severity of what was seen in the fouled samples. The pore size distribution for the coated filters in Figure 5-62 saw an overall decrease when compared with the uncoated samples (represented by the transparent bar graph). The reduction in pore size suggests that the microspheres deposited are closing the pores. This will likely have a negative effect upon the water separation efficiency. If the increase in water separation efficiency provided by the increased hydrophobicity is greater than the negative effect of the pore restriction the coating will be successful in its initial goal of increasing the instantaneous water separation efficiency.

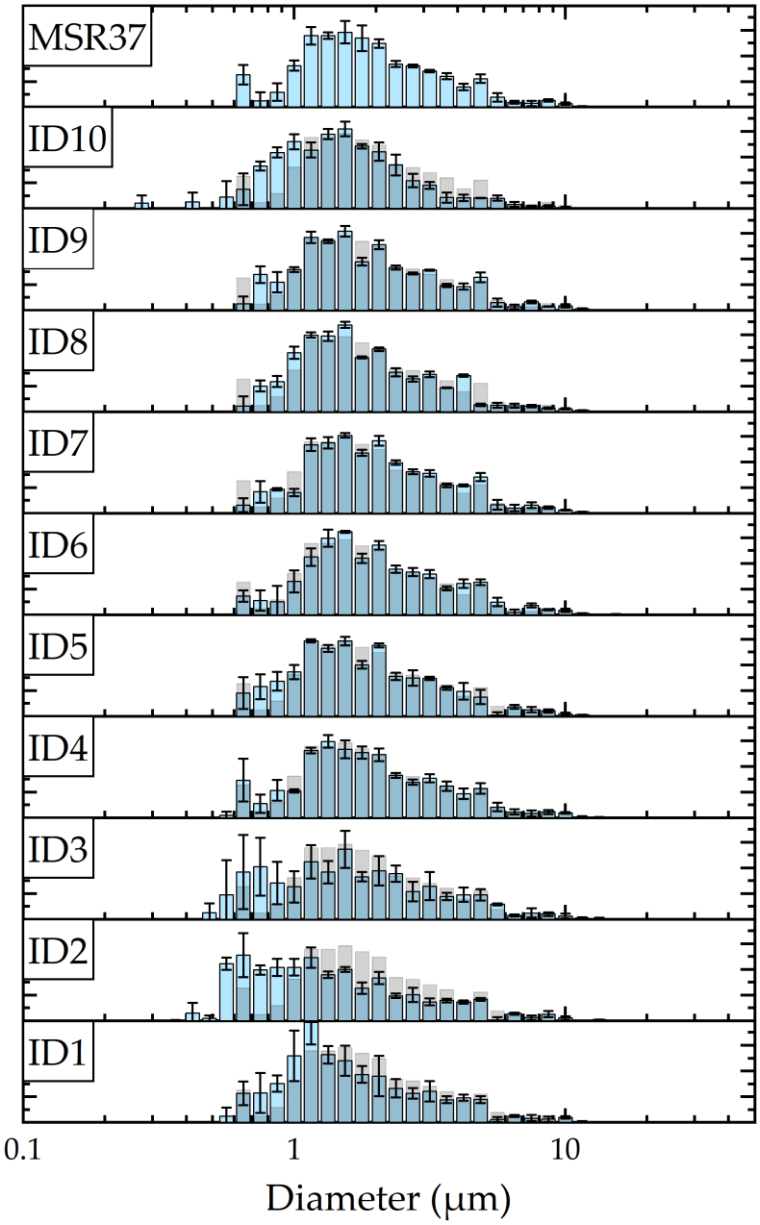

Figure 5-62: Pore size distribution for the coatings functionalised with FAS. (The transparent bars represent the uncoated pore size distribution)

In order to quantify the difference between the uncoated and coated filters the mean squared error was used. The root mean squared error equation is defined in equation 5-4.

$$\mathrm{RMSE} = \sqrt{\frac{1}{\mathrm{n}}\sum_{i=1}^{n}(I_{uncoated} - I_{coated})^2} \qquad \textbf{5-4}$$

Where n is the number of data points, $I_{uncoated}$ is the intensity of the uncoated filter and I_{coated} is the intensity of the coated filter. Interestingly there is a

strong correlation between the concentration of FAS used for functionalising the silica microspheres.

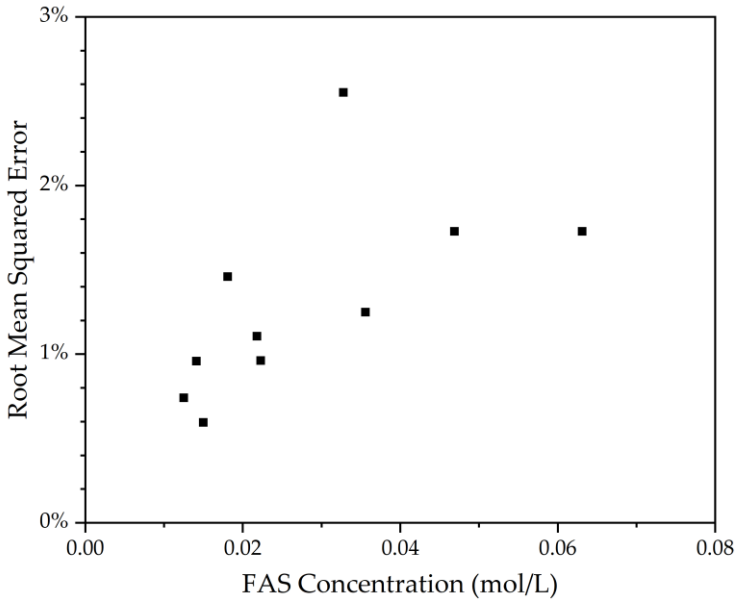

Figure 5-63: Change in error with the increase in functionalising compound concentration (FAS)

Additionally, the effect of the particle size and polydispersity index were examined as well. It was found that the particle size had no effect upon the pore size distribution for the FAS functionalised coatings. However, the polydispersity index had a significant effect. Figure 5-64 shows the correlation between polydispersity index calculated using DLS and the RMSE. Figure 5-65 shows the correlation for the polydispersity index calculated using the SEM images and the RMSE of the pore size distribution.

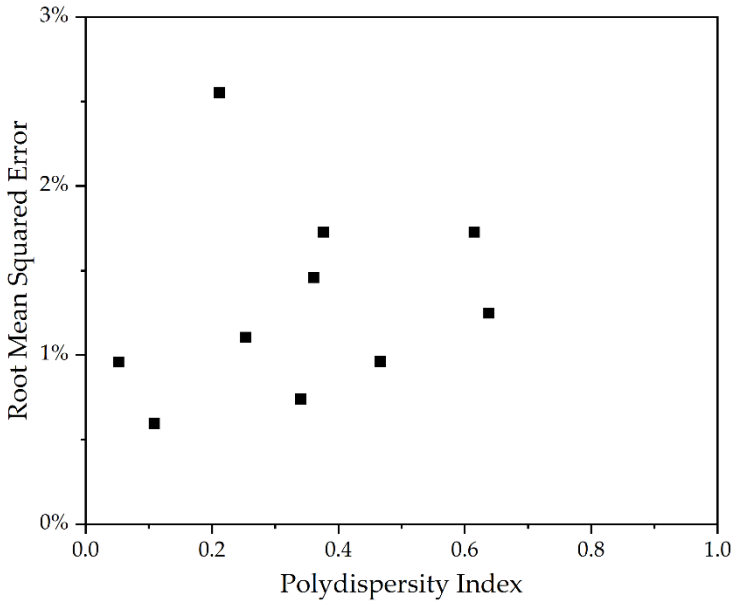

Figure 5-64: RMSE of the pore size distribution vs the polydispersity index calculated using DLS for the FAS functionalised coatings.

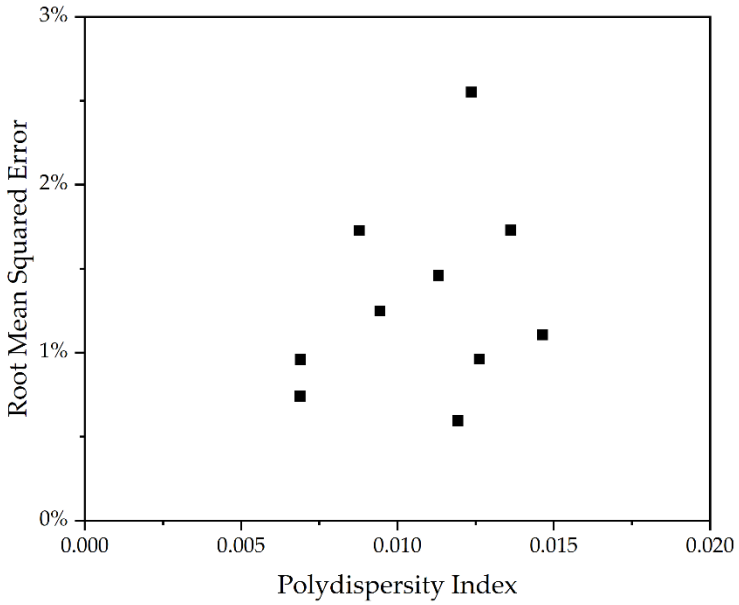

Figure 5-65: RMSE of the pore size distribution vs the polydispersity index calculated using SEM for the FAS functionalised coatings.

There is a positive correlation between in both figures above. As was mentioned previously, the polydispersity index calculated using DLS is an analogue for the tendency for aggregation. The correlation here helps confirm this, as the particles aggregate, they will be more likely to block the pores leading to changes in the pore size distribution and thus an increase in RMSE. It has also been theorised that as the disorder of the particles increase the coating formed will be denser and be more able to form over gaps, blocking

pores. The polydispersity of the discreet particles is a direct measure of the disorder, therefore the positive correlation with the RMSE is expected here.

5.3.4.2 HDTMS

The change in pore size distribution is more pronounced in the HDTMS functionalised coating. In all cases the coating applied has resulted in a reduced pore size. There are two coatings that have significantly reduced pore sizes (ID3 and ID10).

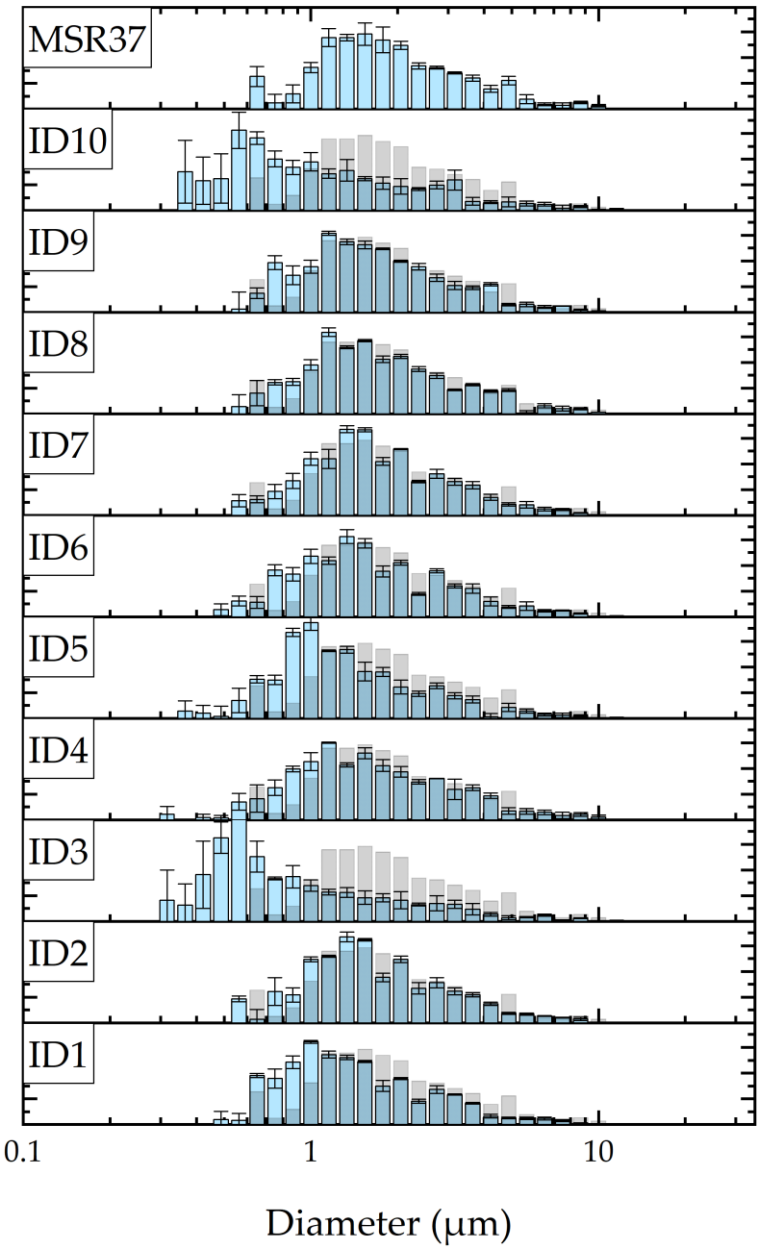

Figure 5-66: Pore size distribution for the coatings functionalised with HDTMS. (The transparent bars represent the uncoated pore size distribution)

Using the root mean squared error it is again possible to determine the extent to which the pore size distribution has been altered. Figure 5-67 shows how the concentration of the compound used for functionalisation is related to the change in pore size distribution. There is a positive correlation between the concentration of the functionalising compound and the error. This is the same as what is seen in the FAS functionalised particles.

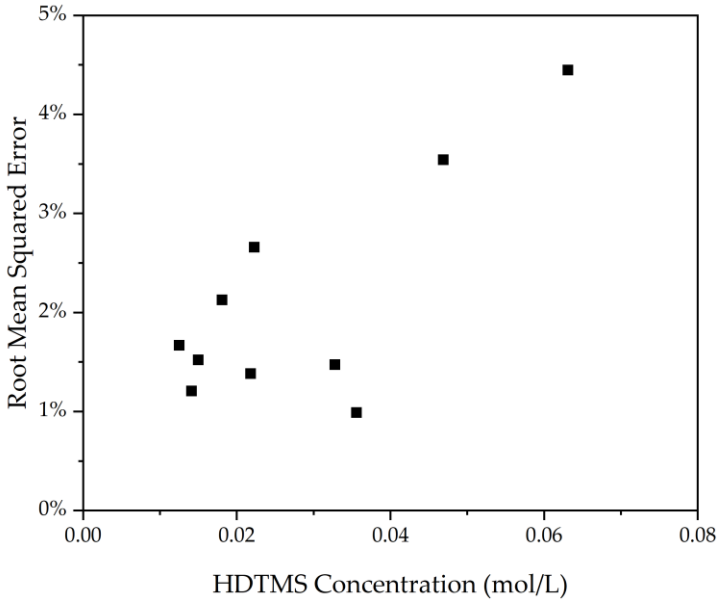

Figure 5-67: Change in error with the increase in functionalising compound concentration (HDTMS)

As was identified, the best analogue for the aggregation tendency is the particle size measured using DLS. Figure 5-68 shows the relationship between the particle size measured using DLS and the RMSE of the pore size distribution. There is again a positive correlation between the tendency to aggregate and the RMSE of the pore size distribution. This shows that as the aggregates form, they are more likely to block and restrict the available pores.

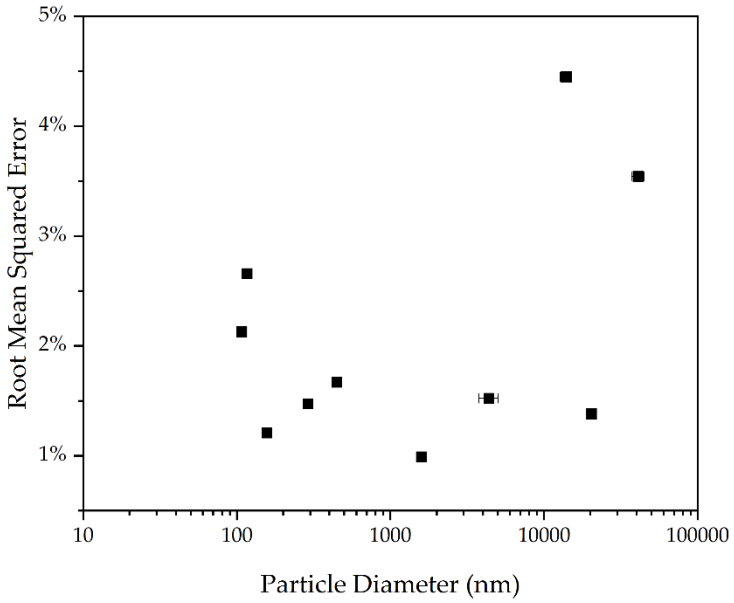

Figure 5-68: RMSE of the pore size distribution vs the particle size measured with DLS for the coatings functionalised with HDTMS.

It was shown that for the FAS functionalised coatings, the more disordered the discreet particles were, the higher the RMSE was. This same trend can be seen in the HDTMS functionalised coatings. Figure 5-69 shows the relationship between the polydispersity index calculated using the SEM data and the RSME. As the particles become more disordered, the pore size distribution is negatively impacted. This further supports the theory that increased disorder results in denser coatings that will more readily block pores.

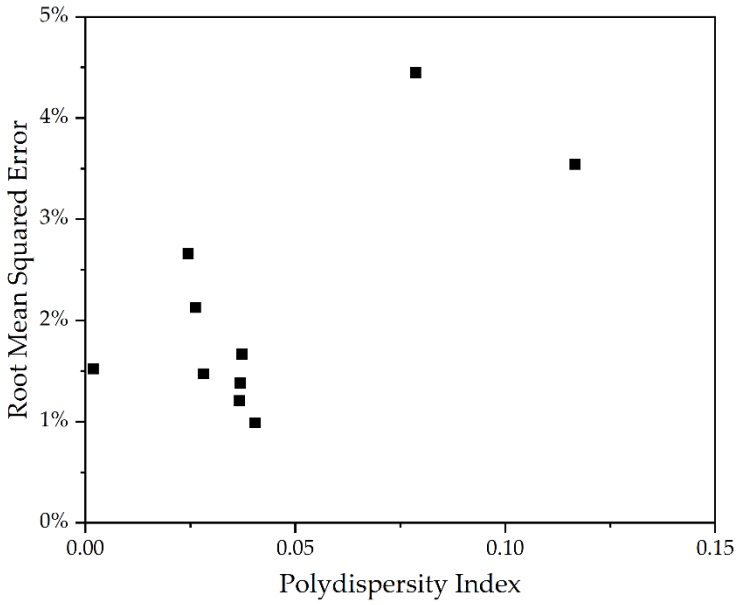

Figure 5-69: RMSE of the pore size distribution vs the polydispersity index calculated using SEM for the HDTMS functionalised coatings.

5.3.4.3 Oleic Acid

The same methodology was implemented for the oleic acid functionalised microspheres. The general trend is for the average pore size to be decreased by the application of the coatings, presented in Figure 5-70. The reduction in pore size is significantly worse for the coating formed using oleic acid as the functionalising compound when compared to the FAS functionalised coating. The average RMSE for the oleic acid functionalised coating is 0.019, significantly higher than for the FAS functionalised (0.013).

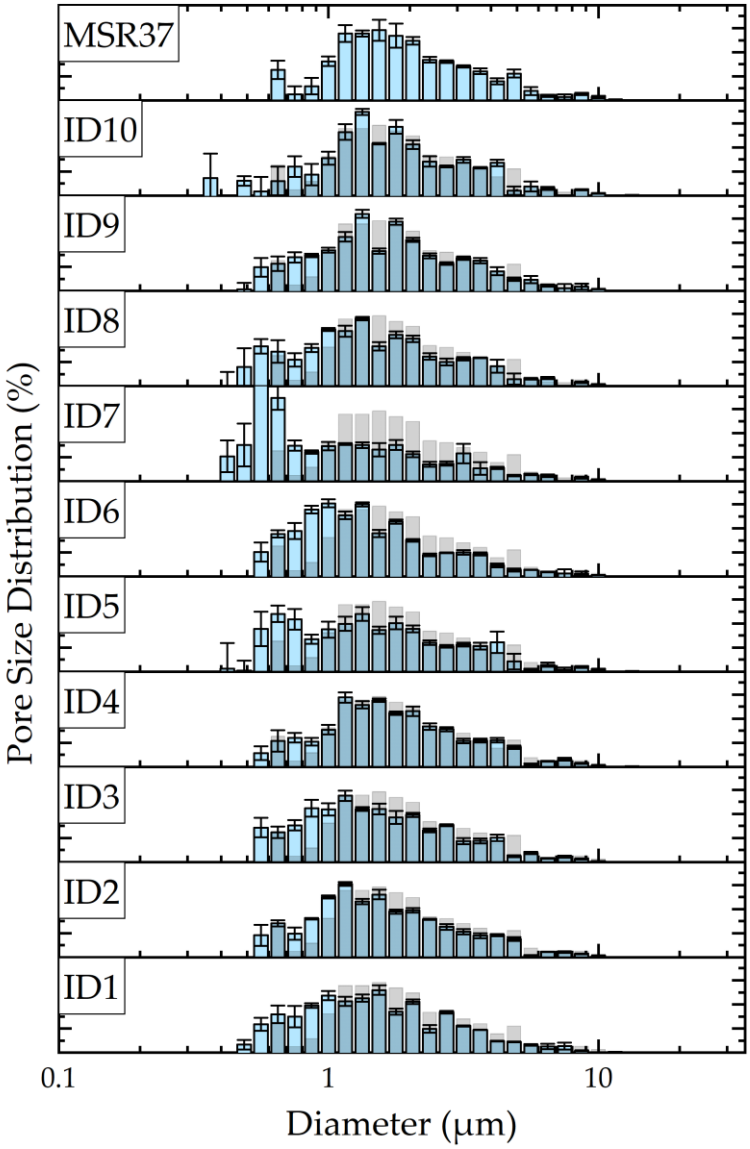

Figure 5-70: Pore size distribution for the coatings functionalised with oleic acid. (The transparent bars represent the uncoated pore size distribution)

While there is a correlation between the concentration of the functionalising compound for both the FAS and HDTMS, there is no correlation for the oleic acid functionalised coating.

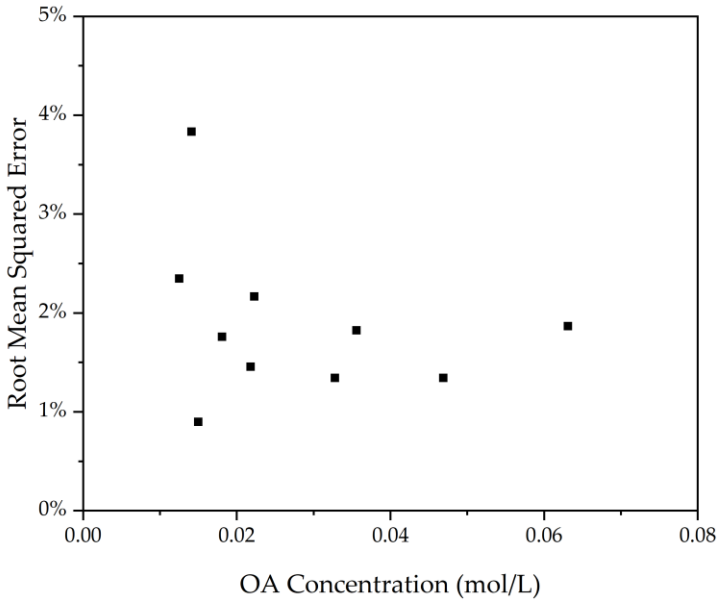

Figure 5-71: Change in error with the increase in functionalising compound concentration (OA)

The effect of aggregation and disorder in the particles must also be examined. Figure 5-72 shows the relationship between the polydispersity calculated from the DLS data. This is used as an analogue for the aggregation tendency. There is a slight correlation between the PDI and the RMSE. However, as was mentioned previously, the OA functionalised particles formed fewer stable aggregates. This is likely the reason that the correlations are weaker.

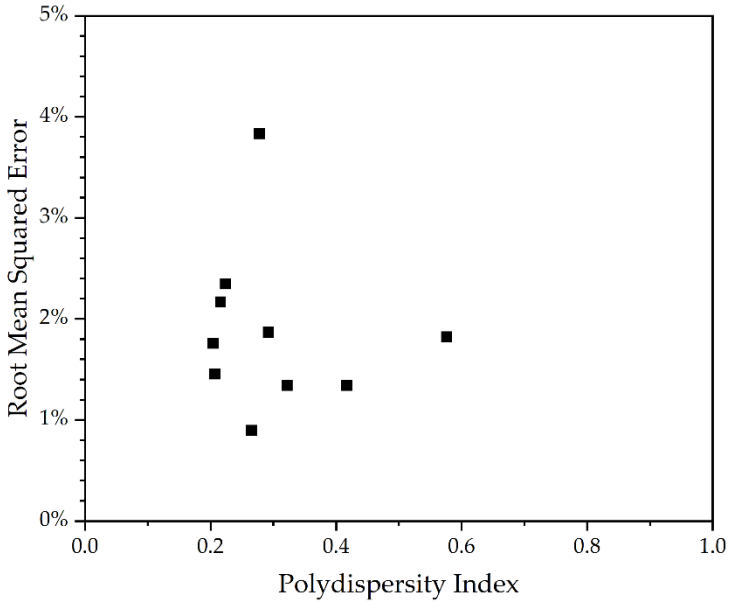

Figure 5-72: RMSE of the pore size distribution vs the polydispersity index calculated with DLS for the OA functionalised coatings.

It has also been found for the other functionalising agents that the disorder of the discreet particles can have an impact upon the final pore size distribution. The reason for this is that more disorder will lead to tighter packing and a

denser final coating that can more readily block pores. Figure 5-73 shows the relationship between the polydispersity index calculated suing the SEM data and the RMSE of the pore size distribution. There is a slight positive correlation between these two parameters, however the correlation is not as strong as was seen for the other two functionalising agents. This is possibly a function of the lower stability of the aggregates formed in the OA functionalised particles.

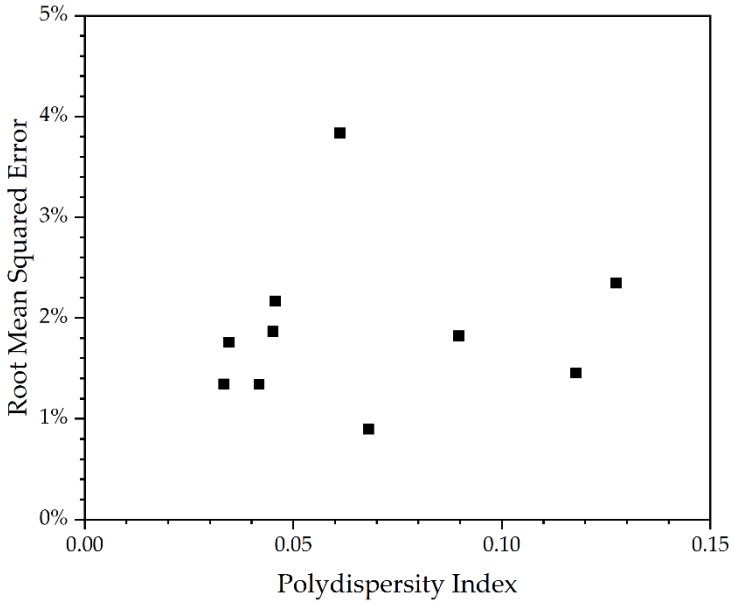

Figure 5-73: RMSE of the pore size distribution vs the polydispersity index calculated with the SEM data for the OA functionalised coatings.

5.4 Discussion

Three different functionalising compounds have been utilised to create hydrophobic silica particles.

- Fluoro-alkyl silane (FAS).
- Alkyl silane (HDTMS).
- Oleic Acid.

Having created these particles, the following testing was performed:

- Particle size via DLS.
    - There was significant amounts of aggregation in these particles, this can be used as the size of the aggregates that have formed.
- Particle size via SEM.
    - This is the true particle sizes formed prior to aggregation.
- Poly dispersity index (DLS)

    - This is significantly affected by the amount of aggregation and is used as an analogue for the degree of aggregation.
- Poly dispersity index (SEM)
    - This is a measure of how uniform the particle sizes created are.
- Contact angle.
    - This is an indication of the hydrophobicity of the particles formed.
- Air permeability.
    - This shows the increased restriction to flow that occurs as a result of applying the coating.
- Pore-size distribution.
    - This gives an indication as to how the particles are blocking the pores. Pore blinding, pore restriction, cake layer etc.

The aim of this chapter is to examine the coatings that were formed, determining the effect of controllable parameters on the final performance of the coating. The parameters that are indirectly controllable are:

- The particle size.
- The size distribution in the particles formed.
- The tendency of the particles to form aggregates.

These parameters have been controlled in this study by changing the concentration of the reagents used in the modified Stöber process, the addition of the functionalising agent made the changes relatively unpredictable as was shown by comparison to the work done by Bogush et al. (204). Figure 5-74 shows the FAS functionalised particles plotted alongside some of results from the literature. One thing that is clear is that the trend identified by Bogush et al.; (204) is not perfect. However, the results from literature do seem to follow a more consistent trend, again this difference is attributed to the one pot method used in this study. Okudera et al. (208) used ethanol as the solvent and ran the experiment at 20°C. Qi et al. (209) also used an ethanol solvent but ran the experiment at 25°C. Wang et al. (210) again used ethanol as the solvent and ran the experiments at 20°C.

It is also possible that other aspects had an impact upon the final particle size. Bogush et al. (204) controlled the reaction temperature to 20°C, in the experiments performed in this chapter all experiments were performed at room temperature. While this will be relatively stable, there will be fluctuations that are not measured. Having said this, over the range of temperatures likely in the laboratory the effect on particle size will likely be

minimal (209). However, it was shown by Qi et al. (209) that the polydispersity is much more sensitive to changes in temperature.

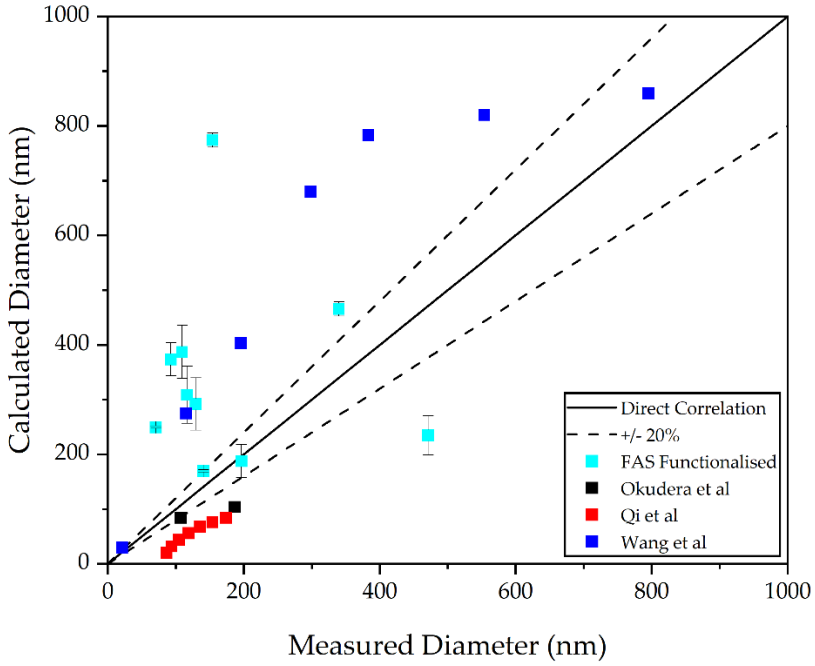

Figure 5-74: FAS functionalised particle diameter plotted alongside results from literature (208) (209) (210).

It would appear that the deviation from what was found in the work by Bogush et al. (204) is primarily caused by the addition of the functionalising agents. The two silane derivative functionalising agents will react in a similar way to the TEOS, hydrolysing and condensing alongside it to form a silica nanoparticle core with a functionalised shell. The reason that a shell will form is that the condensation reaction for the functionalising agents will occur at a slower rate. The accepted reason for the difference in reaction speed is the increased steric hinderance associated with the large functional groups within the functionalising compounds (211).

Once a shell has formed on the surface of the silica the growth of that particle will be impacted. There will be no more free Si-OEt bonds to react with the remaining TEOS in the system. As has been said the rate of reaction of the TEOS will be greater than the functionalising agent. However, there will be an overlap in reaction resulting in a change to the final particle sizes, this will also likely lead to higher polydispersity (212). This was not confirmed in the experiments conducted. However, there is only a relatively small sample size for the number of parameters that were being examined.

The mechanism for the oleic acid functionalising compound will be different. In this case the oleic acid adsorbs onto the surface of the silica molecule. This

was shown by Li et al. (119) using XPS. It was confirmed that similar to the core and shell that is produced using the other functionalising compounds, the oleic acid forms a surface layer. It was not possible to determine whether the oleic acid physically or chemically adsorbs onto the surface. This study was conducted using a two-step process in which oleic acid was added to a solution containing pre prepared silica nanoparticles. The effect of the presence of oleic acid during the hydrolysis and condensation reactions of the Stöber process was not examined. However, from the results that were obtained in this chapter it is likely that the oleic acid alters the production of the silica nanoparticles.

In order to determine whether the particles formed were suitable for increasing the hydrophobicity of the filter material, the contact angle was assessed. For all of the coatings formed, the contact angle was increased when compared to the untreated filter material. This is shown in Figure 5-29, Figure 5-35 and Figure 5-40 for the FAS, HDTMS and OA functionalised coatings respectfully.

Fluoroalkyl silanes have been used to functionalise silica numerous times, with reports of achieving superhydrophobicity. There are several different definitions for superhydrophobicity, the common aspect is having a water contact angle in excess of 150° (203). It has been possible to form 3 coatings that display superhydrophobicity using the FAS functionalising agent. Both HDTMS and Oleic acid have also been used as functionalising agents to form superhydrophobic coatings. HDTMS has been used in one-stage systems similar to the methodology in this work (121) (213) . However, oleic acid is more often used as a second stage functionalising agent (119). It was possible to create superhydrophobic coatings with both functionalising agents in a one-step process in this work.

For each of the functionalising agents, the characteristics of the particles formed were assessed with respect to their impact upon the contact angle. The most significant characteristics that were identified for the FAS functionalised coating were the polydispersity index of the particle size measured using SEM and the polydispersity index of the particle size measured using DLS. The reason these were the most significant parameters is that the SEM measured particle size is considered to be the true particle size, therefore the polydispersity index is a measure of size distribution of these particles. The polydispersity index of the particle size measured with DLS is a measure of the tendency of the particles to aggregate. The size distribution of the particles

has a positive correlation with the contact angle, where the increasing aggregation resulted in decreased contact angles.

The size distribution will have an impact upon the roughness of the formed coating. A larger size distribution will result in a closer packed coating. This will in turn decrease the roughness. The decreased roughness will lessen the Cassie-Baxter effect resulting in overall lower contact angles. For the FAS functionalised coatings, it appears that an increased size distribution increases the contact angle. This is the opposite of what would be expected, looking at Figure 5-33, the range of PDI for the FAS functionalised particles is quite small. It is possible that a greater size distribution resulted in a dual scale roughness, something that is often shown to increase the contact angle (214).

It appears that the aggregation tendency is impacted by the concentration of the functionalising agent. Figure 5-75 shows this relationship. It is possible that the lower reaction rate of the functionalising agent (compared to TEOS) results in the functionalising agent acting as an adhesive to the already formed SiO_2 microspheres. It is not immediately clear why this increase in aggregation has a negative impact upon the contact angle, however, it is likely due to the impact that it has on the amount of air trapped within the structure.

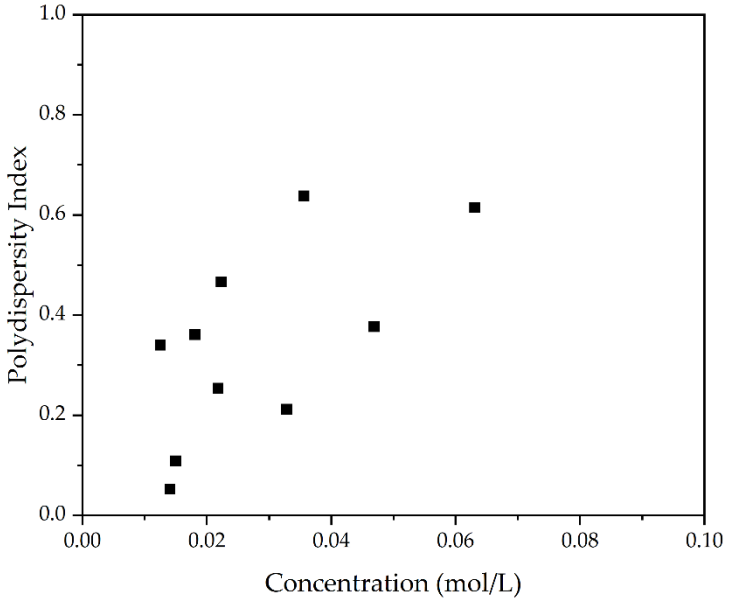

Figure 5-75: Polydispersity index (DLS) vs concentration of the functionalising agent for the FAS functionalised coatings.

For the HDTMS functionalised coatings similar indexes could be used to assess the efficacy of the particles. Again, the SEM was used to measure the true size of the particles formed. The polydispersity index of the particle sizes measured with SEM has a negative correlation with the contact angle, shown in Figure 5-39. This is what would be expected. The increased size distribution

leads to decreased roughness. For the coatings functionalised with HDTMS, the tendency for aggregation was better described by the particle size measured with DLS. This is because the aggregates formed were more consistent and larger the size of the aggregates more accurately represented the aggregation tendency for the HDTMS functionalised particles.

It was shown that the contact angle decreased with increasing aggregation. Particles that aggregate more readily are likely forming more compact coatings with lower roughness. This will decrease the Cassie-Baxter effect leading to decreased contact angles. There is also a negative correlation between the contact angle and the poly dispersity of the particle sizes measured using the SEM. This is not what was seen in the FAS functionalised samples, however the range of poly dispersity in the FAS functionalised samples was much smaller. Increased order in the particles will likely reduce the roughness leading to lower overall contact angles.

Similar trends were seen in the oleic acid functionalised coatings, in this case similar analogues were used as was done for the HDTMS functionalised particles. The average particle size measured using DLS was taken as an indication of the aggregation tendency. The aggregation tendency again had a negative correlation with the contact angle as would be expected. For the Oleic acid functionalised particles, the particle sizes measured using SEM had a negative correlation with the contact angle, this is the opposite of what was seen for both the FAS and HDTMS functionalised particles. It is possible that this difference is due to the differing formation methods between the silane based functionalising agents and the oleic acid functionalising agents.

For all coatings it has been shown that the morphology of the particles has an impact upon the air permeability and the pore size distribution. With regards to air permeability and pore size distribution FAS and HDTMS the coatings have similar effects upon the air permeability and the pore size distribution. Generally, increased disorder reduces the air permeability overall. This is likely caused by tighter packed coatings. For both the FAS and HDTMS functionalised coatings there is a positive correlation between the tendency to aggregate and the change in pore size distribution. This is likely caused by larger aggregates being able to form and block pores.

It has also been shown that the concentration of the functionalising agents for both the FAS and HDTMS functionalised coating agents has a significant correlation with the change in pore size distribution. It is likely that this is because the slower hydrolysing functionalising agents can act as binding

agents for the discreet particles resulting in a decrease in the air permeability and adversely affecting the pore size distribution.

It was found that there was no appreciable trends between any of these variables and the air permeability or the change to pore size distribution for the oleic acid functionalised coatings. It should be noted that the method for coating is relatively prone to variation, this could explain the lack of correlation, especially if the correlation wasn't very strong. The Oleic acid has a different reaction mechanism with the surface of the silica nanoparticle. The acid head of the molecule will form hydrogen bonds with the silanol groups at the surface of the silica nanoparticle (215). This doesn't require any hydrolysation, therefore is free to occur as soon as silanol groups are available. This would likely cause greater disruption to the growth of the silica particles, leading to greater variation in the particle morphology.

5.5 Conclusions

The primary aim of this chapter was to form superhydrophobic particles, the formation of the coatings has been successful, for all of the functionalising agents selected it has been possible to form superhydrophobic coatings. The key objective of achieving this in a one-pot method was also successful. This is something that has not been reported for the Oleic acid functionalised coating before. The aim of forming particles with different morphological properties has been achieved, this allowed the analysis of the most desirable properties for hydrophobicity. It has been shown that the properties of the particles can be controlled by changing the variables in the Stöber process. However, a key finding is that the addition of the functionalizing agents has been shown to affect this significantly alter the way that the Stöber process can be controlled. The addition of the functionalising agents appears to increase aggregation of the particles and cause the size to deviate from what would be expected. However, deviation was not consistent between the functionalising agents, it appeared that oleic acid had a different impact compared to the other two functionalising agents likely caused by the different chemical reaction that forms the outer hydrophobic shell.

The morphology of the particles has a significant effect upon the critical operating parameters of the filters coated. It appears that the contact angle could be tuned by altering the morphology of the particles. It was found that the FAS functionalised coatings formed a dual scale roughness that aided in the Cassie-Baxter effect resulting in higher contact angles. Many of the

correlations between the morphology of the particles and the contact angles were attributed to the effect on roughness.

It was shown that for the FAS and HDTMS functionalised coatings the smaller particles that were more prone to aggregation had a greater negative impact on the pore size distribution and the air permeability. The higher aggregation tendency would allow particles to block pores more readily. It was also shown that there is a correlation between the concentration of functionalising agent and the negative impact on the physical characteristics of the filter. This was attributed to the slower hydrolysation of the functionalising agent being able to act as a binding agent between the particles, leading to more substantial blockages of the pores.

It was shown that the oleic acid performed differently compared to the silane based functionalising agents. The same correlations were not found. This is concluded to be caused by the difference in interaction between the functionalising agent and the surface of the silica particles. The oleic acid would not hydrolyse and form a shell in the same way as the other functionalising agents used, it is more likely that the oleic acid molecules would form a hydrogen bond at the surface of the silica nanoparticle resulting in more variation.

Overall, the aim of creating superhydrophobic particles for coating the as prepared melt blown polymer filter has been successful. Two coatings from each functionalising agent were selected, to be analysed further in the following chapter. This selection was made based on the information obtained in Chapter 4, the two key things that impact the water separation efficiency of the filter are hydrophobicity and restriction to flow. Therefore, for each functionalising agent the coating that caused the lowest physical change as identified by the pore size distribution and the coating which had the highest hydrophobicity as identified by the contact angle.

Chapter 6
Testing the coatings

6.1 Introduction

This chapter will examine the efficacy of the specific coatings that have been created. The coatings that have been applied to the clean filter material will be tested first for the instantaneous water separation efficiency. It is also important to determine whether it has been possible to increase the end-of-life performance. It was not possible to do this by using the filters on engines being run in the real world, therefore two different lab-based methods were used.

The main aim of this chapter is to prove that the coatings formed in Chapter 5 result in an improvement to the filter material. This will be assessed on two fronts, first the instantaneous water separation performance will be assessed. This will be done using the flow rig. The results from this will ensure that increasing the hydrophobicity at the surface of a barrier filter also increases the instantaneous water separation performance in a diesel-water emulsion flow environment.

The second front on which the filters will be assessed is the end-of-life performance. In order to achieve this a facile method of increasing the face velocity and assessing the response was used, as well as the development of a novel laboratory technique for fouling diesel barrier filters. The chapter will also validate that the accelerated fouling process developed is representative of what is seen in the field by comparing the filters that have undergone accelerated fouling with the filters returned from the field.

6.2 Materials and Methods

6.2.1 Selection of the coatings to test

It was not possible to determine the efficacy of all of the coatings that were formed due to time constraints. Therefore, two filters were selected from each of the functionalising compounds. It was shown in Chapter 4 that there were two primary properties that affected the water separation, the contact angle and the pressure drop. It was not possible to determine the pressure drop of each of the samples again due to time constraints; however, it has also been shown that the pore size distribution is related to the pressure drop. For each

functionalising compound the coating with the highest contact angle was chosen, a second coating with the lowest change in pore size distribution (as quantified by RMSE) was also chosen. The selected coatings are listed in Table 6.1.

Table 6.1: Coatings selected for performance evaluation.

Functionalising compound	ID	Reason
FAS	4	Low physical change
FAS	7	High contact angle
HDTMS	8	Low physical change
HDTMS	2	High contact angle
OA	4	Low physical change
OA	3	High contact angle

6.2.2 Methods

Figure 6-1 shows the methodology that is used in this chapter. All of the techniques are completed following the methodologies laid out in Chapter 3.

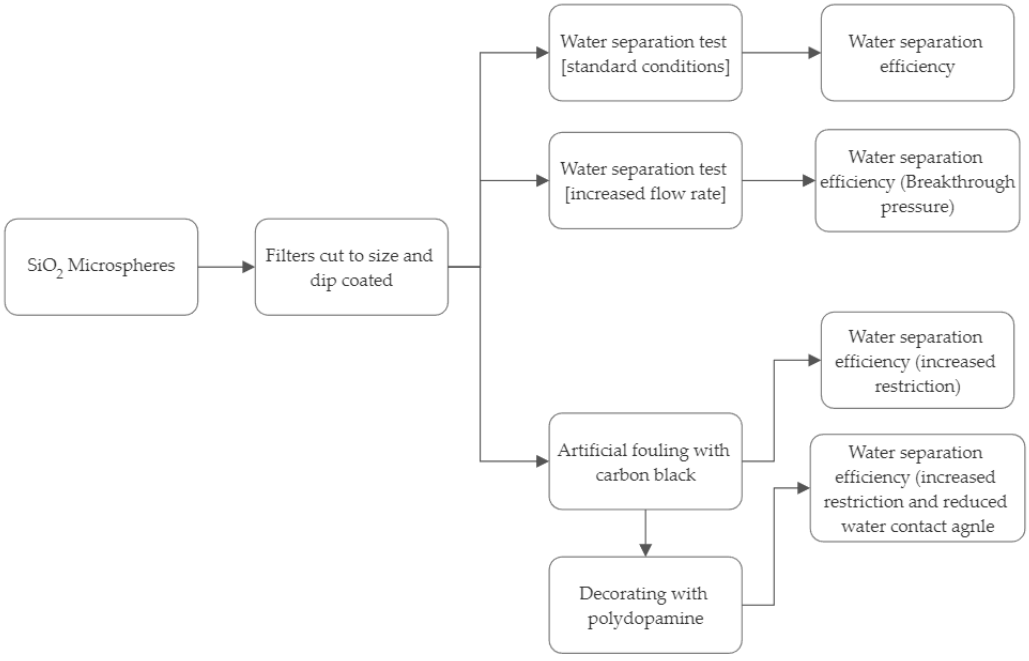

Figure 6-1: Block diagram of the methodology used in evaluating the coatings.

In all cases the experiments were run three times, the values quoted are an average of these three runs and error bars that are shown are the standard deviation between these three values.

6.3 Results

6.3.1 Water separation efficiency

It has been shown that in all cases the water separation efficiency has been improved by applying the microspheres. The performance of the coated filters is far greater than was found for the uncoated filter material, as can be seen in Figure 6-2. One aspect that is of note is that the performance of the filters identified as having a particularly high contact angle outperform the filters showing relatively unchanged pore size distributions for all the functionalising compounds.

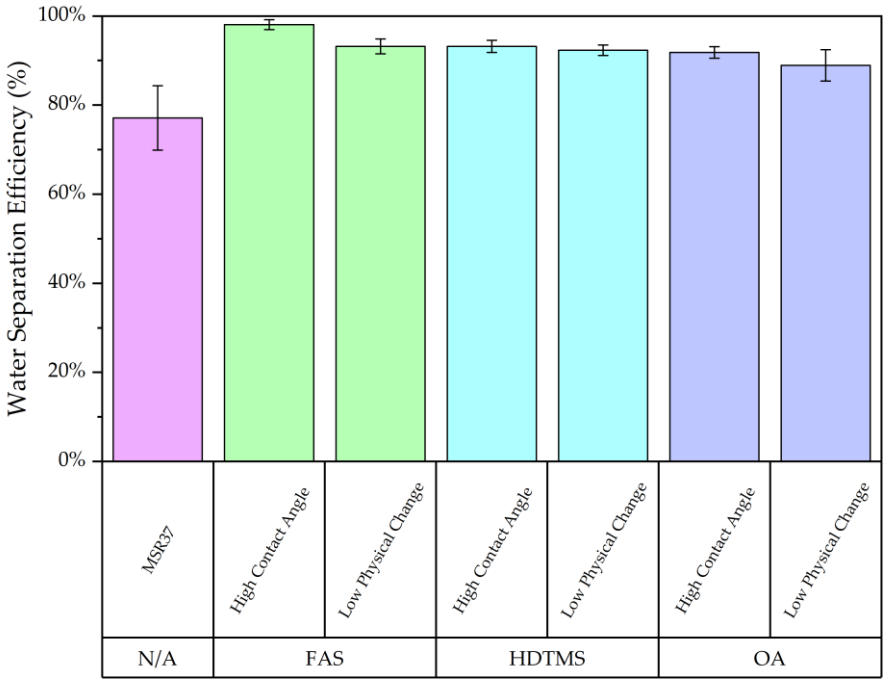

Figure 6-2: Water separation efficiency performance of the coated filters compared to the uncoated filter material.

Having run the experiments pressure drop data was also recorded, shown in Figure 6-3. For all the coatings selected the pressure drop has been increased when compared to the uncoated MSR37 filter. As expected, the filters that have the largest change in pore size distribution have the largest increase in pressure drop. The only coating that does not follow this pattern is the HDTMS functionalised microspheres, it is not immediately clear what has caused this.

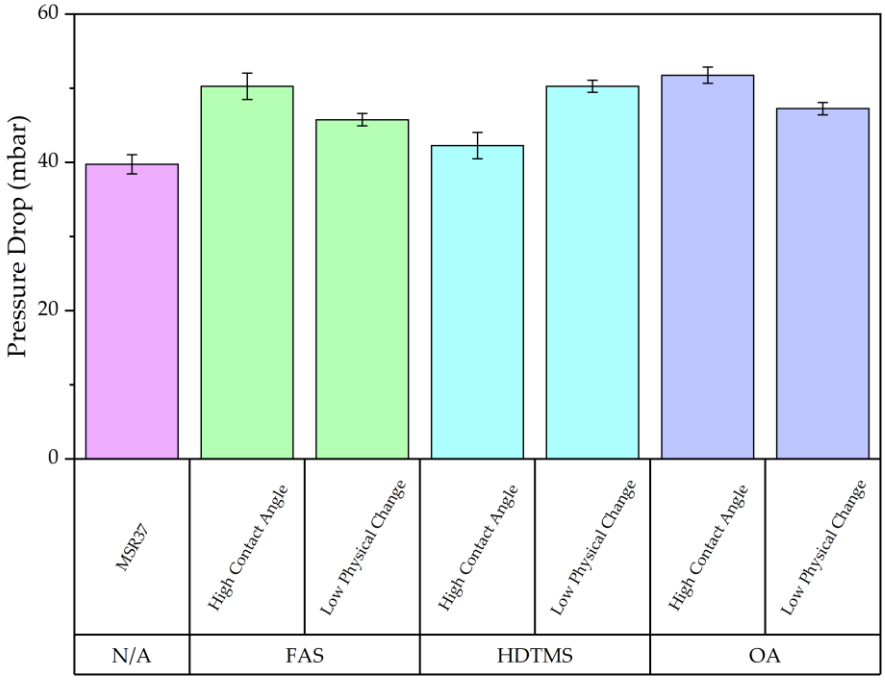

Figure 6-3: Pressure drop of the coated filters compared to the uncoated filter material.

It is known that the pore size distribution cannot be directly used as an analogue for pressure drop. However, looking at there is a clear trend of increasing pressure drop with increasing change in pore size distribution. The HDTMS functionalised coating is a clear outlier to this, further investigation is required to understand what may have caused this.

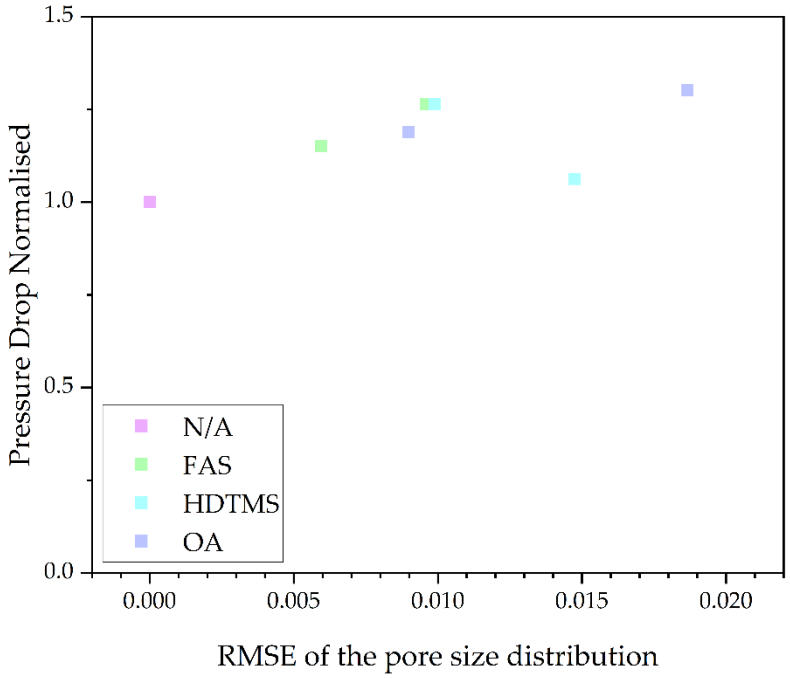

Figure 6-4: The effect of pore size distribution on the pressure drop.

Looking now at the effect the measured contact angle has on the water separation efficiency. The relationship between the contact angle and the water separation efficiency is shown in Figure 6-5. Similar to what was seen in the fouled filters analysed in Chapter 4 as the contact angle increases the water separation efficiency also increases. While this makes intuitive sense, it was not certain that this relationship would hold at very high contact angles.

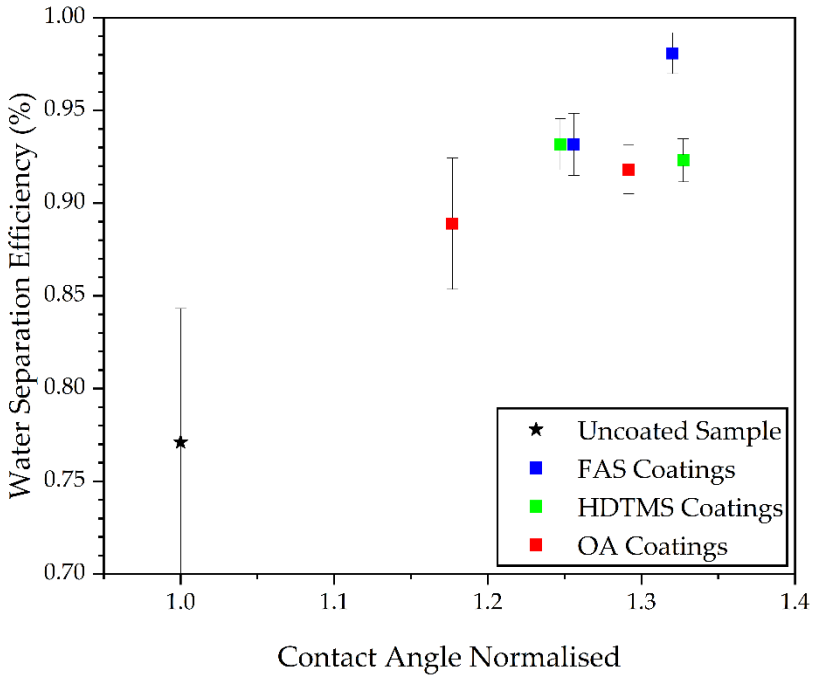

Figure 6-5: Effect of contact angle on the water separation efficiency.

It was also shown in Chapter 4 that the relationship between pressure drop, contact angle and water separation efficiency can be best described using a Boltzmann curve. In order to determine whether this is also true when the contact angle has been increased above that of a clean filter all the data points, including the fouled filters, were plotted. This is shown in Figure 6-6. There is a significant jump in water separation efficiency when comparing the coated samples to the uncoated material. This is likely due to the large increase in contact angle having a much greater impact than the slight increase in pressure drop caused by the deposition of the microspheres.

It is theorized that this increase in separation efficiency would be carried through as the filters become fouled. It was not possible to confirm this because the coated filters could not be used on real engines. However, the fact that the increased pressure drop does not appear to have a significant impact upon the water separation efficiency gives some credence to this theory. The following sections will explore further the effect of fouling on the coated filters.

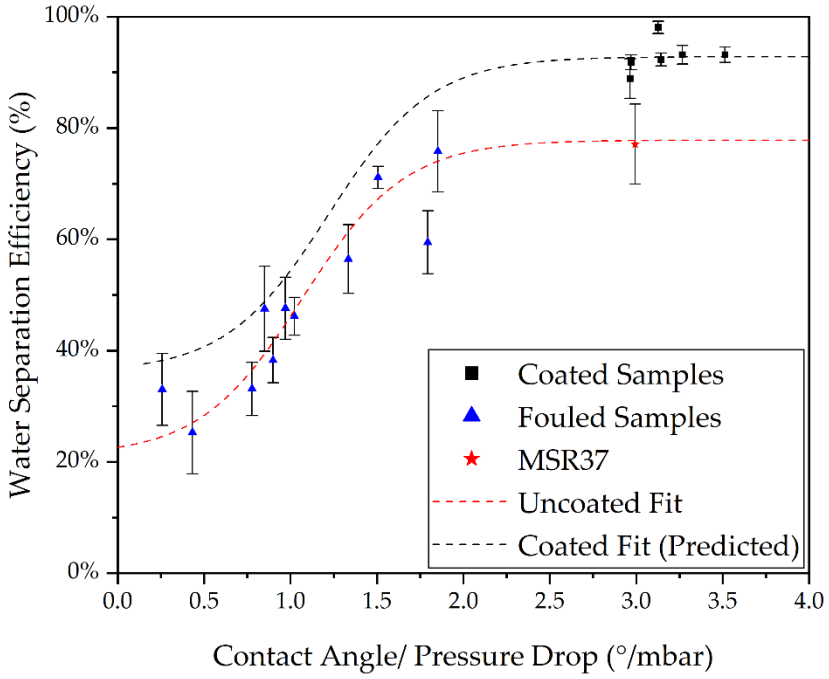

Figure 6-6: Prediction of the effect that fouling will have upon the coated filters.

6.3.2 Increasing face velocity until breakthrough pressure

A possible method of investigating the effect of fouling on the water separation efficiency of the filters is increasing the face velocity. As a filter becomes blocked pores will become unavailable for flow. The reduction in the number of pores will reduce the effective area of the flow, thus increasing the velocity of the fluid through the remaining pores. This is simulated in this section by increasing the flowrate in stages and measuring the resulting water separation efficiency.

For a clean, un-coated filter there is a significant drop in water separation efficiency as the flow rate is increased. This is shown in Figure 6-7. There is a clear strong linear relationship between the face velocity and the pressure drop measured. It will be possible to compare this relationship with the coated samples to determine if the addition of the coatings have an impact upon the increase in pressure drop with increasing flow rate. It is also clear that increasing the face velocity has a significant impact upon the ability of the filter to separate water from the flow. It is clear that at a face velocity of approximately 1.5mm/s the filter completely fails. The aim of the coating will be to improve this failure point.

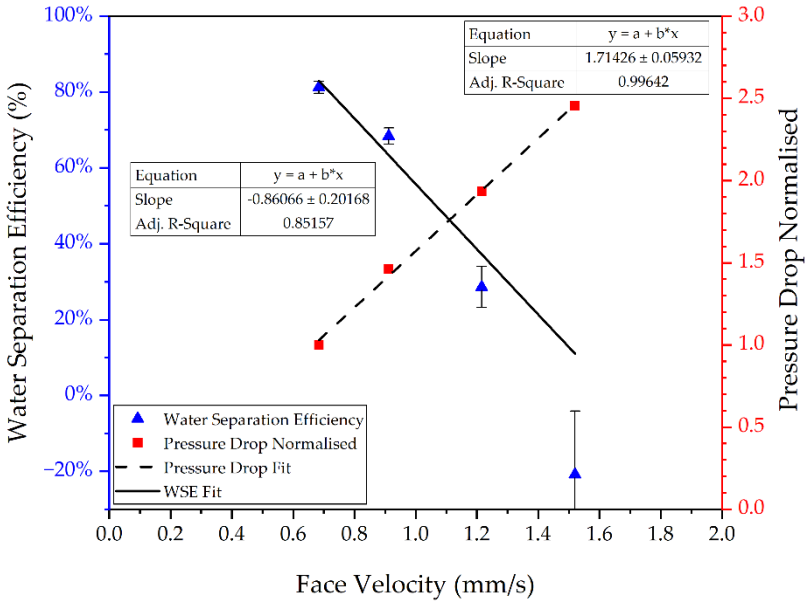

Figure 6-7: Relationship between the face velocity and the water separation efficiency and pressure drop for the uncoated filter material.

Looking first at the effect of increasing the face velocity on the FAS functionalised coatings, it can be seen that for both of the selected coatings the final separation efficiency is improved when compared to the uncoated filter.

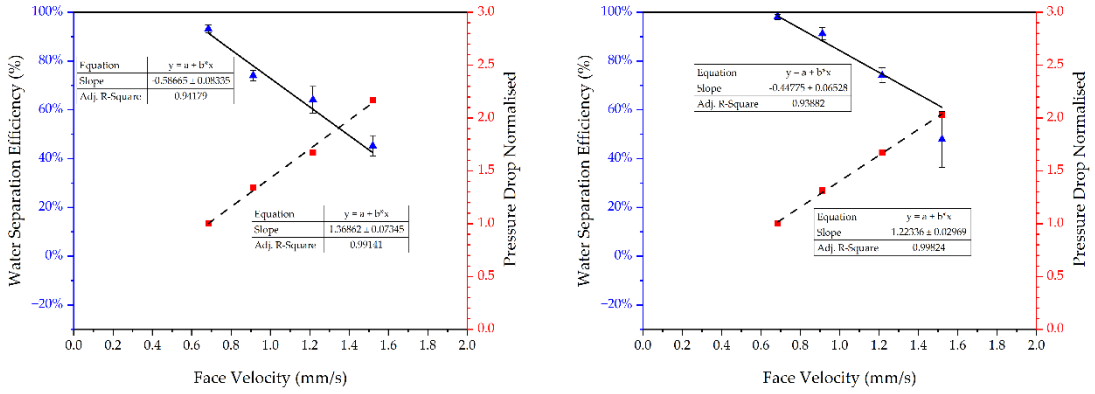

Figure 6-8: Relationship between the face velocity and the water separation efficiency and pressure drop for the FAS functionalised coatings. Left: FAS ID6 (Low physical change). Right: FAS ID7 (Highest contact angle).

The same cannot be said for the coatings formed using HDTMS as the functionalising agent. Figure 6-9 shows that the while the initial water separation efficiency achieved by the high contact angle HDTMS coating was improved compared to the uncoated filter, increasing the face velocity resulted in failure much sooner. With the data collected it is not possible to explain this phenomenon directly. However, the pressure drop was higher for the low physical change filter. This is counter to what would be expected, a possible reason for this is that the droplets of water are entrained at the surface

and are not able to detach. This will lead to fouling of the surface with water droplets, making the pores either impassable or forcing water through reducing the water separation efficiency. This is a function of the sliding angle, a parameter that was not assessed in this study.

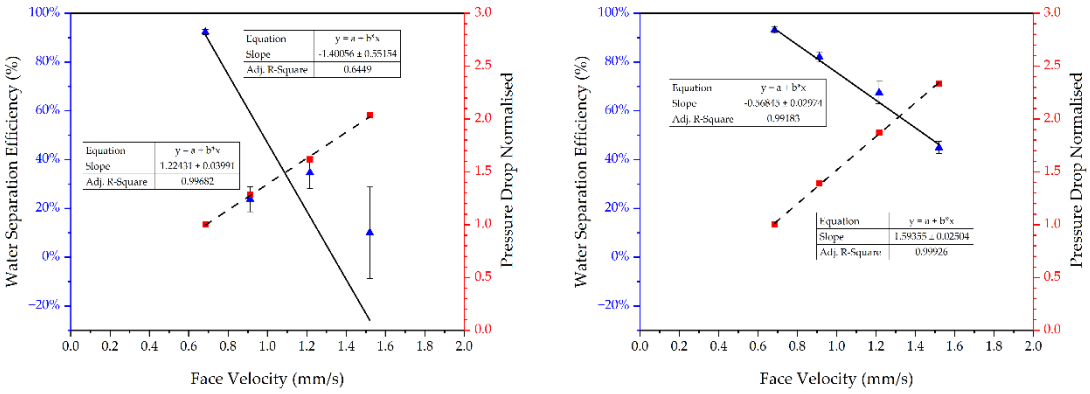

Figure 6-9: Relationship between the face velocity and the water separation efficiency and pressure drop for the FAS functionalised coatings. Left: HDTMS ID8 (Low physical change). Right: HDTMS ID2 (Highest contact angle).

The same analysis has been completed for the coatings functionalised with oleic acid. It appears that the coatings formed with the oleic acid functionalising agent perform the best under increased face velocities as shown in Figure 6-10. It is unclear at this stage what has caused this to occur. The contact angles for these coatings are comparable, if not slightly lower, and the physical change to the filter is also similar.

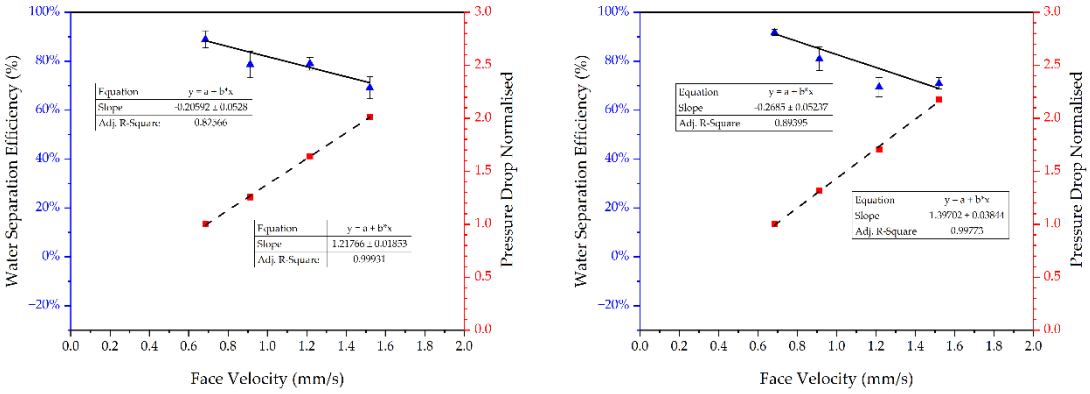

Figure 6-10: Relationship between the face velocity and the water separation efficiency and pressure drop for the FAS functionalised coatings. Left: OA ID4 (Low physical change). Right: OA ID3 (Highest contact angle).

It was shown in Chapter 4 that both the contact angle and the pressure drop appear to have a significant impact on the final water separation efficiency. Looking at Figure 6-6 the relationship begins to breakdown at high contact

angles; however, it is likely that these parameters still have an impact on the water separation efficiency. To explore this, the coated filters response to increased face velocity with regards to pressure drop is examined. For this a linear fit was taken for the relationship between face velocity and pressure drop, and also between face velocity and water separation efficiency.

The gradient of the water separation efficiency and pressure drop with respect to the face velocity is determined by applying a linear trend to the collected data, these trends are shown in the figures shown previously. First looking at the gradient of the water separation efficiency with increasing face velocity, shown in Figure 6-11. The closer the gradient is to 0, the better the filter performs. If the gradient were 0, it would show that the filter is unaffected by an increase in face velocity over the range examined. For the most part the coated filters perform better than the uncoated filter material. The exception to this is the coating formed using HDTMS as the functionalising agent that showed a low change in pore size distribution.

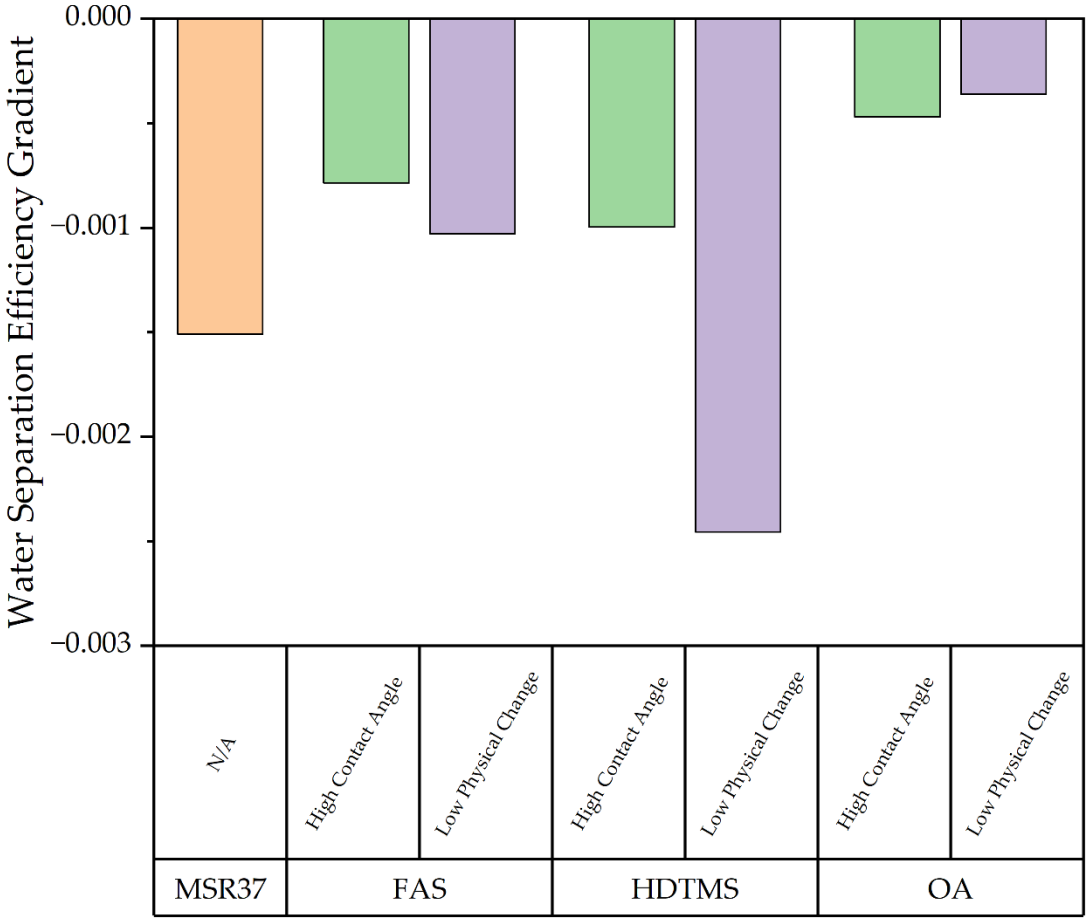

Figure 6-11: Water separation gradient with increasing face velocity for the coatings examined for water separation efficiency.

The same analysis has been conducted for the pressure drop response with increasing face velocity. These two parameters should be highly correlated. However, as the water is separated from the flow, it will be deposited on the surface causing increased restriction. As the droplets attach to the surface and are unable to pass through, they will coalesce until reaching a critical mass, at which the coalesced droplet will fall due to gravity settling. The ability of the droplet to detach from the surface will be influenced by the surface chemistry and the morphology of the surface. Both elements will be altered by the addition of the coatings; therefore, it is expected that the pressure drop response will be related to these changes. If the gradient were 0, the increasing face velocity would have no impact upon the pressure drop, and the higher the gradient the more of an impact the face velocity will have upon the pressure drop. An increase in the gradient can indicate two things, the droplets adhering to the surface are blinding pores and are not being released and/or the coating has blinded or restricted pores resulting in an increase in resistance to flow.

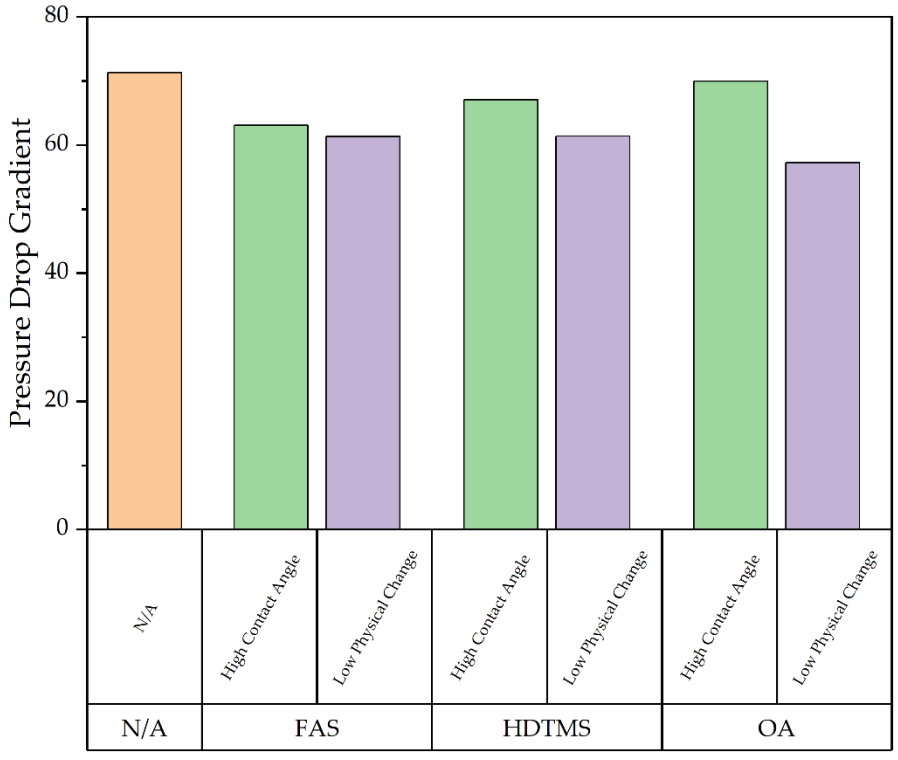

Figure 6-12: Pressure drop gradient with increasing face velocity for the coatings examined for water separation efficiency.

For all the coatings it is apparent that the response of the pressure drop with increasing face velocity is improved. This is not what would be expected for the low physical change HDTMS functionalised coating because the water separation efficiency was very poor. It is not clear what has caused the poor

performance from the measurements taken. This means it must be a result of something that was not possible to measure. The likely cause is the contact angle hysteresis leading droplets not being released from the surface.

6.3.3 Fouling with carbon black

In order to simulate the fouling that occurs in the field carbon black was deposited on the surface of the filters. This will blind pores in a similar way to the foulants found in diesel, but much quicker. This allows the end-of-life performance of the filters to be estimated. The main parameter that is of interest is the water separation efficiency Figure 6-13 shows the water separation efficiency before and after being fouled with carbon black.

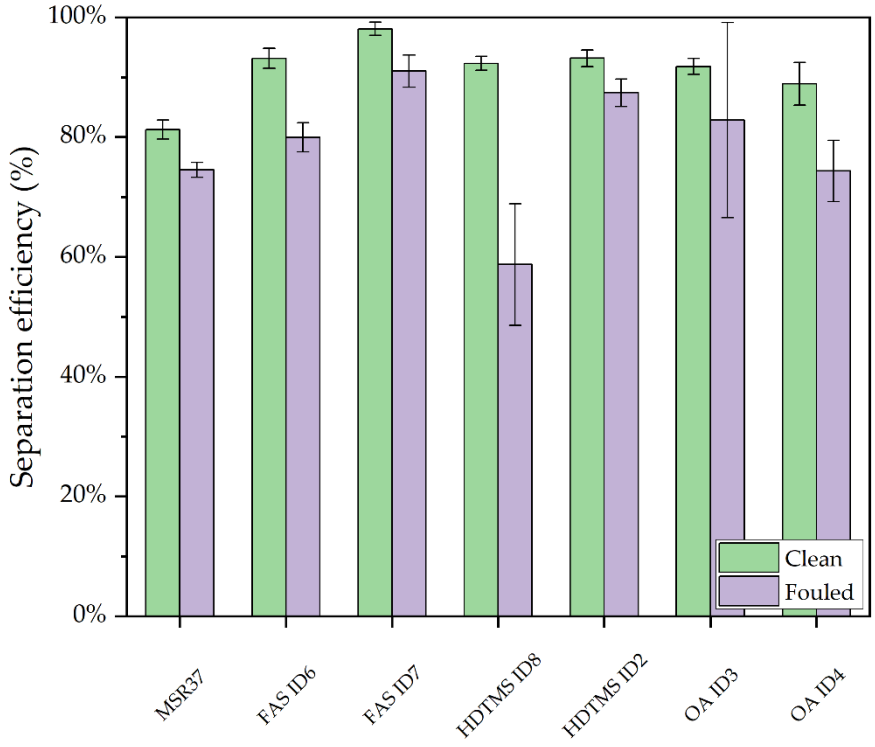

Figure 6-13: Change in separation efficiency after being fouled with carbon black.

As would be expected the water separation efficiency has been decreased for all the coatings fouled with carbon black. It has been shown in the methodology that the contact angle on the surface of the fouled filter is reduced to 120° in all cases. The majority of the reduction in water separation efficiency is likely caused by the increase in pressure drop. Interestingly, similar to what was seen in the increased face velocity experiments, the HDTMS ID8 coating performs significantly worse.

While the primary performance indicator is the water separation efficiency after fouling, it has been shown that pressure drop has a significant impact

upon the water separation efficiency. Therefore, it is beneficial for the coating to have as little pressure drop increase as possible. While the amount of carbon black added to the surface of the filters is maintained at a set amount leading to similar changes in pressure drop. Another factor that contributes to increased pressure drop is the interaction of water droplets with the surface. If the droplets readily fall from the surface after coalescing, the pressure drop should stay relatively low. However, if the droplets coalesce and remain at the surface they will act as an additional barrier to flow. It is likely that the addition of the foulant material will change this property.

Figure 6-14 shows the changes in pressure drop for the coated filters.

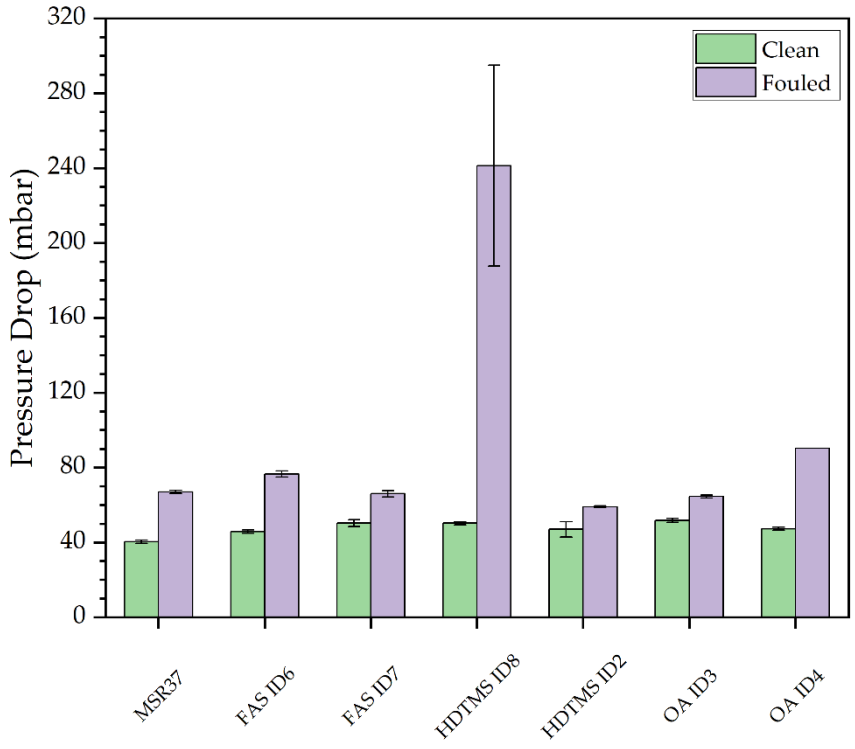

Figure 6-14: Change in pressure drop after being fouled with carbon black.

The two primary indicators of the water separation efficiency have been determined to be contact angle and pressure drop. In order to confirm that this is the case when coated filters are fouled with carbon black, the function of contact angle divided by pressure drop is compared to the water separation efficiency. The function that defines this is shown in equation 6-1. Where PI is the newly defined performance index, CA is the contact angle, dP is the pressure drop, subscript i is the initial value as measured on the pristine filter material and subscript x is the value measured for the filter examined. The comparison is made for both the fouled and unfouled coatings in Figure 6-15.

$$PI = \frac{\left(\frac{CA_x}{CA_i}\right)}{\left(\frac{dP_x}{dP_i}\right)} \qquad \textbf{6-1}$$

For this analysis the contact angle was assumed to be constant between the fouled and unfouled samples. The contact angle is an analogue for the surface energy of the filter, the carbon black will likely primarily create a cake layer on the surface of the filter, meaning that the increased performance caused by the coating will still be effective in the depth of the filter. Figure 6-15 shows this, there is a strong correlation between the function chosen and the water separation efficiency. The main thing that is evident from this figure is that maintaining as low a pressure drop as possible after the fouling process is the most important thing to maintain end of life performance.

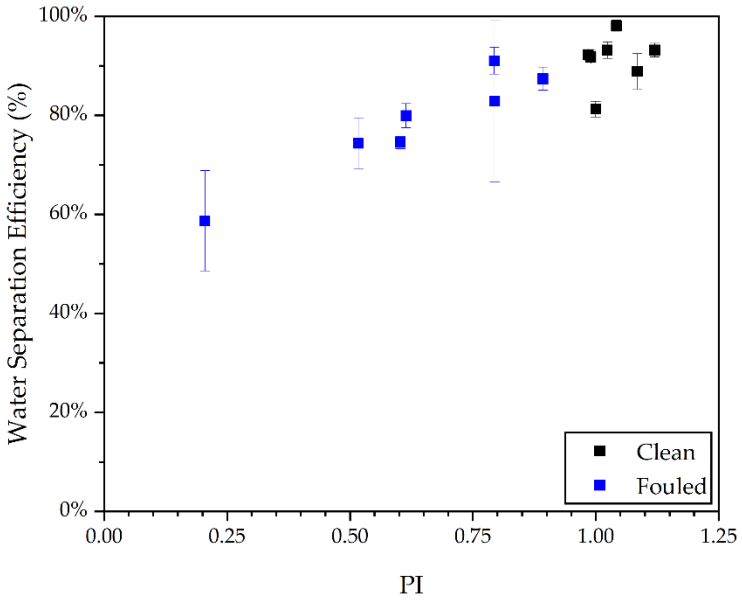

Figure 6-15: Performance index vs water separation efficiency for carbon black fouled filters

Figure 6-16 shows the relationship between the change in water separation efficiency against the change in pressure drop as a result of fouling with carbon black. The change in water separation efficiency is the difference between the water separation efficiency measured for the coated filter and the water separation efficiency measured after laboratory fouling with carbon black. The same was done for the pressure drop, the difference is the difference between the clean coated filter and the laboratory fouled filter. It is clear that the increase in pressure drop has a significant negative effect upon the water separation efficiency. This is what was expected based on the data collected from the field fouled filter. However, fouling with carbon black alone only impacts one of the two identified factors that have a significant

impact on the water separation efficiency. This highlighted the need for a further process in the accelerated fouling process.

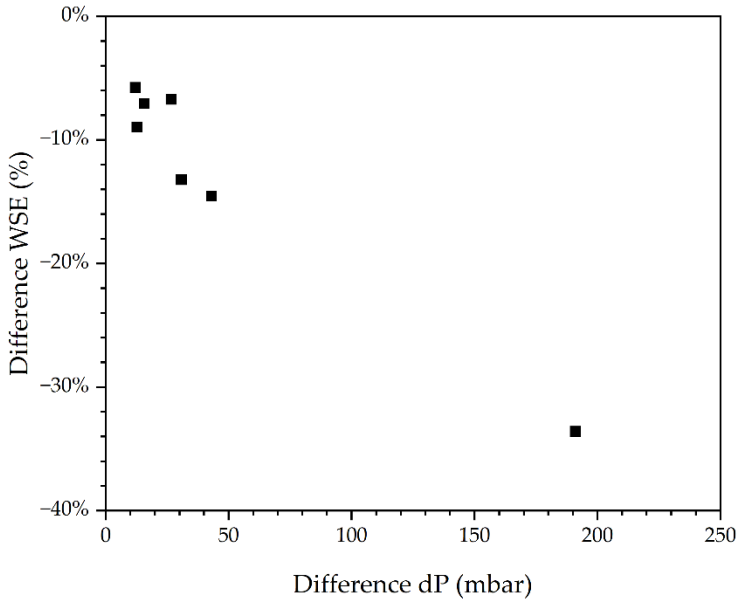

Figure 6-16: Change in water separation efficiency against the change in pressure drop as a result of fouling with carbon black.

6.3.4 Fouling with carbon black decorated with polydopamine.

While fouling with carbon black was able to mimic the physical fouling effect seen in the field relatively well, the chemical changes that occur were not captured. In an attempt to mimic this, the filter that was fouled with carbon black was decorated with polydopamine (pDA). pDA has a high surface energy resulting in a decreased water contact angle, which is what was seen on the field return samples.

Figure 6-17 shows the separation efficiency of the filters coated with pDA decorated carbon black. As would be expected the decrease in contact angle has resulted in decreased water separation efficiency for all the filters. The FAS coated filters have resisted the decrease in water separation efficiency the most effectively achieving water separation efficiencies greater than 70% having been fouled with carbon black decorated with poly dopamine.

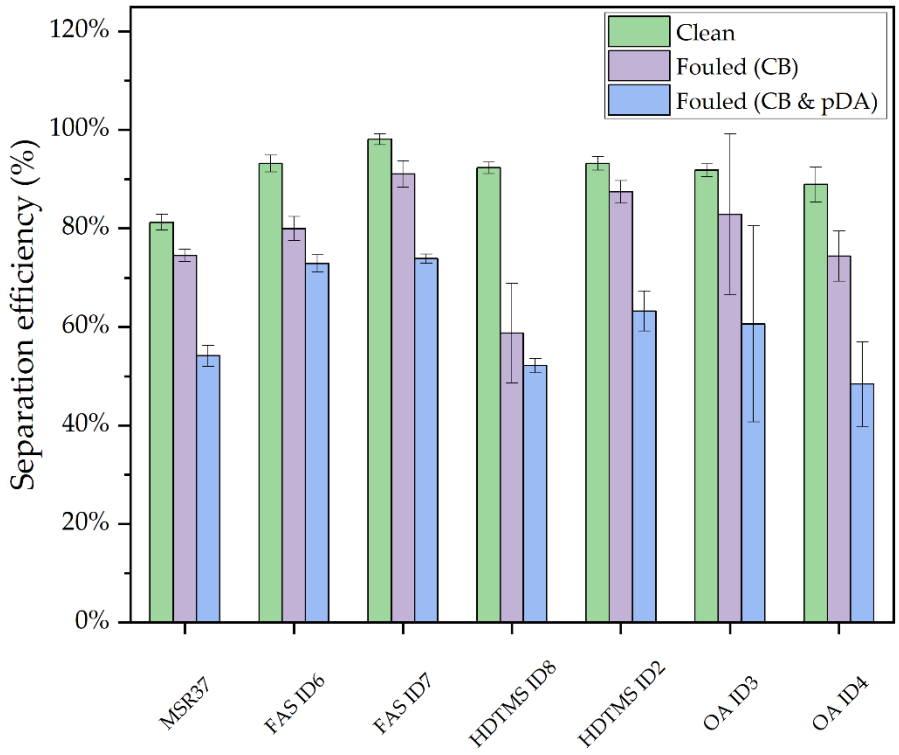

Figure 6-17: Change in separation efficiency after being fouled with carbon black and carbon black decorated with poly dopamine.

The poly dopamine will also have had an impact upon the pressure drop somewhat, being that more material is being added to the surface of the filter. In all but one of the filters the pressure drop was increased for the pDA decorated carbon black fouled filters compared to carbon black alone. This is shown in Figure 6-18. The main reason for this is likely the increase in material that has been added to the surface of the filters. However, it is also possible that the change in surface chemistry will alter the way in which the droplets are released from the surface once they have coalesced. This could also impact the pressure drop.

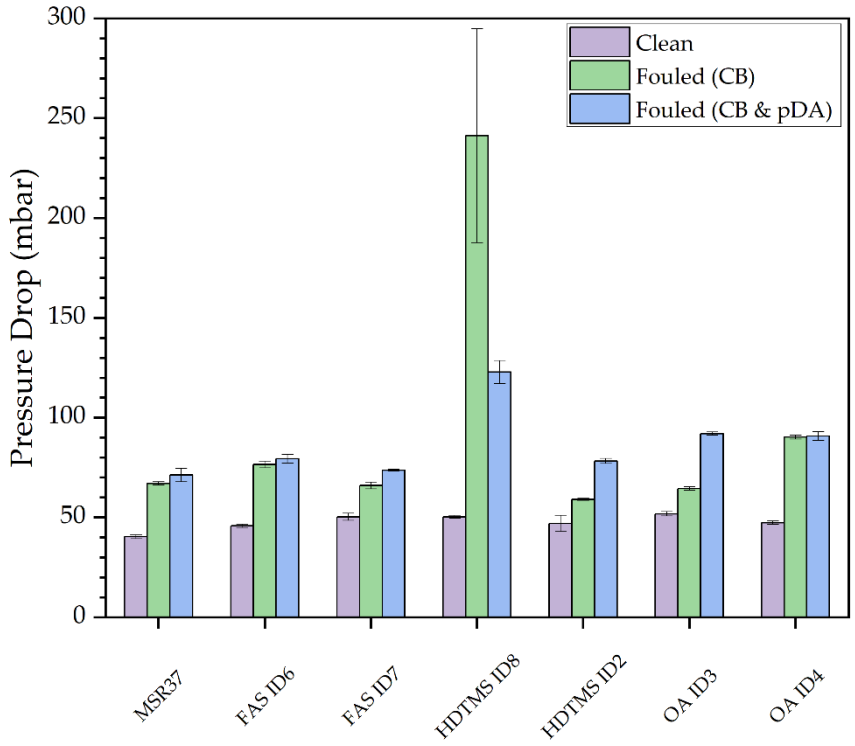

Figure 6-18: Change in pressure drop after being fouled with carbon black and filters fouled with carbon black decorated with poly dopamine.

The main reason for using polydopamine in conjunction with carbon black was to alter the wettability of the surface of the filters. Figure 6-19 below shows the impact that the addition of the poly dopamine has on the contact angle of the coated filters. The poly dopamine has the intended effect, resulting in a decreased contact angle, mimicking what was seen in the field return samples in the first results chapter.

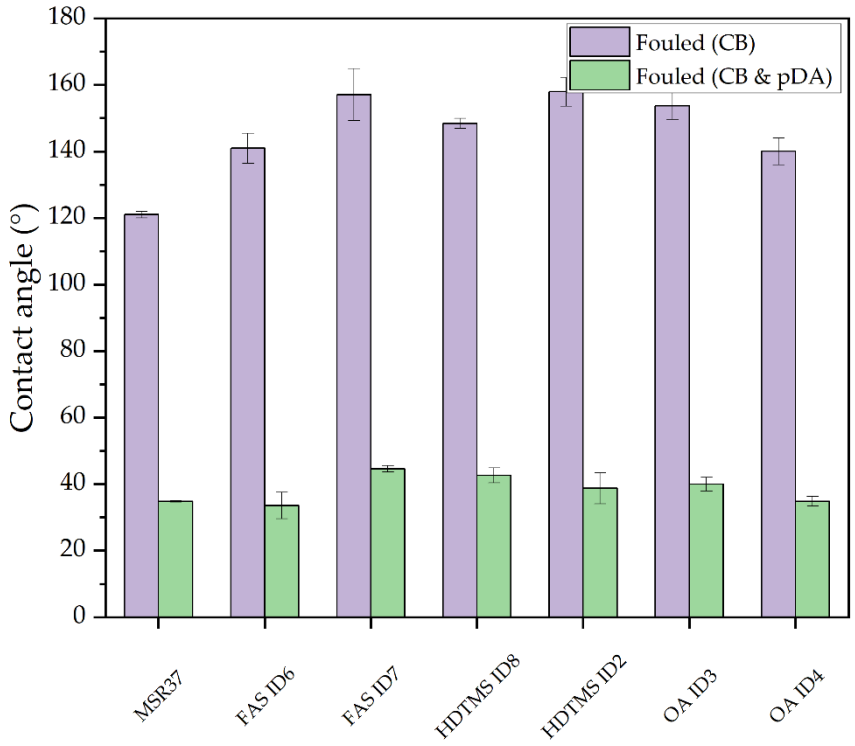

Figure 6-19: Change in contact angle with carbon black and poly dopamine fouling

Using the same metric of contact angle divided by pressure drop for the filters fouled with carbon black and poly dopamine, Figure 6-20 is produced. The general trend shown in the clean and CB only fouled filters is maintained as shown in the left plot in Figure 6-20. It appears that there is a slightly different relationship for the dual fouled filter, the plot on the right of Figure 6-20 includes only these data. The likely reason for this is that there is something that is being altered by the addition of pDA that is not fully accounted for by examining the contact angle and pressure drop.

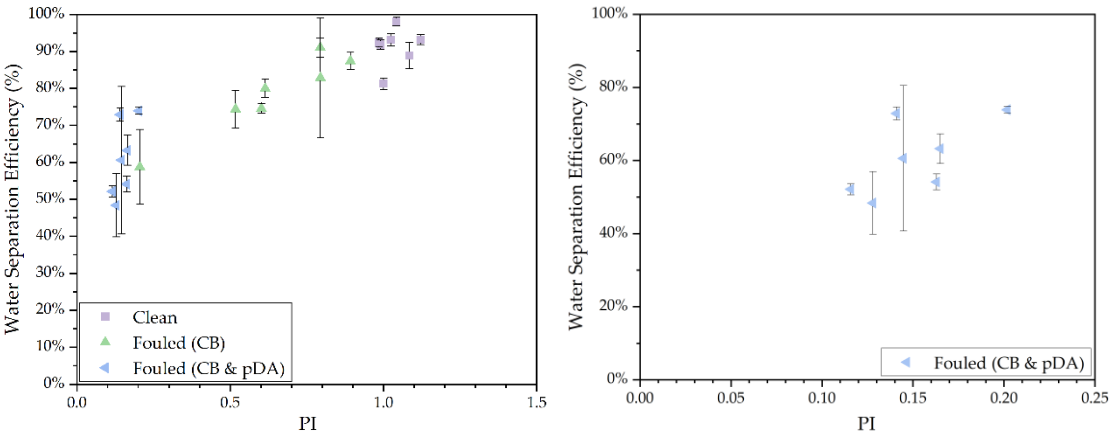

Figure 6-20: Water separation efficiency vs contact angle / differential pressure for all the fouling stages (left). Water separation efficiency vs contact angle / differential pressure for the filters fouled with carbon black and poly dopamine only (right).

Separating the parameters that have been identified as having the biggest impact on the water separation efficiency (contact angle and pressure drop, it is possible to determine the sensitivity to these parameters. Figure 6-21 shows the effect of pressure drop alone. There is an inversely proportional relationship between the pressure drop and the water separation efficiency, this is consistent with what has been previously observed.

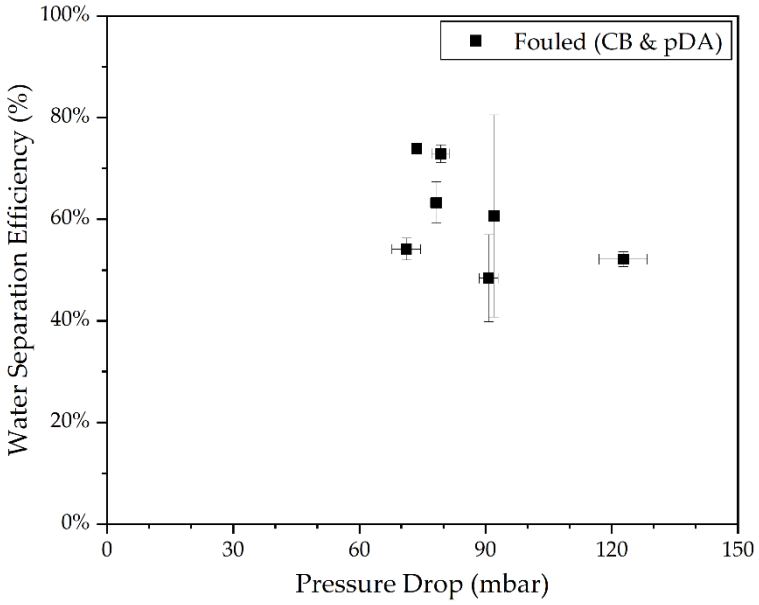

Figure 6-21: Pressure drop vs water separation efficiency for the filters fouled with carbon black decorated with poly dopamine.

The other parameter that has been shown to have an impact on the water separation performance of the filters is the water contact angle. Figure 6-22

Shows the relationship between the water contact angle and the water separation efficiency for the filters artificially fouled with carbon black decorated with poly dopamine. It does not appear that there is the positive correlation that was expected in this data. The likely reason for this is the small range of contact angles, along with the dependency on pressure drop results in the effect being drowned out by the larger variation in pressure drop.

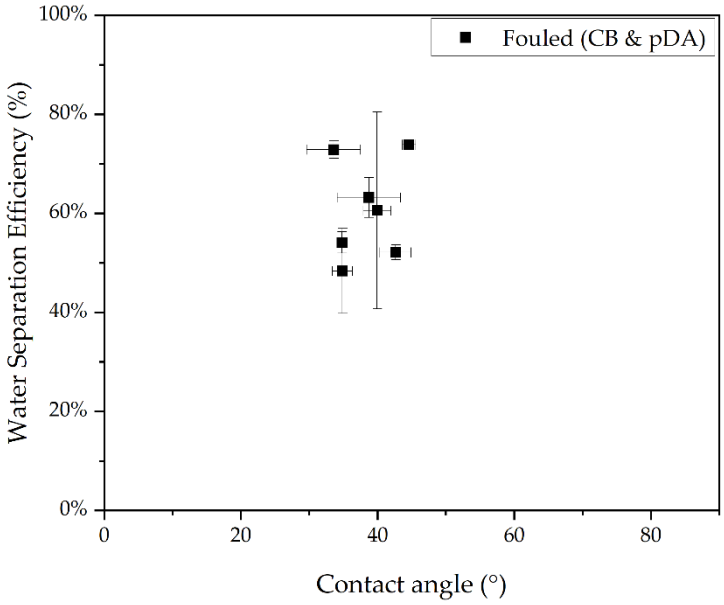

Figure 6-22: Water contact angle vs water separation efficiency for the filters fouled with carbon black decorated with poly dopamine.

Overall, it does appear that the attempt to examine the filters through an accelerated fouling process has been successful. The results match with what was seen in the field samples examined in Chapter 4. It has also been possible to show that through coating, it is possible to increase the end-of-life performance as predicted by the accelerated fouling process.

6.4 Discussion

The table below (Table 2) summarises the testing performed in this chapter on the coated filters. This was done for each type of coating; FAS functionalised, HDTMS functionalised, and OA functionalised.

Table 2: Testing performed in Chapter 6

Technique	Information Obtained	
Standard Water Separation Efficiency (WSE)	Water separation efficiency	Differential Pressure (dP)
Increased face velocity WSE.	WSE response to increased face velocity	dP response to increased face velocity
Carbon black fouled WSE	Physical blockage impact on WSE	Physical blockage impact on dP
pDA & Carbon Black Fouled WSE	Physical & Chemical blockage impact on WSE	Physical & Chemical blockage impact on dP

It has been shown in this chapter that increasing the water contact angle of the fibrous filters does result in a superior performing filter compared to an uncoated filter. Figure 6-2 shows that all of the coated filters result in increased water separation efficiencies when compared to the uncoated filters. It has been shown by numerous authors that increasing the water contact angle results in increased performance of water separating filters, so this was not a surprising result (12, 87, 117). Often this is shown as a result of coating removal through abrasion cycles. For this work, abrasion will not be a problem, therefore this has not been investigated.

It has also been shown in this chapter that the water separation efficiency of coated filters has as strong relationship with the water contact angle. Figure 6-5, shows a proportional relationship between the water contact angle and the water separation efficiency. The relationship between water contact angle and water separation efficiency is not commonly reported. However, in many papers assessing the abrasion resistance in which water contact angle and water separation efficiency is reported, the relationship does appear to be proportional (117, 216).

Something that is not often assessed is the effect of pressure drop on the separation efficiency of the fibrous filter. In most cases where the separation efficiency of filters have been assessed, the driving force of the separation is gravity (117, 216-218) It has been shown in this chapter that increasing pressure drop results in decreased performance of the filter with respect to water separation efficiency, and is therefore an important metric when

considering the performance of a filter coating. Figure 6-3 shows that the pressure drop for the coated filters has been increased compared to the uncoated filter. One of the problems with forming a coating to increase the hydrophobic properties of the filter is the unintended effect of increasing the pressure drop. In this case it has been shown the increase in water contact angle has had a greater positive impact than the negative impact of the pressure drop increase.

The impact of pressure drop has been further investigated by looking at the effect of increasing the face velocity of the filter on the water separation efficiency. It has been shown that increasing the face velocity has a significant impact on both the pressure drop and the water separation efficiency, as would be expected. Two things are important to examine here, the response of the filter to the increased face velocity from both a water separation efficiency and a pressure drop standpoint and also the relationship between pressure drop and water separation efficiency for the different coatings.

For the uncoated filter there is a very pronounced drop in water separation efficiency above a face velocity of approximately 0.9mm/s. The aim of the coating in general would be to increase the face velocity at which the large drop in water separation efficiency occurs. In this case the face velocity is effectively an analogue for the pressure drop, the pressure at which the water separation efficiency drops significantly is the pressure as which the water droplet can be forced through the pores of the filter (breakthrough pressure). It can be seen that for almost all of the coated filters this is improved when compared to the uncoated filter, the exception being HDTMS ID8.

There are a number of variables that will have an impact on the breakthrough pressure. Nazzal et al. (93) created a simple model based on the Young-Laplace equation that describes the critical pressure required to force a droplet through a pore. The equation developed is shown in equation 2-9. The limits of this equation are that the flow regime must be laminar, the hole is a perfect circle, the pores are all equal in size and the droplet diameters are all equal. While the dimensional constraints are not respected, this model may give some insight into the mechanism of breakthrough. The variables that will have an impact upon the critical (or breakthrough) pressure are the contact angle with the droplet, the interfacial tension, the pore size and the droplet size. In this work the droplet sizes should be consistent between experiments as will the interfacial tension, the two factors that are affected by the coating are the water contact angle and the pore size.

Using this model, it has been possible to develop the curve shown in Figure 6-23. There are a number of things that will occur as a result of coating the filters, the nanoparticles will result in a decrease in the pore size this will have a positive impact on the breakthrough pressure. The contact angle will be increased again having a positive impact on the breakthrough pressure. However, due to the fact that in this system the overall face velocity is what is being controlled the reduction in pore size caused by the coating will also increase the pressure. Without knowing the impact of the pore size on the pressure drop, it is difficult to say whether the decrease in pore size has a net positive impact on the water separation efficiency.

The model suggests that there is a very sharp decline in performance of a barrier filter when the contact angle drops below ~100°. It is also shown that there is an exponential increase in critical pressure as the pore size gets smaller. Having said this, it would be expected that as the pores got smaller, the pressure would also increase for a constant flowrate. An attempt was made to relate the water separation efficiencies measured experimentally to the model developed by Nazzal et al. (95), however this was not successful. There are a number of possible reasons for this, one of the primary reasons is that this model is looking at the pressure at which a droplet would deform and pass through a pore. If this were a perfect model for the system being examined the separation mechanism would be purely barrier filtration. In reality it is thought that the system is a combination of both barrier and coalescence filtration.

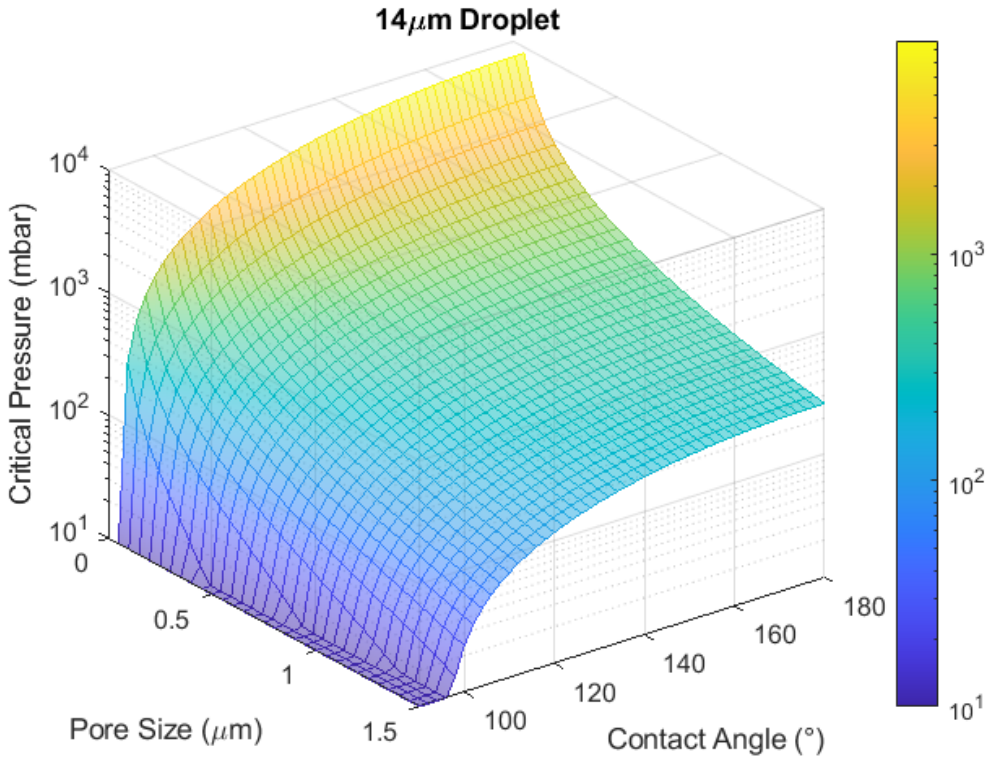

Figure 6-23: Graphical representation of Nazzal et al. model with a droplet diameter of 14μm and an interfacial tension of 22 dynes/cm

In terms of breakthrough pressure, it appears that the oleic acid functionalised coatings result in the most effective filtration media. The increase in face velocity has the least impact on both the low physical change and the highest water contact angle filters with regards to water separation efficiency. This would suggest that these filters will be the most effective at resisting performance degradation due to fouling. It is also shown that the high contact angle coatings outperform the low physical change filters, aside from the oleic acid functionalised coatings where the performance is comparable.

Carbon black was used as an accelerated fouling method. It is expected that the carbon black would form a cake layer on the surface, resulting in an increase in restriction to flow and a subsequent decrease in water separation efficiency. Figure 6-14 shows that the accelerated fouling process was successful in increasing the pressure drop across all of the filters. HDTMS ID8 was found to have an extremely large increase in pressure drop when compared to the other filters. The reason for this is not immediately obvious. Being that these filters were used in water separation experiments, the prevailing theory is that the addition of the foulant material stopped the droplets from being released from the surface resulting in the water acting as an additional foulant material.

Figure 6-15 shows that for the carbon black fouled filters the main variable that affects the water separation efficiency is the pressure drop. The water contact angle was assumed to be constant for the fouled and unfouled filters, while this is not completely true, if the actual water contact angle was used in the calculation, the trend was not as strong. The likely reason for this is that the carbon black formed a cake layer but did not penetrate through the depth of the filter. The fibres that remained uncoated by the fouling material would therefore retain the superhydrophobic properties applied by the coating material.

As a method of attempting to show this phenomenon through analysis, the change in water separation efficiency for the carbon black fouled filters was compared to the un-fouled filters. The results of this are shown in Figure 6-16. The strong negative correlation between the pressure drop and the change in water separation efficiency suggests that the change in water contact angle cause by the carbon black fouling process had little effect. It is known that in real samples that there is a major decrease in water contact angle cause by the fouling process, therefore further experimentation was required.

Using poly dopamine, it was possible to impact the water contact angle of the carbon black fouled samples. The fouled filters were treated as a whole, this was intended to simulate the change to the fibres throughout the depth of the filter, rather than just at the surface. Figure 6-17 shows that the addition of the polydopamine resulted in a decrease in water separation efficiency for all of the filters. The aim of the coatings is to reduce the overall reduction in performance at the end of life. The accelerated fouling process developed appears to give a methodology for assessing this in a short timeframe.

An unintended effect of decreasing the contact angle using polydopamine was the increase in pressure drop across the filter. While this process does add some more material to the filter, the thickness of the coating was expected to only be in the nanometre range. Ball et al. (219) using similar conditions to this work found that the film thickness reaches a constant value of approximately 40nm (independent of substrate). This suggests that the addition of material is not the cause of the increase in pressure drop. The most likely cause of the increased pressure drop is droplet retention leading to pore blinding through a secondary phase blockage.

Figure 6-19 shows that the water contact angle has been significantly decreased as a result of the accelerated fouling process. There are some slight variations in the contact angle, this is likely caused by the roughness imparted by the coating as well as any un-fouled sections remaining. It has been noted

that Figure 6-20 highlights that for the pDA & carbon black fouled filters, there appears to be a slightly different trend than has been observed previously. The factor that is not been fully accounted for is the roughness of the fibres, this will be impacted by the coating and will affect both the contact angle and critically the roll off angle.

Figure 6-21 and Figure 6-22 show the effect of the two variables (pressure drop and water contact angle) found to have the largest impact throughout this study on the water separation efficiency. As has been consistently shown, the pressure drop has a strong inversely proportional relationship with the water separation efficiency. The water contact angle does not appear to have a significant impact on the water separation efficiency for these samples. The reason for this is the interdependency with pressure drop and the small range of water contact angles measured.

There is a significant interest in the fouling behaviour of filters in the literature. However, the majority is not focused on emulsion separation therefore the methods for testing the flux decline are slightly different. For example Lee et al. (220) examined the flux decline in water purification filters, it is shown that there is an immediate flux decline levelling out after approximately 15hrs. In our work the process that results in the production of the insoluble particles that contribute to the blockage of the filters is not present. These processes are not fully understood but it is likely that additive interaction has an impact, as shown by Barker et al. (39). It is also possible that thermal cycling has an impact on the production of the insoluble particles, this is shown by Singer et al. (221).

Shao et al. (222) examined the effect of stabilising emulsions with surfactants and with the addition of contaminants. While the study by Shao et al (222) was looking at the reverse of what is being examined in this thesis (oil in water separation rather than water in oil) similar results were found. In an emulsion that is not surfactant stabilised with no contaminants there is no impact on the trans membrane pressure within the time of the experiment (25mins). It is shown that surfactants have a significant impact for their set up, this is not something that was being examined in this thesis therefore is not completely relevant. However, what is also shown is that the addition of contaminants doesn't result in an additional increase in the transmembrane pressure. They do alter the mechanism by which the surfactants interact with the surface which actually results in an improvement in 'fouling resistance'. This shows that for relatively short experiments simply adding contaminants is not a viable method for replicating long term fouling.

The most important finding from this chapter, alongside the success of the coatings at improving the end-of-life performance of the filters, is that the methodology used to assess the end-of-life performance seems to be successful. It can be shown that filters with different initial performance do have varying end of life performances. It doesn't appear that the initial performance of the filters is a direct indicator of the end-of-life performance. The likely reason for this is that there are parameters that were not analysed that will have an impact on the way in which foulant material is deposited and distributed within the filter. These parameters are likely to be the roughness imparted by the coating and roll off angle for the dispersed phase.

6.5 Conclusions

One of the aims of this chapter was to assess the instantaneous water separation efficiency of the coated filters. It has been possible to shown that the addition of hydrophobic coatings to the polymeric fibres has resulted in increased initial performance of the filtration material. The relationship between water contact angle, pressure drop, and water separation efficiency shown from the field return samples in Chapter 4 was found to apply to the coated samples as well. It was found that although the addition of the coating results in increased pressure drops due to the addition of more material, the increase in contact angle was more significant with respect to water separation efficiency. This achieves the aim of showing that the hydrophobicity is an extremely important factor for the separation of water in diesel emulsions.

One of the issues with developing coatings for increasing water separation efficiency is that while the initial efficiency is of interest, the end-of-life performance is more important. The aim of assessing the end-of0life performance was achieved by developing two methodologies for assessing the end-of-life performance. The first was extremely simple and assessed the breakthrough pressure with increasing flowrate. While this gives an indication of the response of the filter to increased face velocities, it doesn't give a true picture of the end-of-life performance. In these experiments it was found that the oleic acid functionalised coatings performed the best.

The second method developed was the use of carbon black as a fouling agent. It was found that it was vital to also decrease the water contact angle as well as increase the pressure drop. This was achieved by decorating the carbon black fouled filter with poly dopamine. The aim of developing a novel method for determining the end-of-life performance of a filter was achieved. It was

shown that visually the fouling on the surface was similar to what was seen in the field, also the decoration with polydopamine was shown to have similar impacts to the contact angle to what was seen in the field. It was found that this decreased the contact angle to levels that were commonly seen in the return filters that were at the end of life. Using this method, it was found that the FAS functionalised coatings had the best performance at the simulated end of life. Overall, this shows the importance of end-of-life testing when assessing the performance of water separators that are prone to fouling. Overall the aim of producing a coating that improves the instantaneous and end-of-life performance of an as made filter was achieved.

Chapter 7
Discussion, Conclusions and Future Work

7.1 Discussion

7.1.1 Attainment of objectives

The overall aim of this project has been to develop a coating that improves both the instantaneous water separation efficiency of currently used barrier filtration media as well as the end-of-life performance.

Aim 1

The first aim was to assess the fouling that occurs on filters in real engines during operation. Two changes were examined in detail, the physical changes to the filter material caused by the deposition of the foulant material and the chemical changes at the surface. The physical change was assessed in four different ways; the air permeability was measured, the pressure drop across the filter was measured, an SEM image of the surface was captured, and the pore size distribution was determined. The chemical changes at the surface were primarily quantified using water contact angle, to determine whether this could be attributed to a particular foulant, a Fourier transform infrared spectroscopy was taken.

Filters from three different fuel markets were examined, the Brazilian biodiesel market, the Brazilian petroleum diesel market and the Swedish petroleum diesel market. It was found that the fuel market has an impact on the severity of the fouling. This is broadly attributed to the fuel quality, specifically the quality of the biodiesel. It was shown by Ullman et al. (196) that carboxylate soaps are liable to form on diesel injectors. The FTIR data collected shows that there were carboxylic soaps on the surface of the filters examined, these were particularly prominent in the Brazilian fuel market. Fersner and Galante-Fox (33) proved that the biodiesel feedstock has a significant impact on the blocking tendency of the fuel. The feedstock with the worst tendency for blockage out of the feedstocks examined (rapeseed, cooking oil, coconut and soybean) was soybean methyl ester, the feedstock that performed the best was rapeseed methyl ester. This supports the fact that the blockages were occurring more severely and sooner in the Brazilian fuel market, because soybean methyl ester is the most common feedstock used in the Brazilian market, compared to rapeseed in Europe (198).

Even though there were some differences in the fuel market and therefore biodiesel feedstock. Overall, the composition of the fouling material is relatively consistent. The composition is primarily long chain hydrocarbons with some amount of oxygen functionality. There was an attempt to relate the oxygen functionality to the water contact angle, because it was postulated that the polarity of the molecule would correlate with the water contact angle (188). However, it was not possible to find a correlation between the oxygen functionality as identified using FTIR and the water contact angle. One possible reason for this is that the contact angle is affected by more than just the chemistry of the surface. One of the major contributors to the contact angle of a surface is the roughness, this is shown in the well understood models developed by Cassie-Baxter (103) and Wenzel (102).

Looking at the SEM images that were captured of the surface of the filters in Figure 4-10 and Figure 4-15, it is clear even from these images that the roughness imparted by the foulant material varies between filters and fuel markets. In addition to this it has been noted that the fouled material has differing amounts of coverage, leaving fibres exposed in some cases but not in others. This will also have an impact on the contact angle but is not something that would be captured by looking at the oxygen functionality alone. Therefore, even though there was not found to be a correlation between the oxygen functionality determined through FTIR and the contact angle, it cannot be said for certain that no such correlation exists. It would likely require either a significantly more controlled experiment, or an extremely large number of samples for this trend to be identified.

While the differences between the different fuel markets is something that is interesting. It is not completely necessary to understand this in order to create a coating that improves the end-of-life performance of a filter. The most significant finding from examining the returned filters was the correlation between the contact angle and the water separation efficiency, and the pressure drop and the water separation efficiency. It is also shown that by combining these variables into a simple function an even stronger correlation is found with the water separation efficiency. This is important for the formation of the coating, since it identifies the need to maximise the water contact angle while minimising the pressure drop.

Overall, it has been shown that the fuel market does have an impact on the fouling behaviour in diesel fuel filters. The key parameters that impact this are the increase in effective surface free energy as a result of the foulant deposition on the surface. This results in the fibres being more preferentially

wetted by the dispersed phase resulting in the droplets requiring less force to pass through the filter membrane. The second finding was that the restriction to flow caused by the foulant material also decreases the filters effectiveness with respect to water separation efficiency. The reduction is caused by a combination of pore restriction and pore blinding resulting in the force experienced by a droplet of the dispersed phase at the surface being increased because for a smaller effective free area of flow the overall flowrate is smaller. These findings informed the following work on coatings for improved instantaneous and end-of-life water separation efficiency.

Aim 2

This aim is to develop a one-pot method for forming a silica nanoparticle coating functionalised with three different low surface energy compounds. The primary challenge encountered when forming the functionalised nanoparticles in a one pot method was the impact that the functionalising compound had on the Stöber process. Using a model developed by Bogush et al. (204), the equations of which are shown in equation 5-1, 5-2 and 5-3. It is clear that the addition of the functionalising agent has a significant impact on the size of the particles formed. The only aspect of the experiment formed in this work that deviated from that of Bogush et al. (204), aside from the functionalising agent, was that the temperature in this work was not controlled. Qi et al. (209) found that temperature primarily affected the polydispersity of the particles formed therefore the addition of the functionalising agents has been attributed to the observed changes over the standard Stöber process.

Increasing the water contact angle was the primary metric for determining the initial success of the coatings. It has been shown in numerous papers that increasing the water contact angle has a positive impact on the water separation efficiency (56, 66, 79). There are two primary factors that will affect the water contact angle, the surface free energy and the roughness of the surface (84, 166). Using silica nanoparticles alone would not increase the contact angle, applying the nanoparticles to the surface of the fibres would result in an increase in roughness, but would increase the surface free energy. It is likely that this will result in the Wenzel wetting state being achieved, this would reduce the contact angle having the opposite effect to what is desired.

Altering the concentration of the reagents in the Stöber process changed the morphology of the particles being produced, as expected. However, the discrete silica particles were found to form aggregates, this was identified using a combination of SEM images and DLS. The level of aggregation was

found to have an impact on the contact angle, the main performance indicator of the coatings. It has been shown that as the tendency to aggregate increases the contact angle decreases. The tendency of the particles to aggregate likely leads to a less random and more ordered surface, thus decreasing the roughness and resulting in a lower contact angle. It was found that as the particle sizes increased, then the contact angle also increased for both the FAS and HDTMS functionalised particles. This again is attributed to the roughness that would be created by the larger particles allowing a larger fraction of air to be trapped leading to increased contact angles. The opposite was seen for the oleic acid functionalised particles, this is attributed to a difference in the formation of the nanoparticles.

There were some differences between the different functionalising compounds used with regards to contact angle. The FAS functionalised particles resulted in the highest average contact angle (146.4°), followed by the HDTMS functionalised particles (144.5°) and finally the oleic acid resulted in the lowest contact angle (140.2°). This is the result that would be expected due to the differences in surface free energies. However, it was found that an equally important aspect when creating a superhydrophobic coating is the roughness imparted. While it was clear that the roughness did have an impact, the sample size used did not allow for a meaningful correlation of the Stöber process reagent concentrations to the morphology. However, it was found that in general particles that display less aggregation and larger particles resulted in increased contact angles.

As was identified in the field return filters, the pressure drop plays an important role in the ability of the filter to separate the emulsions. It would be expected that by adding a coating to the fibres that the pressure drop across the filter will increase. The goal is to create a coating that maximises the positive impact of increasing contact angle whilst minimising the impact on the flow characteristics. As has been previously mentioned, the secondary function of the filter is to remove any insoluble contaminants from the fuel flow. This will result in the gradual clogging of the filter during use, but accelerating this process through coating is not desired.

In this project the coating was being applied to a prefabricated polymer based fibrous barrier filter. This was fixed, therefore there was little that could be done to improve the restriction to flow. Even though it was shown from the field samples that the restriction to flow has a negative effect upon the water separation efficiency, it is not possible to consider stopping the fouling occurring. Since the secondary function of the filter is to remove insoluble

contaminants from the fuel, therefore the filter will always become blocked during prolonged usage. The aim of the coating is to maintain as much water separating performance as possible once the blockage has occurred. Applying a coating to the surface of the fibres will add material and therefore increase the pressure drop, it was important to ensure that this was minimised.

It is shown that for both the FAS and HDTMS functionalised coatings, increasing concentrations of the functionalising agent resulted in decreased air permeability. The primary reason for this is attributed to the chemical reaction that occurs, the slower hydrolysing functionalising agent may act as a binding agent forming more stable aggregates that more readily block the pores of the filter material (211). The quicker forming silica particles will act like nucleation sites for the slower hydrolysing functionalising agent, as the functionalising agent begins to react it could bind two silica nanoparticles forming a more stable aggregate. This process could occur multiple times, creating much larger aggregates. A schematic of this process is shown in Figure 7-1. The same occurrence was not observed in for the oleic acid functionalised coatings because the reaction governing the functionalisation is an esterification reaction rather than a hydrolysation reaction (119).

This shows that there is an optimum ratio between the concentration of the silica nanoparticles formed and the functionalising agent used to create a superhydrophobic surface. This ratio was not established in detail in this study; however, it is an extremely important finding that would be vital when developing this coating further.

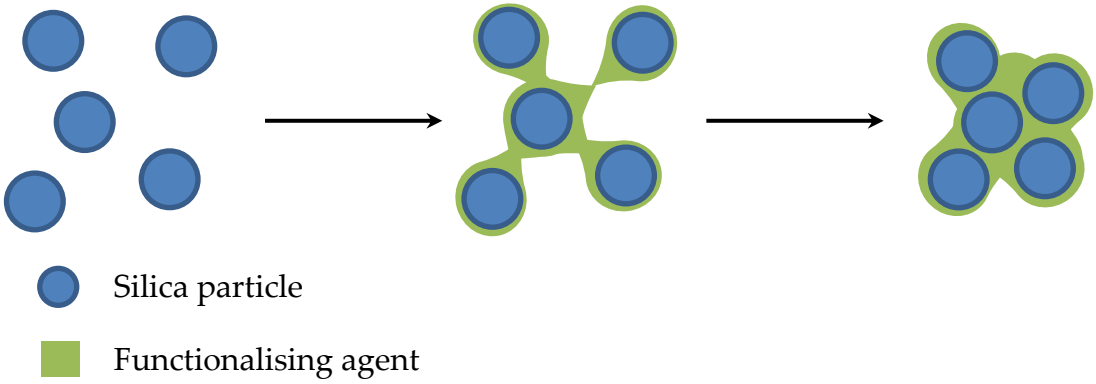

Figure 7-1: Diagram showing the mechanism for aggregation with the slower reacting functionalising agent.

In addition to this, the morphology of the particles is found to have an impact on the pore size distribution and the air permeability. For all the functionalising agents, smaller particles resulted in a lower air permeability. This is the result that would be expected, smaller particles are able to create a

more closely packed layer that is easier to hold together with Van der Waals forces. It was also shown that the samples with FAS and HDTMS with higher polydispersity had a lower air permeability. This is attributed again to the high polydispersity allowing a tighter packed coating to form, making it easier to bridge open pores and block them.

Feng and Hays (223) describe the importance of electrostatic forces on powder particles, this includes Van der Waals forces. The Van der Waals forces will not increase significantly with increasing mass, however the forces due to gravity will. The reason for this is that the force experienced by the particle due to Van der Waals forces is proportional to its radius. However, the force experienced due to gravity is a function of the mass, assuming constant density, this is proportional to the cube of the radius. This will result in the particles becoming less stable at the surface. This explains why the smaller particles are better able to initially block the pores. Obviously if the flow were to be forced through the relatively weak Van der Waals forces would be overcome. However, once the initial build-up of particles has occurred, more particles will be deposited resulting in a significantly stronger blockage.

It is shown that the morphology of the oleic acid functionalised coatings had very little correlation with the air permeability or the pore size distribution. This was attributed to the fact that the coating process was not well controlled. The dip coating process was used because it was simple, however small changes in the speed that the sample is withdrawn from the solution will lead to differences in the thickness of the coating (224). If the changes caused by the morphology of the particles are only small, this could easily be overridden by the differences in film thickness. This is another important limitation of this study, the simplistic nature of the coating method is likely not representative of the methods that would be used in a manufacturing setting. The work has identified that the morphology does have an impact on the tendency of the coating to add restriction to the filter, but the coating method is also likely to have a significant impact on this as well.

Once the coatings had been applied to the surface two coatings were selected from each of the functionalising agents. The coating that exhibited the highest contact angle and the coating that displayed the lowest change to the pore size distribution, or lowest physical change. The lowest physical change was quantified using the root mean squared error between the pore size distribution of the coating and the pore size distribution of an uncoated sample. These coatings were then tested for their water separation efficiency.

The aim of developing a one-pot method for creating superhydrophobic nanoparticles for the application to polymer filter media was achieved. It has been shown that this was possible for three different functionalising compounds. For all functionalising compounds the coatings created were shown to exhibit superhydrophobic tendencies. The understanding of how the particle morphology would impact the additional restriction to flow when applied to the filters was improved, this will allow the recipes to be tuned more accurately to obtain the best results. It was also shown that the functionalising agent's impact on the Stöber process and can lead to aggregation of the particles which is undesired. An optimum ration of functionalising agent concentration to silica particle concentration should be found.

Aim 3

The third aim was to prove that the coatings formed were successful on two fronts, improving the instantaneous water separation efficiency and improving the end-of-life water separation efficiency. It is important that this is done in a flow rig because the flow characteristics were found to be a vital part in the operation of the filter. Additionally, it is necessary to develop an accelerated fouling method for determining the end-of-life water separation performance of the coated filters.

The success of the coatings was universal, each of the coatings selected achieved a greater water separation efficiency than the uncoated filter as seen in Figure 6-2. This achieves the first part of the aim. It is what would be expected, many authors have shown that high water contact angles results in improved water separation efficiency (56, 225-227). The vast majority of the papers published examining the water separation efficiency of superhydrophobic membranes use gravity as the driving force for the mixture. From what has been previously shown in this work, the pressure drop is one of the most important factors when considering the water separation efficiency. In a diesel engine the flux is set based on the requirements of the engine, therefore the pressure drop will vary depending on the level of obstruction. This means that using gravity as the driving force for the experiments will give a skewed perspective of the efficacy of the coating.

In this work the face velocity was used as a crude method for determining the end-of-life performance of the coated filters. The theory being that as the pores become blocked due to foulant material, the face velocity that each individual pore would experience would increase. As expected, increasing the face

velocity resulted in a decrease in water separation efficiency. This is very similar to what was shown by Patel et al. (79). However, it was found that all of the coated filters formed saw a similar decrease in water separation efficiency. The coated filters performed better overall when compared to the uncoated filter.

It was expected that an increase in the contact angle would result in an improved water separation performance. A study previously introduced by Nazzal et al. (95) developed a model based on the Young-Laplace equation. It was shown that the contact angle of the dispersed phase had a direct relationship with the pressure required to deform a droplet through a pore. In this case increasing the face velocity will also increase the pressure drop, therefore increasing the likelihood that a droplet will pass through the filter. In addition to the contact angle, the size of the pores will also have an impact on the pressure required for droplet breakthrough. An attempt was made to relate the findings of this work to the model created by Nazzal et al. (95), however there wasn't a good agreement.

There are a number of possible reasons that the model does not match with the experiment. One thing that is certain is that there must be something that is occurring in reality that is not accounted for in the model. First looking at the assumptions of the model, it is possible to determine some of the reasons. Firstly, the pore is assumed to be rigid, and the droplet is being deformed by the pressure resulting in breakthrough. In reality, as was shown by Patel et al. (79) the fibres can begin to deform under higher pressures, thus changing the pore size. In addition to this, the model assumes that there is one pore size, and this is constant throughout the material, or more accurately this model is looking at the interaction between one droplet and one pore. Applying this to a system in which there are a range of pore sizes, and a range of droplet sizes will likely result in inaccurate results.

In addition to the problems mentioned above, the model is assuming that the mechanism for separation is purely barrier filtration. It is known that there is a combination of both barrier and coalescence filtration occurring, the evidence of this is the observation of secondary phase (water) buildup on the downstream side of the filter within the filter housing. The primary mechanism is barrier filtration, however, is the droplet is not entrained at the surface of the fibres it is possible that is becomes caught in the depth of the filter. More droplets will then coalesce with this droplet as it moves through the filter, providing that it has gained sufficient volume by the time it is exiting the filter it will drop out of the flow due to the gravitational forces

acting upon it. This means that the complete breakdown that is predicted by the model above a threshold pressure will not occur because there will still be some coalescence type filtration occurring.

Using this increase in the face velocity allowed the examination of the mechanisms of water in diesel emulsion separation. It was shown that for the filters being used, while they are primarily barrier filters there is an element of coalescence that occurs. It was also found that due to the complexity of the pore structure and the fact that the droplet size distribution is not uniform, modelling the water separation efficiency from first principles is very complex, and cannot be achieved with the simple equation postulated by Nazzal et al. (95). However, it was conclusively shown that the application of the coatings, while increasing the initial resistance to flow did result in both an improved response to increase in face velocity with respect to both water separation efficiency and pressure drop. This is a good indication that the coated filters will have a better end-of-life performance when compared to the uncoated filter. Further work is required to show this conclusively.

Something that wasn't captured during the increased face velocity testing was the impact of fouling on increased roughness of the fibres introduced by the coating; there was potential for this having no net positive impact on the end-of-life performance of the filter. Looking at the SEM images of the surface of the filters after fouling has occurred (Figure 4-9 - Figure 4-19) the fibres become coated in the foulant material. This will eventually form a cake layer. This was the main driving force behind the development of an accelerated fouling method to allow the impact of a coating to be assessed even after fouling occurs. Figure 7-2 shows a comparison between a filter fouled in the field and a filter fouled using the accelerated method. The fouling achieved in the accelerated methodology is visually very similar to what was observed from the field samples.

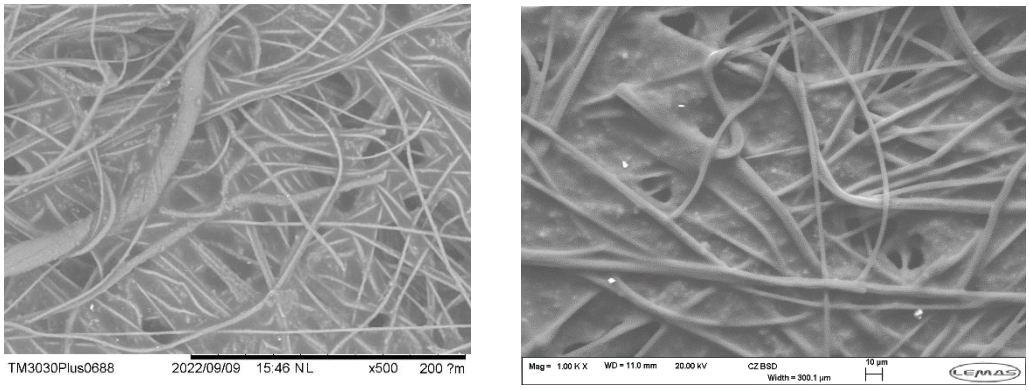

Figure 7-2: Comparison between artificially fouled (right) and field fouled (left) filters.

It has shown that even though the fouling material covers the fibres, the water separation efficiency is still improved when compared to the uncoated sample. This was the case for all the coatings aside from one (HDTMS 8), this shows that this method of improving filter performance is valid even though the foulant material will eventually cover the fibres. One of the most important findings here is that although the filters are primarily barrier filters, once fouled the droplets aren't stopped at the surface alone. If the separation was occurring only at the surface the fibres and the fibres were covered in fouling material, the surface being covered in foulant material should result in complete failure of the filter. This should inform the method of application of this type of coating, using the dip method will result in better penetration that a spray method and will likely lead to improved end-of-life performance.

There were some unexpected results when examining the threshold pressure, the oleic acid functionalised coatings outperformed both the HDTMS and FAS functionalised coatings. This was unexpected because the contact angles for the oleic acid coated filters were lower, and the response to pressure drop was comparable. One important measurement that was not possible to represent in the lab is the roll off angle (contact angle hysteresis); this will represent how easily the droplets caught on the surface would be released before settling due to gravity. It is possible that the superior performance of the oleic acid coatings can be attributed to this. Similarly, HDTMS ID8 showed a significantly increased pressure drop compared to the other filters, it is possible that at higher face velocities the droplets were not able to release from the surface. This caused a chain reaction in which the droplets couldn't release, but were coalescing and blocking more of the pores, hence the increased pressure drop and significant decrease in water separation efficiency.

While this method gave some insight into the performance of the filter, it is not a true representation of the fouling that would occur in the engine. Using carbon black, the engine fouling was mimicked. By using only carbon black initially, the effect of increased pressure drop can be isolated somewhat because the contact angle of the carbon black fouled filters was found to be relatively consistent at 120°. Again, as expected it was found that the water separation efficiency was reduced for all of the filters tested. While it was found that the model developed by Nazzal et al. (95) did not have a good agreement with the experimental results of this work it is a useful tool in describing the reasons that the water separation efficiency is reduced by the fouling. The lack of agreement with a simple pore scale model suggests that

there are more mechanisms governing the capture of a droplet than the simple one postulated by Nazzal et al. (93).

The interfacial tension between the two fluids remained the same throughout the experiments, therefore the interfacial tension portion of the model would be constant. The primary change after fouling with carbon black is that the pores on average will be smaller. The contact angle will be affected as well, reducing to approximately 120° in all cases. The reduction in pore sizes would result in a higher breakthrough pressure, this would result in an improved water separation efficiency. Having said this, the flowrate remained constant therefore the reduction in the open area available for flow will result in an increase in the overall pressure at the surface of the remaining pores. The reduction in contact angle would result in a reduction in water separation efficiency as well.

It was found that the fouling with carbon black resulted in an increase in the pressure drop across the filter, which in turn resulted in a decrease in the water separation efficiency. Interestingly, the relationships between the contact angle, pressure drop, and water separation efficiency observed in the returned filter elements were also found to hold for the artificially fouled filters, as shown in Figure 6-15. All of the filters were fouled with the same mass of carbon black, it would be expected that the increases in pressure drop caused by the fouling process would be similar. This is true for all of the filters, aside from one. This suggests that the physical blockage of the pores is not the only thing that will impact the water separation efficiency. The likely cause of the increase in pressure drop and subsequent decrease in water separation efficiency is that the contact angle hysteresis is increased. This would result in droplets being entrained on the surface as is designed, but the droplets would not be released once they have coalesced. This results in a secondary fouling caused by the dispersed phase. A representation of this is shown in Figure 7-3, if the contact angle hysteresis is high the droplets are not released from the surface, they continue to coalesce, and the pores become blinded. If the contact angle hysteresis is low, the droplets are released from the surface.

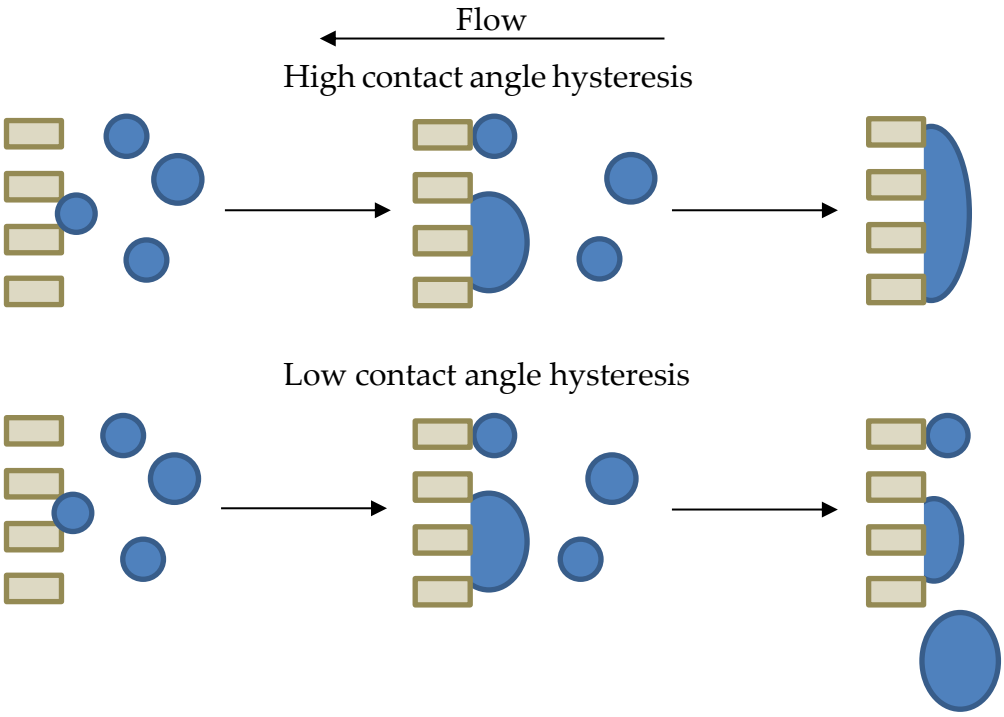

Figure 7-3: Representation of the effect of an increased contact angle hysteresis.

While the fouling with carbon black alone resulted in some interesting data and confirmed the fact that the two primary attributors to the water separation efficiency are contact angle and resistance to flow, it doesn't satisfy the aim of determining the end-of-life performance of the filter. In order to do this the decrease in the contact angle caused by the fouling material also needed to be mimicked. In order to achieve this the fouled filter was coated with polydopamine, this will result in a very thin layer of hydrophilic material being deposited on the filter. It was important to achieve a coating that had as little impact on the size of the pores as possible.

As expected, the reduction in contact angle resulted in a subsequent reduction in the water separation efficiency. Figure 6-17 shows that compared to the clean and filters fouled with only carbon black there is a marked decrease in the water separation efficiency. It is important to compare the performance of the uncoated sample to that of the returned field samples. The water separation efficiency achieved by the uncoated sample that was artificially fouled was 54%, this is comparable to the water separation efficiencies seen in the field return samples examined in Chapter 4. This gives confidence that the technique is able to mimic the fouling process.

Looking at Figure 6-18 for the polydopamine and carbon black fouled process the pressure drop increases for almost all of the filters examined when

compared to the ones fouled only with carbon black. One possible cause for this is that the addition of the polydopamine as a method for reducing the contact angle has added material to the surface. However, as shown by Ball et al. (219), with conditions comparable to the conditions used in this work the maximum film thickness was shown to be approximately 30nm. It is extremely unlikely that this would result in the increases in pressure drop that has been observed.

The mechanism that has caused the increase in pressure drop is most likely caused by the change in the surface free energy as a result of the poly dopamine coating. The effect of increasing contact angle hysteresis has been discussed previously, shown in Figure 7-3. There have been very little if any published work looking at the link between the hydrophilicity and the flux of water in diesel emulsions. However, Shakeri et al. (228) examined the effect of surface modification on the flux in reverse osmosis filters. It was shown that increasing hydrophilicity resulted in increased water fluxes, as would be expected. Another study by He et al. (229) examined a number of different hydrophobic filters for water in oil separation. As a part of this it was shown that as the hydrophobicity increased the flux through the filter increased. This is the same as is seen in this work.

The one exception to the increase in pressure drop with decreasing hydrophobicity is seen for the HDTMS ID8 coated filter, for this filter the pressure drop decreased as the hydrophobicity decreased. What should be noted is that this filter exhibited a significantly higher pressure drop when compared to the other filters. It has been previously suggested that this is a result of the entrainment of the dispersed phase on the surface, this then acts as a secondary blockage to the foulant material. If the chemistry and morphology at the surface is such that the droplets are not able to release and are coalescing to form larger droplets and subsequently restricting flow, the decrease in hydrophobicity will likely aid the droplets in passing through the filter. It has already been noted that Shakeri et al. (228) have shown that higher fluxes are seen for membranes with lower hydrophobicity. Therefore, it is very likely that this is the cause of the decrease in pressure drop for this particular filter.

In terms of end-of-life performance, the filters that performed the best were the ones formed with the FAS functionalising agent. Looking at Figure 6-17 the FAS functionalising agent coatings are the only ones that show a marked improvement in end-of-life performance when compared with the uncoated sample. This is a significant finding; it is known that the C-F bond produces a

lower surface energy product when compared to the C-H bond. For example Ozkan et al. (230) examined the contact angle on the surface of a number of different materials. It was shown that polymers with C-F bonds typically displayed higher contact angles, polymers with C-H bonds displayed lower contact angles and polymers with a combination of C-H and other bonds (e.g., C-O) had even lower contact angles.

This is the primary difference between the other two types of coating and the FAS functionalised coating; therefore, it is theorised that this is the cause of the increased performance. Having said this Zhang et al. (231) found that polydopamine has a greater adhesion to hydrophobic surfaces. However, it was also found that the air/vapour layer found particularly on superhydrophobic surfaces when submerged in water will act as a significant barrier to polydopamine deposition. The polydopamine in this work was applied to the surface in an aqueous solution, meaning that this layer would be present. Being that the fluorine containing compounds would give a more hydrophobic surface it is likely that this layer would be more prominent leading to a reduction in the effectiveness of the polydopamine deposition.

If the air/ vapour barrier is present in the filter during use in a diesel engine, it is possible that this would result in a decrease in fouling during use, drastically increasing the end-of-life performance of the filter. Having said this, an additional finding by Zhang et al. (231) is that ethanol has the ability to displace this layer. This is of particular interest because if ethanol will displace the layer, it is possible that diesel will also displace the layer because diesel has a comparable wetting ability to ethanol (232). This means that the deposition of foulant material when the filter is in use would not have to contend with the air/ vapour barrier. In either case, what has been made clear by this work is that increasing the hydrophobicity will help increase the instantaneous performance of the emulsion separating filter. It has also been shown that it is possible that a marked increase in end-of-life performance will also be seen.

It has been possible to achieve the aim of proving the performance of the coatings that were formed in the previous section. Initially it was shown that the instantaneous water separation efficiency of the coated filters was improved across the board when compared to the uncoated filters. Using the facile method of increasing the face velocity at the filter allowed the mechanisms behind the water separation efficiency to be examined in more detail. It also further indicated the success of the coatings showing improved response in water separation efficiency and pressure drop when compared to

the uncoated filter. Finally, the aim of developing an accelerated fouling technique was successful, it was shown that an uncoated filter had a similar response to the artificial fouling as was seen in the field fouled samples. Using this novel technique, it was then possible to show that the coating has improved the water separation efficiency at the end-of-life of the filters.

7.1.2 Novel Contributions

Hydrophobic silica formation.

Three different compounds were used as functionalising agents in the formation of hydrophobic silica nanospheres, it is well known that fluorine containing compounds have some of the lowest surface free energies (233). Therefore, a fluorine containing silane was used. Fluorine containing carbon compounds have a low surface free energy because the CF bond is very stable and leads to extremely low polarity. For similar reasons CH containing molecules have quite low surface energy as well. The other two functionalising agents used were a long chain silane, which will react in the same way as the fluoro-silane and oleic acid which reacts slightly differently (234). Li et al. (119) postulated that this is an esterification reaction at the surface of the silica sphere.

Super hydrophobic particles were formed in a one step process. The ability to do this in a one step process would have the benefit of being more cost effective. A one pot method has been used by a number of authors to create FAS (Fluoroalkylsilane) functionalised silica nanoparticles (203, 235), only one paper was found to have created HDTMS (Hexadecyltrimethoxysilane) functionalised silica nanoparticles using a one pot method (121) and there were no instances of a one pot method being used for oleic acid functionalisation. The application of these particles to as prepared meltblown PET diesel filters is completely novel.

Flow loop as a test method.

While this is something that seems to be relatively intuitive, the majority of the literature focusses only on improving the water contact angle as a method for increasing the water separation efficiency. This is one of the ways that this study is novel, especially as this applies to the separation of water in diesel emulsions using a barrier filter. For example Zhao et al. (117) created super hydrophobic fabrics similar to those used in this study. However, in the study by Zhao et al. (117), when examining the oil water separation potential, the driving force used was gravity. It has been shown in this study that the pressure drop has a significant impact on the ability of a filter media to

separate two phases, therefore using gravity alone as a driving force may not give a true performance metric of the filtration media.

Using the flow loop method, it is possible to have a set flowrate, this will more accurately determine how the coated filters would behave in a real-world environment. It was only possible to find one other paper that used a similar methodology for assessing the water separation efficiency of a barrier filter. Patel et al. (79) used a pumped system to demonstrate the change in performance of electrospun poly vinylidene fluoride with changing face velocities. This work highlighted the need for this type of experiment, one of the filters formed had an extremely high contact angle, however once the face velocity was increased the water separation efficiency was drastically reduced. The reduction in water separation efficiency with increasing face velocity was attributed to deformation of the pores allowing the droplets to pass through. While this is unlikely to be the case for the membranes used in this work, it highlights the need to mimic a realistic flow system as close as possible.

The fouling experiments highlight the requirement for testing the performance of emulsion separation filters in flow conditions rather than through gravity filtration. If gravity filtration was used, it would not be possible to directly shown the reduction in performance that is caused by the fouling of the filters. Something that is often used when examining the performance of filters using gravity driven filtration is the flux through the filter, with higher flux indicating better performance (111, 142, 144, 226). While this will give an indication of the performance of the filter when combined with the water separation efficiency, using a flow loop gives a more representative outlook of performance in the field. It was shown in this study that increasing the face velocity (and thus the pressure across the filter) had a differing impact depending upon the coating that was used.

Accelerated fouling technique

The most novel aspect of the work is the development of the accelerated fouling technique using a combination of carbon black, for the physical change, and polydopamine, for the chemical change. It is important to note that the accelerated fouling technique developed for assessing the filters in this work is unique. There has been work looking at the performance of filters with respect to fouling. For example Muppalla et al. (236) examined the fouling resistance of nanofiltration membranes for the separation of emulsions. The technique used was to run the experiments for a relatively long time (8hrs) monitoring the flux and oil rejection performance. For a diesel

filter, this would not be sufficient to determine its fouling resistance. It has clearly been shown that there are deposits on the surface that occur in the engine that would not build up in a lab test over 8hrs. Additionally, the conditions in the engine are not easily mimicked in the lab. It is possible, if not likely, that the combination of temperature and pressure cycling that the fuel undergoes in the engine results in the formation of the deposits, this is without considering the interaction of additives.

7.1.3 Limitations and Future Work

During the examination of the filters fouled in the field, some interesting correlations were identified, it was possible to develop this somewhat to the beginnings of a fouling index. However, the data set available was quite small making it difficult to give full confidence to the correlations observed. In addition to this the filters that were returned were predominantly at the end-of-life, it would have been more useful to have some filters that were in the middle of their operational life as well. That way the development of the fouling over operational time could be examined.

When forming the coatings using the modified Stöber process the one parameter which is known to impact the morphology of the particles formed that was not examined was temperature. This parameter was relatively uncontrolled, with the reaction taking place at room temperature. It would be extremely interesting to examine the impact of temperature of the modified Stöber process developed in this thesis.

The method used to coat the filters was relatively crude. This is something that may have had an impact on the performance of the coated filters, especially with regards to the flow characteristics. If the filter was withdrawn at a slower rate for one than another the mass of coating on the surface could have increased resulting in an increased restriction to flow. A more controlled method for coating should be considered, this could either be dip coating with some sort of mechanical control, spin coating or spray coating.

When examining the performance of the coated filters with respect to hydrophobicity water contact angle was the primary method that was used. One of the issues with this was the fibrous nature of the samples making the fitting algorithm required difficult to implement. Additionally, it was not possible to determine the contact angle hysteresis. It would be recommended that a method should be developed to quantify this. The options I see, would be to apply coatings to a solid piece of the fibre material and apply the coating to this. This would make the measurements possible. Another method that

was considered, but ultimately abandoned due to time constraints was atomic force microscope pull off force, this can be used to determine the surface free energy.

It was intended at the beginning of this project that while examining filters from different fuel markets, certain trends would be seen allowing coatings to be developed for specific types of fouling. However, there wasn't sufficient samples from each region to make any solid conclusions on this. However, it was possible to see some slight differences. It would be beneficial to the field of study to continue this work in understanding the effect of different fuel make-ups on the fouling behaviour seen.

Something that was not examined in this work, which could have a large impact on the efficacy of a filter is the size of the pores. Having larger pores would allow the coatings to be applied achieving a final pore size to the clean filter media used in this study. Additionally, the coating process itself was not examined. Using different coating processes could lead to more favourable coating of the fibres such as better fibre coverage without impacting the pores as significantly.

All the laboratory experiments using the flow rig were using pure reference grade diesel as the continuous phase. It would be extremely informative to complete the same testing of the coatings formed using different blends of biodiesel, especially because the fuel market is trending towards having higher percentages of biodiesel in the future. Additionally, there are a significant number of additives in fuel which are known to inadvertently result in the stabilisation of water droplets. This was again not considered as part of this thesis but would be a vital part of ongoing research.

7.2 Conclusions

During the initial research for this project, it was found that there was very little published research looking at the performance of water in diesel emulsion separators after being fouled in the field. Therefore, first stage of this research was examining filters that had been fouled in real engines. Filters were received from three different fuel markets; the petroleum diesel markets in Sweden and Brazil and the biodiesel fuel market in Brazil. Analysing the fouling material on these filters it was possible to determine that in general terms, the composition of the material was relatively consistent. It was shown that the material consisted of long chain hydrocarbons with some oxygen functionality. There was some variation in the samples, however due to the

uncontrolled nature of the samples received from the field, it was not possible to identify any significant trends.

The water separation performance of the returned filters was examined using the flow rig. It was shown that there was a strong correlation between the pressure drop, contact angle and the water separation efficiency. A very simple model was created to show this. This was an important finding and was the primary reason for conducting this initial research. Understanding this relationship was able to help guide the formation and application of the coating. The coating is intended to increase the water separation efficiency of the filters both instantaneously and at the end-of life.

There has been significant research into the formation of superhydrophobic coatings. The next section of this thesis was intended to develop a one pot method to create superhydrophobic microspheres. The reason for this is that having a one-pot method will decrease the cost of the process significantly. It was shown that using a modified Stöber process hydrophobic microspheres could be formed using three different functionalising agents. It was found that the addition of the functionalising agents affected the Stöber process, this was identified by comparing the expected particle size with the measured particle size.

It was also found that the size and morphology had an impact on both of the variables found in the first chapter to have an impact on the water separation performance of the filters. It was observed that the smaller particles had a greater tendency to aggregate, this led to increased pore blockage due to the coating resulting in increased pressure drop and reduced water separation performance. Conversely, the FAS functionalised particles resulted in the smallest spheres. It was observed that these spheres formed a hierarchical structure, this resulted in increased contact angles, likely caused by an increase in the Cassie-Baxter effect.

Once the initial water separation testing was complete, it was clear that the addition of the coatings resulted in an increase in the water separation efficiency when compared to the uncoated media. Having said this, as expected the addition of the coating resulted in higher pressure drops in all cases. The primary finding in this is that the benefit from increasing the hydrophobicity outweighed the negative effect of increasing the resistance to flow.

While increasing the initial performance of the filters is of interest, it was more important to understand the end-of-life performance of the filters. In order to

do this an accelerated fouling process was developed. It was shown that the pressure drop after the fouling process was similar to that seen in the field return samples. Additionally, when examined using the SEM visually, the fouling looked comparable. The initial stage of fouling with carbon black alone had little impact on the contact angle, therefore the surface was treated with polydopamine to increase the hydrophilicity. This was found to be successful.

Using the accelerated fouling method, it was found that not all of the filters coated showed increased end-of-life performance when compared to the uncoated filter. This highlights how vital testing of end-of-life performance is when developing new coatings. The functionalising agent that performed the best during the end-of-life performance was FAS. It is likely that the reason for this is that it has the lowest surface free energy. This would mean that the fouling material used would have the least chance of adhering to the surface of the particles, allowing the coating to retain its hydrophobic properties.

References

1. Stanfel, C. Fuel filtration: Protecting the diesel engine. *Filtration & Separation.* 2009, **46**(3), pp.22-25.
2. Matsui, K., Kashiwaba, Y. and Kishimoto, Y. *Fuel filter provided with a water level detecting means*. Google Patents. 1981.
3. Bansal, S., von Arnim, V., Stegmaier, T. and Planck, H. Effect of fibrous filter properties on the oil-in-water-emulsion separation and filtration performance. *Journal of Hazardous Materials.* 2011, **190**(1), pp.45-50.
4. Arfaoui, M.A., Dolez, P.I., Dubé, M. and David, É. Development and characterization of a hydrophobic treatment for jute fibres based on zinc oxide nanoparticles and a fatty acid. *Applied Surface Science.* 2017, **397**, pp.19-29.
5. Crick, C.R., Gibbins, J.A. and Parkin, I.P. Superhydrophobic polymer-coated copper-mesh; membranes for highly efficient oil–water separation. *Journal of Materials Chemistry A.* 2013, **1**(19), pp.5943-5948.
6. Gao, J., Huang, X., Xue, H., Tang, L. and Li, R.K.Y. Facile preparation of hybrid microspheres for super-hydrophobic coating and oil-water separation. *Chemical Engineering Journal.* 2017, **326**, pp.443-453.
7. Guo, W., Ngo, H.-H. and Li, J. A mini-review on membrane fouling. *Bioresource Technology.* 2012, **122**, pp.27-34.
8. Schommers, J., Duvinage, F., Stotz, M., Peters, A., Ellwanger, S., Koyanagi, K. and Gildein, H. Potential of Common Rail Injection System for Passenger Car DI Diesel Engines. In: *SAE 2000 World Congress*. SAE International, 2000.
9. McClements, D.J. *Food emulsions: principles, practices, and techniques.* Third ed. Boca Raton: CRC Press, 2016.
10. Nurafiatin, L. Regulation vs. Field Data: Managing Fuel Quality. In.: SAE International, 2019.
11. Jakeria, M.R., Fazal, M.A. and Haseeb, A.S.M.A. Influence of different factors on the stability of biodiesel: A review. *Renewable and Sustainable Energy Reviews.* 2014, **30**, pp.154-163.
12. Patel, S.U. and Chase, G.G. Separation of water droplets from water-in-diesel dispersion using superhydrophobic polypropylene fibrous membranes. *Separation and Purification Technology.* 2014, **126**, pp.62-68.
13. Fregolente, P.B.L., Fregolente, L.V. and Wolf Maciel, M.R. Water Content in Biodiesel, Diesel, and Biodiesel–Diesel Blends. *Journal of Chemical & Engineering Data.* 2012, **57**(6), pp.1817-1821.
14. Narayan, S., Moravec, D.B., Hauser, B.G., Dallas, A.J. and Dutcher, C.S. Removing Water from Diesel Fuel: Understanding the Impact of. *Energy and Fuels.* 2018, **32**, pp.7326-7337.

15. Dixson-Declève, S. Differences Between the US and the EU Fuel Regulation Policies: A Comparative Analysis of the U.S. RFG Program and the EU Auto Oil I Program. In.: SAE International, 2000.
16. The European Parliment and the Council of the European Union. DIRECTIVE 98/70/EC OF THE EUROPEAN PARLIAMENT AND OF THE COUNCIL. *Official Journal of the European Communities.* 1998, **350**, pp.58-67.
17. The European Parliment and the Council of the European Union. DIRECTIVE 2009/30/EC OF THE EUROPEAN PARLIAMENT AND OF THE COUNCIL. *Official Journal of the European Union.* 2009, **140**, pp.88-113.
18. The European Parliment and the Council of the European Union. DIRECTIVE 2003/17/EC OF THE EUROPEAN PARLIAMENT AND OF THE COUNCIL. *Official Journal of the European Union.* 2004, **70**, pp.10-19.
19. Thomas, J.W., Brian; Alleman, Teresa; Melendez, Margo; Shirk, Mathew. *History of Significant Vehicle and Fuel Introductions in the United States.* Oak Ridge National Laboratory, 2017.
20. Zhang, K., Hu, J., Gao, S., Liu, Y., Huang, X. and Bao, X. Sulfur content of gasoline and diesel fuels in northern China. *Energy Policy.* 2010, **38**(6), pp.2934-2940.
21. Zhang, S., Wu, Y., Wu, X., Li, M., Ge, Y., Liang, B., Xu, Y., Zhou, Y., Liu, H., Fu, L. and Hao, J. Historic and future trends of vehicle emissions in Beijing, 1998–2020: A policy assessment for the most stringent vehicle emission control program in China. *Atmospheric Environment.* 2014, **89**, pp.216-229.
22. UNION, T.E.P.A.T.C.O.T.E. REGULATION (EC) No 715/2007 OF THE EUROPEAN PARLIAMENT AND OF THE COUNCIL of 20 June 2007 on type approval of motor vehicles with respect to emissions from light passenger and commercial vehicles (Euro 5 and Euro 6) and on access to vehicle repair and maintenance information. *Official Journal of the European Union.* 2007, **30**(13), pp.1-16.
23. Yue, X., Wu, Y., Hao, J., Pang, Y., Ma, Y., Li, Y., Li, B. and Bao, X. Fuel quality management versus vehicle emission control in China, status quo and future perspectives. *Energy Policy.* 2015, **79**, pp.87-98.
24. Vashist, D.K., Naveen; Bindra, Manu. Technical Challenges in Shifting from BS IV to BS-VI Automotive Emissions Norms by 2020 in India: A Review. *Archives of Current Research International.* 2017, **8**(1).
25. Matzke, M., Jess, A. and Litzow, U. Polar nitrogen-containing aromatic compounds as carriers of natural diesel lubricity. *Fuel.* 2015, **140**, pp.770-777.
26. Matzke, M., Litzow, U., Jess, A., Caprotti, R. and Balfour, G. Diesel Lubricity Requirements of Future Fuel Injection Equipment. 2009.

27. Weiß, G. Zur Anthropologie des Todes. Konzeptionen außereuropäischer (Stammes-)Gesellschaften zu Totenkult und Jenseitsglauben. In: Sich, D. et al.. eds. *Sterben und Tod Eine kulturvergleichende Analyse: Verhandlungen der VII. Internationalen Fachkonferenz Ethnomedizin in Heidelberg, 5.–8.4.1984*. Wiesbaden: Vieweg+Teubner Verlag, 1986, pp.217-226.
28. Hsieh, P.Y. and Bruno, T.J. A perspective on the origin of lubricity in petroleum distillate motor fuels. *Fuel Processing Technology.* 2015, **129**, pp.52-60.
29. Voice, A.K., Tzanetakis, T. and Traver, M. Lubricity of Light-End Fuels with Commercial Diesel Lubricity Additives. In.: SAE International, 2017.
30. Hazrat, M.A., Rasul, M.G. and Khan, M.M.K. Lubricity Improvement of the Ultra-low Sulfur Diesel Fuel with the Biodiesel. *Energy Procedia.* 2015, **75**, pp.111-117.
31. Hoekman, S.K., Gertler, A.W., Broch, A., Robbins, C. and Natarajan, M. Biodistillate Transportation Fuels 1. Production and Properties. *Fuels and Lubricants.* 2009, **2**(2).
32. Society of Automotive Engineering. *Alternative Automotive Fuels.* SAE International, 2017.
33. Fersner, A.S. and Galante-Fox, J.M. Biodiesel Feedstock and Contaminant Contributions to Diesel Fuel Filter Blocking. *Fuels and Lubricants.* 2014, **7**(3), pp.783-791.
34. Barbosa, F.C. Biodiesel Use in Transit Fleets - A Summary of Brazilian Experiences. In: *21st SAE Brasil International Congress and Exhibition*. SAE International, 2012.
35. Wadumesthrige, K., Johnson, N., Winston-Galant, M., Tang, H., Ng, K.Y.S. and Salley, S.O. Deterioration of B20 from Compression Ignition Engine Operation. *Fuels and Lubricants.* 2010, **3**(2), pp.638-649.
36. Lopes, S.M. and Geng, P. Estimation of Elemental Composition of Diesel Fuel Containing Biodiesel. *Fuels and Lubricants.* 2013, **6**(3), pp.668-676.
37. Schwab, S.D., Bennett, J.J., Dell, S.J., Galante-Fox, J.M., Kulinowski, A.M. and Miller, K.T. Internal Injector Deposits in High-Pressure Common Rail Diesel Engines. *SAE International Journal of Fuels and Lubricants.* 2010, **3**(2), pp.865-878.
38. Caparella, T. The Complex California Biofuels Market. *Render: The International Magazine of Rendering.* 2017.
39. Barker, J., Cook, S. and Richards, P. Sodium Contamination of Diesel Fuel, its Interaction with Fuel Additives and the Resultant Effects on Filter Plugging and Injector Fouling. *SAE International Journal of Fuels and Lubricants.* 2013, **6**(3), pp.826-838.

40. Fang, H.L., Stehouwer, D.M. and Wang, J.C. Interaction Between Fuel Additive and Oil Contaminant: (II) Its Impact on Fuel Stability and Filter Plugging Mechanism. In: *SAE Powertrain & Fluid Systems Conference & Exhibition*. SAE International, 2003.
41. Grimes, B.A. Population Balance Model for Batch Gravity Separation of Crude Oil and Water Emulsions. Part I: Model Formulation. *Journal of Dispersion Science and Technology.* 2012, **33**(4), pp.578-590.
42. Hahn, A.U. and Mittal, K.L. Mechanism of demulsification of oil-in-water emulsion in the centrifuge. *Colloid and Polymer Science.* 1979, **257**(9), pp.959-967.
43. Cambiella, A., Benito, J.M., Pazos, C. and Coca, J. Centrifugal Separation Efficiency in the Treatment of Waste Emulsified Oils. *Chemical Engineering Research and Design.* 2006, **84**(1), pp.69-76.
44. Eow, J.S. and Ghadiri, M. Electrostatic enhancement of coalescence of water droplets in oil: a review of the technology. *Chemical Engineering Journal.* 2002, **85**, pp.357-368.
45. Mhatre, S., Vivacqua, V., Ghadiri, M., Abdullah, A.M., Al-Marri, M.J., Hassanpour, A., Hewakandamby, B., Azzopardi, B. and Kermani, B. Electrostatic phase separation: A review. *Chemical Engineering Research and Design.* 2015, **96**, pp.177-195.
46. Kwon, W.T., Park, K., Han, S.D., Yoon, S.M., Kim, J.Y., Bea, W. and Rhee, Y.W. Investigation of water separation from water-in-oil emulsion using electric field. *Journal of Industrial and Engineering Chemistry.* 2010, **16**, pp.684-687.
47. Vega, C. and Delgado, M. Treatment of waste-water/oil emulsions using microwave radiation. In: SPE, 2002.
48. Binner, E.R., Robinson, J.P., Silvester, S.A., Kingman, S.W. and Lester, E.H. Investigation into the mechanisms by which microwave heating enhances separation of water-in-oil emulsions. *Fuel.* 2014, **116**, pp.516-521.
49. Fang, C.S., Lai, P.M.C., Chang, B.K.L. and Klaila, W.J. Oil Recovery and Waste Reduction by Microwave Radiation. *Environmental Progress.* 1989, **8**(4), pp.235-238.
50. Mohammed, R.A., Bailey, A.I., Luckham, P.F. and Taylor, S.E. Dewatering of crude oil emulsions 3. Emulsion resolutuion by chemical means. *Colloids and Surfaces A: Physiochemical and Engineering Aspects.* 1994, **83**(3), pp.261-271.
51. Jones, T.J., Neustadter, E.L. and Wittingham, K.P. Water-In-Crude Oil Emulsion Stability And Emulsion Destabilization By Chemical Demulsifiers. *Journal of Canadian Petroleum Technology.* 1978, **17**(2), pp.100-108.

52. Wu, J., Xu, Y., Dabros, T. and Hamza, H. Effect of Demulsifier Properties on Destabilization of Water-in-Oil Emulsion. *Energy and Fuels.* 2003, **17**(2), pp.1554-1559.
53. Temple-Head, C., Davies, C., Wilson, N. and Readman, N. Developing New Surfactant Chemistry for Breaking Emulsions in Heavy Oil. *Journal of Petroleum Technology.* 2014, **66**(1), pp.30-36.
54. Kumbár, V. and Skřivánek, A. Temperature dependence viscosity and density of different biodiesel blends. *Acta Universitatis Agriculturae et Silviculturae Mendelianae Brunensis.* 2015, **63**(4), pp.1147-1151.
55. Kocherginsky, N.M., Tan, C.L. and Lu, W.F. Demulsification of water-in-oil emulsions via filtration through a hydrophilic polymer membrane. *Journal of Membrane Science.* 2003, **220**, pp.117-128.
56. Zhang, W., Shi, Z., Zhang, F., Liu, X., Jin, J. and Jiang, L. Superhydrophobic and Superoleophilic PVDF Membranes for Effective Separation of Water-in-Oil Emulsions with High Flux. *Advanced Materials.* 2013, **25**(14), pp.2071-2076.
57. Shin, C. and Chase, G.G. Separation of Water ‐ in ‐ Oil Emulsions Using Glass Fiber Media Augmented with Polymer Nanofibers. *Journal of Dispersion Science and Technology.* 2006, **27**(4), pp.517-522.
58. Feng, L., Zhang, Z., Mai, Z., Ma, Y., Liu, B., Jiang, L. and Zhu, D. Surface Chemistry A Super-Hydrophobic and Super-Oleophilic Coating Mesh Film for the Separation of Oil and Water. *Surface Chemistry.* 2004, **116**, pp.2046-2048.
59. Han, D. and Steckl, A.J. Superhydrophobic and Oleophobic Fibers by Coaxial Electrospinning. *Langmuir.* 2009, **25**(16), pp.9454-9462.
60. Jiang, L., Zhao, Y. and Zhai, J. A Lotus-Leaf-like Superhydrophobic Surface: A Porous Microsphere/Nanofiber Composite Film Prepared by Electrohydrodynamics. *Angewandte Chemie.* 2004, **116**, pp.4438-4441.
61. Liang, Y., Peng, J., Li, X., Huang, J., Qiu, R., Zhang, Z. and Ren, L. Wettability and Contact Time on a Biomimetic Superhydrophobic Surface. *Materials.* 2017, **10**(3), pp.254-265.
62. Clayfield, E.J., Dixon, A.G., Foulds, A.W. and Miller, L.R.J. The Coalescence of Secondary Dispersions I. The Effect of Wettability and Surface Energy. *Journal of Colloid and Interface Science.* 1985, **104**(2), pp.500-511.
63. Sokolovic′, S.R.M., Vulic′, T.J. and Sokolovic′, S.M. Effect of bed length on steady-state coalescence of oil-in-water emulsion. *Separation and Purification Technology.* 2007, **56**, pp.79-84.
64. Akagi, Y., Okada, K., Dote, T. and Yoshioka, N. Effect of Wettability of Glass Fiber Beds on Separation of Oil Droplets Dispersed in Water. *Journal of Chemical Engineering of Japan.* 1990, **23**(1), pp.105-108.

65. Lee, C. and Baik, S. Vertically-aligned carbon nano-tube membrane filters with superhydrophobicity and superoleophilicity. *Carbon.* 2010, **48**, pp.2192-2197.
66. Cao, Y., Chen, Y., Liu, N., Lin, X., Feng, L. and Wei, Y. Mussel-inspired chemistry and Stöber method for highly stabilized water-in-oil emulsions separation. *Journal of Materials Chemistry A.* 2014, **2**(48), pp.20439-20443.
67. Lee, C.H., Johnson, N., Drelich, J. and Yap, Y.K. The performance of superhydrophobic and superoleophilic carbon nanotube meshes in water–oil filtration. *Carbon.* 2011, **49**, pp.669-676.
68. Viswanadam, G. and Chase, G.G. Water–diesel secondary dispersion separation using superhydrophobic tubes. *Separation and Purification Technology.* 2013, **104**, pp.81-88.
69. Li, H.J., Cao, Y.M., Qin, J.J., Jie, X.M., Wang, T.H., Liu, J.H. and Yuan, Q. Development and characterization of anti-fouling cellulose hollow fiber UF membranes for oil–water separation. *Journal of Membrane Science.* 2006, **279**(2), pp.328-335.
70. Zhang, M., Wang, C., Wang, S., Shi, Y. and Li, J. Fabrication of coral-like superhydrophobic coating on filter paper. *Applied Surface Science.* 2012, **261**, pp.764-769.
71. Han, Q. and Kang, Y. Separation of water-in-oil emulsion with microfiber glass coalescing bed. *Journal of Dispersion Science and Technology.* 2017, **38**(11), pp.1523-1529.
72. Sokolovic, R.M.S., Sokolovic, S.M. and Dokovic, B.D. Effect of Working Conditions on Bed Coalescence of an Oil-in-Water Emulsion Using a Polyurethane Foam Bed. *Industrial Chemical Engineering.* 1997, **36**(11), pp.4949-4953.
73. Sareen, S.S., Rose, P.M., Gudesen, R.C. and Kintner, R.C. Coalescence in Fibrous Beds. *A.I.Ch.E. Journal.* 1966, **12**(6), pp.1045-1050.
74. Basu, S. A Study on the Effect of Wetting on Mechanism of Coalescence in a Model Coalescer. *Journal of Colloid and Interface Science.* 1993, **159**, pp.68-76.
75. Moses, S.F. and Ng, K.M. A visual study of the breakdown of emulsions in porous coalescers. *Chemical Engineering Science.* 1985, **40**(12), pp.2339-2350.
76. Zhang, J., Huang, W. and Han, Y. A Composite Polymer Film with both Superhydrophobicity and Superoleophilicity. *Macromolecular Rapid Communications.* 2006, **27**, pp.804-808.
77. Šećerov Sokolović, R.M., Vulić, T.J. and Sokolović, S.M. Effect of Fluid Flow Orientation on the Coalescence of Oil Droplets in Steady-State Bed Coalescers. *Industrial & Engineering Chemistry Research.* 2006, **45**(11), pp.3891-3895.

78. Angelov, G., Boyadzhiev, L. and Kyutchoukov, G. Separator for Liquid-Liquid Dispersions. *Chemical Engineering Communications.* 1983, **25**(6), pp.311-320.
79. Patel, S.U., Patel, S.U. and Chase, G.G. Electrospun Superhydrophobic Poly(vinylidene fluoride-co-hexafluoropropylene) Fibrous Membranes for the Separation of Dispersed Water from Ultralow Sulfur Diesel. *Energy & Fuels.* 2013, **27**(5), pp.2458-2464.
80. Sherony, D.F. and Kintner, R.C. Coalescence of an Emulsion in a Fibrous Bed: Part I Theory. *The Canadian Journal of Chemical Engineering.* 1971, **49**, pp.314-320.
81. Othman, F.M., Fahim, M.A., Jeffreys, G.V. and Mumford, C.J. Prediction of Predominant Mechanisms in The Seperation of Secondary Dispersions in a Fibrous Bed. *Journal of Dispersion Science and Technology.* 1988, **9**(2), pp.91-113.
82. Austin, D.G. and Jeffreys, G.V. Coalescence Phenomena in Liquid-Liquid Systems *Journal of Chemical Technology.* 1981, **31**, pp.475-488.
83. Kulkarni, P.S., Patel, S.U. and Chase, G.G. Layered hydrophilic/hydrophobic fiber media for water-in-oil coalescence. *Separation and Purification Technology.* 2012, **85**, pp.157-164.
84. Miller, J.D., Veeramasuneni, S., Drelich, J. and Yalamanchili, M.R. Effect of Roughness as Determined by Microscopy on the Wetting Properties Films. *Polymer Engineering and Science.* 1996, **36**(14), pp.1849-1855.
85. Hazlett, R.N. FIBROUS BED COALESCENCE OF WATER. *Industrial Engineering Chemical Fundamentals.* 1969, **8**(4), pp.625-632.
86. Magiera, R. and Blass, E. Separation of liquid-liquid Dispersions by Flow hrough Fibre Beds. *Filtration and Separation.* 1997, **34**(4), pp.369-376.
87. Agarwal, S., von Arnim, V., Stegmaier, T., Planck, H. and Agarwal, A. Role of surface wettability and roughness in emulsion separation. *Separation and Purification Technology.* 2013, **107**, pp.19-25.
88. Zhou, Y.B., Chen, L., Hu, X.M. and Lu, J. Modified Resin Coalescer for Oil-in-Water Emulsion Treatment: Effect of Operarating Conditions on Oil Removal Performance. *Industrial Engineering Chemistry.* 2009, **48**(3), pp.1660-1664.
89. Shin, C., Chase, G.G. and Reneker, D.H. The Effect of Nanofibers on Liquid–LiquidCoalescence Filter Performance. *AIChE Journal.* 2005, **51**(12), pp.3109-3113.
90. Wang, S., Song, Y. and Jiang, L. Microscale and nanoscale hierarchical structured mesh films with superhydrophobic and superoleophilic properies induced by long chain fatty acids. *Nanotechnology.* 2007, **18**(1), pp.1-5.

91. Scott, K., Jachuck, R.J. and Hall, D. Crossflow microfiltration of water-in-oil emulsions using corrugated membranes. *Separation and Purification Technology.* 2001, **22**, pp.431-441.
92. Somasundaran, P. and Zhang, L. Adsorption of surfactants on minerals for wettability control in improved oil recovery processes. *Journal of Petroleum Science and Engineering.* 2006, **52**(2), pp.198-212.
93. Nazzal, F.F. and Wiesner, M.R. Microfiltration of oil-in-water emulsions. *Water Environment Research.* 1996, **68**(7), pp.1187-1191.
94. Yang, L., Weeranoppanant, N., Jensen, K.F.J.I. and Research, E.C. Characterization and modeling of the operating curves of membrane microseparators. 2017, **56**(42), pp.12184-12191.
95. Nazzal, F.F. and Wiesner, M.R. Microfiltration of oil-in-water emulsions. 1996, **68**(7), pp.1187-1191.
96. Vasiljević, J., Gorjanc, M., Tomšič, B., Orel, B., Jerman, I., Mozetič, M., Vesel, A. and Simončič, B. The surface modification of cellulose fibres to create super-hydrophobic, oleophobic and self-cleaning properties. *Cellulose.* 2013, **20**(1), pp.277-289.
97. Fernández-Blázquez, J.P., Fell, D., Bonaccurso, E. and Campo, A.d. Superhydrophilic and superhydrophobic nanostructured surfaces via plasma treatment. *Journal of Colloid and Interface Science.* 2011, **357**(1), pp.234-238.
98. Balu, B., Breedveld, V. and Hess, D.W. Fabrication of "Roll-off" and "Sticky" Superhydrophobic Cellulose Surfaces via Plasma Processing. *Langmuir.* 2008, **24**(9), pp.4785-4790.
99. Yang, C., Li, X.-M., Gilron, J., Kong, D.-f., Yin, Y., Oren, Y., Linder, C. and He, T. CF4 plasma-modified superhydrophobic PVDF membranes for direct contact membrane distillation. *Journal of Membrane Science.* 2014, **456**, pp.155-161.
100. Yin, B., Fang, L., Hu, J., Tang, A.-Q., Wei, W.-H. and He, J. Preparation and properties of super-hydrophobic coating on magnesium alloy. *Applied Surface Science.* 2010, **257**(5), pp.1666-1671.
101. Xue, C.-H., Li, Y.-R., Zhang, P., Ma, J.-Z. and Jia, S.-T. Washable and Wear-Resistant Superhydrophobic Surfaces with Self-Cleaning Property by Chemical Etching of Fibers and Hydrophobization. *ACS Applied Materials & Interfaces.* 2014, **6**(13), pp.10153-10161.
102. Wenzel, R.N. Resistance of solid surfaces to wetting by water. *Industrial and Engineering Chemistry.* 1936, **28**(8), pp.988-994.
103. Cassie, A.B.D. and Baxter, S. Wettability of Porous Structures. *TRansactions of the Faraday Society.* 1944, **40**, pp.546-551.
104. Jin, C., Jiang, Y., Niu, T. and Huang, J. Cellulose-based material with amphiphobicity to inhibit bacterial adhesion by surface modification. *Journal of Materials Chemistry.* 2012, **22**(25), pp.12562-12567.

105. Cheng, Y., Zhu, T., Li, S., Huang, J., Mao, J., Yang, H., Gao, S., Chen, Z. and Lai, Y. A novel strategy for fabricating robust superhydrophobic fabrics by environmentally-friendly enzyme etching. *Chemical Engineering Journal.* 2019, **355**, pp.290-298.
106. Kyzer, J.L. and Martens, M. Metabolism and Toxicity of Fluorine Compounds. *Chemical Research in Toxicology.* 2021, **34**(3), pp.678-680.
107. Wu, J., Xia, J., Lei, W. and Wang, B.-p. Fabrication of superhydrophobic surfaces with double-scale roughness. *Materials Letters.* 2010, **64**(11), pp.1251-1253.
108. Zhu, T., Li, S., Huang, J., Mihailiasa, M. and Lai, Y. Rational design of multi-layered superhydrophobic coating on cotton fabrics for UV shielding, self-cleaning and oil-water separation. *Materials & Design.* 2017, **134**, pp.342-351.
109. Ogawa, T., Ding, B., Sone, Y. and Shiratori, S. Super-hydrophobic surfaces of layer-by-layer structured film-coated electrospun nanofibrous membranes. *Nanotechnology.* 2007, **18**(16), p.165607.
110. Zhang, L., Zha, D.-a., Du, T., Mei, S., Shi, Z. and Jin, Z. Formation of Superhydrophobic Microspheres of Poly(vinylidene fluoride–hexafluoropropylene)/Graphene Composite via Gelation. *Langmuir.* 2011, **27**(14), pp.8943-8949.
111. Gao, J., Wong, J.S.-P., Hu, M., Li, W. and Li, R.K.Y. Facile preparation of hierarchically porous polymer microspheres for superhydrophobic coating. *Nanoscale.* 2014, **6**(2), pp.1056-1063.
112. Polakiewicz, A., Dodiuk, H. and Kenig, S. Super-hydrophilic coatings based on silica nanoparticles. *Journal of Adhesion Science and Technology.* 2014, **28**(5), pp.466-478.
113. Brassard, J.-D., Sarkar, D.K. and Perron, J. Fluorine Based Superhydrophobic Coatings. 2012, **2**(2), pp.453-464.
114. Zhang, Z., Ge, B., Men, X. and Li, Y. Mechanically durable, superhydrophobic coatings prepared by dual-layer method for anti-corrosion and self-cleaning. *Colloids and Surfaces A: Physicochemical and Engineering Aspects.* 2016, **490**, pp.182-188.
115. Vasiljević, J., Zorko, M., Tomšič, B., Jerman, I. and Simončič, B. Fabrication of the hierarchically roughened bumpy-surface topography for the long-lasting highly oleophobic "lotus effect" on cotton fibres. *Cellulose.* 2016, **23**(5), pp.3301-3318.
116. Yu, T., Zhao, Y., Zheng, P., Wang, L., Yan, Z., Ge, D. and Yang, L. Ultra-durable superhydrophobic surfaces from 3D self-similar network via co-spraying of polymer microspheres and nanoparticles. *Chemical Engineering Journal.* 2021, **410**, p.128314.
117. Zhao, X., Li, Y., Li, B., Hu, T., Yang, Y., Li, L. and Zhang, J. Environmentally benign and durable superhydrophobic coatings

based on SiO2 nanoparticles and silanes. *Journal of Colloid and Interface Science.* 2019, **542**, pp.8-14.

118. Xu, B. and Zhang, Q. Preparation and Properties of Hydrophobically Modified Nano-SiO2 with Hexadecyltrimethoxysilane. *ACS Omega.* 2021, **6**(14), pp.9764-9770.
119. Li, Z. and Zhu, Y. Surface-modification of SiO2 nanoparticles with oleic acid. *Applied Surface Science.* 2003, **211**(1), pp.315-320.
120. Baniasadi, H. and Seppälä, J. Novel long-chain aliphatic polyamide/surface-modified silicon dioxide nanocomposites: in-situ polymerization and properties. *Materials Today Chemistry.* 2021, **20**, p.100450.
121. Wang, H., Ding, J., Xue, Y., Wang, X. and Lin, T. Superhydrophobic fabrics from hybrid silica sol-gel coatings: Structural effect of precursors on wettability and washing durability. *Journal of Materials Research.* 2010, **25**(7), pp.1336-1343.
122. Lee, H., Dellatore, S.M., Miller, W.M. and Messersmith, P.B. Mussel-Inspired Surface Chemistry for Multifunctional Coatings. *Science.* 2007, **318**(5849), pp.426-430.
123. Ryu, J.H., Messersmith, P.B. and Lee, H. Polydopamine Surface Chemistry: A Decade of Discovery. *ACS Applied Materials & Interfaces.* 2018, **10**(9), pp.7523-7540.
124. Cao, C., Tan, L., Liu, W., Ma, J. and Li, L. Polydopamine coated electrospun poly(vinyldiene fluoride) nanofibrous membrane as separator for lithium-ion batteries. *Journal of Power Sources.* 2014, **248**, pp.224-229.
125. Orishchin, N., Crane, C.C., Brownell, M., Wang, T., Jenkins, S., Zou, M., Nair, A. and Chen, J. Rapid Deposition of Uniform Polydopamine Coatings on Nanoparticle Surfaces with Controllable Thickness. *Langmuir.* 2017, **33**(24), pp.6046-6053.
126. Kang, S.M., You, I., Cho, W.K., Shon, H.K., Lee, T.G., Choi, I.S., Karp, J.M. and Lee, H. One-Step Modification of Superhydrophobic Surfaces by a Mussel-Inspired Polymer Coating. *Angewandte Chemie International Edition.* 2010, **49**(49), pp.9401-9404.
127. Zhang, W., Luo, J., Ding, L. and Jaffrin, M.Y. A Review on Flux Decline Control Strategies in Pressure-Driven Membrane Processes. *Industrial & Engineering Chemistry Research.* 2015, **54**(11), pp.2843-2861.
128. Chang, Y.-R., Lee, Y.-J. and Lee, D.-J. Membrane fouling during water or wastewater treatments: Current research updated. *Journal of the Taiwan Institute of Chemical Engineers.* 2019, **94**, pp.88-96.
129. Bouhabila, E.H., Ben Aïm, R. and Buisson, H. Fouling characterisation in membrane bioreactors. *Separation and Purification Technology.* 2001, **22-23**, pp.123-132.

130. Trussell, R.S., Merlo, R.P., Hermanowicz, S.W. and Jenkins, D. Influence of mixed liquor properties and aeration intensity on membrane fouling in a submerged membrane bioreactor at high mixed liquor suspended solids concentrations. *Water Research.* 2007, **41**(5), pp.947-958.
131. Hwang, K.-J. and Ku, C.-Y. Model development for estimating microfiltration performance of bio-ethanol fermentation broth. *Journal of the Taiwan Institute of Chemical Engineers.* 2014, **45**(4), pp.1233-1240.
132. Lee, D.-J. and Huang, C. Membrane Fouling Mitigation: Membrane Cleaning AU - Lin, Justin Chun-Te. *Separation Science and Technology.* 2010, **45**(7), pp.858-872.
133. Juang, Y.-C., Adav, S.S., Lee, D.-J. and Lai, J.-Y. Influence of Internal Biofilm Growth on Residual Permeability Loss in Aerobic Granular Membrane Bioreactors. *Environmental Science & Technology.* 2010, **44**(4), pp.1267-1273.
134. Li, X., Mo, Y., Li, J., Guo, W. and Ngo, H.H. In-situ monitoring techniques for membrane fouling and local filtration characteristics in hollow fiber membrane processes: A critical review. *Journal of Membrane Science.* 2017, **528**, pp.187-200.
135. Wang, Z., Wu, Z., Yin, X. and Tian, L. Membrane fouling in a submerged membrane bioreactor (MBR) under sub-critical flux operation: Membrane foulant and gel layer characterization. *Journal of Membrane Science.* 2008, **325**(1), pp.238-244.
136. Johnson, D. and Hilal, N. Characterisation and quantification of membrane surface properties using atomic force microscopy: A comprehensive review. *Desalination.* 2015, **356**, pp.149-164.
137. Yu, S. A review of recent advance in fouling mitigation of NF/RO membranes in water treatment: pretreatment, membrane modification, and chemical cleaning AU - Zhao, Dongsheng. *Desalination and Water Treatment.* 2015, **55**(4), pp.870-891.
138. Mohammad, A.W., Teow, Y.H., Ang, W.L., Chung, Y.T., Oatley-Radcliffe, D.L. and Hilal, N. Nanofiltration membranes review: Recent advances and future prospects. *Desalination.* 2015, **356**, pp.226-254.
139. Kaya, Y., Gönder, Z.B., Vergili, I. and Barlas, H. The effect of transmembrane pressure and pH on treatment of paper machine process waters by using a two-step nanofiltration process: Flux decline analysis. *Desalination.* 2010, **250**(1), pp.150-157.
140. Simon, A., McDonald, J.A., Khan, S.J., Price, W.E. and Nghiem, L.D. Effects of caustic cleaning on pore size of nanofiltration membranes and their rejection of trace organic chemicals. *Journal of Membrane Science.* 2013, **447**, pp.153-162.
141. Gzara, L., Ahmad Rehan, Z., Khan, S.B., Alamry, K.A., Albeirutty, M.H., El-Shahawi, M.S., Rashid, M.I., Figoli, A., Drioli, E. and Asiri,

A.M. Preparation and characterization of PES-cobalt nanocomposite membranes with enhanced anti-fouling properties and performances. *Journal of the Taiwan Institute of Chemical Engineers.* 2016, **65**, pp.405-419.

142. Liu, N., Lin, X., Zhang, W., Cao, Y., Chen, Y., Feng, L. and Wei, Y. A Pure Inorganic ZnO-Co3O4 Overlapped Membrane for Efficient Oil/Water Emulsions Separation. *Scientific Reports.* 2015, **5**, p.9688.
143. Shi, Z., Zhang, W., Zhang, F., Liu, X., Wang, D., Jin, J. and Jiang, L. Ultrafast Separation of Emulsified Oil/Water Mixtures by Ultrathin Free-Standing Single-Walled Carbon Nanotube Network Films. *Advanced Materials.* 2013, **25**(17), pp.2422-2427.
144. Huang, Y., Li, H., Wang, L., Qiao, Y., Tang, C., Jung, C., Yoon, Y., Li, S. and Yu, M. Ultrafiltration Membranes with Structure-Optimized Graphene-Oxide Coatings for Antifouling Oil/Water Separation. *Advanced Materials Interfaces.* 2015, **2**(2), p.1400433.
145. Zhang, Y., Zhao, Y., Chu, H., Dong, B. and Zhou, X. Characteristics of dynamic membrane filtration: structure, operation mechanisms, and cost analysis. *Chinese Science Bulletin.* 2014, **59**(3), pp.247-260.
146. Pearce, G. Introduction to membranes: Fouling control. *Filtration & Separation.* 2007, **44**(6), pp.30-32.
147. Barker, J., Langley, G. and Richards, P.J.S.T.P. Insights into deposit formation in high pressure diesel fuel injection equipment. 2010, **2010**.
148. Csontos, B., Bernemyr, H., Erlandsson, A., Forsberg, O., Pach, M. and Hittig, H. *Characterization of Deposits Collected from Plugged Fuel Filters.* 2019.
149. Arouni, H., Farooq, U., Goswami, P., Kapur, N. and Russell, S.J. Coalescence efficiency of surface modified PBT meltblown nonwovens in the separation of water from diesel fuel containing surfactants. *Results in Engineering.* 2019, **4**, p.100048.
150. Michielsen, S. and Lee, H.J. Design of a Superhydrophobic Surface Using Woven Structures. *Langmuir.* 2007, **23**(11), pp.6004-6010.
151. Young, T. III. An essay on the cohesion of fluids. *Philosophical Transactions: The Royal Society Publishing.* 1805, **95**, pp.65-87.
152. Chau, T.T., Bruckard, W.J., Koh, P.T.L. and Nguyen, A.V. A review of factors that affect contact angle and implications for flotation practice. *Advances in Colloid and Interface Science.* 2009, **150**, pp.106-115.
153. Kaelble, D.H. Dispersion-Polar Surface Tension Properties of Organic Solids. *The Journal of Adhesion.* 1970, **2**(2), pp.66-81.
154. Kirsch, P. *Modern Fluoroorganic Chemistry: Synthesis, Reactivity, Applications.* Weinheim: Wiley, 2013.
155. Marmur, A. Wetting on Hydrophobic Rough Surfaces: To Be. *Langmuir.* 2003, **19**, pp.8343-8348.

156. Zhou, Z. and Wu, X. Electrospinning superhydrophobic–superoleophilic fibrous PVDF membranes for high efficiency water-oil separation. *Material Letters.* 2015, **160**(1), pp.423-427.
157. Zhang, X., Shi, F., Niu, J., Jiang, Y. and Wang, Z. Superhydrophobic surfaces: from structural control to functional application. *Journal of Materials Chemistry.* 2007, **18**(2), pp.621-633.
158. Du, C., Wang, J., Chen, Z. and Chen, D. Durable superhydrophobic and superoleophilic filter paper for oil–water separation prepared by a colloidal deposition method. *Applied Surface Science.* 2014, **313**, pp.304-310.
159. Lander, L.M., Siewierski, L.M., Brittain, W.J. and Vogler, E.A. A Systematic Comparison of Contact Angle Methods. *Langmuir.* 1993, **9**, pp.2237-2239.
160. Zhang, X., Shi, F., Yu, X., Liu, H., Fu, Y., Wang, Z., Jiang, L. and Li, X. Polyelectrolyte Multilayer as Matrix for Electrochemical Deposition of Gold Clusters: Towards Super-Hydrophobic Surface. *Journal of the American Chemical Society.* 2004, **126**(10), pp.3064-3065.
161. Myers, N.O. Characterization of surface roughness. *Wear.* 1962, **5**(3), pp.182-189.
162. Bhushan, B. *Introduction to tribology.* John Wiley & Sons, 2013.
163. Fowkes, F.M. Calculation of work of adhesion by pair potential summation. *Journal of Colloid and Interface Science.* 1968, **28**(4), pp.493-505.
164. Owens, D.K. and Wendt, R.C. Estimation of the surface free energy of polymers. *Journal of Applied Polymer Science.* 1969, **13**(8), pp.1741-1747.
165. Zenkiewicz, M. Methods for the calculation of surface free energy of solids. *Journal of achievements in Materials and Manufacturing Engineering.* 2007, **24**(1), pp.137-145.
166. Fox, H.W. and Zisman, W.A. The Spreading of Liquids on Low Energy Surfaces. I. Polytetrafluoroethylene. *Journal of Colloid Science.* 1950, **5**(6), pp.514-531.
167. Kabza, K.G., Gestwicki, J.E. and McGrath, J.L. Contact Angle Goniometry as a Tool for Surface Tension Measurements of Solids, Using Zisman Plot Method. A Physical Chemistry Experiment. *Journal of Chemical Education.* 2000, **77**(1), p.63.
168. Stöber, W., Fink, A. and Bohn, E. Controlled growth of monodisperse silica spheres in the micron size range. *Journal of Colloid and Interface Science.* 1968, **26**(1), pp.62-69.
169. Van Blaaderen, A., Van Geest, J. and Vrij, A. Monodisperse colloidal silica spheres from tetraalkoxysilanes: Particle formation and growth mechanism. *Journal of Colloid and Interface Science.* 1992, **154**(2), pp.481-501.

170. Greasley, S.L., Page, S.J., Sirovica, S., Chen, S., Martin, R.A., Riveiro, A., Hanna, J.V., Porter, A.E. and Jones, J.R. Controlling particle size in the Stöber process and incorporation of calcium. *Journal of Colloid and Interface Science.* 2016, **469**, pp.213-223.
171. Lee, K., Sathyagal, A.N. and McCormick, A.V. A closer look at an aggregation model of the Stöber process. *Colloids and Surfaces A: Physicochemical and Engineering Aspects.* 1998, **144**(1), pp.115-125.
172. Masalov, V.M., Sukhinina, N.S., Kudrenko, E.A. and Emelchenko, G.A. Mechanism of formation and nanostructure of Stöber silica particles. *Nanotechnology.* 2011, **22**(27), p.275718.
173. Matsoukas, T. and Gulari, E. Dynamics of growth of silica particles from ammonia-catalyzed hydrolysis of tetra-ethyl-orthosilicate. *Journal of Colloid and Interface Science.* 1988, **124**(1), pp.252-261.
174. Matsoukas, T. and Gulari, E. Monomer-addition growth with a slow initiation step: A growth model for silica particles from alkoxides. *Journal of Colloid and Interface Science.* 1989, **132**(1), pp.13-21.
175. Trevor, S. and George, C. Section 1 - Filtration – Introduction, Physical Principles and Ratings. In: Sixth Edition ed. Elsevier Ltd, 2016, pp.1-54.
176. Bruttel, P. and Schlink, R.J.M.m. Water determination by Karl Fischer titration. 2003, **8**(026), p.50003.
177. Scholz, E. *Karl Fischer titration: determination of water.* Springer Science & Business Media, 2012.
178. Stetefeld, J., McKenna, S.A. and Patel, T.R.J.B.r. Dynamic light scattering: a practical guide and applications in biomedical sciences. 2016, **8**(4), pp.409-427.
179. Brinker, C.J. Dip Coating. In: Schneller, T. et al.. eds. *Chemical Solution Deposition of Functional Oxide Thin Films*. Vienna: Springer Vienna, 2013, pp.233-261.
180. Hind, A.R., Bhargava, S.K. and McKinnon, A. At the solid/liquid interface: FTIR/ATR — the tool of choice. *Advances in Colloid and Interface Science.* 2001, **93**(1), pp.91-114.
181. Arouni, H. *Nonwoven Coalescing Fuel-Water Filter Media for Diesel Engines*. thesis, University of Leeds, 2017.
182. Dağtekin, İ. and Ünsal, M. Numerical analysis of axisymmetric and planar sudden expansion flows for laminar regime. *International Journal for Numerical Methods in Fluids.* 2011, **65**(9), pp.1133-1144.
183. Gov.uk. *Energy and environment: data tables (ENV).* [Online]. 2018. [Accessed]. Available from: https://www.gov.uk/government/statistical-data-sets/energy-and-environment-data-tables-env
184. Della Vecchia, N.F., Luchini, A., Napolitano, A., D'Errico, G., Vitiello, G., Szekely, N., d'Ischia, M. and Paduano, L. Tris Buffer Modulates

Polydopamine Growth, Aggregation, and Paramagnetic Properties. *Langmuir.* 2014, **30**(32), pp.9811-9818.

185. Scriven, L.E. Physics and Applications of DIP Coating and Spin Coating. *MRS Online Proceedings Library.* 1988, **121**(1), pp.717-729.
186. Coyle, W.T. *The future of biofuels: a global perspective.* 2007.
187. Fung, H.-L. and Higuchi, T. Molecular Interactions and Solubility of Polar Nonelectrolytes in Nonpolar Solvents. *Journal of Pharmaceutical Sciences.* 1971, **60**(12), pp.1782-1788.
188. Giovambattista, N., Debenedetti, P.G. and Rossky, P.J. Effect of Surface Polarity on Water Contact Angle and Interfacial Hydration Structure. *The Journal of Physical Chemistry B.* 2007, **111**(32), pp.9581-9587.
189. Nandiyanto, A.B.D., Oktiani, R. and Ragadhita, R. How to Read and Interpret FTIR Spectroscope of Organic Material. *2019.* 2019, **4**(1), p.22 %J Indonesian Journal of Science and Technology.
190. Lacey, P., Gail, S., Kientz, J.M., Milovanovic, N. and Gris, C. Internal Fuel Injector Deposits. *SAE International Journal of Fuels and Lubricants.* 2012, **5**(1), pp.132-145.
191. Feld, H. and Oberender, N. Characterization of Damaging Biodiesel Deposits and Biodiesel Samples by Infrared Spectroscopy (ATR-FTIR) and Mass Spectrometry (TOF-SIMS). *SAE International Journal of Fuels and Lubricants.* 2016, **9**(3), pp.717-724.
192. Galante-Fox, J. and Bennett, J. Diesel injector internal deposits in high pressure common rail diesel engines. In: *Fuel systems for IC engines*. Elsevier, 2012, pp.157-166.
193. Mahamuni, N.N. and Adewuyi, Y.G. Fourier Transform Infrared Spectroscopy (FTIR) Method To Monitor Soy Biodiesel and Soybean Oil in Transesterification Reactions, Petrodiesel−Biodiesel Blends, and Blend Adulteration with Soy Oil. *Energy & Fuels.* 2009, **23**(7), pp.3773-3782.
194. Coates, D. *Liquid crystal polymers: synthesis, properties and applications.* iSmithers Rapra Publishing, 2000.
195. Tang, H., De Guzman, R., Salley, S. and Ng, K.S.J.J.o.t.A.O.C.S. Comparing process efficiency in reducing steryl glucosides in biodiesel. 2010, **87**(3), pp.337-345.
196. Ullmann, J., Geduldig, M., Stutzenberger, H., Caprotti, R., Balfour, G. and Hess, D. Effects of fuel impurities and additive interactions on the formation of internal diesel injector deposits. In: *TAE Esslingen Symposium*, 2009.
197. Elgharbawy, A.S., Sadik, W., Sadek, O.M. and Kasaby, M.A.J.J.o.t.C.C.S. A review on biodiesel feedstocks and production technologies. 2021, **66**(1), pp.5098-5109.
198. OECD, Food and Nations, A.O.o.t.U. *OECD-FAO Agricultural Outlook 2021-2030.* 2021.

199. Saeong, P., Saisriyoot, M., Thanapimmetha, A. and Srinophakun, P.J.F. The response surface optimization of steryl glucosides removal in palm biodiesel using silica adsorption. 2017, **191**, pp.1-9.
200. Tang, H., De Guzman, R.C., Salley, S.O. and Ng, K.J.J.o.t.A.O.C.S. Formation of insolubles in palm oil-, yellow grease-, and soybean oil-based biodiesel blends after cold soaking at 4 C. 2008, **85**(12), pp.1173-1182.
201. Heiden, R.W., Schober, S. and Mittelbach, M. Solubility limitations of residual steryl glucosides, saturated monoglycerides and glycerol in commercial biodiesel fuels as determinants of filter blockages. 2021, **98**(12), pp.1143-1165.
202. Costa, C.A.R., Leite, C.A.P. and Galembeck, F. Size Dependence of Stöber Silica Nanoparticle Microchemistry. *The Journal of Physical Chemistry B.* 2003, **107**(20), pp.4747-4755.
203. Wang, H., Fang, J., Cheng, T., Ding, J., Qu, L., Dai, L., Wang, X. and Lin, T. One-step coating of fluoro-containing silica nanoparticles for universal generation of surface superhydrophobicity. *Chemical Communications.* 2008, (7), pp.877-879.
204. Bogush, G.H., Tracy, M.A. and Zukoski, C.F. Preparation of monodisperse silica particles: Control of size and mass fraction. *Journal of Non-Crystalline Solids.* 1988, **104**(1), pp.95-106.
205. Ding, P. and Pacek, A.W. De‐agglomeration of Silica Nanoparticles in the Presence of Surfactants. *Journal of Dispersion Science and Technology.* 2008, **29**(4), pp.593-599.
206. Shrestha, S., Wang, B. and Dutta, P. Nanoparticle processing: Understanding and controlling aggregation. *Advances in Colloid and Interface Science.* 2020, **279**, p.102162.
207. Liu, H., Dong, S., Tang, L., Krishnan, N.M.A., Sant, G. and Bauchy, M. Effects of polydispersity and disorder on the mechanical properties of hydrated silicate gels. *Journal of the Mechanics and Physics of Solids.* 2019, **122**, pp.555-565.
208. Okudera, H. and Hozumi, A. The formation and growth mechanisms of silica thin film and spherical particles through the Stöber process. *Thin Solid Films.* 2003, **434**(1), pp.62-68.
209. Qi, D., Lin, C., Zhao, H., Liu, H. and Lü, T. Size regulation and prediction of the SiO2 nanoparticles prepared via Stöber process. *Journal of Dispersion Science and Technology.* 2017, **38**(1), pp.70-74.
210. Wang, X.-D., Shen, Z.-X., Sang, T., Cheng, X.-B., Li, M.-F., Chen, L.-Y. and Wang, Z.-S. Preparation of spherical silica particles by Stöber process with high concentration of tetra-ethyl-orthosilicate. *Journal of Colloid and Interface Science.* 2010, **341**(1), pp.23-29.

211. Osterholtz, F.D. and Pohl, E.R. Kinetics of the hydrolysis and condensation of organofunctional alkoxysilanes: a review. *Journal of Adhesion Science and Technology.* 1992, **6**(1), pp.127-149.
212. Han, Y., Lu, Z., Teng, Z., Liang, J., Guo, Z., Wang, D., Han, M.-Y. and Yang, W. Unraveling the Growth Mechanism of Silica Particles in the Stöber Method: In Situ Seeded Growth Model. *Langmuir.* 2017, **33**(23), pp.5879-5890.
213. Xu, L., Zhuang, W., Xu, B. and Cai, Z. Superhydrophobic cotton fabrics prepared by one-step water-based sol–gel coating. *The Journal of The Textile Institute.* 2012, **103**(3), pp.311-319.
214. Zhao, Z.-B., Zhang, D.-M., Meng, Y.-F., Tai, L. and Jiang, Y. One-pot fabrication of fluoride-silica@silica raspberry-like nanoparticles for superhydrophobic coating. *Ceramics International.* 2016, **42**(13), pp.14601-14608.
215. Costoyas, Á., Ramos, J. and Forcada, J. Encapsulation of silica nanoparticles by miniemulsion polymerization. *Journal of Polymer Science Part A: Polymer Chemistry.* 2009, **47**(3), pp.935-948.
216. Zhou, X., Zhang, Z., Xu, X., Guo, F., Zhu, X., Men, X. and Ge, B. Robust and Durable Superhydrophobic Cotton Fabrics for Oil/Water Separation. *ACS Applied Materials & Interfaces.* 2013, **5**(15), pp.7208-7214.
217. Sutar, R.S., Latthe, S.S., Gharge, N.B., Gaikwad, P.P., Jundle, A.R., Ingole, S.S., Ekunde, R.A., Nagappan, S., Park, K.H., Bhosale, A.K. and Liu, S. Facile approach to fabricate a high-performance superhydrophobic PS/OTS modified SS mesh for oil-water separation. *Colloids and Surfaces A: Physicochemical and Engineering Aspects.* 2023, **657**, p.130561.
218. Cortese, B., Caschera, D., Federici, F., Ingo, G.M. and Gigli, G. Superhydrophobic fabrics for oil–water separation through a diamond like carbon (DLC) coating. *Journal of Materials Chemistry A.* 2014, **2**(19), pp.6781-6789.
219. Ball, V., Frari, D.D., Toniazzo, V. and Ruch, D. Kinetics of polydopamine film deposition as a function of pH and dopamine concentration: Insights in the polydopamine deposition mechanism. *Journal of Colloid and Interface Science.* 2012, **386**(1), pp.366-372.
220. Lee, A., Elam, J.W. and Darling, S.B. Membrane materials for water purification: design, development, and application. *Environmental Science: Water Research & Technology.* 2016, **2**(1), pp.17-42.
221. Singer, P. and Rühe, J. On the mechanism of deposit formation during thermal oxidation of mineral diesel and diesel/biodiesel blends under accelerated conditions. *Fuel.* 2014, **133**, pp.245-252.
222. Shao, S., Liu, Y., Shi, D., Qing, W., Fu, W., Li, J., Fang, Z. and Chen, Y. Control of organic and surfactant fouling using dynamic membranes

in the separation of oil-in-water emulsions. *Journal of Colloid and Interface Science.* 2020, **560**, pp.787-794.

223. Feng, J.Q. and Hays, D.A. Relative importance of electrostatic forces on powder particles. *Powder Technology.* 2003, **135-136**, pp.65-75.
224. Tang, X. and Yan, X. Dip-coating for fibrous materials: mechanism, methods and applications. *Journal of Sol-Gel Science and Technology.* 2017, **81**(2), pp.378-404.
225. Yang, C., Han, N., Wang, W., Zhang, W., Han, C., Cui, Z. and Zhang, X. Fabrication of a PPS Microporous Membrane for Efficient Water-in-Oil Emulsion Separation. *Langmuir.* 2018, **34**(36), pp.10580-10590.
226. Daksa Ejeta, D., Wang, C.-F., Kuo, S.-W., Chen, J.-K., Tsai, H.-C., Hung, W.-S., Hu, C.-C. and Lai, J.-Y. Preparation of superhydrophobic and superoleophilic cotton-based material for extremely high flux water-in-oil emulsion separation. *Chemical Engineering Journal.* 2020, **402**, p.126289.
227. Wang, D., Zang, J., Wang, Q., Cheng, W., Han, G. and Huan, S. Hierarchical composite membrane with multiscale roughness structures for water-in-oil emulsion separation. *Applied Surface Science.* 2021, **566**, p.150666.
228. Shakeri, A., Mighani, H., Salari, N. and Salehi, H. Surface modification of forward osmosis membrane using polyoxometalate based open frameworks for hydrophilicity and water flux improvement. *Journal of Water Process Engineering.* 2019, **29**, p.100762.
229. He, S., Zhan, Y., Bai, Y., Hu, J., Li, Y., Zhang, G. and Zhao, S. Gravity-driven and high flux super-hydrophobic/super-oleophilic poly(arylene ether nitrile) nanofibrous composite membranes for efficient water-in-oil emulsions separation in harsh environments. *Composites Part B: Engineering.* 2019, **177**, p.107439.
230. Ozkan, O. and Erbil, H.Y. Interpreting contact angle results under air, water and oil for the same surfaces. *Surface Topography: Metrology and Properties.* 2017, **5**(2), p.024002.
231. Zhang, C., Gong, L., Xiang, L., Du, Y., Hu, W., Zeng, H. and Xu, Z.-K. Deposition and Adhesion of Polydopamine on the Surfaces of Varying Wettability. *ACS Applied Materials & Interfaces.* 2017, **9**(36), pp.30943-30950.
232. Patiño-Camino, R., Cova-Bonillo, A., Lapuerta, M., Rodríguez-Fernández, J. and Segade, L. Surface tension of diesel-alcohol blends: Selection among fundamental and empirical models. *Fluid Phase Equilibria.* 2022, **555**, p.113363.
233. Nishino, T., Meguro, M., Nakamae, K., Matsushita, M. and Ueda, Y. The lowest surface free energy based on− CF3 alignment. *Langmuir.* 1999, **15**(13), pp.4321-4323.

234. Dalvi, V.H. and Rossky, P.J. Molecular origins of fluorocarbon hydrophobicity. *Proceedings of the National Academy of Sciences.* 2010, **107**(31), pp.13603-13607.
235. Zeng, C., Wang, H., Zhou, H. and Lin, T. Self-cleaning, superhydrophobic cotton fabrics with excellent washing durability, solvent resistance and chemical stability prepared from an SU-8 derived surface coating. *RSC Advances.* 2015, **5**(75), pp.61044-61050.
236. Muppalla, R., Jewrajka, S.K. and Reddy, A.V.R. Fouling resistant nanofiltration membranes for the separation of oil–water emulsion and micropollutants from water. *Separation and Purification Technology.* 2015, **143**, pp.125-134.